

University of Alberta

Characterization of transport of positron emission tomography tracer 3'-
deoxy-3'-fluorothymidine by nucleoside transporters

by

Robert Joseph Paproski

A thesis submitted to the Faculty of Graduate Studies and Research
in partial fulfillment of the requirements for the degree of

Doctor of Philosophy

Oncology

©Robert Joseph Paproski

Spring 2010
Edmonton, Alberta

Permission is hereby granted to the University of Alberta Libraries to reproduce single copies of this thesis and to lend or sell such copies for private, scholarly or scientific research purposes only. Where the thesis is converted to, or otherwise made available in digital form, the University of Alberta will advise potential users of the thesis of these terms.

The author reserves all other publication and other rights in association with the copyright in the thesis and, except as herein before provided, neither the thesis nor any substantial portion thereof may be printed or otherwise reproduced in any material form whatsoever without the author's prior written permission.

Examining Committee

Dr. Carol Cass, Department of Oncology, University of Alberta

Dr. James Young, Department of Physiology, University of Alberta

Dr. Mary Hitt, Department of Oncology, University of Alberta

Dr. Chris Cheeseman, Department of Physiology, University of Alberta

Dr. James Hammond, Department of Physiology and Pharmacology, University of Western Ontario

To my parents for all their love and support.

Abstract

Positron emission tomography (PET) tracer 3'-fluoro-3'-deoxythymidine (FLT) is used for imaging tumor proliferation. Prior to this work, human equilibrative nucleoside transporter 1 (hENT1) was the only known human nucleoside transporter (hNT) capable of FLT transport. The aim of this research was to determine if other hNTs, including hENT2, human concentrative nucleoside transporter 1 (hCNT1), hCNT2 and hCNT3, were capable/important of/for FLT transport in mammalian cells.

Transport assays performed in *Xenopus laevis* oocytes producing recombinant hNTs demonstrated that hENT1/2 and hCNT1/3 were capable of FLT transport. FLT uptake assays with or without hENT1 inhibitor nitrobenzylmercaptapurine ribonucleoside (NBMPR) in various cultured cancer cell lines demonstrated that hENT1 was responsible for the majority of mediated FLT uptake in all tested cell lines, suggesting that hENT1 was important for FLT uptake.

The *in vivo* role of hENT1 in FLT uptake was determined by performing [¹⁸F]FLT PET on wild-type and ENT1 knockout mice. One hour after [¹⁸F]FLT injection, ENT1 knockout mice displayed significantly reduced [¹⁸F]FLT accumulation in the blood, heart, brain, kidney, liver, and lungs compared to wild-type mice. Interestingly, ENT1 knockout mice displayed increased [¹⁸F]FLT accumulation in the bone marrow and spleen which both have high CNT expression, suggesting that loss of ENT1 significantly alters FLT biodistribution in mice.

hENT1 is a predictive marker of gemcitabine response in pancreatic cancers. Since FLT uptake and gemcitabine toxicity are dependent on hENT1, FLT uptake may predict gemcitabine response in pancreatic cancers. To test this hypothesis, six different pancreatic cancer cell lines were analyzed for FLT uptake and gemcitabine toxicity. hENT1/2 inhibition in cells decreased FLT uptake and gemcitabine sensitivity. In five of six cell lines, a positive correlation was observed between FLT uptake and gemcitabine toxicity, suggesting that FLT PET may be clinically useful for predicting gemcitabine response in pancreatic cancers.

The results from this research suggest that hNTs, especially hENT1, are important for FLT uptake in mammalian cells and that FLT uptake can predict gemcitabine response in most cultured pancreatic cancer cells. The results warrant FLT PET clinical trials in pancreatic cancer patients to determine the potential of FLT PET in predicting gemcitabine response.

Acknowledgements

I thank my supervisor, Dr. Carol Cass, for accepting me as a graduate student and providing me the opportunity to pursue graduate studies in her laboratory. Despite Carol's significant administrative duties, she has always been available to provide assistance whenever I needed help. Carol's mentorship has influenced me both as a scientist and as an individual and I'm thankful to have chosen Carol as a supervisor during the earlier years of my scientific training.

I would also like to thank my two other supervisory committee members, Dr. Mary Hitt and Dr. James Young, for their helpful feedback and support throughout my program. I'm very grateful to have collaborated with Dr. Young's laboratory which has greatly aided the beginning of my own project. In addition to my supervisory committee, I thank Dr. Chris Cheeseman and Dr. James Hammond for taking significant time from their schedules to be part of my final examination committee.

Working in the Cass laboratory has been a very positive experience thanks to the many helpful individuals within the laboratory. In particular, I thank: 1) Delores Mowles and Jolanta Paul for their dedication in ordering and preparing many reagents and solutions which has greatly simplified my responsibilities, 2) Tracy Tackaberry, Frank Visser, Geraldine Baron, and Kathryn Graham for their training and technical assistance, 3) Lorelei Johnson for her work involving immunohistochemistry staining of mice spleens which is part of this thesis, 4) Michelle Kuzma, Cheryl Santos, Pat Carpenter, Vijaya Damaraju, Nancy Zhang,

and Tara Scriver for general assistance, and 5) Adam Elwi and Jing Zhang for discussions and guidance.

Outside of the Cass laboratory, I thank 1) Amy Ng and Sylvia Yao in Dr. Young's laboratory for their work with oocytes that is part of this thesis, 2) Gail Hipperson and Dan McGinn for their assistance and training in regards to housing and working with mice, 3) John Mercer, Alexander McEwan, Steve McQuarrie, Piyush Kumar, John Wilson, Melinda Wuest, Terence Riauka, and Hans-Sonke Jans for their assistance in planning, performing, and analyzing PET experiments, 4) Don Morgan and Randy Whittal from the Mass Spectrometry Laboratory in the Department of Chemistry for performing liquid-chromatography-mass spectrometry of mice plasma samples which is part of this thesis, 5) Michael Sawyer for scientific discussions, 6) Cheryl Erickson, Lori Kiernan, Cathy Walsh, and Pat Caley for administrative support, and 7) Linda Harris for assistance in obtaining various scientific articles.

Finally, I thank my immediate family including my brother and my parents for their love, support, and encouragement throughout my post-secondary education and life in general.

Table of Contents

Chapter 1: Introduction.....	1
1.1 Nucleosides.....	2
1.2 Nucleoside transport.....	3
1.3 Concentrative nucleoside transporters (CNTs).....	4
<i>1.3.1 hCNT permeants and inhibitors</i>	<i>5</i>
<i>1.3.2 hCNT regulation.....</i>	<i>7</i>
1.4 Equilibrative nucleoside transporters (ENTs).....	8
<i>1.4.1 hENT permeants and inhibitors</i>	<i>9</i>
<i>1.4.2 hENT regulation.....</i>	<i>10</i>
1.5 hNT distribution	12
1.6 Anti-cancer nucleoside analogs.....	17
<i>1.6.1 Nucleoside transporters and nucleoside drug response.....</i>	<i>22</i>
1.7 Diagnostic nucleoside analogs.....	27
<i>1.7.1 Positron Emission Tomography (PET).....</i>	<i>27</i>
<i>1.7.2 Hypoxia PET tracers.....</i>	<i>31</i>
<i>1.7.3 Deoxycytidine kinase PET tracer.....</i>	<i>32</i>
<i>1.7.4 Proliferation PET tracers.....</i>	<i>32</i>
1.8 3'-Deoxy-3'-fluorothymidine (FLT).....	36
<i>1.8.1 FLT pharmacology.....</i>	<i>37</i>
<i>1.8.2 Clinical [¹⁸F]FLT PET</i>	<i>38</i>
1.9 Goals of present work.....	46
1.10 Bibliography.....	56

Chapter 2: Materials and methods.....	78
2.1 Materials.....	79
2.2 Cell culture.....	81
2.2.1 Generation of A549-pSUPER-SC and A549-pSUPER-hENT1 cell lines.....	82
2.3 Protein determination assays.....	84
2.4 Transport and uptake assays.....	85
2.4.1 Inhibitor-sensitivity assays with <i>Saccharomyces cerevisiae</i>.....	85
2.4.2 Transport and uptake in <i>Xenopus laevis</i> oocytes.....	86
2.4.3 Transport and uptake in cultured cell lines.....	87
2.5 Taqman quantitative real-time reverse transcriptase polymerase chain reaction (RT-PCR).....	88
2.6 Equilibrium [³H]NBMPR binding assays.....	89
2.7 Gemcitabine toxicity assays.....	91
2.8 [¹⁸F]FLT uptake in mice.....	91
2.8.1 Mice models.....	91
2.8.2 [¹⁸F]FLT small animal PET.....	92
2.8.3 [¹⁸F]FLT PET image analysis.....	93
2.9 TK1 Immunoblotting.....	95
2.10 Immunohistochemistry.....	97
2.11 Liquid chromatography-mass spectrometry (LC-MS).....	98
2.12 Statistical analysis.....	99
2.13 Bibliography.....	103

Chapter 3: Characterization of FLT transport by human nucleoside transporters and the role of hENT1 for uptake of FLT in human cancer cell lines	105
3.1 Introduction.....	106
3.2 Results.....	109
3.2.1 <i>Interaction of FLT with recombinant hNTs in yeast cells.....</i>	<i>109</i>
3.2.2 <i>Transportability of FLT by recombinant hNTs in oocytes.....</i>	<i>109</i>
3.2.3 <i>Relative quantification of hNTs in cell lines.....</i>	<i>110</i>
3.2.4 <i>hNTs responsible for [³H]FLT uptake in cell lines.....</i>	<i>111</i>
3.2.5 <i>NBMPR binding and inhibition of [³H]FLT uptake in cell lines.....</i>	<i>112</i>
3.2.6 <i>Cellular hENT1 location in cell lines.....</i>	<i>112</i>
3.2.7 <i>Correlation between FLT uptake and extracellular NBMPR binding sites.....</i>	<i>113</i>
3.3 Discussion.....	114
3.4 Bibliography.....	129

Chapter 4: Biodistribution and uptake of 3'-deoxy-3'-fluorothymidine in equilibrative nucleoside transporter 1 (ENT1) knockout mice and in an ENT1 knockdown tumor model	133
4.1 Introduction.....	134
4.2 Results.....	136

4.2.1	<i>Characterization of ENT1 transcript levels in spleens of individual ENT1^{+/+} and ENT1^{-/-} mice</i>	136
4.2.2	<i>[¹⁸F]FLT PET with ENT1 altered mice</i>	136
4.2.3	<i>TKI immunoblots of mouse spleens</i>	138
4.2.4	<i>NT immunohistochemistry of mouse spleens</i>	138
4.2.5	<i>Thymidine levels in mouse plasma</i>	139
4.2.6	<i>In vitro characterization of transfected A549 cells</i>	139
4.2.7	<i>In vivo characterization of transfected A549 cells</i>	141
4.3	Discussion.....	144
4.4	Bibliography.....	162

Chapter 5: Predicting gemcitabine transport and toxicity in human pancreatic cancer cell lines with the positron emission tomography tracer 3'-deoxy-3'-fluorothymidine.....		
166		
5.1	Introduction.....	167
5.2	Results.....	170
5.2.1	<i>Quantification of extracellular hENT1 levels with [³H]NBMPR binding.....</i>	170
5.2.2	<i>Quantification of relative levels of hNTs, dCK, TK1, and RRM1 mRNA with real-time PCR.....</i>	171
5.2.3	<i>Correlation between FLT and gemcitabine transport in five cell lines.....</i>	173
5.2.4	<i>Dependence of FLT and gemcitabine uptake on hNT activity.....</i>	174

5.2.5	<i>Dependence of gemcitabine toxicity on hNT activity.....</i>	175
5.2.6	<i>Correlations between gemcitabine uptake, FLT uptake, or RRM1 mRNA expression and gemcitabine toxicity in five cell lines.....</i>	176
5.3	Discussion.....	178
5.4	Bibliography.....	196
 Chapter 6: General discussion and conclusions.....		200
6.1	Human nucleoside transporters (hNTs) capable of 3'-deoxy-3'- fluorothymidine (FLT) transport.....	201
6.2	Importance of hNTs for FLT uptake.....	203
6.3	Clinical implications of FLT transport by hNTs.....	207
6.4	Future work.....	211
6.5	Bibliography.....	214

List of Tables

Table 1-1.	Nucleoside and nucleoside analog permeants of hNTs.....	50
Table 1-2.	Decay characteristics of positron emitting isotopes commonly used in PET.....	51
Table 2-1.	Real-time PCR probe and primer concentrations and sequences.....	101
Table 3-1.	Kinetic parameters of [³H]FLT influx mediated by hNTs in oocytes.....	120
Table 3-2.	NBMPR binding parameters and IC₅₀ values for inhibition of [³H]FLT uptake in various cell lines.....	121
Table 4-1.	[¹⁸F]FLT biodistribution in mice with various ENT1 activity.....	149
Table 4-2.	[¹⁸F]FLT apparent kinetic values for A549-pSUPER-SC and A549-pSUPER-hENT1 tumors in NIH-III mice using a 3-compartment model.....	150
Table 5-1.	Total and extracellular NBMPR binding sites per cell in pancreatic cancer cell lines.....	184
Table 5-2.	Rates of uptake of FLT and gemcitabine with or without hNT inhibitors between 1-45 s in pancreatic cancer cell lines.....	185
Table 5-3.	FLT and gemcitabine uptake with or without hNT inhibitors after 1 h in pancreatic cancer cell lines.....	186
Table 5-4.	Gemcitabine toxicity with or without hNT inhibitors in pancreatic cancer cell lines.....	187

List of Figures

Figure 1-1.	Chemical structures of physiological nucleosides and nucleoside analogs.....	52
Figure 1-2.	Coincidence detection events in PET.....	53
Figure 1-3.	Thymidine metabolism in mammalian cells.....	54
Figure 1-4.	[¹⁸ F]FLT PET images in human cancer patients.....	55
Figure 3-1.	FLT inhibition of [³ H]uridine uptake in yeast cells producing recombinant hNTs.....	122
Figure 3-2.	[³ H]FLT uptake and kinetic analysis in oocytes producing recombinant hNTs.....	123
Figure 3-3.	Relative quantitation of hNT transcript levels in various cell lines by real-time PCR.....	124
Figure 3-4.	Characterization of hNTs responsible for FLT uptake in various cultured cancer cell lines.....	125
Figure 3-5.	[³ H]NBMPR binding sites and the effect of NBMPR on [³ H]FLT uptake in MCF-7 cells.....	126
Figure 3-6.	Extracellular and intracellular NBMPR binding in various cell lines.....	127
Figure 3-7.	Linear regression analysis of [³ H]FLT uptake and extracellular NBMPR binding sites per cell for all cell lines excluding MIA PaCa-2.....	128
Figure 4-1.	Analysis of mENT1 transcript levels in spleens of ENT1 ^{+/+} and ENT1 ^{-/-} mice.....	151

Figure 4-2.	FLT PET maximum intensity projection images of ENT1^{+/+} mice, ENT1^{+/+} mice injected with 15 mg/kg NBMPR-P 1 h before imaging, ENT1^{+/-} mice, and ENT1^{-/-} mice.....	152
Figure 4-3.	Characterization of TK1 and mNT levels in ENT1 altered mice.....	153
Figure 4-4.	LC-MS analysis of plasma thymidine levels in ENT1^{+/+} and ENT1^{-/-} mice.....	155
Figure 4-5.	Characterization of hENT1 and TK1 transcript levels, NBMPR binding sites, and [³H]FLT uptake in A549-derived cells.....	156
Figure 4-6.	[¹⁸F]FLT uptake in A549-pSUPER-hENT1 and A549-pSUPER-SC xenograft tumors.....	158
Figure 4-7.	Three compartment model describing FLT kinetics.....	160
Figure 4-8.	Models of FLT uptake mediated by hNTs in the absence of TK1.....	161
Figure 5-1.	Quantification hENT1 sites with NBMPR binding in pancreatic cancer cells.....	188
Figure 5-2.	Quantification of hNT, dCK, TK1, and RRM1 mRNA levels in pancreatic cancer cell lines by real-time RT-PCR.....	189
Figure 5-3.	FLT and gemcitabine uptake in pancreatic cancer cell lines over short periods of time.....	191
Figure 5-4.	Linear regression analysis of FLT and gemcitabine initial	

	rates of uptake in pancreatic cancer cell lines.....	192
Figure 5-5.	Uptake of 100 nM [³ H]FLT and [³ H]gemcitabine in pancreatic cancer cell lines.....	193
Figure 5-6.	Linear regression analysis of gemcitabine toxicity in pancreatic cell lines with gemcitabine uptake, FLT uptake, or RRM1 expression.....	194

List of Symbols, Nomenclature, or Abbreviations

%	percent
×	multiply
±	plus or minus
°C	degree Celsius
2D	two-dimensional
3D	three-dimensional
³H	tritium
5-FdU	5-fluoro-2'-deoxyuridine
A₁	adenosine receptor subtype 1
A_{2A}	adenosine receptor subtype 2A
A_{2B}	adenosine receptor subtype 2B
A₃	adenosine receptor subtype 3
ALL	acute lymphocytic leukemia
AML	acute myeloid leukemia
ATP	adenosine-5'-triphosphate
AZT	3'-deoxy-3'-azidothymidine
BBB	blood brain barrier
B_{max}	maximum number of binding sites
BSA	bovine serum albumin
cDNA	complementary DNA
CK2	casein kinase II
CLL	chronic lymphocytic leukemia
CML	chronic myelogenous leukemia
CMM	complete minimal media
CNTs	concentrative nucleoside transporters
Ci	Curie
CS	calf serum
C_T	cycle threshold
CT	computed tomography
dCK	deoxycytidine kinase

DMEM	Dulbecco's modified Eagle's medium
DNA	deoxyribonucleic acid
dUMP	2'-deoxyuridine monophosphate
<i>E. coli</i>	<i>Escherichia coli</i>
<i>e.g.</i>	<i>exempli gratia</i> ('for example')
EC₅₀	concentration of reagent resulting in 50% effectiveness
ECL	enhanced chemiluminescence
EDTA	ethylenediaminetetraacetic acid
<i>ei</i>	equilibrative insensitive; insensitive to inhibition by NBMPR
ENT	equilibrative nucleoside transporter
ERE	estrogen response element
<i>es</i>	equilibrative sensitive; sensitive to inhibition by NBMPR
FAC	1-(2'-deoxy-2'-fluoroarabinofuranosyl) cytosine
FAM	6-carboxy-fluorescein
FAZA	1- α -D-(5-deoxy-5-[¹⁸ F]-fluoroarabinofuranosyl)-2-nitroimidazole
FBAU	1-(2'-deoxy-2'-fluoro- β -D-arabinofuranosyl)-5-bromouracil
FBS	fetal bovine serum
<i>fbv</i>	fractional blood volume
FDG	2-fluoro-2-deoxyglucose
FFUdR	5-fluoro-1-(2'-fluoro-2'-deoxy- β -D-ribofuranosyl)-uracil
Fig.	figure
FLT	3'-deoxy-3'-fluorothymidine
FMAU	1-(2'-Deoxy-2'-fluoro-1- β -D-arabinofuranosyl)-thymine
FMISO	fluoromisonidazole
fmol	femtomole
FTH-SAENTA	5-S-{2-(1-[(fluorescein-5-yl)thioureido]hexanamido)ethyl}-6-N-(4-nitrobenzyl)-5-thioadenosine
<i>g</i>	relative centrifugal force
<i>g</i>	gram

GAPDH	glyceraldehyde-3-phosphate dehydrogenase
GFP	green fluorescence protein
GLU	glucose
h	hour
hCNT	human concentrative nucleoside transporter
hCNT1	human concentrative nucleoside transporter 1
hCNT2	human concentrative nucleoside transporter 2
hCNT3	human concentrative nucleoside transporter 3
hENT	human equilibrative nucleoside transporter
hENT1	human equilibrative nucleoside transporter 1
hENT2	human equilibrative nucleoside transporter 2
hENT3	human equilibrative nucleoside transporter 3
hENT4	human equilibrative nucleoside transporter 4
HEPES	4-(2-hydroxyethyl)-1-piperazineethanesulfonic acid
HIV	human immunodeficiency virus
HNF3	hepatocyte nuclear factor 3
HNF4	hepatocyte nuclear factor 4
hNT	human nucleoside transporter
HUVEC	human umbilical vein endothelial cells
IAZA	iodoazomycin arabinoside
IC₅₀	concentration of inhibitor causing 50% inhibition of protein activity
<i>i.e.</i>	<i>id est</i> ('that is to say')
IgG	Immunoglobulin G
inh.	inhibitor
IT	inhibits transporter activity
keV	kiloelectron volt
<i>K_d</i>	dissociation constant
<i>K_i</i>	inhibitor dissociation constant
Ki-67	protein expressed in proliferating cells that can be bound by the Ki-67 antibody

K_M	Michaelis-Menten constant; the permeant concentration resulting in half the maximum transport rate
L-NAME	N(G)-nitro-L-arginine methyl ester
LC-MS	liquid chromatography-mass spectrometry
MAP	mitogen-activated protein
MBq	megaBecquerel
mCNT1	mouse concentrative nucleoside transporter 1
mCNT2	mouse concentrative nucleoside transporter 2
mCNT3	mouse concentrative nucleoside transporter 3
MDCK	Madin-Darby canine kidney
mENT1	mouse equilibrative nucleoside transporter 1
mENT2	mouse equilibrative nucleoside transporter 2
MeV	megaelectron volt
mg	milligram
min	minute
MLL	mixed lineage leukemia
mM	millimolar
mNT	mouse nucleoside transporter
MRI	magnetic resonance imaging
mRNA	messenger ribonucleic acid
MRPs	multidrug resistance-associated proteins
MTS	[3-(4,5-dimethylthiazol-2-yl)-5-(3-carboxymethoxyphenyl)-2-(4-sulfophenyl)-2H-tetrazolium
N1	transport system describing CNT2 transport activity
N2	transport system describing CNT1 transport activity
N3	transport system describing CNT3 transport activity
N4	transport system describing CNT3-like transport activity without inosine transport
N5	transport system describing CNT transport of guanosine that is NBMPR-sensitive
NBMPR	nitrobenzylmercaptapurine ribonucleoside

NBMPR-P	nitrobenzylmercaptapurine ribonucleoside phosphate
nm	nanometer
nM	nanomolar
NMDG	N-methyl-D-glucamine
NP	not a permeant
NSCLC	non-small cell lung cancer
NTs	nucleoside transporters
OATs	organic anion transporters
OCTs	organic cation transporters
P	probability of obtaining a result at least as extreme as the one that was actually observed assuming that the null hypothesis is true
P	permeant
PBS	phosphate buffered saline
PBS-T	phosphate buffered saline with 0.05% Tween-20
PCR	polymerase chain reaction
PET	positron emission tomography
pH	measure of hydrogen ion concentration
PHID	pigmented hypertrichotic dermatosis with insulin-dependent diabetes
PKC	protein kinase C
pM	picomolar
PMA	12-myristate 13-acetate
pmol	picomole
PP	poor permeant
r	correlation coefficient
RNA	ribonucleic acid
RPMI	Roswell Park Memorial Institute
RRM1	ribonucleotide reductase subunit 1
RRM2	ribonucleotide reductase subunit 2
RT-PCR	reverse-transcription polymerase chain reaction

s	second
SAENTA	5'-S-(2-aminoethyl)-N6-(4-nitrobenzyl)-5'-thioadenosine
SCID	severely compromised immunodeficient mice
SDS	sodium dodecyl sulphate
SEM	standard error of the mean
shRNA	short hairpin ribonucleic acid
SLC28	solute carrier family 28; concentrative nucleoside transporter family
SLC29	solute carrier family 29; equilibrative nucleoside transporter family
Sp1	human transcription factor
SUV	standardized uptake values
SUV_{max}	maximum standardized uptake values
TAC	time-activity curve
TAC_{tumor}	tumor time-activity curve
TATA box	DNA sequence containing 5'-TATAAA-3' or similar sequence
TDP	thymidine diphosphate
TK1	thymidine kinase 1
TMP	thymidine monophosphate
Tris	tris(hydroxymethyl)aminomethane
TTP	thymidine triphosphate
μM	micromolar
μm	micrometer
V_{max}	maximum transport velocity
v/v	volume per volume
w/v	weight (gram) per volume (100 millilitres)
<i>X. laevis</i>	<i>Xenopus laevis</i>

Chapter 1: Introduction

1.1 Nucleosides

Nucleosides are the chemical precursors to nucleic acids such as DNA and RNA. Nucleosides are composed of a ribose group attached to a pyrimidine or purine nucleobase (Figure 1-1A). The most common physiological nucleosides found in prokaryotes and eukaryotes include thymidine, cytidine, and uridine (pyrimidine nucleosides) as well as adenosine, guanosine, and inosine (purine nucleosides).

Adenosine may be phosphorylated repeatedly and become adenosine-5'-triphosphate (ATP), which is the main cellular energy intermediate involved in the synthesis of DNA, RNA, and proteins. Removal of the 5'-phosphates from ATP provides energy for many enzymes and non-phosphorylated adenosine is highly produced in cells and tissues with reduced energy levels. Endogenous extracellular adenosine concentrations in tissues are relatively constant (30-300 nM) but may increase to 10 μ M under hypoxic conditions [1].

Adenosine is an important signaling molecule due to its central role in energy metabolism. Various physiological processes in the cardiovascular, neurological, inflammatory, immune, gastrointestinal, and respiratory systems are regulated by adenosine [2-5]. Adenosine exerts its effects on cells by binding to the G-protein coupled A_1 , A_{2A} , A_{2B} , and A_3 receptors which have various effects in tissues. In general, increased adenosine signaling in the human body increases delivery of nutrients to tissues while decreasing energy utilization. Elevated adenosine levels in the cardiovascular system increases heart rate and dilates

coronary arteries [2], while elevated adenosine levels in the brain have a sedative effect by inhibiting neurotransmitter secretion and neuronal activity [3].

1.2 Nucleoside transport

Due to the importance of nucleosides for nucleotide and nucleic acid synthesis, cells incapable of *de novo* nucleotide synthesis, such as bone marrow cells, leukocytes and blood platelets [6], require nucleoside salvage pathways. Nucleosides and many nucleoside analogs are relatively hydrophilic molecules and cannot efficiently cross plasma membranes. Various transporter families, including concentrative nucleoside transporters (CNTs), equilibrative nucleoside transporters (ENTs), organic cation transporters (OCTs), organic anion transporters (OATs), and multidrug resistance proteins (MRPs), have demonstrated nucleoside, nucleobase, and/or nucleotide transport activities [7-11]. In mammals, the majority of nucleoside transport is mediated by nucleoside transporters (NTs, which include ENTs and CNTs) since physiological nucleosides are the primary endogenous permeants of NTs [8].

Extracellular adenosine concentrations are influenced by NTs and ENT inhibitors have been clinically used as coronary vasodilators [12, 13]. Various anti-cancer nucleoside analogs (see section 1.6) require nucleoside transport for efficient cellular uptake and inhibition of nucleoside transport activity typically increases resistance to nucleoside analog therapy [14]. Inactivating mutations of human ENT3 (hENT3) are known to cause H-syndrome [15], which is characterized by cutaneous hyperpigmentation, hypertrichosis, hepatosplenomegaly, heart anomalies, hearing loss, hypogonadism and short

stature, and the closely related pigmented hypertrichotic dermatosis with insulin-dependent diabetes (PHID) syndrome in humans, although further studies are required to determine how mutation of hENT3 can cause these syndromes. Taken together, nucleoside transport and nucleoside transporters are important in various aspects of human health and disease.

1.3 Concentrative nucleoside transporters (CNTs)

CNTs are symporters that transport nucleosides and Na^+ (and/or H^+ for CNT3) along the cation's electrochemical gradient, normally into cells. CNT transport activities were identified before the transporters were cloned. Five Na^+ -dependent nucleoside transport systems, including N1, N2, N3, N4 and N5, were identified and distinguished based on their transport profiles [16]. N1 transports mainly purine nucleosides and uridine while N2 transports mainly pyrimidine nucleosides and adenosine. N3 and N4 transports purine and pyrimidine nucleosides although N4 did not transport inosine. N5 transports guanosine and, unlike the other concentrative nucleoside transport systems, was sensitive to nitrobenzylmercaptapurine ribonucleoside (NBMPR) inhibition. The genes encoding the N2, N1, and N3 systems have been identified and the proteins have been called CNT1, CNT2, and CNT3, respectively [17-19]. Studies of the human genome suggest no other hCNT proteins exist and the transport systems N4 and N5 may belong to other gene families or may be CNT splice variants. hCNT1/2/3, which are considered plasma membrane transporters, are comprised of 649/658/691 amino acids, respectively [17-19]. Initial hydrophobicity plots suggested that CNT1 contains 14 transmembrane domains although subsequent

analysis of CNT1 structure suggested that it contains 13 transmembrane domains [20, 21]. Recent cysteine scanning analysis with hCNT3 suggested hCNT3, and perhaps the other hCNTs, may contain 15 transmembrane domains [22]. hCNTs contain an intracellular N-terminus and an extracellular C-terminus with several potential glycosylation sites [23].

1.3.1 hCNT permeants and inhibitors

hCNT transport activities have been analyzed in mammalian cells, as well as *Xenopus laevis* oocytes and yeast cells producing recombinant hCNTs. hCNT transport studies have primarily relied on monitoring cellular uptake of radiolabeled nucleosides although transport may also be analyzed by monitoring current changes in oocytes using the two-electrode voltage clamp system [24]. Table 1-1 displays hCNT transport profiles and K_M values for hCNT permeants.

hCNT1 produced in oocytes transports uridine, thymidine, cytidine, and adenosine, but not guanosine or inosine [18, 25]. hCNT1 can also transport some clinical nucleoside analogs, including gemcitabine, 5-fluoro-2'-deoxyuridine (metabolite of 5-fluorouracil and capecitabine) and, to a lesser extent, cladribine and cytarabine [26, 27]. Electrophysiological studies with oocytes producing hCNT1 suggest that Na^+ and uridine are co-transported with a 1:1 ratio and approximately 10 uridine molecules per second are transported by each hCNT1 molecule when the oocytes are clamped at -50 mV [27].

hCNT2 produced in oocytes efficiently transports uridine, adenosine, guanosine and inosine, but not thymidine or cytidine [19]. Interestingly, murine CNT2 (mCNT2) produced in COS-2 cells demonstrated significant cytidine

transport, although with a K_M value 13-fold larger than that of uridine, suggesting differences in transportability characteristics between CNT2 orthologs [28]. When produced in CEM-derived cells or oocytes, hCNT2 demonstrated transport of 5-fluoro-2'-deoxyuridine, clofarabine and, to a lesser extent, cladribine [29, 30]. Electrophysiological studies of hCNT2 produced in oocytes suggest that hCNT2 has a Na^+ /nucleoside stoichiometry of 1:1 [31].

hCNT3 produced in oocytes transports all physiological nucleosides, including uridine, thymidine, cytidine, adenosine, guanosine, and inosine as well pharmacological nucleosides, including fludarabine, cladribine, clofarabine, 5-fluoro-2'-deoxyuridine, and gemcitabine [17, 29]. Electrophysiological studies with oocytes producing hCNT3 suggest that Na^+ or H^+ may be co-transported with uridine with 2:1 or 1:1 stoichiometries, respectively [32].

CNTs are relatively resistant to inhibition by ENT inhibitors, including NBMPR, dilazep and dipyridamole [17]. Currently, no specific CNT inhibitors have been identified although some progress has been made in the design of hCNT3 inhibitors. Phloridzin displayed an hCNT3 K_i value of 16 μM as measured by the concentration that inhibited 50% of uridine uptake in nucleoside transport deficient PK15NTD (porcine kidney nucleoside transport deficient) cells producing hCNT3 [33]. One phloridzin derivative (compound 16 in the study) displayed a K_i value of 2.9 μM for hCNT3. The K_i values of these compounds for hENT1 were greater than 1 mM, suggesting the compounds are relatively specific for hCNT3 [33]. It is currently unknown whether or not these compounds have inhibitory activity for the other hCNTs.

1.3.2 hCNT regulation

Relatively little is known about the regulation of hCNTs although some studies have provided clues toward understanding hCNT regulation. For some cell types, hCNT expression increases with cell differentiation [23]. Human promyelocytic leukemia HL-60 cells undergo differentiation into adherent macrophage-like cells when cultured with phorbol esters and incubation of HL-60 cells with phorbol 12-myristate 13-acetate (PMA) increased expression of hCNT3 mRNA and transport activity [17, 34]. Similar results were observed when human lymphoma U937 cells were incubated with PMA [35]. Differentiation of cultured hepatocyte-derived BC2 cells by continuous culturing caused increased mRNA expression of hCNT1 which was dependent on hepatocyte nuclear factor 4 (HNF4) alpha [36]. Hepatocyte-derived HepG2 cells displayed increased hCNT2 mRNA expression when co-transfected with CCAAT/enhancer binding protein (C/EBP) alpha and hepatocyte nuclear factor 3 (HNF3) gamma, suggesting these transcription factors are important for regulating hCNT2 expression in hepatocytes [36].

Tumor necrosis factor alpha has been shown to increase hCNT1 and hCNT3 mRNA levels when incubated in cultured adipocytes [37]. Hypoxia affects hCNT2, but not hCNT1, expression since culturing various human cancer cell lines in hypoxic conditions decreased hCNT2 mRNA levels to 25-50% of those of cells that were cultured in normoxic conditions [38]. Further studies are required to fully elucidate the molecular mechanisms that control hCNT regulation.

1.4 Equilibrative nucleoside transporters (ENTs)

ENTs are membrane transporters that facilitate the bidirectional diffusion of nucleosides across membranes. ENT transport processes were originally identified as being sensitive or insensitive to NBMPR and were designated equilibrative sensitive (*es*) or equilibrative insensitive (*ei*), respectively [16]. The human genes encoding the *es* and *ei* transport proteins have been identified and have been called hENT1 and hENT2, respectively [39, 40]. After the completion of the human genome project, two more hENT genes were identified and designated hENT3 and hENT4 [41, 42]. hENT1/2/3/4 have 456/456/475/530 amino acids, respectively, and, based on detailed studies with hENT1, are believed to contain 11 putative transmembrane domains with an intracellular N-terminus and an extracellular C-terminus [43]. For hENT1 and hENT2, the extracellular loop between transmembrane domains 1 and 2 contains one and two potential glycosylation sites, respectively, which are not required for hENT function [44, 45]. hENT4 in the human heart is glycosylated with two predicted glycosylation sites near the C-terminus [42].

hENT1/2/4 are considered plasma membrane transporters although hENT1 has been observed on mitochondrial membranes and hENT1/2 have been observed on nuclear membranes [46, 47]. hENT3 was originally characterized as an intracellular membrane transporter that partly co-localized with lysosomal markers [41]. Immunofluorescent microscopy analysis of hENT3 in a panel of cell lines found that hENT3 localization varied between cell lines and was sometimes observed on plasma membranes and mitochondrial membranes [48].

1.4.1 *hENT permeants and inhibitors*

Similar to the hCNTs, hENTs have been functionally characterized as recombinant proteins in oocytes as well as yeast or mammalian cells and transport studies have involved the use of radiolabeled permeants in transport assays. Table 1-1 displays hENT transport profiles and K_M values for hENT permeants.

hENT1/2/3 can transport all physiological nucleosides including uridine, thymidine, cytidine, adenosine, guanosine and inosine [41, 49]. When produced in MDCK (Madin-Darby canine kidney) cells or oocytes, hENT4 demonstrated transport of several monoamines (including dopamine and serotonin) and of adenosine but not uridine, suggesting that hENT4 cannot transport pyrimidine nucleosides [42, 50]. Interestingly, hENT3/4 transport is pH-dependent and is optimal at pH 5.5 although it is unclear whether protons are co-transported with nucleosides [41, 42]. hENT1 is capable of transporting many nucleoside analogs, including fludarabine, cladribine, clofarabine, 5-fluoro-2'-deoxyuridine, cytarabine, and gemcitabine [26, 29, 51]. hENT2 transports clofarabine, 5-fluoro-2'-deoxyuridine, gemcitabine and, to a lesser extent, cytarabine [26, 29, 51]. When incubated with yeast cells producing recombinant hENT2, fludarabine and cladribine inhibited [^3H]adenosine uptake with K_i values of 168 μM and 50 μM , respectively, suggesting hENT2 may also transport these nucleoside analogs [29]. hENT3 is capable of transporting a broad range of nucleoside analogs, including fludarabine, cladribine, 5-fluoro-2'-deoxyuridine, and gemcitabine [41, 48]. Clofarabine and cytarabine have not yet been tested as permeants for hENT3. Currently, no studies have addressed whether hENT4 can transport clinical

nucleoside analogs although hENT4 is not expected to be important for uptake of many nucleoside analogs due to its apparent selectivity for adenosine [42].

Several ENT inhibitors have been synthesized and some, including dilazep, dipyridamole and draflazine, have been clinically used as coronary vasodilators and cardioprotective agents [12, 52, 53]. Before the hENTs were cloned, NBMPR was used to identify and characterize hENT1 transport since NBMPR inhibits hENT1 at nanomolar concentrations (K_d value 0.1-10 nM) and hENT1 and hENT2 at high micromolar concentrations [16, 40]. hENT3 and hENT4 transport activities in oocytes are not inhibited when incubated with 1 μ M NBMPR [41, 42]. Dilazep, dipyridamole, and draflazine inhibit both hENT1 and hENT2 although hENT1 is several orders of magnitude more sensitive to inhibition from these inhibitors than hENT2 [40, 49, 54]. High micromolar concentrations of dilazep, dipyridamole, and draflazine are necessary for inhibition of both hENT1 and hENT2 [40, 49, 54]. When produced in oocytes, hENT3 was only partially inhibited when incubated with 10 μ M dilazep or dipyridamole and no inhibition of hENT3 transport was observed at 1 μ M concentrations [41]. Compared to hENT3, hENT4 was more sensitive to inhibition by dilazep and dipyridamole since, when produced in oocytes, hENT4 was partially inhibited by 1 μ M dilazep or dipyridamole [42].

1.4.2 hENT regulation

Regulation of hENTs is relatively poorly understood with all currently published studies focusing on hENT1 and, to a lesser extent, hENT2. However, substantial progress has been made with the characterization of the hENT1

promoter [55]. The hENT1 promoter has one transcriptional initiation site 58 base pairs downstream of the TATA box and the promoter contains consensus sites for various transcription factors including estrogen response element (ERE), MAZ, Sp1, AP-2, myogenin, IRF-2, CREB, and PTF- β [55].

Protein kinase C has an important role in regulating hENT1 activity since its stimulation by PMA in HeLa (cervical carcinoma) and MCF-7 (breast adenocarcinoma) cells increased hENT1-dependent uridine uptake [56]. However, incubation of PMA or lipopolysaccharide with human lymphoma BLS-1 cells caused hENT1 down-regulation which was also dependent on protein kinase C [57]. When human umbilical vein endothelial cells (HUVEC) were exposed to hyperglycemic conditions (25 mM glucose), hENT1 mRNA, cell surface hENT1 protein abundance, and adenosine transport were all reduced [58]. hENT1 downregulation by hyperglycemia was dependent on nitric oxide, the MAP kinase pathway, and protein kinase C since incubation of HUVEC with N(G)-nitro-L-arginine methyl ester (L-NAME, nitric oxide synthase inhibitor), PD-98059 (MEK1/2 inhibitor), or calphostin C (PKC inhibitor) inhibited the hENT1 downregulatory effects of elevated glucose concentrations [59]. Hyperglycemic conditions also increased Sp1 protein abundance which decreased hENT1 promoter activity, suggesting Sp1 may be a negative transcriptional regulator for hENT1 [59]. hENT2 mRNA levels decreased in HUVEC when cells were cultured in hyperglycemic conditions although hENT2 protein levels and hENT2-mediated adenosine transport remained constant [58]. However, hENT2

expression and activity in HUVEC were increased with insulin, suggesting that hENT2 expression and function may fluctuate with diet [60].

Earlier experiments suggest that hENT1 gene expression may be cell cycle dependent since increased NBMPR binding and hENT1 activity were observed during late G1 and S-phase [61, 62]. Inhibitors of deoxynucleotide synthesis increased ENT1 abundance, suggesting that it may be partly regulated by intracellular deoxynucleotide pools [62]. hENT1 and hENT2 contain phosphorylation sites for casein kinase II (CK2) which is important for regulating proliferation [39, 40, 63]. CK2 may inhibit hENT1 expression and/or internalize hENT1 since inhibition of CK2 in human osteosarcoma cells increased NBMPR binding sites per cell as well as hENT1-mediated uptake of 2-chloro-[³H]-adenosine [64]. CK2 inhibition in human osteosarcoma cells also caused a transient decrease in hENT2 mRNA expression [64].

Hypoxia also regulates hNT expression since when HUVEC were cultured in hypoxic conditions, hENT1 mRNA, NBMPR binding sites per cell, and adenosine uptake all significantly decreased [65]. Various cultured human cancer cell lines, including hepatic-derived HepG2 and HepB3, pancreatic-derived PANC-1, and skeletal muscle-derived A673, also exhibited reduced hENT1 and hENT2 expression when cells were cultured in hypoxic conditions, suggesting hypoxia is a significant regulator of hENT expression [38].

1.5 hNT distribution

Analyses of mammalian ENT RNA levels suggest that ENTs are widely distributed throughout most tissues [66]. Northern dot blot analyses of hENT1/2

and hCNT1/2 mRNA in 50 different human tissues indicated that hENT1 was the most ubiquitously expressed hNT since hENT1 mRNA was detectable in all tissues tested with high expression in most tissues except those in the central nervous system which displayed lower hENT1 expression [67]. hENT2 mRNA was found in almost half of the tissues tested with highest expression in skeletal muscle, pituitary gland, fetal kidney, kidney, and small intestine [67]. Northern dot blot analyses of hENT3 in 76 different human tissues suggested that it is widely expressed in many different tissues with the highest levels in placenta, uterus, ovary, spleen, lymph node, and bone marrow [41]. Similarly, RNA dot blot analyses of hENT4 suggest that it is also ubiquitously expressed with highest levels in the brain, heart, intestine, pancreas, skeletal muscle, liver, bone marrow, and lymph node [42].

Although hCNTs can be found in various tissues, expression of their mRNAs is typically less ubiquitous than that of the hENTs [8]. hCNT1 mRNA expression was highest in liver, kidney, small intestine, and medulla oblongata with little to no detectable hCNT1 mRNA in the other tested tissues [67]. hCNT2 mRNA was also mainly expressed in highly specialized tissues such as the stomach, small intestine, colon, and kidney [67]. Compared to hCNT1/2, hCNT3 mRNA was relatively ubiquitous with highest expression in mammary gland, pancreas, bone marrow, trachea followed by modest mRNA levels in various other tissues including liver, lung, placenta, prostate, testis, and heart [17].

Many hNTs are found concentrated on plasma membranes although the exact distribution of hNTs on plasma membranes can differ substantially. In the

small intestine, hNTs are important for the absorption of dietary nucleosides. Immunohistochemical analyses of human small intestine determined that hENT1/2 and hCNT1/2 staining was found on plasma membranes of enterocytes although hCNT1/2 staining was predominantly found on apical membranes compared to that of hENT1/2 staining which was predominantly found on apical and lateral membranes [68]. hCNT1/2 staining was more abundant in enterocytes than crypt cells, suggesting that differentiation of enterocytes in the small intestine may increase hCNT1/2 expression [68]. Interestingly, sodium-dependent guanosine and thymidine transport is greatest near the proximal jejunum and decreases toward the terminal ileum, suggesting that hCNT activity is greatest near the beginning of the small intestine, where levels of dietary nucleosides are expected to be highest, and decreases toward the more distal small intestine regions [69].

hNTs also have important roles with reabsorption of nucleosides in the kidney [70]. In immunohistochemical analyses of human kidney sections hCNT1/2 staining was found on apical membranes of proximal and distal tubules while hENT1/2 staining was found on basolateral membranes of proximal and distal tubules [68]. Subsequent immunohistochemical analyses of human kidney sections showed hENT1 primarily on apical membranes of proximal tubules and apical and basolateral membranes in the thick ascending loops of Henle and collecting ducts [71]. Immunofluorescence microscopy of human kidney sections showed hCNT3 primarily on apical membranes of proximal tubules and thick ascending loops of Henle [71]. Functional analyses of primary human renal

proximal tubule cells from different individuals suggested that nucleoside transport on apical membranes is dominated by hCNT3 with some hENT1 and hENT2 activity while nucleoside transport on basolateral membranes is primarily mediated by hENT2 [72]. Primary human renal proximal tubule cells may also display net basolateral to apical flux of some nucleoside analogs such as 2'-deoxyadenosine [72]. Net nucleoside flux across proximal tubule membranes is dependent on 1) which hNTs are present on apical and basolateral membranes, 2) the transport efficiencies of the hNTs for the nucleoside, and 3) nucleoside concentration differences across the membranes. hCNT3 and hENT2 are considered primarily responsible for the reabsorption of nucleosides across proximal tubules [72].

The liver is important in the metabolism of nucleosides and nucleoside analogs in the blood and hNTs are important for nucleoside transport in hepatocytes. Immunohistochemical staining of human liver sections demonstrated hENT1/2 and hCNT1/2 staining on apical (sinusoidal) membranes, suggesting that these hNTs are important for nucleoside transport into hepatocytes [68, 73]. Immunofluorescence microscopy of cultured primary hepatocytes suggested that hENT1 and hCNT1/2 also localized to canalicular membranes, consistent with the involvement of these hNTs in nucleoside absorption/secretion in the bile canaliculus [73]. hCNTs are involved in nucleoside uptake in hepatocytes while hENT1/2 appear to be involved in nucleoside uptake or secretion.

Although hENT4 was identified by molecular cloning and functional expression relatively recently, several studies have analyzed the protein

distribution of hENT4 in human tissues. Immunoblot analysis of human kidney displayed hENT4 staining and MDCK cells stably transfected with hENT4 cDNA displayed apical localization when cells were cultured on transwell filters [74]. Immunofluorescence analysis of human kidney displayed significant hENT4 staining specifically in podocytes of the glomerulus, suggesting that hENT4 is not involved in tubular reabsorption/secretion of adenosine/monoamines but may have a role in regulating dopamine levels at the glomerulus [75]. Immunofluorescence microscopy of human small intestine displayed apical hENT4 staining in enterocytes at the tips of villi, suggesting involvement of hENT4 in the absorption of adenosine/monoamines in the small intestine [76]. Immunofluorescence analysis of mENT4 in mouse brain displays significant staining throughout the brain with the greatest staining in the forebrain cortex, olfactory tubercle, hippocampus, cerebellum and choroid plexus [77]. Dual-immunofluorescence microscopy using phenotypic markers suggests that mENT4 is produced in neurons but not in astrocytes [77]. The high abundance and wide distribution of mENT4 in the brain suggests that it may be involved in maintaining low levels of extracellular dopamine and serotonin, which are both permeants of mENT4 [77]. Immunofluorescence analysis of rENT4 in the rat heart displayed significant staining in ventricular cardiomyocytes and vascular endothelial cells, suggesting involvement of ENT4 in regulating extracellular adenosine levels in the heart [42].

Studies of endogenous hNT distribution in various tissues have focused on hENT1/2 and hCNT1/2. Less is known about the endogenous distribution of the

relatively recently discovered hCNT3 and hENT3 proteins. Most studies analyzing hCNT3 distribution have focused on the human kidney (see above). Immunoblots of rat tissues found significant staining of rENT3 in the heart, liver, spleen, and kidney [41]. Further analysis of hNT distribution, especially that of hENT3 and hCNT3, is necessary for elucidating the physiological functions of hNTs.

1.6 Anti-cancer nucleoside analogs

Due to the importance of nucleosides in cell metabolism as well as DNA and RNA synthesis, many nucleoside analogs have been tested as anti-cancer drugs and several nucleoside analogs, including fludarabine, cladribine, clofarabine, capecitabine, cytarabine, and gemcitabine, are clinically used in the treatment of cancer [14]. All of these nucleoside analogs require NTs for efficient entry into cells. Once inside cells, nucleoside analogs are phosphorylated by specific nucleoside kinases and the resulting nucleotide analogs exert their toxic effects by enzymatic inhibition and/or incorporation into nucleic acids thereby interfering with transcription and/or genomic replication [14]. The chemical structures of various anti-cancer nucleoside analogs are shown in Figure 1-1B.

Fludarabine

Fludarabine (9- β -D-arabinosyl-2-fluoroadenine) is used in the treatment of chronic lymphocytic leukemia (CLL) and has anti-cancer activity for various other hematological malignances including low-grade non-Hodgkins lymphoma [78]. Due to its poor water solubility, fludarabine is commonly given as an infusion of fludarabine monophosphate [79], which is readily degraded in the

blood as unphosphorylated fludarabine [80]. Fludarabine is a permeant for hENT1, hCNT3, and perhaps hENT2 [17, 81, 82] and upon gaining intracellular access, is phosphorylated by deoxycytidine kinase which is considered the rate-limiting step in fludarabine phosphorylation [83]. Fludarabine monophosphate is subsequently phosphorylated to the diphosphate and triphosphate forms and fludarabine triphosphate is an inhibitor of ribonucleotide reductase with low micromolar IC₅₀ values [84-86]. Ribonucleotide reductase is involved in the conversion of ribonucleoside diphosphates into deoxyribonucleoside diphosphates and its inhibition decreases the pool of deoxyadenosine triphosphate available for incorporation into DNA [87]. Since fludarabine triphosphate is a substrate for DNA polymerase α , β , and γ , its inhibition of ribonucleotide reductase increases its incorporation into DNA due to decreased substrate competition from deoxyadenosine triphosphate [84]. This is an important self-potentiating mechanism of action since incorporation of fludarabine into DNA inhibits DNA elongation [84].

Cladribine

Cladribine (2-chloro-2'-deoxyadenosine) is structurally similar to fludarabine and both compounds have similar mechanisms of action. Cladribine is used in the treatment of CLL and has anti-cancer activity for some other hematological malignances including hairy cell leukemia [88, 89]. Similar to fludarabine, cladribine is a permeant of hENT1, hCNT3, and perhaps hENT2 [17, 29, 90]. Intracellular cladribine is phosphorylated by deoxycytidine kinase and mitochondrial 2'-deoxyguanosine kinase [83, 91]. Cladribine-monophosphate is

subsequently phosphorylated to the diphosphate and triphosphate forms, and cladribine triphosphate is a stronger inhibitor of ribonucleotide reductase than the natural regulator deoxyadenosine triphosphate by approximately two orders of magnitude [92]. DNA polymerase α , β , and γ can incorporate cladribine triphosphate into DNA which inhibits DNA elongation [84], leading to cladribine's anti-proliferative effects.

Clofarabine

Clofarabine [2-chloro-9-(2'-deoxy-2'-fluoro- β -D-arabinofuranosyl) adenine] is a next generation purine nucleoside analog that is structurally similar to cladribine but contains a fluoro group in the 2' arabino configuration which protects the glycosidic bond from phosphorylase activity [93]. Clofarabine has activity for hematological malignancies, including acute leukemias and myelodysplastic syndrome [94], and is currently approved for treating pediatric patients with relapsed or refractory acute lymphoblastic leukemia (ALL) after at least two prior treatment regimens [95, 96]. Based on transport assays with hNT-transfected oocytes, clofarabine is a permeant for hENT1, hENT2, hCNT2, and hCNT3 [29]. Compared to fludarabine and cladribine, clofarabine is a better substrate for deoxycytidine kinase [97] and compared to fludarabine triphosphate, clofarabine triphosphate is a 10-fold more potent inhibitor of ribonucleotide reductase [98]. Unlike fludarabine triphosphate and cladribine triphosphate, clofarabine triphosphate selectively inhibits DNA polymerase α at low micromolar concentrations [98] and like the other two nucleoside analogs, its incorporation into DNA causes termination of DNA elongation [99]. Unlike

fludarabine, clofarabine directly disrupts mitochondrial integrity which leads to the release of pro-apoptotic factors including cytochrome C and apoptosis inducing factor [100].

Capecitabine

Capecitabine (5'-deoxy-5-N-[(pentoxycarbonyl)]-cytidine) is a cytidine nucleoside analog that is used in the treatment of locally advanced or metastatic breast and colorectal cancers [101]. Designed as an orally available pro-drug of 5-fluorouracil, capecitabine is metabolized to 5-fluorouracil in three enzymatic steps [102]. When taken orally, capecitabine is absorbed in the gastrointestinal tract and transported to the liver where it is hydrolyzed to 5'-deoxy-5-fluorocytidine by carboxylesterase. Cytidine deaminase then converts 5'-deoxy-5-fluorocytidine to 5'-deoxy-5-fluorouridine, which is a permeant for hENT1 since incubation of hENT1 inhibitor NBMPR with cultured MDA-MB-435s breast cancer cells increased 5'-deoxy-5-fluorouridine resistance [103]. hCNT1 also transports 5'-deoxy-5-fluorouridine [104]. hCNT3 has relatively high affinity for 5'-deoxy-5-fluorouridine, suggesting that it may also be capable of transporting this capecitabine intermediate [105]. Thymidine phosphorylase, an enzyme that is upregulated in various cancers [106, 107], converts 5'-deoxy-5-fluorouridine into 5-fluorouracil, which is subsequently converted into other toxic metabolites, including 1) 5-fluorouridine monophosphate, which inhibits thymidylate synthase and reduces levels of phosphorylated thymidine needed for DNA replication, 2) 5-fluorouridine triphosphate, which is incorporated into RNA and interferes with

RNA processing, and 3) 5-fluoro-2'-deoxyuridine triphosphate, which is incorporated into DNA and eventually causes DNA strand breaks [108].

Cytarabine

Cytarabine (1- β -D-arabinofuranosylcytosine) is a cytidine nucleoside analog that has been extensively used in the treatment of acute myeloid leukemia (AML) [109] and has shown activity for other hematological malignances, including CML [110] and refractory non-Hodgkin's lymphoma [111]. hENT1, hENT2, and hCNT1 are capable of cytarabine transport although hENT1 is considered the primary nucleoside transporter involved in cytarabine uptake [51]. All three hCNTs have low affinities for cytarabine and are unlikely to be important for cytarabine transport [51]. Upon cell entry, cytarabine is phosphorylated by deoxycytidine kinase [112] and subsequently phosphorylated to cytarabine triphosphate, which may be incorporated into DNA and cause strand breaks through stabilization of topoisomerase 1-DNA cleavage complexes [113]. In resting B-CLL cells, cytarabine triphosphate may also exert toxicity through interference with RNA synthesis [114].

Gemcitabine

Gemcitabine (2',2'-difluoro-2'-deoxycytidine) is a cytidine nucleoside analog used in the treatment of pancreatic, ovarian, metastatic breast, and non-small cell lung cancers [115]. hENT1, hENT2, hCNT1, and hCNT3 are capable of gemcitabine transport [26, 116] and upon entering cells, gemcitabine is phosphorylated by deoxycytidine kinase which has a 2-3 fold greater affinity for gemcitabine than for cytarabine [117]. Gemcitabine is subsequently

phosphorylated to gemcitabine diphosphate, which is a potent inhibitor of ribonucleotide reductase [118]. Inhibition of ribonucleotide reductase decreases deoxycytidine triphosphate levels thereby increasing gemcitabine incorporation into DNA [118]. Incorporation of gemcitabine immediately 3' of topoisomerase 1 cleavage sites on the non-scissile strand can lead to DNA strand breaks by stabilization of topoisomerase 1-DNA cleavage complexes [119]. Gemcitabine triphosphate may also be incorporated into RNA resulting in toxicity to non-proliferating cells [120].

1.6.1 Nucleoside transporters and nucleoside drug response

As previously stated, most anti-cancer nucleoside analog drugs are hydrophilic molecules and require hNTs for efficient cellular influx [14]. These drugs require intracellular access to exert their toxicities and the absence of hNTs in cancer cells generally confers resistance to nucleoside drugs [14]. As described in detail below, various pre-clinical and clinical studies have established the importance of hNTs, especially that of hENT1, in nucleoside analog anti-cancer therapies [14].

Pre-clinical studies

Several in vitro studies have observed correlations between nucleoside analog toxicities and either hNT mRNA levels or protein abundance in various cancer cells [121-125]. For example, hENT2 immunostaining in patient-derived CLL cells displayed a positive correlation with fludarabine *ex vivo* sensitivity ($P = 0.006$) [123]. In leukemic blasts from pediatric AML patients, hENT1 mRNA levels positively correlated with cytarabine ($P = 0.001$), cladribine ($P = 0.04$), and

gemcitabine ($P = 0.02$) *ex vivo* sensitivities [122]. In myeloblasts from AML patients, there was a positive correlation between hENT1 abundance, as measured by binding of the hENT1 inhibitor SAENTA fluorescein, and *ex vivo* cytarabine sensitivity ($P < 0.03$) [121]. A positive correlation was observed between hENT1 mRNA levels and cytarabine *ex vivo* sensitivity ($P = 0.006$) in mixed lineage leukemia (MLL) gene-rearranged infant ALL cells [125]. In a study with several pancreatic and biliary tract carcinoma cell lines, hENT1 mRNA levels positively correlated with gemcitabine toxicity ($P = 0.037$), suggesting that hNTs are also important for nucleoside analog treatment of solid tumors [124].

It is possible to assess the involvement of hENTs in nucleoside analog toxicity by incubating cancer cells with or without hENT inhibitors and monitoring changes in nucleoside analog toxicity. Resistance to cytarabine toxicity in cultured acute leukemia cell lines, derived from either AML or ALL patients, significantly increased (2 to 40-fold) as NBMPR concentrations were increased [126]. MDA-MB-431 breast cancer cells displayed several-fold increased resistance to 5'-deoxy-5-fluorouridine (metabolite of capecitabine and 5-fluorouracil) in the presence of 100 nM NBMPR compared to that of cells in the absence of NBMPR, suggesting that hENT1 activity in breast cancer may influence 5'-deoxy-5-fluorouridine toxicity [103]. Gemcitabine resistance in cultured K562, CEM, or HeLa cell lines (derived from erythroid leukemia, lymphoblastic leukemia, and cervical cancer, respectively) was increased 39 to over 1800-fold when cells were incubated with 10 μ M dipyridamole (hENT1/2 inhibitor), suggesting that hENT1 and hENT2 were important for gemcitabine

toxicity in these cell lines [127]. However, colon cancer derived CaCo-2 cells, which possess hENT1/2 and hCNT3 transport activities, did not display significantly increased gemcitabine resistance when incubated with 10 μ M dipyridamole, suggesting that the combined nucleoside transport activities of the hNTs capable of transporting gemcitabine (i.e., hENT1/2 and hCNT1/3) will influence gemcitabine resistance in cancer cells [127].

Several *in vitro* studies have introduced hNTs in cancer cells by transfection and analyzed changes in nucleoside analog toxicities [29, 128-130]. Transfection of cDNAs encoding hENT1, hENT2, hCNT1, or hCNT2 in transport-deficient CEM/ara-C cells increased CEM/ara-C sensitivity to fludarabine, cladribine, and clofarabine, although some hNTs, such as hENT1, displayed a greater drug sensitizing effect than the other hNTs for the nucleoside analogs tested [29]. Transfection of cDNAs encoding hENT1 or hCNT1 in MDCK cells increased gemcitabine sensitivity by several-fold when compared to mock-transfected MDCK cells [130]. Transfection of pancreatic cancer derived NP-9 cells with cDNA encoding hCNT1 increased cell sensitivity to gemcitabine by almost three-fold [128]. Furthermore, introduction of hENT1 into pancreatic cancer derived NP-9 xenograft tumors using a hENT1 over-expressing adenovirus caused an increase in tumor sensitivity to gemcitabine as observed by reduced tumor growth rates [129]. Taken together, the pre-clinical data suggests nucleoside analog toxicity is dependant on the activities of hNTs capable of transporting nucleoside analogs.

Clinical studies

Most clinical studies that have analyzed tumor hNT levels and response to nucleoside analog treatment have focused on hENT1 due to the transporter's broad transport profile and abundance in cancer cells (see section 1.4). A retrospective study with 123 AML patients who received cytarabine-containing treatment regimens found that deficiency of hENT1 expression, determined by mRNA levels, correlated with shorter disease-free survival [131]. In another study with 24 non-small cell lung cancer patients that received gemcitabine-containing chemotherapy, a lack of hENT1 immunohistochemical staining in tumor specimens correlated with a lack of treatment response (i.e., stable disease or progressive disease) [132].

Not all clinical studies have found a positive correlation between hNT expression and treatment response. Surprisingly, increased mRNA expression of hCNT3 in CLL cells was associated with a greater risk of disease progression in CLL patients receiving fludarabine therapy [133]. A similar study analyzing hCNT3 protein levels with immunohistochemistry in CLL cells obtained from patients receiving fludarabine treatment provided similar results [134], suggesting hCNT3 may have increased CLL cell resistance to fludarabine. It is not fully understood why hCNT3, which is capable of fludarabine transport [17], could potentially cause fludarabine resistance in CLL cells but it may be due to increased cellular accumulation of physiological nucleosides which may compete with fludarabine for downstream cellular events necessary for fludarabine toxicity (e.g., phosphorylation and nucleic acid incorporation). hCNT3 expression in CLL cells may also be regulated by other genes that influence fludarabine resistance.

Further research is warranted to determine why hCNT3 expression is linked to fludarabine resistance in CLL.

Several clinical studies have analyzed whether hENT1 and/or hCNT3 mRNA or protein levels are prognostic or predictive markers of gemcitabine response in pancreatic cancer [135-138]. A retrospective study determined that pancreatic cancer patients with less than 90% of tumor cells positive for hENT1 staining, as determined by immunohistochemistry, who were subsequently treated with gemcitabine displayed significantly reduced overall survival compared to pancreatic cancer patients with greater levels of hENT1 staining (median survival: 13 vs 4 months, $P = 0.01$), suggesting that hENT1 is a prognostic marker of gemcitabine response in pancreatic cancer [138]. A subsequent retrospective study determined that hENT1 mRNA levels in pancreatic tumors positively correlated with overall survival in pancreatic cancer patients who subsequently received gemcitabine therapy [136]. A larger prospective study determined that pancreatic cancer patients with less than 50% of tumor cells positive for hENT1 using immunohistochemistry staining who were subsequently treated with gemcitabine displayed significantly reduced overall survival and disease-free survival compared to pancreatic cancer patients with greater levels of tumor hENT1 staining, suggesting that hENT1 is a predictive marker for gemcitabine response in pancreatic cancer [135]. Another similar retrospective study provided similar results and concluded that hENT1 and hCNT3 are both prognostic markers for gemcitabine response in pancreatic cancer [137]. Interestingly, pancreatic cancer patients with high elevated levels of both markers (hENT1 and

hCNT3) displayed significantly increased overall survival (median: 94.8 months) compared to patients with elevated levels of only one marker (median survival: 18.7 months) or low levels of both markers (median survival: 12.2 months) [137]. With the exception of hCNT3 in CLL, the clinical data suggest that hNTs may be prognostic/predictive markers of nucleoside analog response in cancer.

1.7 Diagnostic nucleoside analogs

Nucleoside analogs have not only been used as therapeutic agents but also as diagnostic agents. If a positron emitting radionuclide (e.g. ^{11}C , ^{13}N , ^{15}O , or ^{18}F ; Table 1-2) is present in a nucleoside analog, the radioactive nucleoside analog (radiotracer) is capable of being detected non-invasively using positron emission tomography (PET). Many nucleoside analogs have been synthesized and radiolabeled with a positron emitting radionuclide for use in PET imaging, including radiotracers used for imaging adenosine receptors [139-141], hypoxia [142, 143], deoxycytidine kinase activity [144], and proliferation [145]. The chemical structures for various diagnostic nucleoside analogs are shown in Figure 1-1C. The following review will focus on nucleoside based PET tracers developed for oncological purposes.

1.7.1 Positron Emission Tomography (PET)

Positron emission tomography (PET) is a non-invasive imaging modality that allows the visualization of biological processes within a subject (See [146, 147] for a reviews on PET). Unlike other commonly used imaging modalities, including magnetic resonance imaging (MRI), computed tomography (CT), and ultrasound, PET requires preparation of short-lived radiotracers that are injected

inside subjects. The physical locations of these radiotracers can be determined with PET, which allows analysis of various biological processes depending on the pharmacokinetics of the radiotracer in the subject's body.

PET Physics

Positron-emitting radionuclides are unstable isotopes that usually have fewer neutrons than protons. These radionuclides can be artificially produced by particle collisions using charged particle accelerators [148] and chemically incorporated into molecules of interest typically using automated chemical synthesis apparatuses. When injected into subjects, the radiotracers have the same pharmacokinetics as non-radioactive molecules of the same structures. When the radionuclides emit positrons, which are positively charged electrons, the positrons quickly lose kinetic energy and eventually collide with electrons. For each collision, both particles are annihilated, since matter (electron) and anti-matter (positron) cannot co-exist together, and two gamma photons are created with 511 keV energy. These gamma photons travel at approximately 180 degrees from each other and can be detected using various detector systems [149].

Since two gamma photons are produced from each positron-electron annihilation event, coincidence detection is used to determine the location of annihilation events. If two detectors 180 degrees from each other detect photons of appropriate energy within a specific coincidence time frame (usually several nanoseconds), these detection events signify a true annihilation event between the detectors (Figure 1-2A). Scattered coincidence events may also occur when one or both photons from an annihilation event are scattered before reaching the detector

(Figure 1-2B). Annihilation events from scattered coincidence events are recorded but will usually incorrectly place annihilation events thus reducing image quality. Finally, random coincidence events may happen when two opposite detectors are activated within the coincidence time frame by photons originating from different annihilation events (Figure 1-2C). Random coincidence events occur uniformly throughout the detectors and the majority of these events may be subtracted before image reconstruction.

PET Image Reconstruction

During image acquisition, the detection events are stored in a computer that can be subsequently analyzed to reconstruct a three-dimensional image using specialized software. The software may analyze the data in different modes including 2D or 3D acquisition mode which determines the detection events that will be used for image reconstruction [150]. The 2D acquisition mode only accepts detection events from detectors that are in the same ring or nearby rings of detectors, allowing faster image reconstruction, smaller data sizes, and reduced detection of scatter events. The 3D acquisition mode accepts coincidence detection events from detectors in many different detector rings, allowing a greater number of accepted coincidence detection events and greater sensitivity although image reconstruction is slower, data sizes are larger, and more scatter events are recorded.

Before image reconstruction, PET imaging software is capable of correcting the data for several potential image altering issues. Different detectors will have different efficiencies for detecting photons. These differences in

efficiencies may be corrected by a normalization file produced by scanning a known uniform radioactive source and comparing the scanned results with the theoretical results. PET imaging software may also correct for signal attenuation. Photons may be absorbed within the body and this prevents the detection of annihilation events. Photons produced in deep tissues have a greater chance of being absorbed causing increased signal reduction in deep tissues. Signal attenuation may be corrected by an attenuation file produced by transmission or transmissionless based methods [151]. Scatter events can also reduce image quality and several computational algorithms have been created to compensate for these scatter events [152].

Each reconstructed image requires a specific acquisition time frame where the sum of all detection events within the time frame is used for image reconstruction. Static imaging produces one image by summing all the detection events over the entire imaging session while dynamic imaging create several images by allocating specific acquisition time frames for specific images (e.g., image 1, 0-5 min; image 2, 5-10 min; etc). Dynamic imaging allows kinetic analysis and rate constants of radiotracer uptake can be calculated.

Upon reconstruction of the PET image, two-dimensional coronal, sagittal, or transverse images of the subject may be viewed and analyzed. The two-dimensional images may be reconstructed into a three-dimensional image and two or three dimensional regions of interest may be selected and analyzed for radioactivity. The information provided by PET is dependent on the radiotracer used and many PET radiotracers have been synthesized in the past few decades.

1.7.2 Hypoxia PET tracers

Tumor hypoxia commonly occurs heterogeneously in advanced tumors and is a poor prognostic marker for many cancers [153-155]. In tumors, hypoxia not only increases the malignant phenotype but also provides resistance to chemotherapy and radiotherapy [156, 157]. Although oxygen sensing electrodes may be used to detect oxygen levels in tissues, they are not routinely used clinically due to their invasiveness. The PET radiotracer [^{18}F]fluoromisonidazole ([^{18}F]FMISO) was developed to monitor hypoxia non-invasively [158]. [^{18}F]FMISO contains a 2-nitroimidazole ring that, when under hypoxic conditions, undergoes reductive metabolism and can react and bind to cellular macromolecules (e.g., proteins, lipids, nucleic acids) [159]. [^{18}F]FMISO accumulation in cells is dependent on oxygen levels although [^{18}F]FMISO displays relative high retention within various organs, including the brain and liver due to its non-specific lipophilic uptake [143, 158].

Another PET radiotracer, 1- α -D-(5-deoxy-5-[^{18}F]fluoroarabinofuranosyl)-2-nitroimidazole ([^{18}F]FAZA), was synthesized for imaging hypoxia [143]. [^{18}F]FAZA contains the 2-nitroimidazole ring attached to a modified ribose group. [^{18}F]FAZA accumulation in Walker 256 rat tumors was dependent on oxygen levels and [^{18}F]FAZA was rapidly cleared from the body via the renal system [143]. The [^{18}F]FAZA analog iodoazomycin arabinoside ([^{124}I]IAZA) was also synthesized as a hypoxic radiotracer with the longer half-life radionuclide ^{124}I and found to display reduced tumor to background ratios in A431 xenograft tumors compared to [^{18}F]FAZA [142]. An initial clinical study with [^{18}F]FAZA

has demonstrated acceptable tumor to background ratios for squamous cell carcinomas of the head and neck, small-cell and non-small cell lung cancers, malignant lymphomas, and high grade gliomas with no patient side effects [160], suggesting that ^{18}F -FAZA may be clinically useful for imaging hypoxia.

1.7.3 Deoxycytidine kinase PET tracer

Deoxycytidine kinase is involved in the phosphorylation of various anti-cancer nucleoside analogs, including fludarabine, cladribine, clofarabine, cytarabine, and gemcitabine (see section 1.6 for a review of anti-cancer nucleoside analogs). Decreased deoxycytidine kinase activity in ovarian carcinoma cell line A2780 cells correlated with both *in vitro* and *in vivo* gemcitabine resistance since deoxycytidine kinase is necessary for gemcitabine activation [161]. The gemcitabine analog radiotracer 1-(2'-deoxy-2'-fluoroarabinofuranosyl) cytosine (^{18}F)-FAC was developed to non-invasively monitor deoxycytidine kinase activity using PET [144]. ^{18}F -FAC was a slightly better substrate for deoxycytidine kinase than gemcitabine and uptake of both ^{18}F -FAC and gemcitabine was similar in a variety of cultured L1210 murine leukemic cell lines with different levels of deoxycytidine kinase [144]. L1210 tumors with low levels of deoxycytidine kinase in severely compromised immunodeficient mice (SCID) mice were relatively resistant to gemcitabine and displayed significantly lower ^{18}F -FAC uptake compared to that of L1210 tumors with 'normal' deoxycytidine kinase levels [144], suggesting that ^{18}F -FAC may be clinically useful in identifying gemcitabine resistant tumors.

1.7.4 Proliferation PET tracers

Tumor proliferation is an important prognostic marker in various cancers and is commonly analyzed in *ex vivo* tumor samples [162-164]. Tumor cell proliferation has been analyzed by various methods including [³H]thymidine DNA incorporation assays [165], bromodeoxyuridine staining [166], and Ki-67 staining [167], although these methods are of limited use for non-resectable or metastasizing cancers.

Most minimally non-invasive methods for analyzing cell proliferation have focused on the development of radiotracers for PET [145]. Most PET proliferation radiotracers are based on thymidine since thymidine is the only physiological nucleoside incorporated into DNA but not into RNA. Thymidine is transported across plasma membranes by human nucleoside transporters (hENT1, hENT2, hCNT1, and hCNT3) and is metabolized by a series of enzymes (Figure 1-3). The cytosolic enzyme thymidine kinase 1 (TK1), which is up-regulated during late G1 and S phase [168], phosphorylates thymidine, thereby “trapping” it inside cells since thymidine nucleotides do not readily diffuse through biological membranes and are not permeants of human nucleoside transporters (or other known transporters). The constitutively expressed mitochondrial thymidine kinase 2 also phosphorylates thymidine, which allows moderate thymidine uptake in non-proliferating cells [168].

Studies analyzing [³H]thymidine uptake in rodents showed specific [³H]thymidine uptake and retention in proliferating tissues such as spleen, intestines, thymus, and various tumors types, including sarcomas, lymphomas, hepatomas, and osteosarcomas [169, 170], suggesting that a positron emitting

form of thymidine would be useful for non-invasive imaging of proliferation. [¹¹C]Thymidine was synthesized and used in clinical PET imaging studies on patients with gliomas [171, 172] and head and neck tumors [173]. [¹¹C]Thymidine PET image quality has been hampered by rapid radiotracer catabolism since the majority of [¹¹C]thymidine is converted to [¹¹C]CO₂ within 10 minutes of radiotracer injection [174]. Elaborate modeling algorithms have been used to account for thymidine metabolites in [¹¹C]thymidine PET images and these mathematical models require many assumptions that may or may not be true for each patient [145]. The rapid catabolism of thymidine in the human body, coupled with the short half-life of [¹¹C], has increased interest in synthesizing thymidine analogs that are resistant to catabolism as PET radiotracers for imaging proliferation.

When the thymidine analog 5-fluoro-1-(2'-fluoro-2'-deoxy-β-D-ribofuranosyl)-uracil (FFUdR) was synthesized, radiolabeled, and injected in Lewis Lung tumor bearing BDF₁ mice, the tracer displayed relatively high uptake in the tumor and spleen after 1 hour [175]. The 2'-fluoro group of FFUdR provided resistance to catabolism since the majority of the tracer in the urine was unmodified eight hours after tracer injection [175]. When injected into EMT6 tumor-bearing mice, [³H]FFUdR displayed tumor to blood ratios of approximately two [176], suggesting that FFUdR PET would allow tumor visualization, although with relatively low contrast.

Another 2'-fluorothymidine analog, 1-(2'-Deoxy-2'-fluoro-1-β-D-arabinofuranosyl)-thymine (FMAU), has been tested as a proliferation radiotracer

[177]. Incubation of [^{14}C]FMAU with cultured Dunning R3327 rat prostate cells resulted in [^{14}C]FMAU incorporation into DNA and cellular accumulation of [^{14}C]FMAU was dependent on cell line growth rates [178]. In rodents, [^{14}C]FMAU preferentially accumulated in the small intestine and bone marrow with almost no [^{14}C]FMAU metabolism one hour after injection [179]. Initial clinical [^{18}F]FMAU PET studies using patients with various cancers (brain, prostate, colorectal, lung, and breast) determined that [^{18}F]FMAU uptake was high in liver, kidney, and spleen and most tumors were visible with mean standardized uptake values ranging from 0.24-6.31 [180]. Unfortunately, FMAU is preferentially phosphorylated by the constitutively expressed mitochondrial thymidine kinase 2 [181] thus reducing the ability of FMAU to accumulate specifically in proliferating cells.

Bromodeoxyuridine has traditionally been used with immunohistochemical staining to determine proliferation [182]. Although attempts have been made to use [^{76}Br]bromodeoxyuridine as a PET radiotracer for proliferation, the majority of the radionuclide dissociates as free [^{76}Br]bromide relatively soon after radiotracer injection in pigs [183]. 1-(2'-Deoxy-2'-fluoro- β -D-arabinofuranosyl)-5-bromouracil (FBAU) was synthesized as a catabolic resistant bromodeoxyuridine analog and, when injected into rats, [^{76}Br]FBAU displayed selective accumulation in proliferating tissues (e.g., spleen and intestine) with significant [^{76}Br]FBAU incorporation within the DNA of these tissue [184]. Analysis of urine two hours after [^{76}Br]FBAU injection demonstrated that the majority of the tracer was unmodified, suggesting that the

2'-fluoro group provided resistance to tracer catabolism [184]. [¹⁸F]FBAU has also been synthesized and used to image dogs with similar results [185]. Compared to [³H]FMAU, [³H]FBAU displayed greater uptake and DNA incorporation in cultured U-937 and MOLT-4 cells (lymphoma and ALL derived cell lines, respectively) [185], suggesting that FBAU may be a better proliferation tracer than FMAU.

When tested, the proliferation PET tracers described above have not demonstrated selectivity for TK1 and some are preferentially phosphorylated by the constitutively expressed thymidine kinase 2, causing significant tracer accumulation in non-proliferating tissues [145, 186]. Currently, the only thymidine analog used for proliferation imaging that has demonstrated selective phosphorylation by thymidine kinase 1 is 3'-deoxy-3'-fluorothymidine (FLT).

1.8 3'-Deoxy-3'-fluorothymidine (FLT)

Before FLT was tested as a proliferation tracer, it was tested as an anti-viral agent due to its potent inhibition of human immunodeficiency virus (HIV) reverse transcriptase and HIV replication [187]. Clinical trials with FLT (alovudine) were halted prematurely due to excessive hepatic toxicity causing the death of two patients [188, 189]. [¹⁸F]FLT was later tested as a PET proliferation tracer and demonstrated significant uptake in the liver, bone marrow, and the tumor of a non-small cell lung cancer patient [190]. Since FLT concentrations used in PET imaging are approximately 0.0003-fold those causing any form of toxicity in the clinical trials with FLT, it may be safely used in PET [191]. When comparing all of the thymidine analog PET proliferation tracers, FLT has been the

most extensively studied due to its relative high tumor to background uptake ratios and its selective phosphorylation by thymidine kinase 1 [188].

1.8.1 FLT pharmacology

FLT is chemically identical to thymidine except that a 3'-fluoro group is substituted for the 3'-hydroxyl group. When FLT is injected in humans, the majority of the tracer is unmodified in the blood 1 hour after tracer injection, suggesting that the 3'-fluoro group prevents tracer catabolism by thymidine phosphorylase [192]. The primary metabolite of FLT is FLT-glucuronide, which likely explains the relatively high liver uptake of FLT since glucuronidation occurs in the liver [190, 193]. FLT and FLT-glucuronide are rapidly excreted through the renal system, allowing high contrast FLT PET images within 1 hour of tracer injection [190, 193]. Negative and positive FLT PET images of two human cancer patients are displayed in Figure 1-4.

At the time the work described in this thesis was undertaken, FLT was considered a permeant of hENT1 since the majority of FLT uptake in cultured HL-60 cells was inhibited by incubating cells with the hENT1 inhibitor NBMPR-phosphate (NBMPR-P) [194]. It was not known whether FLT was a permeant for the other hNTs or how well each hNT could transport FLT.

Upon gaining intracellular access, FLT is selectively phosphorylated by TK1; the 3'-fluoro group prevents phosphorylation of FLT by the mitochondrial thymidine kinase 2 [195]. FLT-monophosphate is then trapped inside cells since it does not diffuse readily through plasma membranes and the nucleoside transporters do not accept nucleotides as permeants. Similar to other nucleoside-

monophosphates, FLT-monophosphate may be subsequently phosphorylated to the diphosphate and triphosphate forms [196]. When FLT was incubated in cultured A549 cells, FLT-monophosphate and FLT-triphosphate levels were relatively high compared to FLT-diphosphate, suggesting that the rate limiting phosphorylation step in FLT metabolism is thymidylate kinase [196]. Since FLT lacks a 3'-hydroxyl group, FLT-triphosphate acts as a DNA chain terminator which limits FLT incorporation into DNA [197]. When incubated with cultured CEM cells, FLT caused significant DNA fragmentation and apoptosis at concentrations that were relatively non-toxic for the structurally similar anti-viral 3'-deoxy-3'-azidothymidine (AZT, zidovudine), which likely explains the high hematological toxicities that were clinically observed with FLT [189, 197].

When 22 different cultured cancer cell lines were incubated with [³H]FLT for one hour, FLT uptake correlated with thymidine uptake ($r = 0.88$, $P < 0.0001$) and percent S-phase fraction ($r = 0.76$, $P < 0.0001$), suggesting that FLT uptake is dependent on cellular proliferation [198]. FLT uptake in mouse lymphoma L5178Y xenograft tumors correlated with ATP and TK1 protein levels ($r = 0.86$, $P = 0.003$), further suggesting that FLT uptake is dependent on the cell cycle regulated TK1 [199].

1.8.2 Clinical [¹⁸F]FLT PET

[¹⁸F]FLT PET clinical studies have been performed on patients with various cancers, including lung, breast, brain and pancreatic cancers, as well as lymphomas, soft tissue sarcomas and melanomas [191]. Earlier clinical studies have focused on validating [¹⁸F]FLT PET for tumor visualization as well as

analyzing correlations between [¹⁸F]FLT uptake and tumor proliferation while more recent clinical trials have explored whether or not [¹⁸F]FLT PET is useful for predicting tumor response to therapy.

[¹⁸F]FLT PET in Lung Cancer

The first multi-patient clinical study using [¹⁸F]FLT PET was performed on non-small cell lung cancer (NSCLC) patients [200]. Two patients had benign lesions and [¹⁸F]FLT uptake in these lesions was significantly smaller than in the nine other patients with malignant disease. Correlations were demonstrated between both average and maximum [¹⁸F]FLT standardized uptake values (SUV) in the lesions and the Ki-67 scores ($P < 0.005$), suggesting that [¹⁸F]FLT PET was useful for distinguishing between benign and malignant lung tumors [200]. Other larger studies of [¹⁸F]FLT PET with lung cancer patients have reported similar results, supporting the potential utility of using [¹⁸F]FLT PET for monitoring lung tumor proliferation. A study by Buck et al. [201] compared [¹⁸F]FLT PET with [¹⁸F]FDG PET in 18 lung patients and determined that mean [¹⁸F]FLT uptake was only 41% of that of mean [¹⁸F]FDG uptake. [¹⁸F]FLT PET and [¹⁸F]FDG PET displayed, respectively, 83% and 94% sensitivity (percent of cancers that were detected) and 100% and 81% specificity (percent of detected lesions that were true cancers), suggesting that [¹⁸F]FDG PET allows greater lung cancer detection but more false positives compared to [¹⁸F]FLT PET [201]. [¹⁸F]FLT PET displayed a stronger correlation to Ki-67 scores ($r = 0.92$, $P < 0.0001$) than [¹⁸F]FDG PET ($r = 0.59$, $P < 0.001$), suggesting that [¹⁸F]FLT PET is more specific than [¹⁸F]FDG PET for imaging proliferating tumors [201]. Other studies

comparing [¹⁸F]FLT PET and [¹⁸F]FDG PET in patients with lung cancer have demonstrated similar results [202-204].

[¹⁸F]FLT PET has also been studied for its ability to predict lung tumor response to different anti-cancer therapies [205, 206]. In a study by Sohn et al. [206], patients with advanced lung adenocarcinomas underwent serial [¹⁸F]FLT PET scans before and seven days after receiving gefitinib and response was determined six weeks after treatment using CT scans. [¹⁸F]FLT maximum SUV significantly differed for responding ($64 \pm 15\%$ of baseline) and non-responding patients ($110 \pm 20\%$ of baseline) and, when using a greater than 10.4 % decrease in [¹⁸F]FLT maximum SUV as criterion for differentiating between gefitinib responders and non-responders, the sensitivity of [¹⁸F]FLT PET for predicting response to gefitinib treatment was 92.9% [206]. In another study by Everitt et al. [205], five patients with locally advanced NSCLC received serial [¹⁸F]FLT PET scans during chemo (carboplatin and paclitaxel)-radiotherapy. Eight of nine [¹⁸F]FLT PET scans displayed a mean of 58% [¹⁸F]FLT uptake in treated tumors compared to that of non-treated tumors and irradiated bone marrow displayed approximately 50% reduction in [¹⁸F]FLT uptake even with one radiotherapy treatment of 2 Gy radiation [205]. It remains to be determined whether [¹⁸F]FLT PET or [¹⁸F]FDG PET is more accurate for determining lung cancer response to anti-cancer therapy since no clinical studies have directly compared the two tracers for measuring tumor response.

[¹⁸F]FLT PET in Breast Cancer

A pilot study in which 12 breast cancer patients were imaged with [¹⁸F]FLT PET demonstrated focally increased [¹⁸F]FLT uptake in 13 of 14 primary tumors (93% sensitivity) with seven of eight lymph node metastases also being detectable with [¹⁸F]FLT PET [207]. Another [¹⁸F]FLT PET study performed on 15 breast cancer patients determined that [¹⁸F]FLT SUV correlated with Ki-67 scores ($r = 0.79$) and that the correlation became stronger when comparing Ki-67 scores to advanced kinetic parameters of [¹⁸F]FLT retention that had been corrected for radiotracer metabolites ($r = 0.92-0.94$) [208].

Two clinical studies analyzed whether or not [¹⁸F]FLT PET could be used to predict treatment response in breast cancer patients [209, 210]. A study by Pio et al. [210] performed serial [¹⁸F]FLT PET scans in 14 breast cancer patients who were treated with hormonal therapy or chemotherapy. Changes in average [¹⁸F]FLT SUV correlated with changes in CA27.29 breast tumor marker levels ($r = 0.79$, $P = 0.001$) after the first course of treatment. Changes in average [¹⁸F]FLT SUV after one course of treatment also correlated with changes in tumor size (measured by CT scans) after the entire treatment regimen ($r = 0.74$, $P = 0.01$) [210]. A study by Kenny et al. [209] performed [¹⁸F]FLT PET on 13 breast cancer patients prior to and one week after chemotherapy (5-fluorouracil, epirubicin, cyclophosphamide) and clinical response was determined 60 days after therapy. A significant difference was observed between responders (complete or partial response) and non-responders (stable disease) with respect to changes in [¹⁸F]FLT SUV one week after treatment ($P = 0.022$) [209]. Similar to the lung cancer studies described above, [¹⁸F]FLT PET appears promising for predicting breast

cancer response to therapy although further studies are necessary to compare [¹⁸F]FLT PET and [¹⁸F]FDG PET for monitoring treatment response.

[¹⁸F]FLT PET in Brain Cancer

A study by Chen et al. [211] compared [¹⁸F]FLT PET and [¹⁸F]FDG PET on 25 patients with brain tumors. Increased focal uptake of [¹⁸F]FLT occurred in all high grade (Grade 3 and 4) tumors although [¹⁸F]FLT uptake in lower grade tumors was significantly lower and many of these tumors were not detectable with [¹⁸F]FLT PET. Although [¹⁸F]FLT maximum SUVs were significantly lower than those of [¹⁸F]FDG, [¹⁸F]FLT displayed greater tumor to background ratios due to greater non-specific [¹⁸F]FDG uptake in the brain, allowing more brain tumors to be visualized by [¹⁸F]FLT PET than by [¹⁸F]FDG PET [211]. Stronger correlations were observed between Ki-67 score and maximum tracer SUV with [¹⁸F]FLT ($r = 0.84$, $P < 0.0001$) than with [¹⁸F]FDG ($r = 0.51$, $P = 0.07$), suggesting that [¹⁸F]FLT PET allows better visualization of tumor proliferation than [¹⁸F]FDG PET [211]. Compared to [¹⁸F]FDG PET, [¹⁸F]FLT PET also provided stronger correlations with progression-free survival ($P = 0.03$, $P = 0.0005$, respectively) and probability of survival ($P = 0.06$, $P = 0.001$, respectively) [211]. Another study by Choi et al. [212] provided similar results when comparing [¹⁸F]FLT PET and [¹⁸F]FDG PET with brain tumors. Brain lesions with disrupted blood brain barrier (BBB) function display significantly higher levels of FLT uptake that is dominated by FLT transport to the lesion, suggesting that BBB function should be known before grading brain tumors with [¹⁸F]FLT PET [213, 214]. When comparing [¹⁸F]FLT PET and [¹¹C]methionine

PET in brain tumors, the two tracers provided similar sensitivities for detecting high grade brain tumors although [¹⁸F]FLT PET provided higher tumor to non-tumor ratios for high grade tumors and stronger correlations with Ki-67 scores [215, 216].

The predictive value of [¹⁸F]FLT PET for glioma response to therapy was analyzed in patients with recurrent gliomas receiving bevacizumab and irinotecan treatment [217]. Patients underwent serial [¹⁸F]FLT PET scans before, 1-2 weeks and 6 weeks after treatment and changes in [¹⁸F]FLT SUV were compared to clinical response at six weeks (using MRI) and overall survival. Patients who displayed at least a 25% decrease in glioma [¹⁸F]FLT SUV survived over three-fold longer than the other patients (10.8 vs 3.4 months, P = 0.003) and [¹⁸F]FLT SUV at both 1-2 weeks and six weeks were better predictors of patient survival than MRI at six weeks (P = 0.006, P = 0.002, P = 0.06, respectively), suggesting that [¹⁸F]FLT PET may be useful for predicting glioma response to therapy [217].

[¹⁸F]FLT PET in Pancreatic Cancer

An initial study of [¹⁸F]FLT PET in five pancreatic cancer patients compared [¹⁸F]FLT PET/CT to [¹⁸F]FDG PET/CT for visualizing pancreatic tumors [218]. Focally increased [¹⁸F]FLT and [¹⁸F]FDG uptake was observed in 40% and 100% of patients, respectively, suggesting that [¹⁸F]FDG PET is more appropriate for diagnosing pancreatic tumors than [¹⁸F]FLT PET. A subsequent larger study by Herrmann et al. [219], which performed [¹⁸F]FLT PET in 31 patients with unknown pancreatic lesions, found that increased focal [¹⁸F]FLT uptake was exclusively in malignant pancreatic tumors since none of the ten

benign tumors displayed focally increased [¹⁸F]FLT uptake. Focal [¹⁸F]FLT uptake was demonstrated in 15 of 21 malignant pancreatic tumors (71% sensitivity), suggesting that [¹⁸F]FLT PET is better for visualizing malignant pancreatic tumors than originally reported [218, 219]. Currently, no studies have been published regarding the predictive value of [¹⁸F]FLT PET for treatment response in pancreatic cancers.

[¹⁸F]FLT PET in Lymphomas

The initial clinical [¹⁸F]FLT PET study with lymphomas was performed on 11 patients with indolent or aggressive lymphomas [220]. Patients underwent [¹⁸F]FLT PET and [¹⁸F]FDG PET and both tracers detected a similar number of malignant lesions. [¹⁸F]FLT SUV correlated with Ki-67 score in nine of ten selected biopsies ($r = 0.95$, $P < 0.005$), suggesting that [¹⁸F]FLT PET may be useful for visualizing and staging lymphomas [220]. A subsequent larger study with 34 patients demonstrated similar results [221]. [¹⁸F]FLT PET detected 490 malignant lesions compared to 420 malignant lesions using standard detection methodologies [221]. Furthermore, mean [¹⁸F]FLT SUVs were significantly higher in aggressive lymphomas than in indolent lymphomas ($P = 0.0001$) [221].

A study by Kasper et al. [222] compared the value of [¹⁸F]FLT PET and [¹⁸F]FDG PET for predicting overall survival in 48 patients with Hodgkin's ($n = 15$) and non-Hodgkin's lymphoma ($n = 33$). Patients received chemo-radiotherapy and underwent [¹⁸F]FLT PET and [¹⁸F]FDG PET at least six weeks after treatment. Compared to [¹⁸F]FLT PET, [¹⁸F]FDG PET detected a greater number of lymphomas and provided a stronger correlation to overall survival in tracer

positive and tracer negative patients ($P = 0.002$ and $P = 0.016$, respectively). Another study by Herrmann et al. [223] performed serial [^{18}F]FLT PET scans on 22 patients with high grade non-Hodgkin's lymphoma before and after chemotherapy (cyclophosphamide, adriamycin, vincristine, and prednisone). Mean [^{18}F]FLT SUV was 23% that of baseline seven days after chemotherapy, suggesting that chemotherapy had significantly affected the lymphoma's thymidine metabolism. It was not possible to assess correlations with FLT uptake and clinical response since only two patients developed clinical relapse after initial response (median clinical follow-up = 12.6 months) [223]. The ability of [^{18}F]FLT PET to predict lymphoma response to therapy will likely depend on the chemotherapies used and the timing of [^{18}F]FLT PET after treatment. Further studies are required to determine the potential of [^{18}F]FLT PET for predicting lymphoma response to therapy.

[^{18}F]FLT PET in Soft Tissue Sarcomas

[^{18}F]FLT PET has demonstrated significant potential for detecting malignant soft tissue sarcomas [224, 225]. A study by Cobben et al. [225], which performed [^{18}F]FLT PET on 19 patients with soft tissue sarcomas of the extremities, demonstrated focally increased [^{18}F]FLT uptake in 19 of 20 tumors. Mean and maximal [^{18}F]FLT SUVs as well as [^{18}F]FLT tumor to non-tumor ratios all correlated with Ki-67 scores ($P < 0.05$) and the same three [^{18}F]FLT parameters also differentiated between low (grade 1) and high (grade 2 and 3) grade sarcomas ($P < 0.05$) [225]. A subsequent study by Buck et al. [224] performed [^{18}F]FLT PET in 22 sarcoma patients and compared [^{18}F]FLT PET

with [¹⁸F]FDG PET in 15 sarcoma patients. Both [¹⁸F]FLT and [¹⁸F]FDG allowed detection of all tumors (100% sensitivity) but only [¹⁸F]FLT mean and maximal SUVs in sarcoma lesions correlated with tumor grading [224].

[¹⁸F]FLT PET was also performed before and 28-49 days after hyperthermic isolated limb perfusion treatment on ten soft tissue sarcoma patients [226]. Pretreatment sarcoma mean and maximal [¹⁸F]FLT SUVs correlated with sarcoma mitotic index scores ($r = 0.82$ and 0.87 , respectively, $P < 0.05$) and pretreatment mean [¹⁸F]FLT SUV correlated with percent cellular tumor necrosis after treatment ($P < 0.05$) [226]. However, changes in [¹⁸F]FLT SUV before and after treatment did not correlate with percent cellular tumor necrosis since two tumors displayed at least 75% necrosis but had less than a 25% decrease in [¹⁸F]FLT SUV after treatment [226]. Current data suggest [¹⁸F]FLT PET may be useful for detecting and grading soft tissue sarcomas.

[¹⁸F]FLT PET in Melanomas

Only one study has been performed with [¹⁸F]FLT PET in melanoma patients [227]. Ten patients with stage three metastatic melanomas underwent [¹⁸F]FLT PET and all locoregional metastases had focally increased [¹⁸F]FLT uptake [227]. [¹⁸F]FLT PET had a sensitivity of 88% for detecting lymph node metastases, which was similar to results of previously published studies using [¹⁸F]FDG PET in melanoma patients [227, 228]. Published studies have not directly compared [¹⁸F]FLT PET with [¹⁸F]FDG PET for detecting and staging melanomas and such studies are warranted.

1.9 Goals of present work

FLT is used as a PET tracer for imaging proliferation based on the selective phosphorylation and “trapping” of FLT in cells by TK1, the activity of which is greatest in S-phase [168, 190]. Unfortunately, not all clinical studies have found positive correlations between FLT uptake and Ki-67 scores in tumors [229-231], suggesting that FLT uptake in tumor cells is not completely dependent on TK1 activity. Given the importance of hNTs in the uptake of nucleosides and many clinical nucleoside analogs, it is likely that hNTs are important for FLT uptake in normal and cancer cells.

Most [^{18}F]FLT PET clinical trials have focused on determining if [^{18}F]FLT PET is a valid method for imaging tumor proliferation [191] based on the assumption that [^{18}F]FLT PET predicts tumor response to therapy due to changes in tumor proliferation. Interestingly, several clinical anti-cancer drugs are nucleoside analogs and have relatively similar structures to that of FLT. The clinical efficacy of these nucleoside analog drugs is partly dependent on the levels of hNTs and low levels of hNTs may cause clinical resistance to these drugs (see section 1.6.1). If hNTs are also important for FLT uptake in cancer cells, then analysis of uptake of [^{18}F]FLT PET may be useful in determining the nucleoside transport capacity of tumors for nucleoside analog anti-cancer drugs such as gemcitabine.

The research described in this thesis focused on understanding the importance of hNTs in cellular FLT accumulation. Before this work was initiated, the only membrane transporter that had been tested for FLT transport was hENT1 [194]. To determine which hNTs could interact with FLT, [^3H]uridine transport

assays were performed with or without graded FLT concentrations using yeast cells producing individual recombinant hNTs (Chapter 3). Inhibition of [³H]uridine uptake by FLT suggested that FLT 1) interacts with the recombinant hNT produced in yeast cells, and 2) may be a permeant for the recombinant hNT produced in yeast cells. Yeast cells used in this study were genetically modified and displayed very little endogenous nucleoside transport, therefore, nucleoside uptake in yeast cells was almost exclusively mediated by recombinant hNTs [232]. To directly determine which hNTs are capable of FLT transport, *Xenopus laevis* oocytes producing individual recombinant hNTs were incubated with [³H]FLT and analyzed for mediated [³H]FLT uptake (Chapter 3). Oocytes display relatively little endogenous thymidine transport or metabolism, allowing analysis of nucleoside transport by recombinant hNTs [233]. [³H]FLT transport assays with or without hNT permeants/inhibitors were also performed with cultured human cancer cell lines with various origins to determine the importance of each hNT for FLT uptake (Chapter 3).

To determine the role of ENT1 in FLT uptake in normal tissues, wildtype FVB/N mice (ENT1^{+/+}) and ENT1 knockout mENT1-m1-cec mice (ENT1^{-/-}) underwent [¹⁸F]FLT microPET imaging (Chapter 4). ENT1^{+/+} mice injected with NBMPR-P one hour before imaging also underwent [¹⁸F]FLT microPET to determine how pharmacological inhibition of ENT1 by the NBMPR-P metabolite NBMPR affected FLT biodistribution in mice (Chapter 4). FLT uptake was also analyzed in lung carcinoma A549 xenograft tumors which have been stably transfected with pSUPER encoding shRNA against either hENT1 (A549-

pSUPER-hENT1 tumors) or a scrambled sequence with no homology to any known mammalian gene (A549-pSUPER-SC tumors). To determine if alterations in hENT1 protein levels in tumors affects tumor FLT uptake, [^{18}F]FLT microPET was performed with immunocompromised NIH-III mice with A549-pSUPER-SC and A549-pSUPER-hENT1 tumors over their left and right thighs, respectively, (Chapter 4).

FLT uptake in pancreatic cancer cells may be able to predict gemcitabine toxicity since 1) hENT1 is a predictive marker of gemcitabine response in pancreatic cancer [135], and 2) FLT uptake in pancreatic cancer cell lines Capan-2 and MIA-PaCa-2 was significantly reduced by inhibition of hENT1 with NBMPR (results from Chapter 3). To test this hypothesis, [^3H]FLT and [^3H]gemcitabine transport assays as well as gemcitabine toxicity assays were performed with cultured pancreatic cancer cell lines Capan-2, AsPC-1, BxPC-3, PL45, MIA PaCa-2, and PANC-1 (Chapter 5). Correlations were analyzed between FLT and gemcitabine uptake over short (45 s) and long (1 h) periods as well as gemcitabine toxicity to determine if FLT uptake may predict gemcitabine uptake and/or toxicity in pancreatic cancer cells.

Table 1-1. Nucleoside and nucleoside analog permeants of hNTs

The nucleosides listed in the Table are permeants for the hNTs when the K_M value is given. Unless otherwise indicated, hCNT K_M values were obtained from experiments with oocytes and hENT K_M values were obtained from experiments with cultured mammalian cells.

Permeant	hCNT1	hCNT2	hCNT3	hENT1	hENT2	hENT3	hENT4
<i>Nucleosides</i>				Apparent K_M values (μM)			
Uridine	45	40	22	480	270	2020 *	NP
Thymidine	27	NP	21	240	620	P, ND	ND
Cytidine	34	NP	15	680	5210	P, ND	ND
Adenosine	PP, ND	8	15	50	140	1860 *	780 *
Guanosine	NP	P, ND	43	140	2700	P, ND	ND
Inosine	NP	P, ND	53	200	50	P, ND	ND
<i>Nucleoside analogs</i>							
Fludarabine	NP	NP	P, ND	107	IT, ND	P, ND	ND
Cladribine	PP, ND	PP, ND	P, ND	23	IT, ND	P, ND	ND
Clofarabine	NP	81	52	108	328 *	ND	ND
5-FdU	15	P, ND	P, ND	P, ND	P, ND	P, ND	ND
Cytarabine	PP, ND	NP	NP	P, ND	PP, ND	ND	ND
Gemcitabine	24	NP	60	160 *	740 *	P, ND	ND
Zidovudine	P, ND	NP	310	NP	P, ND	P, ND	ND
References	[18, 24, 26, 27, 29, 51, 234]	[19, 26, 29, 30, 51, 81]	[17, 29, 51, 116]	[26, 29, 49, 51, 235]	[26, 29, 49, 51, 235]	[41, 48]	[42]

P = Permeant, PP = Poor permeant, NP = Not a permeant, ND = Not determined, IT = Inhibits transporter activity (no direct transport data), * = Data from experiments with oocytes

Table 1-2. Decay characteristics of positron emitting isotopes commonly used in PET

Isotope	Half-life	Decay Energy (max)	Decay Product
	min	MeV	
¹¹ C	20.4	0.96	¹¹ B
¹³ N	9.96	1.19	¹³ C
¹⁵ O	2.07	1.72	¹⁵ N
¹⁸ F	109	0.64	¹⁸ O

Half-life and decay energy values from Phelps (1991)
PET: A Biological Imaging Technique [236]

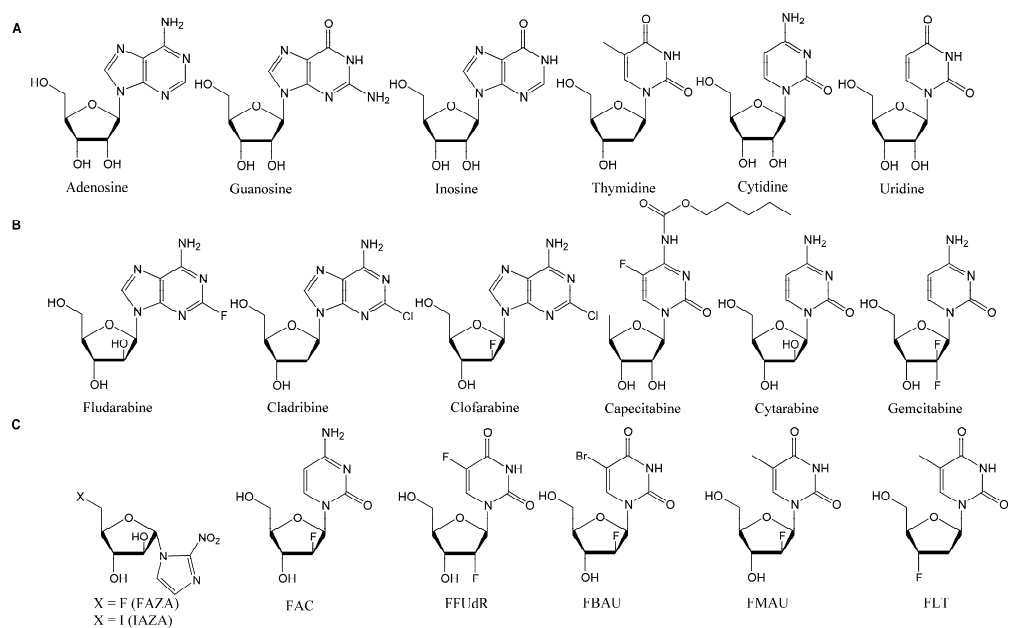


Figure 1-1. Chemical structures of physiological nucleosides and nucleoside analogs. (A) Physiological nucleosides include adenosine, guanosine, inosine, thymidine, cytidine, and uridine. (B) Clinical anti-cancer nucleoside analogs include fludarabine (9- β -D-arabinosyl-2-fluoroadenine), cladribine (2-chloro-2'-deoxyadenosine), clofarabine [2-chloro-9-(2'-deoxy-2'-fluoro- β -D-arabinofuranosyl) adenine], capecitabine (5'-deoxy-5-N-[(pentoxy)carbonyl]-cytidine), cytarabine (1- β -D-arabinofuranosylcytosine), and gemcitabine (2',2'-difluoro-2'-deoxycytidine). (C) Diagnostic nucleoside analogs include FAZA (1- α -D-(5-deoxy-5-[18 F]-fluoroarabinofuranosyl)-2-nitroimidazole), IAZA (iodoazomycin arabinoside), FAC (1-(2'-deoxy-2'-fluoroarabinofuranosyl) cytosine), FFUdR (5-fluoro-1-(2'-fluoro-2'-deoxy- β -D-ribofuranosyl)-uracil), FBAU (1-(2'-deoxy-2'-fluoro- β -D-arabinofuranosyl)-5-bromouracil), FMAU (1-(2'-deoxy-2'-fluoro-1- β -D-arabinofuranosyl)-thymine), and FLT (3'-deoxy-3'-fluorothymidine).

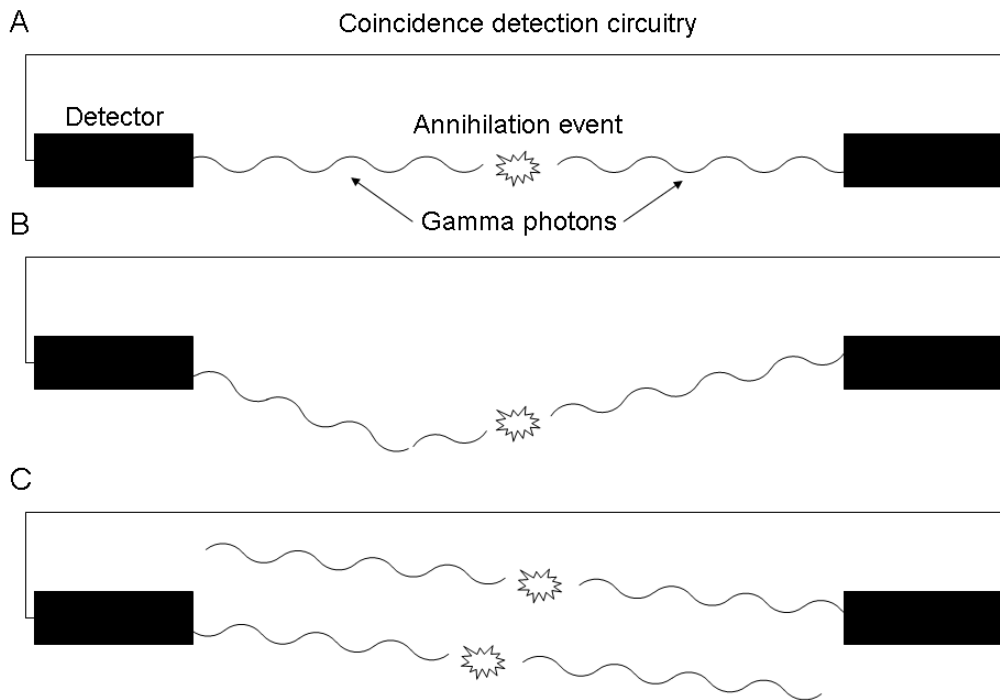


Figure 1-2. Coincidence detection events in PET. (A) A true coincidence detection event occurs when an annihilation event produces two photons that simultaneously activate detectors linked with coincidence detection circuitry. **(B)** A scatter coincidence detection event occurs when one or both photons from an annihilation event is/are scattered and both photons activate detectors linked with coincidence detection circuitry. **(C)** A random coincidence detection event occurs when two photons from two different annihilation events activate detectors linked with coincidence detection circuitry. Both scatter and random coincidence detection events will misplace annihilation events and reduce image quality.

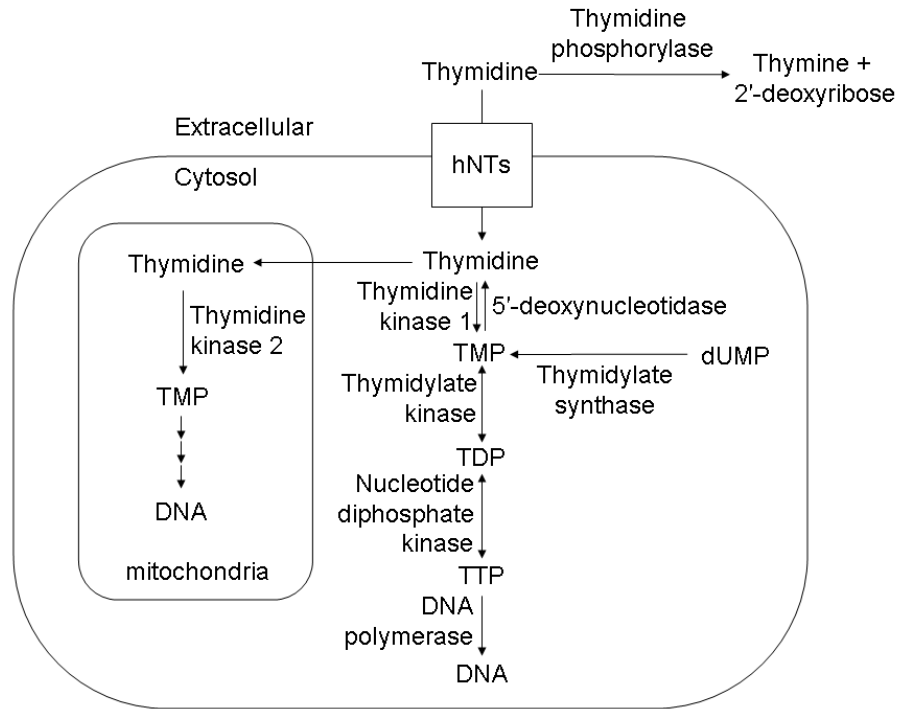


Figure 1-3. Thymidine metabolism in mammalian cells. Extracellular thymidine may be 1) hydrolysed to thymine and 2'-deoxyribose by thymidine phosphorylase, or 2) transported into cells by human nucleoside transporters (hNTs). Within the cytosol, thymidine may be subsequently phosphorylated by thymidine kinase 1, thymidylate kinase, and nucleotide diphosphate kinase to form thymidine-monophosphate (TMP), thymidine-diphosphate (TDP), and thymidine triphosphate (TTP), respectively. TTP may then be incorporated in DNA by DNA polymerases. Within the mitochondria, thymidine may be phosphorylated by thymidine kinase 2 and after subsequent phosphorylations, may be incorporated into mitochondrial DNA. TMP may also be produced by methylation of 2'-deoxyuridine-monophosphate by thymidylate synthase.

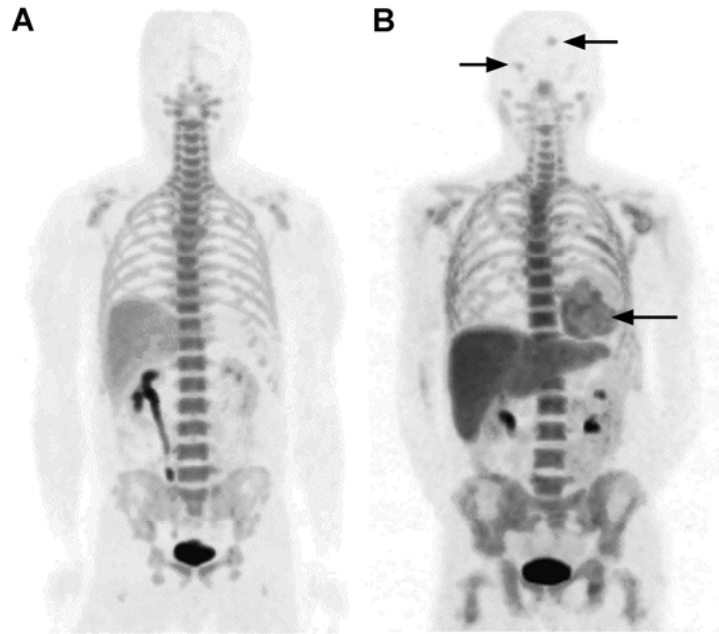


Figure 1-4. [¹⁸F]FLT PET images in human cancer patients. (A) Patient has normal FLT biodistribution with focal FLT uptake in the bladder, bone marrow, and liver. **(B)** Patient displays focal FLT uptake in tumors (indicated by arrows) throughout the head and torso. [¹⁸F]FLT PET images were acquired from the Department of Nuclear Medicine at the Cross Cancer Institute.

1.10 Bibliography

- [1] Schulte G, Fredholm BB. Signalling from adenosine receptors to mitogen-activated protein kinases. *Cell Signal* 2003;15:813-27.
- [2] Cohen MV, Downey JM. Adenosine: trigger and mediator of cardioprotection. *Basic Res Cardiol* 2008;103:203-15.
- [3] Haas HL, Selbach O. Functions of neuronal adenosine receptors. *Naunyn Schmiedebergs Arch Pharmacol* 2000;362:375-81.
- [4] Hasko G, Linden J, Cronstein B, Pacher P. Adenosine receptors: therapeutic aspects for inflammatory and immune diseases. *Nat Rev Drug Discov* 2008;7:759-70.
- [5] Wilson CN. Adenosine receptors and asthma in humans. *Br J Pharmacol* 2008;155:475-86.
- [6] Murray AW. The biological significance of purine salvage. *Annu Rev Biochem* 1971;40:811-26.
- [7] Ciarimboli G. Organic cation transporters. *Xenobiotica* 2008;38:936-71.
- [8] Kong W, Engel K, Wang J. Mammalian nucleoside transporters. *Curr Drug Metab* 2004;5:63-84.
- [9] Kruh GD, Guo Y, Hopper-Borge E, Belinsky MG, Chen ZS. ABCC10, ABCC11, and ABCC12. *Pflugers Arch* 2007;453:675-84.
- [10] Ritter CA, Jedlitschky G, Meyer zu Schwabedissen H, Grube M, Kock K, Kroemer HK. Cellular export of drugs and signaling molecules by the ATP-binding cassette transporters MRP4 (ABCC4) and MRP5 (ABCC5). *Drug Metab Rev* 2005;37:253-78.
- [11] Srimaroeng C, Perry JL, Pritchard JB. Physiology, structure, and regulation of the cloned organic anion transporters. *Xenobiotica* 2008;38:889-935.
- [12] Marzilli M, Simonetti I, Levantesi D, Trivella MG, De Nes M, Perissinotto A, et al. Effects of dilazep on coronary and systemic hemodynamics in humans. *Am Heart J* 1984;108:276-85.
- [13] Schaper W. Dipyridamole, an underestimated vascular protective drug. *Cardiovasc Drugs Ther* 2005;19:357-63.
- [14] Zhang J, Visser F, King KM, Baldwin SA, Young JD, Cass CE. The role of nucleoside transporters in cancer chemotherapy with nucleoside drugs. *Cancer Metastasis Rev* 2007;26:85-110.

- [15] Molho-Pessach V, Lerer I, Abeliovich D, Agha Z, Abu Libdeh A, Broshtilova V, et al. The H syndrome is caused by mutations in the nucleoside transporter hENT3. *Am J Hum Genet* 2008;83:529-34.
- [16] Griffith DA, Jarvis SM. Nucleoside and nucleobase transport systems of mammalian cells. *Biochim Biophys Acta* 1996;1286:153-81.
- [17] Ritzel MW, Ng AM, Yao SY, Graham K, Loewen SK, Smith KM, et al. Molecular identification and characterization of novel human and mouse concentrative Na⁺-nucleoside cotransporter proteins (hCNT3 and mCNT3) broadly selective for purine and pyrimidine nucleosides (system cib). *J Biol Chem* 2001;276:2914-27.
- [18] Ritzel MW, Yao SY, Huang MY, Elliott JF, Cass CE, Young JD. Molecular cloning and functional expression of cDNAs encoding a human Na⁺-nucleoside cotransporter (hCNT1). *Am J Physiol* 1997;272:C707-14.
- [19] Ritzel MW, Yao SY, Ng AM, Mackey JR, Cass CE, Young JD. Molecular cloning, functional expression and chromosomal localization of a cDNA encoding a human Na⁺/nucleoside cotransporter (hCNT2) selective for purine nucleosides and uridine. *Mol Membr Biol* 1998;15:203-11.
- [20] Hamilton SR, Yao SY, Ingram JC, Hadden DA, Ritzel MW, Gallagher MP, et al. Subcellular distribution and membrane topology of the mammalian concentrative Na⁺-nucleoside cotransporter rCNT1. *J Biol Chem* 2001;276:27981-8.
- [21] Huang QQ, Yao SY, Ritzel MW, Paterson AR, Cass CE, Young JD. Cloning and functional expression of a complementary DNA encoding a mammalian nucleoside transport protein. *J Biol Chem* 1994;269:17757-60.
- [22] Slugoski MD, Ng AM, Yao SY, Lin CC, Mulinta R, Cass CE, et al. Substituted Cysteine Accessibility Method Analysis of Human Concentrative Nucleoside Transporter hCNT3 Reveals a Novel Discontinuous Region of Functional Importance within the CNT Family Motif (G/A)XKX3NEFVA(Y/M/F). *J Biol Chem* 2009;284:17281-92.
- [23] Pastor-Anglada M, Cano-Soldado P, Errasti-Murugarren E, Casado FJ. SLC28 genes and concentrative nucleoside transporter (CNT) proteins. *Xenobiotica* 2008;38:972-94.
- [24] Lostao MP, Mata JF, Larrayoz IM, Inzillo SM, Casado FJ, Pastor-Anglada M. Electrogenic uptake of nucleosides and nucleoside-derived drugs by the human nucleoside transporter 1 (hCNT1) expressed in *Xenopus laevis* oocytes. *FEBS Lett* 2000;481:137-40.

- [25] Loewen SK, Ng AM, Yao SY, Cass CE, Baldwin SA, Young JD. Identification of amino acid residues responsible for the pyrimidine and purine nucleoside specificities of human concentrative Na(+) nucleoside cotransporters hCNT1 and hCNT2. *J Biol Chem* 1999;274:24475-84.
- [26] Mackey JR, Yao SY, Smith KM, Karpinski E, Baldwin SA, Cass CE, et al. Gemcitabine transport in xenopus oocytes expressing recombinant plasma membrane mammalian nucleoside transporters. *J Natl Cancer Inst* 1999;91:1876-81.
- [27] Smith KM, Ng AM, Yao SY, Labedz KA, Knaus EE, Wiebe LI, et al. Electrophysiological characterization of a recombinant human Na⁺-coupled nucleoside transporter (hCNT1) produced in *Xenopus* oocytes. *J Physiol* 2004;558:807-23.
- [28] Nagai K, Nagasawa K, Koma M, Hotta A, Fujimoto S. Cytidine is a novel substrate for wild-type concentrative nucleoside transporter 2. *Biochem Biophys Res Commun* 2006;347:439-43.
- [29] King KM, Damaraju VL, Vickers MF, Yao SY, Lang T, Tackaberry TE, et al. A comparison of the transportability, and its role in cytotoxicity, of clofarabine, cladribine, and fludarabine by recombinant human nucleoside transporters produced in three model expression systems. *Mol Pharmacol* 2006;69:346-53.
- [30] Lang TT, Selner M, Young JD, Cass CE. Acquisition of human concentrative nucleoside transporter 2 (hcnt2) activity by gene transfer confers sensitivity to fluoropyrimidine nucleosides in drug-resistant leukemia cells. *Mol Pharmacol* 2001;60:1143-52.
- [31] Smith KM, Slugoski MD, Cass CE, Baldwin SA, Karpinski E, Young JD. Cation coupling properties of human concentrative nucleoside transporters hCNT1, hCNT2 and hCNT3. *Mol Membr Biol* 2007;24:53-64.
- [32] Smith KM, Slugoski MD, Loewen SK, Ng AM, Yao SY, Chen XZ, et al. The broadly selective human Na⁺/nucleoside cotransporter (hCNT3) exhibits novel cation-coupled nucleoside transport characteristics. *J Biol Chem* 2005;280:25436-49.
- [33] Gupte A, Buolamwini JK. Synthesis and biological evaluation of phloridzin analogs as human concentrative nucleoside transporter 3 (hCNT3) inhibitors. *Bioorg Med Chem Lett* 2009;19:917-21.
- [34] Rovera G, Santoli D, Damsky C. Human promyelocytic leukemia cells in culture differentiate into macrophage-like cells when treated with a phorbol diester. *Proc Natl Acad Sci U S A* 1979;76:2779-83.

- [35] Errasti-Murugarren E, Molina-Arcas M, Casado FJ, Pastor-Anglada M. A splice variant of the SLC28A3 gene encodes a novel human concentrative nucleoside transporter-3 (hCNT3) protein localized in the endoplasmic reticulum. *FASEB J* 2009;23:172-82.
- [36] Fernandez-Veledo S, Jover R, Casado FJ, Gomez-Lechon MJ, Pastor-Anglada M. Transcription factors involved in the expression of SLC28 genes in human liver parenchymal cells. *Biochem Biophys Res Commun* 2007;353:381-8.
- [37] Guallar JP, Cano-Soldado P, Aymerich I, Domingo JC, Alegre M, Domingo P, et al. Altered expression of nucleoside transporter genes (SLC28 and SLC29) in adipose tissue from HIV-1-infected patients. *Antivir Ther* 2007;12:853-63.
- [38] Lam W, Leung CH, Bussom S, Cheng YC. The impact of hypoxic treatment on the expression of phosphoglycerate kinase and the cytotoxicity of troxacitabine and gemcitabine. *Mol Pharmacol* 2007;72:536-44.
- [39] Griffiths M, Beaumont N, Yao SY, Sundaram M, Boumah CE, Davies A, et al. Cloning of a human nucleoside transporter implicated in the cellular uptake of adenosine and chemotherapeutic drugs. *Nat Med* 1997;3:89-93.
- [40] Griffiths M, Yao SY, Abidi F, Phillips SE, Cass CE, Young JD, et al. Molecular cloning and characterization of a nitrobenzylthioinosine-insensitive (ei) equilibrative nucleoside transporter from human placenta. *Biochem J* 1997;328 (Pt 3):739-43.
- [41] Baldwin SA, Yao SY, Hyde RJ, Ng AM, Foppolo S, Barnes K, et al. Functional characterization of novel human and mouse equilibrative nucleoside transporters (hENT3 and mENT3) located in intracellular membranes. *J Biol Chem* 2005;280:15880-7.
- [42] Barnes K, Dobrzynski H, Foppolo S, Beal PR, Ismat F, Scullion ER, et al. Distribution and functional characterization of equilibrative nucleoside transporter-4, a novel cardiac adenosine transporter activated at acidic pH. *Circ Res* 2006;99:510-9.
- [43] Young JD, Yao SY, Sun L, Cass CE, Baldwin SA. Human equilibrative nucleoside transporter (ENT) family of nucleoside and nucleobase transporter proteins. *Xenobiotica* 2008;38:995-1021.
- [44] Sundaram M, Yao SY, Ingram JC, Berry ZA, Abidi F, Cass CE, et al. Topology of a human equilibrative, nitrobenzylthioinosine (NBMPR)-sensitive nucleoside transporter (hENT1) implicated in the cellular uptake of adenosine and anti-cancer drugs. *J Biol Chem* 2001;276:45270-5.

- [45] Ward JL, Leung GP, Toan SV, Tse CM. Functional analysis of site-directed glycosylation mutants of the human equilibrative nucleoside transporter-2. *Arch Biochem Biophys* 2003;411:19-26.
- [46] Lai Y, Tse CM, Unadkat JD. Mitochondrial expression of the human equilibrative nucleoside transporter 1 (hENT1) results in enhanced mitochondrial toxicity of antiviral drugs. *J Biol Chem* 2004;279:4490-7.
- [47] Mani RS, Hammond JR, Marjan JM, Graham KA, Young JD, Baldwin SA, et al. Demonstration of equilibrative nucleoside transporters (hENT1 and hENT2) in nuclear envelopes of cultured human choriocarcinoma (BeWo) cells by functional reconstitution in proteoliposomes. *J Biol Chem* 1998;273:30818-25.
- [48] Govindarajan R, Leung GP, Zhou M, Tse CM, Wang J, Unadkat JD. Facilitated Mitochondrial Import of Anti-viral and Anti-cancer Nucleoside Drugs by Human Equilibrative Nucleoside Transporter-3 (hENT3). *Am J Physiol Gastrointest Liver Physiol* 2009.
- [49] Ward JL, Sherali A, Mo ZP, Tse CM. Kinetic and pharmacological properties of cloned human equilibrative nucleoside transporters, ENT1 and ENT2, stably expressed in nucleoside transporter-deficient PK15 cells. ENT2 exhibits a low affinity for guanosine and cytidine but a high affinity for inosine. *J Biol Chem* 2000;275:8375-81.
- [50] Engel K, Zhou M, Wang J. Identification and characterization of a novel monoamine transporter in the human brain. *J Biol Chem* 2004;279:50042-9.
- [51] Clarke ML, Damaraju VL, Zhang J, Mowles D, Tackaberry T, Lang T, et al. The role of human nucleoside transporters in cellular uptake of 4'-thio-beta-D-arabinofuranosylcytosine and beta-D-arabinosylcytosine. *Mol Pharmacol* 2006;70:303-10.
- [52] Kim HH, Liao JK. Translational therapeutics of dipyridamole. *Arterioscler Thromb Vasc Biol* 2008;28:s39-42.
- [53] Rongen GA, Smits P, Ver Donck K, Willemsen JJ, De Abreu RA, Van Belle H, et al. Hemodynamic and neurohumoral effects of various grades of selective adenosine transport inhibition in humans. Implications for its future role in cardioprotection. *J Clin Invest* 1995;95:658-68.
- [54] Visser F, Vickers MF, Ng AM, Baldwin SA, Young JD, Cass CE. Mutation of residue 33 of human equilibrative nucleoside transporters 1 and 2 alters sensitivity to inhibition of transport by dilazep and dipyridamole. *J Biol Chem* 2002;277:395-401.

- [55] Abdulla P, Coe IR. Characterization and functional analysis of the promoter for the human equilibrative nucleoside transporter gene, hENT1. *Nucleosides Nucleotides Nucleic Acids* 2007;26:99-110.
- [56] Coe I, Zhang Y, McKenzie T, Naydenova Z. PKC regulation of the human equilibrative nucleoside transporter, hENT1. *FEBS Lett* 2002;517:201-5.
- [57] Soler C, Felipe A, Mata JF, Casado FJ, Celada A, Pastor-Anglada M. Regulation of nucleoside transport by lipopolysaccharide, phorbol esters, and tumor necrosis factor-alpha in human B-lymphocytes. *J Biol Chem* 1998;273:26939-45.
- [58] Aguayo C, Casado J, Gonzalez M, Pearson JD, Martin RS, Casanello P, et al. Equilibrative nucleoside transporter 2 is expressed in human umbilical vein endothelium, but is not involved in the inhibition of adenosine transport induced by hyperglycaemia. *Placenta* 2005;26:641-53.
- [59] Puebla C, Farias M, Gonzalez M, Vecchiola A, Aguayo C, Krause B, et al. High D-glucose reduces SLC29A1 promoter activity and adenosine transport involving specific protein 1 in human umbilical vein endothelium. *J Cell Physiol* 2008;215:645-56.
- [60] Munoz G, San Martin R, Farias M, Cea L, Vecchiola A, Casanello P, et al. Insulin restores glucose inhibition of adenosine transport by increasing the expression and activity of the equilibrative nucleoside transporter 2 in human umbilical vein endothelium. *J Cell Physiol* 2006;209:826-35.
- [61] Cass CE, Dahlig E, Lau EY, Lynch TP, Paterson AR. Fluctuations in nucleoside uptake and binding of the inhibitor of nucleoside transport, nitrobenzylthioinosine, during the replication cycle of HeLa cells. *Cancer Res* 1979;39:1245-52.
- [62] Pressacco J, Wiley JS, Jamieson GP, Erlichman C, Hedley DW. Modulation of the equilibrative nucleoside transporter by inhibitors of DNA synthesis. *Br J Cancer* 1995;72:939-42.
- [63] Guerra B, Issinger OG. Protein kinase CK2 and its role in cellular proliferation, development and pathology. *Electrophoresis* 1999;20:391-408.
- [64] Stolk M, Cooper E, Vilk G, Litchfield DW, Hammond JR. Subtype-specific regulation of equilibrative nucleoside transporters by protein kinase CK2. *Biochem J* 2005;386:281-9.
- [65] Casanello P, Torres A, Sanhueza F, Gonzalez M, Farias M, Gallardo V, et al. Equilibrative nucleoside transporter 1 expression is downregulated by hypoxia in human umbilical vein endothelium. *Circ Res* 2005;97:16-24.

- [66] Baldwin SA, Beal PR, Yao SY, King AE, Cass CE, Young JD. The equilibrative nucleoside transporter family, SLC29. *Pflugers Arch* 2004;447:735-43.
- [67] Pennycooke M, Chaudary N, Shuralyova I, Zhang Y, Coe IR. Differential expression of human nucleoside transporters in normal and tumor tissue. *Biochem Biophys Res Commun* 2001;280:951-9.
- [68] Govindarajan R, Bakken AH, Hudkins KL, Lai Y, Casado FJ, Pastor-Anglada M, et al. In situ hybridization and immunolocalization of concentrative and equilibrative nucleoside transporters in the human intestine, liver, kidneys, and placenta. *Am J Physiol Regul Integr Comp Physiol* 2007;293:R1809-22.
- [69] Ngo LY, Patil SD, Unadkat JD. Ontogenic and longitudinal activity of Na(+)-nucleoside transporters in the human intestine. *Am J Physiol Gastrointest Liver Physiol* 2001;280:G475-81.
- [70] Elwi AN, Damaraju VL, Baldwin SA, Young JD, Sawyer MB, Cass CE. Renal nucleoside transporters: physiological and clinical implications. *Biochem Cell Biol* 2006;84:844-58.
- [71] Damaraju VL, Elwi AN, Hunter C, Carpenter P, Santos C, Barron GM, et al. Localization of broadly selective equilibrative and concentrative nucleoside transporters, hENT1 and hCNT3, in human kidney. *Am J Physiol Renal Physiol* 2007;293:F200-11.
- [72] Elwi AN, Damaraju VL, Kuzma ML, Mowles DA, Baldwin SA, Young JD, et al. Transepithelial fluxes of adenosine and 2'-deoxyadenosine across human renal proximal tubule cells: roles of nucleoside transporters hENT1, hENT2, and hCNT3. *Am J Physiol Renal Physiol* 2009;296:F1439-51.
- [73] Govindarajan R, Endres CJ, Whittington D, LeCluyse E, Pastor-Anglada M, Tse CM, et al. Expression and hepatobiliary transport characteristics of the concentrative and equilibrative nucleoside transporters in sandwich-cultured human hepatocytes. *Am J Physiol Gastrointest Liver Physiol* 2008;295:G570-80.
- [74] Xia L, Engel K, Zhou M, Wang J. Membrane localization and pH-dependent transport of a newly cloned organic cation transporter (PMAT) in kidney cells. *Am J Physiol Renal Physiol* 2007;292:F682-90.
- [75] Xia L, Zhou M, Kalhorn TF, Ho HT, Wang J. Podocyte-specific expression of organic cation transporter PMAT: implication in puromycin aminonucleoside nephrotoxicity. *Am J Physiol Renal Physiol* 2009;296:F1307-13.

- [76] Zhou M, Xia L, Wang J. Metformin transport by a newly cloned proton-stimulated organic cation transporter (plasma membrane monoamine transporter) expressed in human intestine. *Drug Metab Dispos* 2007;35:1956-62.
- [77] Dahlin A, Xia L, Kong W, Hevner R, Wang J. Expression and immunolocalization of the plasma membrane monoamine transporter in the brain. *Neuroscience* 2007;146:1193-211.
- [78] Plunkett W, Saunders PP. Metabolism and action of purine nucleoside analogs. *Pharmacol Ther* 1991;49:239-68.
- [79] Montgomery JA, Clayton SD, Shortnacy AT. An improved procedure for the preparation of 9-fl-D-arabinofuranosyl-2-fluoroadenine. *J Heterocyc Chem* 1979;16:157-60.
- [80] Hersh MR, Kuhn JG, Phillips JL, Clark G, Ludden TM, Von Hoff DD. Pharmacokinetic study of fludarabine phosphate (NSC 312887). *Cancer Chemother Pharmacol* 1986;17:277-80.
- [81] Lang TT, Young JD, Cass CE. Interactions of nucleoside analogs, caffeine, and nicotine with human concentrative nucleoside transporters 1 and 2 stably produced in a transport-defective human cell line. *Mol Pharmacol* 2004;65:925-33.
- [82] Molina-Arcas M, Bellosillo B, Casado FJ, Montserrat E, Gil J, Colomer D, et al. Fludarabine uptake mechanisms in B-cell chronic lymphocytic leukemia. *Blood* 2003;101:2328-34.
- [83] Carson DA, Wasson DB, Kaye J, Ullman B, Martin DW, Jr., Robins RK, et al. Deoxycytidine kinase-mediated toxicity of deoxyadenosine analogs toward malignant human lymphoblasts in vitro and toward murine L1210 leukemia in vivo. *Proc Natl Acad Sci U S A* 1980;77:6865-9.
- [84] Parker WB, Bapat AR, Shen JX, Townsend AJ, Cheng YC. Interaction of 2-halogenated dATP analogs (F, Cl, and Br) with human DNA polymerases, DNA primase, and ribonucleotide reductase. *Mol Pharmacol* 1988;34:485-91.
- [85] Tseng WC, Derse D, Cheng YC, Brockman RW, Bennett LL, Jr. In vitro biological activity of 9-beta-D-arabinofuranosyl-2-fluoroadenine and the biochemical actions of its triphosphate on DNA polymerases and ribonucleotide reductase from HeLa cells. *Mol Pharmacol* 1982;21:474-7.
- [86] White EL, Shaddix SC, Brockman RW, Bennett LL, Jr. Comparison of the actions of 9-beta-D-arabinofuranosyl-2-fluoroadenine and 9-beta-D-arabinofuranosyladenine on target enzymes from mouse tumor cells. *Cancer Res* 1982;42:2260-4.

- [87] Cerqueira NM, Fernandes PA, Ramos MJ. Ribonucleotide reductase: a critical enzyme for cancer chemotherapy and antiviral agents. *Recent Pat Anticancer Drug Discov* 2007;2:11-29.
- [88] Beutler E. Cladribine (2-chlorodeoxyadenosine). *Lancet* 1992;340:952-6.
- [89] Robak T. Therapy of chronic lymphocytic leukaemia with purine nucleoside analogues: facts and controversies. *Drugs Aging* 2005;22:983-1012.
- [90] Schaner ME, Wang J, Zevin S, Gerstin KM, Giacomini KM. Transient expression of a purine-selective nucleoside transporter (SPNTint) in a human cell line (HeLa). *Pharm Res* 1997;14:1316-21.
- [91] Wang L, Karlsson A, Arner ES, Eriksson S. Substrate specificity of mitochondrial 2'-deoxyguanosine kinase. Efficient phosphorylation of 2-chlorodeoxyadenosine. *J Biol Chem* 1993;268:22847-52.
- [92] Griffig J, Koob R, Blakley RL. Mechanisms of inhibition of DNA synthesis by 2-chlorodeoxyadenosine in human lymphoblastic cells. *Cancer Res* 1989;49:6923-8.
- [93] Carson DA, Wasson DB, Esparza LM, Carrera CJ, Kipps TJ, Cottam HB. Oral antilymphocyte activity and induction of apoptosis by 2-chloro-2'-arabino-fluoro-2'-deoxyadenosine. *Proc Natl Acad Sci U S A* 1992;89:2970-4.
- [94] Kantarjian H, Gandhi V, Cortes J, Verstovsek S, Du M, Garcia-Manero G, et al. Phase 2 clinical and pharmacologic study of clofarabine in patients with refractory or relapsed acute leukemia. *Blood* 2003;102:2379-86.
- [95] Harned TM, Gaynon PS. Treating refractory leukemias in childhood, role of clofarabine. *Ther Clin Risk Manag* 2008;4:327-36.
- [96] Jeha S, Gandhi V, Chan KW, McDonald L, Ramirez I, Madden R, et al. Clofarabine, a novel nucleoside analog, is active in pediatric patients with advanced leukemia. *Blood* 2004;103:784-9.
- [97] Lotfi K, Mansson E, Spasokoukotskaja T, Pettersson B, Liliemark J, Peterson C, et al. Biochemical pharmacology and resistance to 2-chloro-2'-arabino-fluoro-2'-deoxyadenosine, a novel analogue of cladribine in human leukemic cells. *Clin Cancer Res* 1999;5:2438-44.
- [98] Parker WB, Shaddix SC, Chang CH, White EL, Rose LM, Brockman RW, et al. Effects of 2-chloro-9-(2-deoxy-2-fluoro-beta-D-arabinofuranosyl)adenine on K562 cellular metabolism and the inhibition of human ribonucleotide reductase and DNA polymerases by its 5'-triphosphate. *Cancer Res* 1991;51:2386-94.

- [99] Xie C, Plunkett W. Metabolism and actions of 2-chloro-9-(2-deoxy-2-fluoro-beta-D- arabinofuranosyl)-adenine in human lymphoblastoid cells. *Cancer Res* 1995;55:2847-52.
- [100] Genini D, Adachi S, Chao Q, Rose DW, Carrera CJ, Cottam HB, et al. Deoxyadenosine analogs induce programmed cell death in chronic lymphocytic leukemia cells by damaging the DNA and by directly affecting the mitochondria. *Blood* 2000;96:3537-43.
- [101] Aprile G, Mazzer M, Moroso S, Puglisi F. Pharmacology and therapeutic efficacy of capecitabine: focus on breast and colorectal cancer. *Anticancer Drugs* 2009;20:217-29.
- [102] Miwa M, Ura M, Nishida M, Sawada N, Ishikawa T, Mori K, et al. Design of a novel oral fluoropyrimidine carbamate, capecitabine, which generates 5-fluorouracil selectively in tumours by enzymes concentrated in human liver and cancer tissue. *Eur J Cancer* 1998;34:1274-81.
- [103] Mackey JR, Jennings LL, Clarke ML, Santos CL, Dabbagh L, Vsianska M, et al. Immunohistochemical variation of human equilibrative nucleoside transporter 1 protein in primary breast cancers. *Clin Cancer Res* 2002;8:110-6.
- [104] Mata JF, Garcia-Manteiga JM, Lostao MP, Fernandez-Veledo S, Guillen-Gomez E, Larrayoz IM, et al. Role of the human concentrative nucleoside transporter (hCNT1) in the cytotoxic action of 5[Prime]-deoxy-5-fluorouridine, an active intermediate metabolite of capecitabine, a novel oral anticancer drug. *Mol Pharmacol* 2001;59:1542-8.
- [105] Zhang J, Visser F, Vickers MF, Lang T, Robins MJ, Nielsen LP, et al. Uridine binding motifs of human concentrative nucleoside transporters 1 and 3 produced in *Saccharomyces cerevisiae*. *Mol Pharmacol* 2003;64:1512-20.
- [106] Imazano Y, Takebayashi Y, Nishiyama K, Akiba S, Miyadera K, Yamada Y, et al. Correlation between thymidine phosphorylase expression and prognosis in human renal cell carcinoma. *J Clin Oncol* 1997;15:2570-8.
- [107] Moghaddam A, Zhang HT, Fan TP, Hu DE, Lees VC, Turley H, et al. Thymidine phosphorylase is angiogenic and promotes tumor growth. *Proc Natl Acad Sci U S A* 1995;92:998-1002.
- [108] Longley DB, Harkin DP, Johnston PG. 5-fluorouracil: mechanisms of action and clinical strategies. *Nat Rev Cancer* 2003;3:330-8.
- [109] Blum W, Marcucci G. New approaches in acute myeloid leukemia. *Best Pract Res Clin Haematol* 2008;21:29-41.

- [110] Reiter A, Hochhaus A, Berger U, Kuhn C, Hehlmann R. AraC-based pharmacotherapy of chronic myeloid leukaemia. *Expert Opin Pharmacother* 2001;2:1129-35.
- [111] Wang WS, Tzeng CH, Chiou TJ, Liu JH, Hsieh RK, Yen CC, et al. High-dose cytarabine and mitoxantrone as salvage therapy for refractory non-Hodgkin's lymphoma. *Jpn J Clin Oncol* 1997;27:154-7.
- [112] Momparler RL, Fischer GA. Mammalian deoxynucleoside kinase. I. Deoxycytidine kinase: purification, properties, and kinetic studies with cytosine arabinoside. *J Biol Chem* 1968;243:4298-304.
- [113] Pourquier P, Takebayashi Y, Urasaki Y, Gioffre C, Kohlhagen G, Pommier Y. Induction of topoisomerase I cleavage complexes by 1-beta-D-arabinofuranosylcytosine (ara-C) in vitro and in ara-C-treated cells. *Proc Natl Acad Sci U S A* 2000;97:1885-90.
- [114] de Vries JF, Falkenburg JH, Willemze R, Barge RM. The mechanisms of Ara-C-induced apoptosis of resting B-chronic lymphocytic leukemia cells. *Haematologica* 2006;91:912-9.
- [115] Toschi L, Finocchiaro G, Bartolini S, Gioia V, Cappuzzo F. Role of gemcitabine in cancer therapy. *Future Oncol* 2005;1:7-17.
- [116] Hu H, Endres CJ, Chang C, Umaphathy NS, Lee EW, Fei YJ, et al. Electrophysiological characterization and modeling of the structure activity relationship of the human concentrative nucleoside transporter 3 (hCNT3). *Mol Pharmacol* 2006;69:1542-53.
- [117] Heinemann V, Hertel LW, Grindey GB, Plunkett W. Comparison of the cellular pharmacokinetics and toxicity of 2',2'-difluorodeoxycytidine and 1-beta-D-arabinofuranosylcytosine. *Cancer Res* 1988;48:4024-31.
- [118] Heinemann V, Xu YZ, Chubb S, Sen A, Hertel LW, Grindey GB, et al. Inhibition of ribonucleotide reduction in CCRF-CEM cells by 2',2'-difluorodeoxycytidine. *Mol Pharmacol* 1990;38:567-72.
- [119] Pourquier P, Gioffre C, Kohlhagen G, Urasaki Y, Goldwasser F, Hertel LW, et al. Gemcitabine (2',2'-difluoro-2'-deoxycytidine), an antimetabolite that poisons topoisomerase I. *Clin Cancer Res* 2002;8:2499-504.
- [120] Ruiz van Haperen VW, Veerman G, Vermorken JB, Peters GJ. 2',2'-Difluoro-deoxycytidine (gemcitabine) incorporation into RNA and DNA of tumour cell lines. *Biochem Pharmacol* 1993;46:762-6.
- [121] Gati WP, Paterson AR, Belch AR, Chlumecky V, Larratt LM, Mant MJ, et al. Es nucleoside transporter content of acute leukemia cells: role in cell sensitivity to cytarabine (araC). *Leuk Lymphoma* 1998;32:45-54.

- [122] Hubeek I, Stam RW, Peters GJ, Broekhuizen R, Meijerink JP, van Wering ER, et al. The human equilibrative nucleoside transporter 1 mediates in vitro cytarabine sensitivity in childhood acute myeloid leukaemia. *Br J Cancer* 2005;93:1388-94.
- [123] Molina-Arcas M, Marce S, Villamor N, Huber-Ruano I, Casado FJ, Bellosillo B, et al. Equilibrative nucleoside transporter-2 (hENT2) protein expression correlates with ex vivo sensitivity to fludarabine in chronic lymphocytic leukemia (CLL) cells. *Leukemia* 2005;19:64-8.
- [124] Mori R, Ishikawa T, Ichikawa Y, Taniguchi K, Matsuyama R, Ueda M, et al. Human equilibrative nucleoside transporter 1 is associated with the chemosensitivity of gemcitabine in human pancreatic adenocarcinoma and biliary tract carcinoma cells. *Oncol Rep* 2007;17:1201-5.
- [125] Stam RW, den Boer ML, Meijerink JP, Ebus ME, Peters GJ, Noordhuis P, et al. Differential mRNA expression of Ara-C-metabolizing enzymes explains Ara-C sensitivity in MLL gene-rearranged infant acute lymphoblastic leukemia. *Blood* 2003;101:1270-6.
- [126] Gati WP, Paterson AR, Larratt LM, Turner AR, Belch AR. Sensitivity of acute leukemia cells to cytarabine is a correlate of cellular es nucleoside transporter site content measured by flow cytometry with SAENTA-fluorescein. *Blood* 1997;90:346-53.
- [127] Mackey JR, Mani RS, Selner M, Mowles D, Young JD, Belt JA, et al. Functional nucleoside transporters are required for gemcitabine influx and manifestation of toxicity in cancer cell lines. *Cancer Res* 1998;58:4349-57.
- [128] Garcia-Manteiga J, Molina-Arcas M, Casado FJ, Mazo A, Pastor-Anglada M. Nucleoside transporter profiles in human pancreatic cancer cells: role of hCNT1 in 2',2'-difluorodeoxycytidine- induced cytotoxicity. *Clin Cancer Res* 2003;9:5000-8.
- [129] Perez-Torras S, Garcia-Manteiga J, Mercade E, Casado FJ, Carbo N, Pastor-Anglada M, et al. Adenoviral-mediated overexpression of human equilibrative nucleoside transporter 1 (hENT1) enhances gemcitabine response in human pancreatic cancer. *Biochem Pharmacol* 2008;76:322-9.
- [130] Veltkamp SA, Pluim D, van Eijndhoven MA, Bolijn MJ, Ong FH, Govindarajan R, et al. New insights into the pharmacology and cytotoxicity of gemcitabine and 2',2'-difluorodeoxyuridine. *Mol Cancer Ther* 2008;7:2415-25.
- [131] Galmarini CM, Thomas X, Calvo F, Rousselot P, Rabilloud M, El Jaffari A, et al. In vivo mechanisms of resistance to cytarabine in acute myeloid leukaemia. *Br J Haematol* 2002;117:860-8.

- [132] Oguri T, Achiwa H, Muramatsu H, Ozasa H, Sato S, Shimizu S, et al. The absence of human equilibrative nucleoside transporter 1 expression predicts nonresponse to gemcitabine-containing chemotherapy in non-small cell lung cancer. *Cancer Lett* 2007;256:112-9.
- [133] Mackey JR, Galmarini CM, Graham KA, Joy AA, Delmer A, Dabbagh L, et al. Quantitative analysis of nucleoside transporter and metabolism gene expression in chronic lymphocytic leukemia (CLL): identification of fludarabine-sensitive and -insensitive populations. *Blood* 2005;105:767-74.
- [134] Tsang RY, Santos C, Ghosh S, Dabbagh L, King K, Young J, et al. Immunohistochemistry for human concentrative nucleoside transporter 3 protein predicts fludarabine sensitivity in chronic lymphocytic leukemia. *Mod Pathol* 2008;21:1387-93.
- [135] Farrell JJ, Elsaleh H, Garcia M, Lai R, Ammar A, Regine WF, et al. Human equilibrative nucleoside transporter 1 levels predict response to gemcitabine in patients with pancreatic cancer. *Gastroenterology* 2009;136:187-95.
- [136] Giovannetti E, Del Tacca M, Mey V, Funel N, Nannizzi S, Ricci S, et al. Transcription analysis of human equilibrative nucleoside transporter-1 predicts survival in pancreas cancer patients treated with gemcitabine. *Cancer Res* 2006;66:3928-35.
- [137] Marechal R, Mackey JR, Lai R, Demetter P, Peeters M, Polus M, et al. Human equilibrative nucleoside transporter 1 and human concentrative nucleoside transporter 3 predict survival after adjuvant gemcitabine therapy in resected pancreatic adenocarcinoma. *Clin Cancer Res* 2009;15:2913-9.
- [138] Spratlin J, Sangha R, Glubrecht D, Dabbagh L, Young JD, Dumontet C, et al. The absence of human equilibrative nucleoside transporter 1 is associated with reduced survival in patients with gemcitabine-treated pancreas adenocarcinoma. *Clin Cancer Res* 2004;10:6956-61.
- [139] Herzog H, Elmenhorst D, Winz O, Bauer A. Biodistribution and radiation dosimetry of the A1 adenosine receptor ligand 18F-CPFPX determined from human whole-body PET. *Eur J Nucl Med Mol Imaging* 2008;35:1499-506.
- [140] Kiesewetter DO, Lang L, Ma Y, Bhattacharjee AK, Gao ZG, Joshi BV, et al. Synthesis and characterization of [76Br]-labeled high-affinity A3 adenosine receptor ligands for positron emission tomography. *Nucl Med Biol* 2009;36:3-10.

- [141] Todde S, Moresco RM, Simonelli P, Baraldi PG, Cacciari B, Spalluto G, et al. Design, radiosynthesis, and biodistribution of a new potent and selective ligand for in vivo imaging of the adenosine A(2A) receptor system using positron emission tomography. *J Med Chem* 2000;43:4359-62.
- [142] Reischl G, Dorow DS, Cullinane C, Katsifis A, Roselt P, Binns D, et al. Imaging of tumor hypoxia with [124I]IAZA in comparison with [18F]FMISO and [18F]FAZA--first small animal PET results. *J Pharm Pharm Sci* 2007;10:203-11.
- [143] Sorger D, Patt M, Kumar P, Wiebe LI, Barthel H, Seese A, et al. [18F]Fluoroazomycin-arabinofuranoside (18FAZA) and [18F]Fluoromisonidazole (18FMISO): a comparative study of their selective uptake in hypoxic cells and PET imaging in experimental rat tumors. *Nucl Med Biol* 2003;30:317-26.
- [144] Laing RE, Walter MA, Campbell DO, Herschman HR, Satyamurthy N, Phelps ME, et al. Noninvasive prediction of tumor responses to gemcitabine using positron emission tomography. *Proc Natl Acad Sci U S A* 2009;106:2847-52.
- [145] Bading JR, Shields AF. Imaging of cell proliferation: status and prospects. *J Nucl Med* 2008;49 Suppl 2:64S-80S.
- [146] Depresseux JC. The positron emission tomography and its applications. *J Belge Radiol* 1977;60:483-500.
- [147] Raichle ME. Positron emission tomography. *Annu Rev Neurosci* 1983;6:249-67.
- [148] Saha GB, MacIntyre WJ, Go RT. Cyclotrons and positron emission tomography radiopharmaceuticals for clinical imaging. *Semin Nucl Med* 1992;22:150-61.
- [149] Lewellen TK. Recent developments in PET detector technology. *Phys Med Biol* 2008;53:R287-317.
- [150] Gundlich B, Musmann P, Weber S, Nix O, Semmler W. From 2D PET to 3D PET: issues of data representation and image reconstruction. *Z Med Phys* 2006;16:31-46.
- [151] Zaidi H, Hasegawa B. Determination of the attenuation map in emission tomography. *J Nucl Med* 2003;44:291-315.
- [152] Zaidi H, Koral KF. Scatter modelling and compensation in emission tomography. *Eur J Nucl Med Mol Imaging* 2004;31:761-82.

- [153] Bertout JA, Patel SA, Simon MC. The impact of O₂ availability on human cancer. *Nat Rev Cancer* 2008;8:967-75.
- [154] Vaupel P, Mayer A. Hypoxia in cancer: significance and impact on clinical outcome. *Cancer Metastasis Rev* 2007;26:225-39.
- [155] Vaupel P, Mayer A, Hockel M. Tumor hypoxia and malignant progression. *Methods Enzymol* 2004;381:335-54.
- [156] Harrison L, Blackwell K. Hypoxia and anemia: factors in decreased sensitivity to radiation therapy and chemotherapy? *Oncologist* 2004;9 Suppl 5:31-40.
- [157] Vaupel P, Mayer A. Hypoxia and anemia: effects on tumor biology and treatment resistance. *Transfus Clin Biol* 2005;12:5-10.
- [158] Rasey JS, Koh WJ, Grierson JR, Grunbaum Z, Krohn KA. Radiolabelled fluoromisonidazole as an imaging agent for tumor hypoxia. *Int J Radiat Oncol Biol Phys* 1989;17:985-91.
- [159] Nunn A, Linder K, Strauss HW. Nitroimidazoles and imaging hypoxia. *Eur J Nucl Med* 1995;22:265-80.
- [160] Postema EJ, McEwan AJ, Riauka TA, Kumar P, Richmond DA, Abrams DN, et al. Initial results of hypoxia imaging using 1-alpha-D: -(5-deoxy-5-[(18)F]-fluoroarabinofuranosyl)-2-nitroimidazole ((18)F-FAZA). *Eur J Nucl Med Mol Imaging* 2009.
- [161] Ruiz van Haperen VW, Veerman G, Eriksson S, Boven E, Stegmann AP, Hermsen M, et al. Development and molecular characterization of a 2',2'-difluorodeoxycytidine-resistant variant of the human ovarian carcinoma cell line A2780. *Cancer Res* 1994;54:4138-43.
- [162] Ignatiadis M, Sotiriou C. Understanding the molecular basis of histologic grade. *Pathobiology* 2008;75:104-11.
- [163] Pich A, Chiusa L, Navone R. Prognostic relevance of cell proliferation in head and neck tumors. *Ann Oncol* 2004;15:1319-29.
- [164] Qin LX, Tang ZY. The prognostic molecular markers in hepatocellular carcinoma. *World J Gastroenterol* 2002;8:385-92.
- [165] Lederer B, Butterich D, Moore GW, Mittermayer C. Autoradiographic studies on the incorporation rate of 3H thymidine during the S-phase of the mitotic cycle. *Beitr Pathol* 1970;141:75-80.
- [166] Dolbeare F. Bromodeoxyuridine: a diagnostic tool in biology and medicine, Part III. Proliferation in normal, injured and diseased tissue,

growth factors, differentiation, DNA replication sites and in situ hybridization. *Histochem J* 1996;28:531-75.

- [167] Scholzen T, Gerdes J. The Ki-67 protein: from the known and the unknown. *J Cell Physiol* 2000;182:311-22.
- [168] Arner ES, Eriksson S. Mammalian deoxyribonucleoside kinases. *Pharmacol Ther* 1995;67:155-86.
- [169] Larson SM, Weiden PL, Grunbaum Z, Rasey JS, Kaplan HG, Graham MM, et al. Positron imaging feasibility studies. I: Characteristics of [3H]thymidine uptake in rodent and canine neoplasms: concise communication. *J Nucl Med* 1981;22:869-74.
- [170] Shields AF, Larson SM, Grunbaum Z, Graham MM. Short-term thymidine uptake in normal and neoplastic tissues: studies for PET. *J Nucl Med* 1984;25:759-64.
- [171] Vander Borgh T, Pauwels S, Lambotte L, Labar D, De Maeght S, Stroobandt G, et al. Brain tumor imaging with PET and 2-[carbon-11]thymidine. *J Nucl Med* 1994;35:974-82.
- [172] Wells JM, Mankoff DA, Eary JF, Spence AM, Muzi M, O'Sullivan F, et al. Kinetic analysis of 2-[11C]thymidine PET imaging studies of malignant brain tumors: preliminary patient results. *Mol Imaging* 2002;1:145-50.
- [173] Goethals P, van Eijkeren M, Lodewyck W, Dams R. Measurement of [methyl-carbon-11]thymidine and its metabolites in head and neck tumors. *J Nucl Med* 1995;36:880-2.
- [174] Shields AF, Graham MM, Kozawa SM, Kozell LB, Link JM, Swenson ER, et al. Contribution of labeled carbon dioxide to PET imaging of carbon-11-labeled compounds. *J Nucl Med* 1992;33:581-4.
- [175] Mercer JR, Knaus EE, Wiebe LI. Synthesis and tumor uptake of 5-halo-1-(2'-fluoro-2'-deoxy-beta-D-ribofuranosyl)[2-14C]uracils. *J Med Chem* 1987;30:670-5.
- [176] Shields AF, Grierson JR, Kozawa SM, Zheng M. Development of labeled thymidine analogs for imaging tumor proliferation. *Nucl Med Biol* 1996;23:17-22.
- [177] Conti PS, Alauddin MM, Fissekis JR, Schmall B, Watanabe KA. Synthesis of 2'-fluoro-5-[11C]-methyl-1-beta-D-arabinofuranosyluracil ([11C]-FMAU): a potential nucleoside analog for in vivo study of cellular proliferation with PET. *Nucl Med Biol* 1995;22:783-9.

- [178] Bading JR, Shahinian AH, Bathija P, Conti PS. Pharmacokinetics of the thymidine analog 2'-fluoro-5-[(14)C]-methyl-1-beta-D-arabinofuranosyluracil ([14C]FMAU) in rat prostate tumor cells. *Nucl Med Biol* 2000;27:361-8.
- [179] Bading JR, Shahinian AH, Vail A, Bathija P, Koszalka GW, Koda RT, et al. Pharmacokinetics of the thymidine analog 2'-fluoro-5-methyl-1-beta-D-arabinofuranosyluracil (FMAU) in tumor-bearing rats. *Nucl Med Biol* 2004;31:407-18.
- [180] Sun H, Sloan A, Mangner TJ, Vaishampayan U, Muzik O, Collins JM, et al. Imaging DNA synthesis with [18F]FMAU and positron emission tomography in patients with cancer. *Eur J Nucl Med Mol Imaging* 2005;32:15-22.
- [181] Wang J, Eriksson S. Phosphorylation of the anti-hepatitis B nucleoside analog 1-(2'-deoxy-2'-fluoro-1-beta-D-arabinofuranosyl)-5-iodouracil (FIAU) by human cytosolic and mitochondrial thymidine kinase and implications for cytotoxicity. *Antimicrob Agents Chemother* 1996;40:1555-7.
- [182] Gratzner HG. Monoclonal antibody to 5-bromo- and 5-iododeoxyuridine: A new reagent for detection of DNA replication. *Science* 1982;218:474-5.
- [183] Bergstrom M, Lu L, Fasth KJ, Wu F, Bergstrom-Pettermann E, Tolmachev V, et al. In vitro and animal validation of bromine-76-bromodeoxyuridine as a proliferation marker. *J Nucl Med* 1998;39:1273-9.
- [184] Lu L, Bergstrom M, Fasth KJ, Langstrom B. Synthesis of [76Br]bromofluorodeoxyuridine and its validation with regard to uptake, DNA incorporation, and excretion modulation in rats. *J Nucl Med* 2000;41:1746-52.
- [185] Nimmagadda S, Mangner TJ, Sun H, Klecker RW, Jr., Muzik O, Lawhorn-Crews JM, et al. Biodistribution and radiation dosimetry estimates of 1-(2'-deoxy-2'-(18)F-Fluoro-1-beta-D-arabinofuranosyl)-5-bromouracil: PET imaging studies in dogs. *J Nucl Med* 2005;46:1916-22.
- [186] Johansson NG, Eriksson S. Structure-activity relationships for phosphorylation of nucleoside analogs to monophosphates by nucleoside kinases. *Acta Biochim Pol* 1996;43:143-60.
- [187] Bazin H, Chattopadhyaya J, Datema R, Ericson AC, Gilljam G, Johansson NG, et al. An analysis of the inhibition of replication of HIV and MuLV by some 3'-blocked pyrimidine analogs. *Biochem Pharmacol* 1989;38:109-19.

- [188] Been LB, Suurmeijer AJ, Cobben DC, Jager PL, Hoekstra HJ, Elsinga PH. [18F]FLT-PET in oncology: current status and opportunities. *Eur J Nucl Med Mol Imaging* 2004;31:1659-72.
- [189] Flexner C, van der Horst C, Jacobson MA, Powderly W, Duncanson F, Ganes D, et al. Relationship between plasma concentrations of 3'-deoxy-3'-fluorothymidine (alovudine) and antiretroviral activity in two concentration-controlled trials. *J Infect Dis* 1994;170:1394-403.
- [190] Shields AF, Grierson JR, Dohmen BM, Machulla HJ, Stayanoff JC, Lawhorn-Crews JM, et al. Imaging proliferation in vivo with [F-18]FLT and positron emission tomography. *Nat Med* 1998;4:1334-6.
- [191] Salskov A, Tammisetti VS, Grierson J, Vesselle H. FLT: measuring tumor cell proliferation in vivo with positron emission tomography and 3'-deoxy-3'-[18F]fluorothymidine. *Semin Nucl Med* 2007;37:429-39.
- [192] Shields AF, Briston DA, Chandupatla S, Douglas KA, Lawhorn-Crews J, Collins JM, et al. A simplified analysis of [18F]3'-deoxy-3'-fluorothymidine metabolism and retention. *Eur J Nucl Med Mol Imaging* 2005;32:1269-75.
- [193] Schinazi RF, Boudinot FD, Doshi KJ, McClure HM. Pharmacokinetics of 3'-fluoro-3'-deoxythymidine and 3'-deoxy-2',3'-didehydrothymidine in rhesus monkeys. *Antimicrob Agents Chemother* 1990;34:1214-9.
- [194] Kong XB, Zhu QY, Vidal PM, Watanabe KA, Polsky B, Armstrong D, et al. Comparisons of anti-human immunodeficiency virus activities, cellular transport, and plasma and intracellular pharmacokinetics of 3'-fluoro-3'-deoxythymidine and 3'-azido-3'-deoxythymidine. *Antimicrob Agents Chemother* 1992;36:808-18.
- [195] Eriksson S, Kierdaszuk B, Munch-Petersen B, Oberg B, Johansson NG. Comparison of the substrate specificities of human thymidine kinase 1 and 2 and deoxycytidine kinase toward antiviral and cytostatic nucleoside analogs. *Biochem Biophys Res Commun* 1991;176:586-92.
- [196] Grierson JR, Schwartz JL, Muzi M, Jordan R, Krohn KA. Metabolism of 3'-deoxy-3'-[F-18]fluorothymidine in proliferating A549 cells: validations for positron emission tomography. *Nucl Med Biol* 2004;31:829-37.
- [197] Sundseth R, Joyner SS, Moore JT, Dornsife RE, Dev IK. The anti-human immunodeficiency virus agent 3'-fluorothymidine induces DNA damage and apoptosis in human lymphoblastoid cells. *Antimicrob Agents Chemother* 1996;40:331-5.
- [198] Toyohara J, Waki A, Takamatsu S, Yonekura Y, Magata Y, Fujibayashi Y. Basis of FLT as a cell proliferation marker: comparative uptake studies

with [3H]thymidine and [3H]arabinothymidine, and cell-analysis in 22 asynchronously growing tumor cell lines. *Nucl Med Biol* 2002;29:281-7.

- [199] Barthel H, Perumal M, Latigo J, He Q, Brady F, Luthra SK, et al. The uptake of 3'-deoxy-3'-[18F]fluorothymidine into L5178Y tumours in vivo is dependent on thymidine kinase 1 protein levels. *Eur J Nucl Med Mol Imaging* 2005;32:257-63.
- [200] Vesselle H, Grierson J, Muzi M, Pugsley JM, Schmidt RA, Rabinowitz P, et al. In vivo validation of 3'-deoxy-3'-[(18)F]fluorothymidine ([18F]FLT) as a proliferation imaging tracer in humans: correlation of [18F]FLT uptake by positron emission tomography with Ki-67 immunohistochemistry and flow cytometry in human lung tumors. *Clin Cancer Res* 2002;8:3315-23.
- [201] Buck AK, Halter G, Schirrmeister H, Kotzerke J, Wurziger I, Glatting G, et al. Imaging proliferation in lung tumors with PET: 18F-FLT versus 18F-FDG. *J Nucl Med* 2003;44:1426-31.
- [202] Yamamoto Y, Nishiyama Y, Ishikawa S, Gotoh M, Bandoh S, Kanaji N, et al. 3'-Deoxy-3'-18F-fluorothymidine as a proliferation imaging tracer for diagnosis of lung tumors: comparison with 2-deoxy-2-18f-fluoro-D-glucose. *J Comput Assist Tomogr* 2008;32:432-7.
- [203] Yamamoto Y, Nishiyama Y, Ishikawa S, Nakano J, Chang SS, Bandoh S, et al. Correlation of 18F-FLT and 18F-FDG uptake on PET with Ki-67 immunohistochemistry in non-small cell lung cancer. *Eur J Nucl Med Mol Imaging* 2007;34:1610-6.
- [204] Yap CS, Czernin J, Fishbein MC, Cameron RB, Schiepers C, Phelps ME, et al. Evaluation of thoracic tumors with 18F-fluorothymidine and 18F-fluorodeoxyglucose-positron emission tomography. *Chest* 2006;129:393-401.
- [205] Everitt S, Hicks RJ, Ball D, Kron T, Schneider-Kolsky M, Walter T, et al. Imaging Cellular Proliferation During Chemo-Radiotherapy: A Pilot Study of Serial (18)F-FLT Positron Emission Tomography/Computed Tomography Imaging for Non-Small-Cell Lung Cancer. *Int J Radiat Oncol Biol Phys* 2009.
- [206] Sohn HJ, Yang YJ, Ryu JS, Oh SJ, Im KC, Moon DH, et al. [18F]Fluorothymidine positron emission tomography before and 7 days after gefitinib treatment predicts response in patients with advanced adenocarcinoma of the lung. *Clin Cancer Res* 2008;14:7423-9.
- [207] Smyczek-Gargya B, Fersis N, Dittmann H, Vogel U, Reischl G, Machulla HJ, et al. PET with [18F]fluorothymidine for imaging of primary breast cancer: a pilot study. *Eur J Nucl Med Mol Imaging* 2004;31:720-4.

- [208] Kenny LM, Vigushin DM, Al-Nahhas A, Osman S, Luthra SK, Shousha S, et al. Quantification of cellular proliferation in tumor and normal tissues of patients with breast cancer by [18F]fluorothymidine-positron emission tomography imaging: evaluation of analytical methods. *Cancer Res* 2005;65:10104-12.
- [209] Kenny L, Coombes RC, Vigushin DM, Al-Nahhas A, Shousha S, Aboagye EO. Imaging early changes in proliferation at 1 week post chemotherapy: a pilot study in breast cancer patients with 3'-deoxy-3'-[18F]fluorothymidine positron emission tomography. *Eur J Nucl Med Mol Imaging* 2007;34:1339-47.
- [210] Pio BS, Park CK, Pietras R, Hsueh WA, Satyamurthy N, Pegram MD, et al. Usefulness of 3'-[F-18]fluoro-3'-deoxythymidine with positron emission tomography in predicting breast cancer response to therapy. *Mol Imaging Biol* 2006;8:36-42.
- [211] Chen W, Cloughesy T, Kamdar N, Satyamurthy N, Bergsneider M, Liau L, et al. Imaging proliferation in brain tumors with 18F-FLT PET: comparison with 18F-FDG. *J Nucl Med* 2005;46:945-52.
- [212] Choi SJ, Kim JS, Kim JH, Oh SJ, Lee JG, Kim CJ, et al. [18F]3'-deoxy-3'-fluorothymidine PET for the diagnosis and grading of brain tumors. *Eur J Nucl Med Mol Imaging* 2005;32:653-9.
- [213] Muzi M, Spence AM, O'Sullivan F, Mankoff DA, Wells JM, Grierson JR, et al. Kinetic analysis of 3'-deoxy-3'-18F-fluorothymidine in patients with gliomas. *J Nucl Med* 2006;47:1612-21.
- [214] Saga T, Kawashima H, Araki N, Takahashi JA, Nakashima Y, Higashi T, et al. Evaluation of primary brain tumors with FLT-PET: usefulness and limitations. *Clin Nucl Med* 2006;31:774-80.
- [215] Hatakeyama T, Kawai N, Nishiyama Y, Yamamoto Y, Sasakawa Y, Ichikawa T, et al. 11C-methionine (MET) and 18F-fluorothymidine (FLT) PET in patients with newly diagnosed glioma. *Eur J Nucl Med Mol Imaging* 2008;35:2009-17.
- [216] Ullrich R, Backes H, Li H, Kracht L, Miletic H, Kesper K, et al. Glioma proliferation as assessed by 3'-fluoro-3'-deoxy-L-thymidine positron emission tomography in patients with newly diagnosed high-grade glioma. *Clin Cancer Res* 2008;14:2049-55.
- [217] Chen W, Delaloye S, Silverman DH, Geist C, Czernin J, Sayre J, et al. Predicting treatment response of malignant gliomas to bevacizumab and irinotecan by imaging proliferation with [18F] fluorothymidine positron emission tomography: a pilot study. *J Clin Oncol* 2007;25:4714-21.

- [218] Quon A, Chang ST, Chin F, Kamaya A, Dick DW, Loo BW, Jr., et al. Initial evaluation of 18F-fluorothymidine (FLT) PET/CT scanning for primary pancreatic cancer. *Eur J Nucl Med Mol Imaging* 2008;35:527-31.
- [219] Herrmann K, Eckel F, Schmidt S, Scheidhauer K, Krause BJ, Kleeff J, et al. In vivo characterization of proliferation for discriminating cancer from pancreatic pseudotumors. *J Nucl Med* 2008;49:1437-44.
- [220] Wagner M, Seitz U, Buck A, Neumaier B, Schultheiss S, Bangerter M, et al. 3'-[18F]fluoro-3'-deoxythymidine ([18F]-FLT) as positron emission tomography tracer for imaging proliferation in a murine B-Cell lymphoma model and in the human disease. *Cancer Res* 2003;63:2681-7.
- [221] Buck AK, Bommer M, Stilgenbauer S, Juweid M, Glatting G, Schirrmeister H, et al. Molecular imaging of proliferation in malignant lymphoma. *Cancer Res* 2006;66:11055-61.
- [222] Kasper B, Egerer G, Gronkowski M, Haufe S, Lehnert T, Eisenhut M, et al. Functional diagnosis of residual lymphomas after radiochemotherapy with positron emission tomography comparing FDG- and FLT-PET. *Leuk Lymphoma* 2007;48:746-53.
- [223] Herrmann K, Wieder HA, Buck AK, Schoffel M, Krause BJ, Fend F, et al. Early response assessment using 3'-deoxy-3'-[18F]fluorothymidine-positron emission tomography in high-grade non-Hodgkin's lymphoma. *Clin Cancer Res* 2007;13:3552-8.
- [224] Buck AK, Herrmann K, Buschenfelde CM, Juweid ME, Bischoff M, Glatting G, et al. Imaging bone and soft tissue tumors with the proliferation marker [18F]fluorodeoxythymidine. *Clin Cancer Res* 2008;14:2970-7.
- [225] Cobben DC, Elsinga PH, Suurmeijer AJ, Vaalburg W, Maas B, Jager PL, et al. Detection and grading of soft tissue sarcomas of the extremities with (18)F-3'-fluoro-3'-deoxy-L-thymidine. *Clin Cancer Res* 2004;10:1685-90.
- [226] Been LB, Suurmeijer AJ, Elsinga PH, Jager PL, van Ginkel RJ, Hoekstra HJ. 18F-fluorodeoxythymidine PET for evaluating the response to hyperthermic isolated limb perfusion for locally advanced soft-tissue sarcomas. *J Nucl Med* 2007;48:367-72.
- [227] Cobben DC, Jager PL, Elsinga PH, Maas B, Suurmeijer AJ, Hoekstra HJ. 3'-18F-fluoro-3'-deoxy-L-thymidine: a new tracer for staging metastatic melanoma? *J Nucl Med* 2003;44:1927-32.
- [228] Mijnhout GS, Hoekstra OS, van Tulder MW, Teule GJ, Deville WL. Systematic review of the diagnostic accuracy of (18)F-fluorodeoxyglucose

positron emission tomography in melanoma patients. *Cancer* 2001;91:1530-42.

- [229] Kameyama R, Yamamoto Y, Izuishi K, Takebayashi R, Hagiike M, Murota M, et al. Detection of gastric cancer using 18F-FLT PET: comparison with 18F-FDG PET. *Eur J Nucl Med Mol Imaging* 2009;36:382-8.
- [230] Linecker A, Kermer C, Sulzbacher I, Angelberger P, Kletter K, Dudczak R, et al. Uptake of (18)F-FLT and (18)F-FDG in primary head and neck cancer correlates with survival. *Nuklearmedizin* 2008;47:80-5; quiz N12.
- [231] van Westreenen HL, Cobben DC, Jager PL, van Dullemen HM, Wesseling J, Elsinga PH, et al. Comparison of 18F-FLT PET and 18F-FDG PET in esophageal cancer. *J Nucl Med* 2005;46:400-4.
- [232] Vickers MF, Yao SY, Baldwin SA, Young JD, Cass CE. Nucleoside transporter proteins of *Saccharomyces cerevisiae*. Demonstration of a transporter (FUI1) with high uridine selectivity in plasma membranes and a transporter (FUN26) with broad nucleoside selectivity in intracellular membranes. *J Biol Chem* 2000;275:25931-8.
- [233] Jarvis SM, Griffith DA. Expression of the rabbit intestinal N2 Na⁺/nucleoside transporter in *Xenopus laevis* oocytes. *Biochem J* 1991;278 (Pt 2):605-7.
- [234] Slugoski MD, Loewen SK, Ng AM, Smith KM, Yao SY, Karpinski E, et al. Specific mutations in transmembrane helix 8 of human concentrative Na⁺/nucleoside cotransporter hCNT1 affect permeant selectivity and cation coupling. *Biochemistry* 2007;46:1684-93.
- [235] Yao SY, Ng AM, Sundaram M, Cass CE, Baldwin SA, Young JD. Transport of antiviral 3'-deoxy-nucleoside drugs by recombinant human and rat equilibrative, nitrobenzylthioinosine (NBMPR)-insensitive (ENT2) nucleoside transporter proteins produced in *Xenopus* oocytes. *Mol Membr Biol* 2001;18:161-7.
- [236] Phelps ME. PET: a biological imaging technique. *Neurochem Res* 1991;16:929-40.

Chapter 2: Materials and methods

2.1 Materials

Research grade 3'-deoxy-3'-fluorothymidine (FLT), N-methyl-D-glucamine (NMDG), dilazep, nitrobenzylmercaptapurine ribonucleoside (NBMPR), bovine serum albumin (BSA), dimethyl sulfoxide, ampicillin, glucose, CuSO₄, lithium carbonate, 4-(2-hydroxyethyl)-1-piperazineethanesulfonic acid (HEPES), 5-iodo-2'-deoxyuridine, deoxycholate, dithiothreitol, phenylmethylsulphonyl fluoride and, unless otherwise indicated, all nucleosides and amino acids were purchased from Sigma-Aldrich (St. Louis, MO). Gemcitabine was provided by Eli Lilly (Indianapolis, IN). Sodium dodecyl sulfate (SDS), NaCl, sodium bicarbonate, ethylenedinitrilotetraacetic acid (EDTA), Tween 20, H₂O₂, formic acid, NaOH, and methanol were obtained from Fisher Scientific (Fair Lawn, NJ). Xylene, Na₂HPO₄, KH₂PO₄, ZnCl₂, and KOH were obtained from BDH Inc. (Toronto, ON). Haematoxylin was obtained from Inter-Medica (Markham, ON) while Nonidet P-40 was obtained from Calbiochem-Novabiochem Corporation (La Jolla, CA). Dako "Antibody Diluent with Background Reducing Components" solution, diamino-benzidine solution, DAKO tris(hydroxymethyl)aminomethane (Tris) buffer, and Dako "EnVision+ System-HRP (DAB) for Use with Rabbit Primary Antibodies" solution were obtained from Dako (Glostrup, Denmark). DNA staining dye 4',6-diamidino-2-phenylindole (DAPI) was acquired from Molecular Probes (Eugene, OR). Bacto™ Peptone, Bacto™ Yeast Extract, Bacto™ Agar, Matrigel™ Basement Membrane Matrix High Concentration, and BD Vacutainer™ sodium heparin tubes were obtained from Becton Dickinson (Franklin Lakes, NY). Yeast nitrogen

base was obtained from Difco (Detroit, MI). KCl was obtained from Caledon Laboratories Ltd. (Georgetown, ON). Tris HCl was obtained from Invitrogen (Carlsbad, CA). Skim milk powder was obtained from Safeway Inc. (Pleasanton, CA). Complete protease inhibitor cocktail tablets and FuGENE[®] 6 Transfection Regent were obtained from Roche Applied Science (Penzberg, Germany). Acetonitrile and glacial acetic acid were obtained from EMD Chemicals Inc. (Darmstadt, Germany). Isoflurane was obtained from Benson Medical Industries Inc. (Markham, ON). Bio-Rad protein assay dye and 30% acrylamide solution were obtained from Bio-Rad Laboratories (Hercules, CA). NBMPR analog 5-*S*-{2-(1-[(fluorescein-5-yl)thioureido]hexanamido)ethyl}-6-*N*-(4-nitrobenzyl)-5-thioadenosine (FTH-SAENTA) was synthesized and provided by Dr. Morris Robins (Brigham Young University, Provo, UT) and NBMPR phosphate (NBMPR-P) was provided by Dr. Wendy Gati (University of Alberta, Edmonton, AB). Cell culture reagents including Roswell Park Memorial Institute (RPMI) 1640 medium, Dulbecco's modified Eagle's medium (DMEM), McCoy's 5A medium, fetal bovine serum (FBS), calf serum (CS), horse serum, goat serum, and geneticin were purchased from Gibco (Carlsbad, CA).

Polyclonal antibodies against individual mouse nucleoside transporters (NTs) were generated by immunizing rabbits with carrier proteins conjugated to synthetic mouse NT peptide fragments based on sequence information for mouse equilibrative nucleoside transporter 2 (mENT2), mouse concentrative nucleoside transporter 1 (mCNT1), and mCNT3 corresponding to amino acids 261-278, 30-55, and 61-84, respectively. Mouse polyclonal antibodies against mouse

thymidine kinase 1 were purchased from Abcam, Inc. (Cambridge, MA) and mouse monoclonal antibodies against β -actin were purchased from Ambion (Austin, TX). Peroxidase-conjugated goat anti-mouse IgG antibodies were purchased from Jackson ImmunoResearch Laboratories, Inc (West Grove, PA).

Radioactive compounds including [methyl- ^3H (N)]-3'-deoxy-3'-fluorothymidine (^3H FLT), [methyl- ^3H]-thymidine (^3H thymidine), [5, 6- ^3H]-uridine (^3H uridine), and [^3H (G)]-S-(p-nitrobenzyl)-6-thioinosine (^3H NBMPR) were purchased from Moravек Biochemicals (Brea, CA). [^{18}F]FLT radiosynthesis was carried out at the Edmonton PET Center according to the procedure of *Machulla et al.* [1] using a TracerLab-FX automated synthesis unit (GE Healthcare, Little Chalfont, United Kingdom) and 5'-O-(4,4'-dimethoxytrityl)-2,3'-anhydrothymidine as a precursor (ABX GmbH, Radeberg, Germany).

2.2 Cell culture

Due to the potential utility of FLT PET in lung, breast, and brain cancers [2], A549, MCF-7, and U251 cells, which were derived from a lung carcinoma, breast adenocarcinoma, and glioblastoma, respectively, were used in studies of FLT uptake. In addition, the pancreatic carcinoma cell lines Capan-2, AsPC-1, BxPC-3, PL45, MIA PaCa-2, and PANC-1 were also included since FLT PET may have applications in treatment planning of pancreatic cancer. The renal carcinoma cell line A498 was included because it is one of the few cell lines known to possess hCNT3, which is capable of transporting FLT, and FLT PET may be useful for detecting renal tumors [3]. All cell lines were obtained from the American Type Culture Collection (Manassas, VA).

Cells were subcultured every 2-4 days under aseptic conditions using class 2 biological safety cabinets. All solutions and buffers used in maintaining cells were sterilized by passage through 0.2 μm filters. MCF-7, A549, U251, A498, AsPC-1, BxPC-3, and PL45 cells were maintained in antibiotic-free RPMI 1640 medium containing 10% (v/v) FBS; MIA PaCa-2 cells and PANC-1 cells were maintained in antibiotic-free DMEM medium containing 10% (v/v) FBS; and Capan-2 cells were maintained in antibiotic-free McCoy's 5A medium with 10% (v/v) FBS. Cells were cultured at 37°C in humidified incubators with 5% CO₂. Cells used as stocks were kept in their respective medium with 5-10% dimethyl sulfoxide and placed in liquid nitrogen. Cell stocks were periodically tested for *Mycoplasma* using DAPI staining to ensure *Mycoplasma*-free cells were used in experiments.

2.2.1 Generation of A549-pSUPER-SC and A549-pSUPER-hENT1 cell lines

To knockdown hENT1 in A549 cells, the pSUPER.neo+green fluorescence protein (GFP) vector (Oligoengine, Seattle, WA) was stably transfected into A549 cells following manufacturer's instructions. Briefly, two complementary 60-nucleotide oligomers for the control vector (5'-GAT CCC CAG CGC ACT CCG TTC TTC ATT TCA AGA GAT TGA AGA ACG GAG TGC GCT TTT TTA-3' and 5'-AGC TTA AAA AAG CGC ACT CCG TTC TTC ATT CTC TTG AAT TGA AGA ACG GAG TGC GCT GGG-3') and for the hENT1 vector (5'-GAT CCC CCG GGC AAT TGT GTG ACA AAT TCA AGA GAT TTG TCA CAC AAT TGC CCG TTT TTA-3' and 5'-AGC TTA AAA ACG GGC AAT TGT GTG ACA AAT CTC TTG AAT TTG TCA CAC

AAT TGC CCG GGG-3') were purchased from Oligoengine (Seattle, WA) and dissolved in sterile water at 3 mg/ml. For each pair of oligomers, 1 µl of oligomer mixtures were incubated together in 48 µl of annealing buffer (100 mM NaCl and 50 mM HEPES pH 7.4) and then incubated at 90°C for 4 min, 70°C for 10 min, 37°C for 20 min, and room temperature for 10 min. Annealed oligomers were ligated into linearized pSUPER vector by incubating 2 µl of annealed oligomers, 0.5 µg of pSUPER vector, 400 units of T4 DNA ligase (New England BioLabs Inc., Pickering, ON), 1 µl of T4 DNA ligase buffer, and 5 µl of nuclease-free water in PCR reaction tubes. Ligation mixtures were left at room temperature overnight and the pSUPER-SC (control) and pSUPER-hENT1 (hENT1 short hairpin RNA) vectors were generated.

Circularized pSUPER vectors were transformed into Fusion-Blue competent cells (*Escherichia coli* K-12 strain, Clontech Laboratories, Inc., Mountain View, CA) according to the manufacturer's instructions and transformed bacterial cells were grown in 100 µg/ml ampicillin-containing lysogeny broth plates overnight at 37°C. Individual colonies were picked and expanded in 5 ml of 100 µg/ml ampicillin-containing LB medium overnight at 37°C. Plasmids from the bacterial cultures were isolated using the QIAprep Miniprep kit (Qiagen, Germantown, MD) following the manufacturer's instructions. The identity of plasmid inserts were verified by DNA sequencing using an ABI PRISM 310 sequence detection system (PerkinElmer Life and Analytical Sciences, Boston, MA).

A549 cells were transfected with either pSUPER-SC or pSUPER-hENT1 using the FuGENE[®] 6 Transfection Reagent according to manufacturer's instructions and 24 h after transfection, cells were grown in RPMI + 10% FBS medium with 350 µg/ml of geneticin for at least two weeks to select for transfected cells. Individual cells with geneticin resistance were obtained by limited dilution and placed in 96-well plates (approximately 1 cell/well). Cells were visually inspected for GFP fluorescence using an Olympus IX70 inverted microscope (Olympus Corporation, Tokyo, Japan) and cells within each well that displayed relatively high levels of GFP fluorescence were expanded and tested for hENT1 levels by NBMPR binding assays (section 2.6). A549 cells transfected with pSUPER-hENT1 with the smallest amount of NBMPR binding were designated A549-pSUPER-hENT1 and A549 cells transfected with pSUPER-SC that expressed the largest amount of GFP fluorescence and unchanged levels of NBMPR binding sites (compared to that of untransfected A549 cells) were designated A549-pSUPER-SC. Frozen stocks of A549-pSUPER-SC and A549-pSUPER-hENT1 cells were prepared for later use in experiments.

2.3 Protein determination assays

Bio-Rad protein assays were performed to determine protein content in biological samples. Disposable spectrophotometer plastic cuvettes had 0, 2, 4, 6, 8, or 10 µg BSA protein added in 800 µl water to create standard curves. Several microliters of samples with unknown protein content were added to other disposable cuvettes with 800 µl water. Cuvettes had 200 µl Bio-Rad protein assay dye added and all samples were thoroughly mixed and analyzed for absorbance at

595 nm light using a spectrophotometer (Beckman Coulter DU[®] 640, Beckman Coulter Inc., Fullerton, CA). Protein content in samples was determined by comparing the optical absorbance of samples to those of the standard curve. At least 2 replicates were used for each sample with unknown protein content.

2.4 Transport and uptake assays

2.4.1 Inhibitor-sensitivity assays with *Saccharomyces cerevisiae*

Inhibitor-sensitivity assays were performed as previously described [4, 5]. Briefly, yeast cultures producing a particular recombinant human NT (hNT) (see [5-7] for construction of yeast strains) were maintained in complete minimal medium (CMM) containing 0.67% (w/v) yeast nitrogen base, amino acids (to maintain auxotrophic selection) and 2% (w/v) glucose (CMM/GLU). Yeast cells were washed three times with CMM/GLU (pH 7.4), resuspended so that optical density of the culture at 600 nm was 4, and added to “preloaded” 96-well plates containing CMM/GLU (pH 7.4) with either FLT or thymidine (at desired concentrations) and [³H]uridine. Non-specific binding and uptake of [³H]uridine were determined by incubating wells with 10 mM uridine. Mediated [³H]uridine uptake was determined from the difference in [³H]uridine uptake between cells in the absence and presence of 10 mM uridine. Yeast cells producing recombinant hENT1, hENT2, hCNT1, hCNT2, or hCNT3 were incubated with [³H]uridine for 20, 20, 30, 30, or 10 min, respectively. Yeast cells producing hCNT3 displayed greater [³H]uridine uptake than the other yeast strains and were therefore incubated with [³H]uridine for a shorter duration than the other yeast strains to maintain linear initial rates of uptake. After incubation, yeast cells were harvested

and washed with a Micro96 Harvester (Skatron Intruments, Lier, Norway) and radioactivity in yeast cells was determined by liquid scintillation counting (LS 6500, Beckman Coulter, Fullerton, CA). IC_{50} values (concentration of thymidine or FLT that inhibited [3H]uridine uptake by 50%) were determined and converted to K_i values using the Cheng-Prusoff equation [8], $K_i = IC_{50}/(1+([L]/K_M))$ in which [L] was the concentration of [3H]uridine (1 μM) and apparent K_M values were obtained from previous publications (hENT1, 43 μM ; hENT2, 190 μM ; hCNT1, 9.2 μM ; hCNT2, 29 μM ; hCNT3, 8.7 μM [4, 5, 7]). Studies were not undertaken to determine if FLT has affects on uridine metabolism in yeast and it is therefore possible that FLT may have altered [3H]uridine uptake.

2.4.2 Transport and uptake in *Xenopus laevis* oocytes

Oocyte experiments were performed by Amy Ng and Sylvia Yao in Dr. James Young's laboratory (Department of Physiology, University of Alberta). hNT complementary DNAs (cDNAs) in the *Xenopus* expression vector pGEM-HE were transcribed with T7 polymerase using the mMESSAGING mMACHINETM (Ambion, Austin, TX) transcription system. Healthy defolliculated stage VI oocytes were microinjected with 20 nl water alone or containing RNA transcripts (20 ng) and incubated in modified Barth's medium (changed daily) at 18°C for 72 h prior to transport assays [9].

Transport assays were performed at room temperature on groups of 10-12 oocytes in 200 μl transport buffer as previously described [10]. Incubations were for 30 min to measure cellular uptake or 1 min to measure initial rates of transport. Unless otherwise indicated, the concentration of radiolabeled permeant

was 20 μM . Following incubation periods, oocytes were rapidly washed six times in ice-cold transport medium to remove extracellular radioactivity. Oocytes were dissolved in 5% (w/v) sodium dodecyl sulfate and measured for radioactivity by liquid scintillation counting. Presented as pmol/oocyte/30 min (cellular uptake) or pmol/oocyte/min (initial rate of transport), values were corrected for non-mediated uptake as measured in control, water-injected oocytes.

2.4.3 Transport and uptake in cultured cell lines

In Chapter 3, cells were inoculated in 12-well plates at 5×10^4 (MCF-7 and Capan-2), 4×10^4 (U251 and A498), 3×10^4 (MIA PaCa-2), and 2.5×10^4 (A549) cells/well and incubated at 37°C for 72 h in a humidified incubator with 5% CO_2 prior to using cells for uptake assays. Inoculations were at different cell densities to ensure cell confluency was similar (approximately 50%) between cell lines when experiments were performed. In Chapters 4 and 5, A549, Capan-2, AsPC-1, BxPC-3, PL45, MIA PaCa-2, and PANC-1 cells were inoculated in 24-well plates at 1×10^5 cells/well and incubated at 37°C for 24 h in a humidified incubator with 5% CO_2 prior to using cells for uptake assays. Unless otherwise indicated, 12-well plates were washed with either Na^+ buffer (20 mM Tris, 3 mM K_2HPO_4 , 5 mM glucose, and 145 mM NaCl) or NMDG buffer (20 mM Tris, 3 mM K_2HPO_4 , 5 mM glucose, and 155 mM NMDG) while 24-well plates were washed with phosphate buffered saline (PBS, 137 mM NaCl, 2.7 mM KCl, 8.1 mM Na_2HPO_4 , and 1.5 mM KH_2PO_4). Wash buffers were used at room temperature. Buffers containing [^3H]permeants were similar to wash buffers except that 24-well plates had [^3H]permeants added to DMEM + 10% CS

medium. Buffer volumes used for 12-well and 24-well plates were 1 ml/well and 0.5 ml/well, respectively.

For uptake assays, cells in plates were washed once followed by incubation for up to 45 min with buffer with or without hNT inhibitors (100 nM NBMPR or 100-200 μ M dilazep) or permeants (1-10 mM uridine, 1 mM inosine, or 1 mM thymidine, or 1 mM FLT) to allow interaction between inhibitors/permeants and hNTs. Cells were then incubated with buffer containing 74 nM to 1 μ M [3 H]permeant with or without hNT inhibitors/permeants for various time periods at 37°C. After incubation, radioactive buffer was removed and cells were washed up to three times. Cells were lysed by incubation in 0.5 M KOH for at least 45 min and cell lysates were analyzed for radioactivity by liquid scintillation counting.

Mediated [3 H]FLT uptake was determined from the difference in [3 H]FLT uptake between cells incubated without (total) or with 200 μ M dilazep and 10 mM uridine or 1 mM FLT (non-mediated). [3 H]FLT uptake inhibited by NBMPR was analyzed in concentration-effect curves, for which 100% and 0% uptake represented the largest and smallest amounts of [3 H]FLT uptake observed, respectively, over the graded concentrations of NBMPR.

2.5 Taqman quantitative real-time reverse transcriptase polymerase chain reaction (RT-PCR)

RNA was isolated from cell lines using the RNeasy kit (Qiagen, Mississauga, Ontario) according to manufacturer's instructions and 2 μ g RNA for each reaction was reverse transcribed into DNA using the TaqMan Gold RT-PCR

kit (Applied Biosystems, Foster City, CA) following the manufacturer's instructions. For each real-time PCR reaction, cDNA (0.53 μ l/well) was added to 2x TaqMan Universal PCR Master Mix (Applied Biosystems), that contained primers and probes (see Table 2-1) in a final volume of 20 μ l/well. Reactions were run in triplicate on 96-well plates using an Applied Biosystems 7900HT Fast Real-Time PCR system using standard default settings. Relative quantification of RNA was determined using the delta-delta C_T method [11] using glyceraldehyde-3-phosphate dehydrogenase (GAPDH) to control for RNA loading differences. The probes and primers for hENT1 displayed an amplification efficiency of 83%. When compared to the probes and primers for hENT1, the probes and primers of the other human genes displayed no significant differences in amplification efficiencies.

2.6 Equilibrium [3 H]NBMPR binding assays

In the experiments of Chapter 3, cells were inoculated in 12-well plates at 5×10^4 (MCF-7 and Capan-2), 4×10^4 (U251 and A498), 3×10^4 (MIA PaCa-2), and 2.5×10^4 (A549) cells/well and incubated at 37°C for 72 h in a humidified incubator with 5% CO₂ prior to NBMPR binding assays. Cells in 12-well plates were washed with Na⁺ buffer and then incubated for 90 min at 37°C with 1 ml/well Na⁺ buffer containing graded concentrations (0.1 – 2.5 nM) of [3 H]NBMPR in the presence or absence of 1 μ M NBMPR. After incubation, 50- μ l aliquots were removed from each well to determine the free concentration of [3 H]NBMPR. Radioactive buffer was removed and cells were washed and then incubated with 0.5 ml/well 0.5 M KOH for 45 min and radioactive content was

determined by liquid scintillation counting. Binding of [³H]NBMPR to cells in the presence or absence of 1 μM NBMPR represented non-specific and total binding, respectively, and the difference between the two, which represented specific binding, was used to determine binding parameters (B_{\max} and K_d values).

Equilibrium binding experiments were also performed using FTH-SAENTA to determine the relative proportions of extracellular and intracellular NBMPR binding sites. FTH-SAENTA, being membrane impermeant, only interacts with the extracellular NBMPR binding sites [12]. Cells in 12-well plates were washed twice and then incubated for 60 min with 1 ml/well Na⁺ buffer containing 10 nM [³H]NBMPR alone, 10 nM [³H]NBMPR with 100 nM FTH-SAENTA, or 10 nM [³H]NBMPR with 10 μM NBMPR. Cells were washed three times and lysed by incubation with 1 ml/well 5% Triton X-100 for at least 2 h. The radioactive content of the lysates was determined by liquid scintillation counting. Total specifically bound [³H]NBMPR (extracellular and intracellular) was calculated from the difference between [³H]NBMPR bound in the presence and absence 10 μM NBMPR. Extracellular specifically bound [³H]NBMPR was calculated from the difference of [³H]NBMPR bound with or without FTH-SAENTA. The percentage of specifically bound extracellular [³H]NBMPR was calculated as (extracellular/total bound [³H]NBMPR) x 100.

Chapters 4 and 5 used a similar equilibrium binding procedure as described above with FTH-SAENTA but with the following three modifications: 1) cells were inoculated in 24-well plates at 1 x 10⁵ cells/well and incubated at 37°C for 24 h in a humidified incubator with 5% CO₂ prior to NBMPR binding

assays, 2) 0.5 ml/well volumes were used for all solution, and 3) cells were lysed with a one hour incubation of 0.5 M KOH.

2.7 Gemcitabine toxicity assays

Gemcitabine toxicity assays were performed using the CellTiter 96[®] AQueous One Solution Cell Proliferation Assay (Promega, Madison, WI). Briefly, pancreatic cancer cells were plated on 96-well plates (Corning, Lowell, MA) at 5×10^3 cells/well. Medium was removed 24 h after inoculating cells onto 96-well plates and fresh medium (100 μ l/well) with or without graded amounts of gemcitabine (final concentrations: 10 pM-100 μ M) was added to wells with or without cells. Cells were incubated at 37°C for 72 h, after which 20 μ l [3-(4,5-dimethylthiazol-2-yl)-5-(3-carboxymethoxyphenyl)-2-(4-sulfophenyl)-2H-tetrazolium (MTS) reagent was added to the medium in each well. Plates were shaken on a Titer Plate Shaker (Lab-Line Instruments, Melrose Park, IL) on speed setting 5 for 15 s and then incubated at 37°C for up to 4 h. The 490-nm absorbance in each well was determined using a SpectroMAX 190 (Molecular Devices, Sunnyvale, CA) and absorbance values from wells without cells (background) were subtracted from values from wells with cells. Data were analyzed with GraphPad Prism software (version 4.03; GraphPad Prism, Inc., La Jolla, CA) using non-linear regression analysis to determine gemcitabine EC₅₀ values (concentration that produced 50% of maximum cell death caused by gemcitabine).

2.8 [¹⁸F]FLT uptake in mice

2.8.1 Mice models

For all small animal PET experiments, female mice of at least 10 weeks of age were used. Heterozygote ENT1^{+/-} mice were obtained from Lexicon Pharmaceuticals, Inc. (The Woodlands, TX). The gene trap method was used for gene inactivation in 129/SvEv mouse stem cells. ENT1^{-/-} mice have a retroviral vector insert between exons 2 and 3 of the mouse ENT1 (mENT1) locus. The retroviral insert contained splice acceptor and splice donor sequences that created a fusion gene which altered ENT1 function. The heterozygotes, generated in C57B16-albino mice, were subsequently back-crossed with FVB/N mice for six generations and FVB/N mice (ENT1^{+/+} mice) were therefore used as controls. ENT1^{-/-} (mENT1-m1-cec) mice were generated by crossing ENT1^{+/-} mice and selecting for ENT1^{-/-} mice.

A549 xenograft tumors were developed in NIH-III mice (Charles River Laboratories, Wilmington, MA). A549-pSUPER-SC and A549-pSUPER-hENT1 cells were 1) resuspended at 3x10⁶ cells per 100 µl with equal amounts of RPMI + 10% FBS and MatrigelTM Basement Membrane Matrix High Concentration, and 2) kept on ice. Each NIH-III mouse was anesthetized by isoflurane inhalation and injected subcutaneously with 100 µl of A549-pSUPER-SC and A549-pSUPER-hENT1 cell suspension (3x10⁶ cells) above the left and right thighs, respectively, to minimize tumor movement due to breathing during PET imaging. After three to six weeks, when tumors had reached approximately 250 mm³ in volume, mice were used for experiments.

2.8.2 [¹⁸F]FLT small animal PET

Dan McGinn, Gail Hipperson, and Melinda Wuest provided assistance in performing small animal PET experiments. For biodistribution experiments with ENT1^{+/+}, ENT1^{+/-}, and ENT1^{-/-} mice, animals were anesthetized with isoflurane and injected with 100 µl saline containing a maximum of 4% ethanol and 2-10 MBq [¹⁸F]FLT via either the jugular or lateral tail vein prior to image acquisition. Some ENT1^{+/+} mice were given an intraperitoneal injection of 15 mg/kg NBMPR-P 1 h before imaging. For each imaging experiment, one or two mice were anesthetized with isoflurane, placed in a small animal PET scanner (microPET[®] R4, Siemens preclinical solutions, Knoxville, TN), and dynamically imaged with 60-min emission scans using microPET[®] Manager 2.1.5.0 software (Siemens preclinical solutions). Frames from sinograms were reconstructed using 2D (for biodistribution experiments) or 3D (for experiments with xenograft tumor-bearing mice) ordered subset expectation maximization algorithms. For PET scans involving tumor-bearing NIH-III mice, animals were imaged as described above except that mice had catheters placed in the lateral tail veins and 60-min emission scans were started 15 s prior to ¹⁸F-FLT injection. After imaging, mice were euthanized by cardiac puncture or cervical dislocation and organs and tissues of interest were collected, weighed, and analyzed for radioactivity using a Wizard 3" 1480 automatic gamma-counter (Perkin Elmer, Waltham, MA).

2.8.3 [¹⁸F]FLT PET image analysis

The PET images were analysed by Melinda Wuest (Department of Oncology, University of Alberta) using ROVER v2.0.21 software (ABX GmbH,

Radeberg, Germany). Masks for defining three-dimensional regions of interest (ROI) were set and the ROIs were defined by thresholding. ROI time-activity curves (TAC) were generated for subsequent data analysis. Standardized uptake values [SUV = (activity/ml tissue) / (injected activity/body weight), g/ml] were calculated for each ROI.

Tracer kinetics were analyzed by Hans-Sonke Jans (Department of Oncology, Division of Medical Physics, University of Alberta) using a three-compartment model as previously described for [¹⁸F]FLT [13]. Volumes of interest were defined in each mouse for both tumors and the blood input function. ROIs for the blood input function were drawn over the heart. Kim et al. [14] reported a partial volume correction factor of 0.924 for volumes of interest drawn over a volume of 17 mm³ (3 consecutive slices of thickness 0.8 mm with a circular ROI of 3 mm diameter). Thresholding of 80% maximum over the heart was used to obtain ROIs between 5 and 15 mm³ and the volume correction factor described above was applied. The model is described by four kinetic parameters (K_1, k_2, k_3, k_4) and the fractional blood volume (fbv), which accounts for the non-zero vascular space within the tumor ROI. The analysis was carried out by fitting the measured tumor TACs with a two-exponential model of the general form:

$$TAC_{tumor} = (A_1 \exp(-\alpha_1 t) + A_2 \exp(-\alpha_2 t)) \otimes TAC_{blood} + fbv \cdot TAC_{blood} \quad (1)$$

where \otimes denotes convolution and $A_1, \alpha_1, A_2, \alpha_2$ and fbv are fit parameters representing the amplitude and time dependence of the exponentials. They are related to the kinetic parameters by:

$$\left. \begin{aligned}
\alpha_1 &= 0.5 \cdot \left(k_2 + k_3 + k_4 - \sqrt{(k_2 + k_3 + k_4)^2 - 4k_2k_4} \right) \\
\alpha_2 &= 0.5 \cdot \left(k_2 + k_3 + k_4 + \sqrt{(k_2 + k_3 + k_4)^2 - 4k_2k_4} \right) \\
A_1 &= \frac{K_1}{\alpha_2 - \alpha_1} (k_3 + k_4 - \alpha_1) \\
A_2 &= \frac{K_1}{\alpha_2 - \alpha_1} (\alpha_2 - k_3 - k_4)
\end{aligned} \right\} \quad (2)$$

The fit of equation (1) to the experimentally acquired tumor TACs was implemented in Matlab software (version 7.3; The MathWorks, Inc., Natick, MA), utilizing a Nelder-Mead simplex direct search. The fit was governed by the minimization of the sum over all time points of square differences between the measured values and the model prediction.

2.9 TK1 Immunoblotting

Spleen and tumor tissues were excised from euthanized mice and immediately frozen in liquid nitrogen. At a later date, spleen tissues were pulverized using a mortar and pestle containing liquid nitrogen and resuspended in 100 μ l lysis buffer (10 mM Tris HCl pH 7.5, 150 mM NaCl, 1% Nonidet P-40, 1% deoxycholate, 2 mM EDTA, 0.1% SDS, and protease inhibitors). Spleen samples were incubated at 4°C for 60 min followed by centrifugation at 15,000 x g for 10 min and supernatants were frozen at -80°C and used later for TK1 immunoblotting. Tumor samples were also pulverized using a mortar and pestle containing liquid nitrogen and resuspended in 1 ml swelling buffer (1 mM ZnCl₂, 10 mM Tris-HCl, 0.3 mM phenylmethylsulfonyl fluoride, 0.5 mM dithiothreitol) containing protease inhibitors. Tumor resuspensions were passed through a 21-gauge needle at least 15 times to lyse cells and lysates were centrifuged at 13,500 x g for 30 min at 4°C. The supernatants were placed in a -80°C freezer and used

later for TK1 immunoblots. Protein content in supernatants was determined using the Bio-Rad protein assay kit (Bio-Rad, Hercules, CA).

Spleen and tumor samples were heated to 95°C for 5 min, loaded at 200 and 20 µg protein per lane, respectively, and subjected to electrophoresis on 12% polyacrylamide gels. Proteins in gels were transferred onto polyvinylidene fluoride membranes and membranes were incubated overnight at 4°C in 0.2% Tween 20, Tris-buffered saline containing 5% (w/v) skim milk powder (blocking buffer). Blocked membranes were then incubated for 2 h at room temperature with blocking buffer containing antibodies against either mouse TK1 or β-actin using a 1 in 500 or 5000 dilution, respectively. Membranes were washed three times with Tris-buffered saline with 0.2% Tween 20 (15 min incubation per wash) and then incubated for 1 h with blocking buffer containing goat anti-mouse IgG antibodies conjugated with horseradish peroxidase using a 1 in 15,000 dilution. Membranes were washed three more times and proteins were visualized by incubation of membranes with ECLTM Western Blotting Detection Reagents (GE Healthcare, Little Chalfont, United Kingdom) and subsequent exposure to X-ray films.

Films were scanned and digital images were analyzed with MetaMorph Offline software (version 7.6.4.0; MDS Analytical Technologies, Concord, ON) to determine relative levels of TK1. Images had colors inverted (protein bands were brighter than the background film) and ROIs were drawn around TK1 and β-actin bands. Average band intensities were subtracted by the average intensity of a ROI with no protein bands to remove background intensity. Background-

subtracted ROI intensities for protein bands were multiplied by ROI area to determine total ROI intensity and these values for TK1 bands were divided by those of β -actin to determine normalized TK1 protein levels.

2.10 Immunohistochemistry

The immunohistochemistry procedure was performed by Lorelei Johnson (who was previously a technician in Dr. Carol Cass' laboratory) as previously described with minor modifications [15, 16]. Mice were euthanized by CO₂ inhalation and spleen tissues were excised, formalin-fixed, and paraffin-embedded. Tissue sections of 4-6 μ m were dried in an oven for 2 h at 60°C and later rehydrated for 10 min in xylene followed by brief washes with decreasing concentrations of ethanol (100-50%). Slides were rinsed in cold water and incubated in PBS-T (0.05% Tween-20 in phosphate buffered saline) for 5 min. Slides were incubated in DAKO Tris (tris(hydroxymethyl)aminomethane) buffer (pH 9.9) and heated at 100°C for 6 min, cooled in cold water, and incubated in PBS-T for 5 min. Tissue sections were blocked in PBS-T with 10% goat serum and 1% bovine serum albumin for 20 min followed by a 3-min wash with PBS-T. Slides were incubated in "Dako Antibody Diluent with Background Reducing Components" solution that contained primary antibodies at 58 μ g/ml, 60 μ g/ml, and 57 μ g/ml for mENT2, mCNT1, and mCNT3, respectively, overnight in a humidity chamber at 4°C followed by three rinses with PBS and then three washes with PBS-T for 10 min. Peroxidase blocking was achieved by incubating slides in 3% H₂O₂ for 10 min followed by a water rinse and two incubations in PBS-T for 2 min. Slides were incubated in "EnVision+ System-HRP (DAB) for

Use with Rabbit Primary Antibodies” solution for 30 min in a humidity chamber, rinsed three times with PBS, washed three times with PBS-T for 10 min, incubated in a diamino-benzidine solution, and rinsed with running water for 10 min. Slides were incubated in 1% CuSO₄ for 5 min, haematoxylin for 60 sec, and lithium carbonate for 1 min with water rinses between incubations. Samples were dehydrated through graded alcohols and xylene, and covered with coverslips. Negative controls were obtained by omitting primary antibodies from the procedure.

2.11 Liquid chromatography-mass spectrometry (LC-MS)

Plasma thymidine levels in ENT1^{+/+} and ENT1^{-/-} mice were analyzed with LC-MS as previously described [17]. Briefly, blood from ENT1^{+/+} and ENT1^{-/-} mice was collected by cardiac exsanguination and placed in pre-chilled heparin-containing tubes on ice. Blood was centrifuged at 3,300 x g at 4°C for 15 min and 200- μ l supernatants were frozen at -80°C. At a later date, supernatants were thawed and mixed with 1 ml cold acetonitrile and placed on ice for 10 min. Samples were centrifuged at 16,000 x g at 4°C for 10 min and the supernatants were transferred to new microcentrifuge tubes and alkalinized by mixing with 40 μ l 2 M NaOH. Alkalinized samples were passed through Extract-CleanTM anion-exchange solid-phase extraction columns (Grace Davison Discovery Science, Deerfield, IL) that were preconditioned with two solutions: 1 ml acetonitrile followed by 1 ml 0.01 M NaOH. Columns were rinsed with 2 ml acetonitrile and analytes were eluted with two 1 ml aliquots of 10% glacial acetic acid in water. Eluted samples were dried in a SpeedVac SC100 (Savant Instruments Inc.,

Farmingdale, NY) and resuspended in 50 μ l 10 mM formic acid in 5% (v/v) acetonitrile. Samples were centrifuged to remove debris and frozen at -80°C until their transfer to the Mass Spectrometry Laboratory in the Department of Chemistry at the University of Alberta where samples underwent LC-MS.

LC-MS was performed by Don Morgan and Randy Whittal. Sample separation was achieved with a 150 mm x 3 mm PlatinumTM C18-EPS 3 μ m column (Grace Davison Discovery Science, Deerfield, IL) on an Agilent 1100 system (Agilent Technologies, Santa Clara, CA) using a gradient mobile-phase including 10 mM formic acid in 5% acetonitrile (mobile-phase A) and acetonitrile:water (90:10; mobile-phase B) at a flow rate of 0.3 ml/min. Samples were ionized using atmospheric pressure chemical ionization in an Agilent 1946D mass spectrometer (Agilent Technologies) with the following settings: negative polarity, 5 L/min drying rate, 30 psig nebulizer pressure, 350°C drying gas temperature, 325°C vaporizer temperature, -2 kV capillary voltage, and 18 μ A corona current. Data acquisition and analysis were performed using Agilent ChemStation 10.02 software.

2.12 Statistical analysis

Unless otherwise indicated, experiments were analyzed using either Microsoft Excel 2003 software or GraphPad Prism software (version 4.03) using the following three GraphPad Prism analysis functions: linear regression analysis, nonlinear regression analysis, and column statistics. Unless otherwise indicated, values shown are mean \pm standard error of the mean (SEM) and unpaired t-tests were used to compare groups of values except xenograft tumor data which used

paired t-tests for comparing tumors in the same mouse. Values were considered statistically significant if $P < 0.05$.

Table 2-1. Real-time PCR probe and primer concentrations and sequences

Oligos	Conc. (nM)	Sequence
hENT1-F ^a	280	5'-CACCAGCCTCAGGACAGATACAA
hENT1-R	280	5'-GTGAAATACTGAGTGGCCGTCAT
hENT1-P	130	5'-FAM-CCACGGGAGCAGCGTTCCCA
hENT2-F	280	5'-ATGAGAACGGGATTCCCAGTAG
hENT2-R	280	5'-GCTCTGATTCCGGCTCCTT
hENT2-P	53	5'-FAM-CAGAAAGTAGCTCTGACCCTGGATCTTGACCT
hCNT1-F	280	5'-TCTGTGGATTTGCCAATTTTCAG
hCNT1-R	280	5'-CGGAGCACTATCTGGGAGAAGT
hCNT1-P	130	5'-FAM-TGGGAGGCTTGACCTCCATGGTCC
hCNT2-F	900	Purchased as a kit from Applied Biosystems
hCNT2-R	900	Assay ID: Hs00188407_m1
hCNT2-P	400	(Sequences not given)
hCNT3-F	280	5'-GGGTCCCTAGGAATCGTGATC
hCNT3-R	280	5'-CGAGGCGATATCACGCTTTC
hCNT3-P	27	5'-FAM-CGGACTCACATCCATGGCTCCTTC
GAPDH-F	280	5'-GAAGGTGAAGGTCGGAGTC
GAPDH-R	280	5'-GAAGATGGTGATGGGATTTTC
GAPDH-P	130	5'-FAM-CAAGCTTCCCGTTCTCAGCC

dCK-F	280	5'-AAACCTGAACGATGGTCTTTTACC
dCK-R	280	5'-CTTTGAGCTTGCCATTCAGAGA
dCK-P	53	5'-FAM-CAAACATATGCCTGTCTCAGTCGAATAAGAGCTC
TK1-F	900	Purchased as a kit from Applied Biosystems
TK1-R	900	Assay ID: Hs01062127_g1
TK1-P	400	(Sequences not given)
RRM1-F	900	Purchased as a kit from Applied Biosystems
RRM1-R	900	Assay ID: Hs01040706_m1
RRM1-P	400	(Sequences not given)
mENT1-F	900	Purchased as a kit from Applied Biosystems
mENT1-R	900	Assay ID: Mm01270578_g1
mENT1-P	400	(Sequences not given)

^a F indicates forward (5') primer; R, reverse (3') primer; P, probe; FAM, 6-carboxyfluorescein.

2.13 Bibliography

- [1] Machulla H, Blocher A, Kuntzsch M, Grierson J. Simplified labeling approach for synthesizing 3'-deoxy-3'-[18F]fluorothymidine ([18F]FLT). *J Radioanal Nucl Chem* 2000;243:843-6.
- [2] Been LB, Suurmeijer AJ, Cobben DC, Jager PL, Hoekstra HJ, Elsinga PH. [18F]FLT-PET in oncology: current status and opportunities. *Eur J Nucl Med Mol Imaging* 2004;31:1659-72.
- [3] Lawrentschuk N, Poon AM, Scott AM. Fluorine-18 Fluorothymidine: A New Positron Emission Radioisotope for Renal Tumors. *Clin Nucl Med* 2006;31:788-9.
- [4] Vickers MF, Zhang J, Visser F, Tackaberry T, Robins MJ, Nielsen LP, et al. Uridine recognition motifs of human equilibrative nucleoside transporters 1 and 2 produced in *Saccharomyces cerevisiae*. *Nucleosides Nucleotides Nucleic Acids* 2004;23:361-73.
- [5] Zhang J, Visser F, Vickers MF, Lang T, Robins MJ, Nielsen LP, et al. Uridine binding motifs of human concentrative nucleoside transporters 1 and 3 produced in *Saccharomyces cerevisiae*. *Mol Pharmacol* 2003;64:1512-20.
- [6] Visser F, Vickers MF, Ng AM, Baldwin SA, Young JD, Cass CE. Mutation of residue 33 of human equilibrative nucleoside transporters 1 and 2 alters sensitivity to inhibition of transport by dilazep and dipyridamole. *J Biol Chem* 2002;277:395-401.
- [7] Zhang J, Smith KM, Tackaberry T, Visser F, Robins MJ, Nielsen LP, et al. Uridine binding and transportability determinants of human concentrative nucleoside transporters. *Mol Pharmacol* 2005;68:830-9.
- [8] Cheng Y, Prusoff WH. Relationship between the inhibition constant (K_i) and the concentration of inhibitor which causes 50 per cent inhibition (I_{50}) of an enzymatic reaction. *Biochem Pharmacol* 1973;22:3099-108.
- [9] Yao SYM, Cass CE, Young JD. Membrane Transport: A Practical Approach. In: Baldwin SA, editor. Oxford and New York: Oxford University Press, 2000. p. 47-78.
- [10] King KM, Damaraju VL, Vickers MF, Yao SY, Lang T, Tackaberry TE, et al. A comparison of the transportability, and its role in cytotoxicity, of clofarabine, cladribine, and fludarabine by recombinant human nucleoside transporters produced in three model expression systems. *Mol Pharmacol* 2006;69:346-53.

- [11] Livak KJ, Schmittgen TD. Analysis of relative gene expression data using real-time quantitative PCR and the $2(-\Delta\Delta C(T))$ Method. *Methods* 2001;25:402-8.
- [12] Visser F, Sun L, Damaraju V, Tackaberry T, Peng Y, Robins MJ, et al. Residues 334 and 338 in transmembrane segment 8 of human equilibrative nucleoside transporter 1 are important determinants of inhibitor sensitivity, protein folding, and catalytic turnover. *J Biol Chem* 2007;282:14148-57.
- [13] Muzi M, Mankoff DA, Grierson JR, Wells JM, Vesselle H, Krohn KA. Kinetic modeling of 3'-deoxy-3'-fluorothymidine in somatic tumors: mathematical studies. *J Nucl Med* 2005;46:371-80.
- [14] Kim SJ, Lee JS, Im KC, Kim SY, Park SA, Lee SJ, et al. Kinetic modeling of 3'-deoxy-3'-¹⁸F-fluorothymidine for quantitative cell proliferation imaging in subcutaneous tumor models in mice. *J Nucl Med* 2008;49:2057-66.
- [15] Damaraju VL, Elwi AN, Hunter C, Carpenter P, Santos C, Barron GM, et al. Localization of broadly selective equilibrative and concentrative nucleoside transporters, hENT1 and hCNT3, in human kidney. *Am J Physiol Renal Physiol* 2007;293:F200-11.
- [16] Mackey JR, Galmarini CM, Graham KA, Joy AA, Delmer A, Dabbagh L, et al. Quantitative analysis of nucleoside transporter and metabolism gene expression in chronic lymphocytic leukemia (CLL): identification of fludarabine-sensitive and -insensitive populations. *Blood* 2005;105:767-74.
- [17] Li KM, Clarke SJ, Rivory LP. Quantitation of plasma thymidine by high-performance liquid chromatography—atmospheric pressure chemical ionization mass spectrometry and its application to pharmacodynamic studies in cancer patients. *Analytica Chimica Acta* 2003;486:51-61.

**Chapter 3: Characterization of FLT transport by human
nucleoside transporters and the role of hENT1 for uptake of FLT
in human cancer cell lines¹**

¹ A version of this chapter has been published:

Paproski et al. (2008) *The role of human nucleoside transporters in uptake of 3'-deoxy-3'-fluorothymidine*. *Mol. Pharmacol.* **74**:1372–1380.

3.1 Introduction

Positron emission tomography (PET) is a useful imaging modality that allows visualization and quantification of molecular markers or processes in tissues. The thymidine analog 3'-deoxy-3'-fluorothymidine (FLT) is considered to be an indirect proliferation-indicating PET imaging agent because, although it is not incorporated into DNA, its intracellular accumulation correlates well with proliferating cells [1]. Increased FLT accumulation in proliferating cells is believed to be due to a proliferation-dependent increase in thymidine kinase 1 (TK1) activity, leading to increased intracellular phosphorylation and 'trapping' of FLT [2-4]. However, FLT must cross plasma membranes before it can interact with TK1 and human nucleoside transporters (hNTs) are thought to be involved in this process since FLT uptake in HL-60 cells was significantly reduced by inhibiting human equilibrative nucleoside transporter 1 (hENT1) [5].

hNTs are involved in the cellular uptake of physiological nucleosides, nucleoside analogs and in some instances nucleobases [6]. Extracellular adenosine concentrations, which affect various cardiovascular and neurological processes, are influenced by hNTs [7, 8]. Many clinical antineoplastic and antiviral nucleoside analogs gain intracellular access by hNT-mediated transport across plasma membranes [9, 10].

There are two different families of hNTs: the hENTs (also known as the SLC29 family) and the concentrative nucleoside transporters (hCNTs, also known as the SLC28 family). hENTs mediate bidirectional transport of nucleosides across biological membranes and are found in most tissues in the body. The four

hENT family members are hENT1/2/3/4 [11-14]. hENT1 appears to be ubiquitously distributed in cells and tissues and has broad permeant selectivity, transporting a structurally diverse array of natural and synthetic nucleosides. Nitrobenzylmercaptapurine ribonucleoside (NBMPR) selectively inhibits hENT1 at nanomolar concentrations and has been used to functionally distinguish hENT1 from other hNTs [13]. hENT2 is also broadly selective, transporting natural and some synthetic nucleosides as well as some nucleobases. hENT3 is a pH-dependent low-affinity transporter of broad nucleoside selectivity with a N-terminal dileucine motif that targets the transporter toward intracellular membranes that co-localize with lysosomal markers [11]. hENT4, found predominantly in the heart and brain, displays pH-dependent adenosine-selective transport [12].

hCNTs couple the transport of nucleosides and sodium or, in the case of hCNT3, protons down their electrochemical gradients to concentrate nucleosides within cells. The three hCNT family members are hCNT1/2/3 [15-17]. hCNT1 is pyrimidine nucleoside-selective, transporting uridine, cytidine, and thymidine most efficiently [16]. hCNT2 is purine nucleoside-selective and efficiently transports adenosine, guanosine, and inosine, although it also transports uridine [17]. hCNT3 is broadly selective, transporting both purine and pyrimidine nucleosides with high affinities [15]. The Na^+ -nucleoside coupling ratio for hCNT1 and hCNT2 is 1:1 whereas hCNT3 has a Na^+ -nucleoside ratio of 2:1 and H^+ -nucleoside ratio of 1:1 [18].

Although the permeant selectivities of hNTs have been extensively characterized for many nucleoside analogs, relatively little is known about how hNTs transport FLT. The main objectives of the work described in this chapter were to determine how well the hNTs interact with and transport FLT and to determine which hNTs are important for FLT uptake in various human cancer cell lines. Using [³H]FLT to follow cellular uptake, it was shown that FLT was transported by hENT1, hENT2, hCNT1 and hCNT3 and that hENT1 was responsible for the majority of hNT-mediated [³H]FLT uptake in the cell lines tested. In five of the six cell lines tested, a strong correlation was observed between the abundance of hENT1 at the extracellular surface and FLT uptake.

3.2 Results

3.2.1 Interaction of FLT with recombinant hNTs in yeast cells

Zhang *et al.* developed an assay that assesses the ability of nucleoside analogs to inhibit uridine uptake by yeast producing various recombinant hNTs that provides a measure of the apparent affinities of the hNTs for nucleoside analogs [19, 20]. Graded concentrations of thymidine and FLT were used to inhibit [³H]uridine uptake in yeast cells producing individual hNTs (Fig. 3-1) to determine IC₅₀ values (concentration of thymidine or FLT that inhibited [³H]uridine uptake by 50%) that were converted to K_i values. Thymidine K_i values for hENT1, hENT2, hCNT1, hCNT2, and hCNT3 were 74 ± 17, 160 ± 10, 20 ± 3, 1200 ± 200, and 31 ± 5 μM, respectively. FLT displayed K_i values for hENT1, hENT2, hCNT1, hCNT2, and hCNT3 that were 12-, 3.4-, 5.0-, >8.3-, and 15-fold larger than thymidine K_i values, respectively, suggesting that substitution of fluorine for the 3'-hydroxyl group significantly decreased the affinities of the hNTs for FLT. hCNT1 displayed the lowest K_i value (*i.e.*, highest apparent affinity) for FLT, followed by hCNT3, hENT2, hENT1 and hCNT2.

3.2.2 Transportability of FLT by recombinant hNTs in oocytes

Xenopus laevis oocytes, which have low endogenous transport of nucleosides [21], have been used extensively to assess membrane transport of nucleosides and nucleoside analogs by recombinant hNTs. Although oocytes were injected with similar amounts of RNA encoding hNTs, expression of hNTs may have varied between oocytes injected with different hNT RNAs which may have resulted in different levels of nucleoside uptake. Values for mediated [³H]FLT

uptake in *Xenopus* oocytes producing recombinant hNTs were robust and relatively similar to those of [³H]thymidine (Fig. 3-2A). When hNT-producing oocytes were incubated with 20 μM [³H]FLT, hCNT1 displayed the greatest (pmol/oocyte/30 min) FLT uptake (48 ± 8), followed by hCNT3 (32 ± 5), hENT2 (12 ± 1), hENT1 (11 ± 0.8), and hCNT2 (2.0 ± 0.2). The weak interaction between FLT and hCNT2 likely explains the poor transportability of [³H]FLT by hCNT2.

Influx of [³H]FLT by hENT1, hENT2, hCNT1 and hCNT3 was concentration dependent and conformed to Michaelis-Menten kinetics (Fig. 3-2B); the K_M and V_{max} values are presented in Table 3-1. hENT1 and hENT2 displayed greater transport capacities and lower apparent affinities (larger V_{max} and K_M values, respectively) for [³H]FLT than hCNT1 and hCNT3. The V_{max}/K_M ratio, a measure of transport efficiency, was about 6-fold greater for hCNT1 and hCNT3 than for hENT1 and hENT2, suggesting that hCNT1 and hCNT3 transport [³H]FLT more efficiently than hENT1 and hENT2 at lower (μM) concentrations.

3.2.3 Relative quantification of hNTs in cell lines

Since FLT was shown to be a permeant of several recombinant hNTs, it was expected that cellular accumulation of FLT would be influenced by the levels of hNT mRNA transcripts in the cancer cell lines used in this study. Relative quantification of hNT-transcript levels was determined by TaqMan real-time reverse transcriptase polymerase chain reaction (RT-PCR) (Fig. 3-3). All genes analyzed were amplified with equal efficiencies and glyceraldehyde-3-phosphate dehydrogenase (GAPDH) was used as the RNA loading control. Transcript levels

of hENT1 were 7-, 11-, 25-, and 340-fold greater than those of hENT2, the second most abundant hNT, in A549, MIA PaCa-2, U251, and A498 cells, respectively, whereas transcript levels of hENT2 were equal to and 3-fold greater than those of hENT1 in MCF-7 and Capan-2 cells, respectively. For all cell lines, hENT1 transcripts were at least 300-fold greater than hCNT1/2/3 transcripts and only hCNT2 was detectable in A549 cells, suggesting that hCNT1, hCNT2 and hCNT3 play minor roles in cellular uptake of nucleosides in the cell lines tested.

3.2.4 hNTs responsible for [³H]FLT uptake in cell lines

[³H]FLT uptake assays were performed in different transport buffers to determine the functional hNTs that were involved in [³H]FLT uptake (Fig. 3-4A). Na⁺ buffer allowed tracer uptake mediated by both hENTs and hCNTs while N-methyl-D-glucamine (NMDG) buffer, which lacks Na⁺, allowed tracer uptake mediated by only hENTs. Buffers with 100 μM dilazep inhibited both hENT1 and hENT2 transport while buffers with 100 nM NBMPR inhibited only hENT1 transport. NMDG buffer with 200 μM dilazep and 10 mM uridine was used to determine non-mediated tracer uptake. [³H]FLT uptake in NMDG buffer was 76, 78, 90, and 98% of uptake in Na⁺-containing buffer for Capan-2, A549, MCF-7, and U251 cells, respectively, suggesting that hCNTs were relatively unimportant for [³H]FLT uptake in these cell lines. Addition of 100 nM NBMPR to Na⁺ buffer reduced mediated [³H]FLT uptake (determined by the difference of [³H]FLT uptake in buffers with or without 200 μM dilazep and 10 mM uridine) by 50, 63, 68, 71, 77, and 77% in Capan-2, MCF-7, U251, A549, MIA PaCa-2, and A-498

cells, respectively, suggesting that hENT1 was the main hNT involved in [³H]FLT uptake in these cell lines (Fig. 3-4B).

3.2.5 NBMPR binding and inhibition of [³H]FLT uptake in cell lines

To determine the importance of hENT1 for [³H]FLT uptake in the cell lines used in this study, [³H]NBMPR equilibrium binding assays (Fig. 3-5A) and concentration-effect assays with NBMPR inhibiting [³H]FLT uptake (Fig. 3-5B) were performed. [³H]NBMPR binding parameters are displayed in Table 3-2. NBMPR B_{\max} values varied significantly between cell lines (180 – 1300 fmol/10⁶ cells). MIA PaCa-2 cells displayed the largest amount of NBMPR binding sites, followed by MCF-7, A549, U251, A498, and Capan-2. Unlike B_{\max} values, the K_d values were similar for all of the cell lines (0.18 – 0.43 nM). When comparing NBMPR, K_d and IC₅₀ values (Table 3-2), MCF-7, A549, and Capan-2 cells displayed IC₅₀ values smaller or equal to K_d values, suggesting that binding and inhibition of 50% of hENT1 transporters by NBMPR decreased NBMPR-sensitive FLT uptake by at least 50%.

3.2.6 Cellular hENT1 location in cell lines

Although hENT1 is considered a plasma membrane transporter, it has been found in nuclear and mitochondrial membranes [22, 23]. To determine the proportion of intracellular and extracellular NBMPR binding sites (*i.e.*, hENT1 on intracellular and plasma membranes, respectively), [³H]NBMPR equilibrium binding assays were performed with or without 5-S-{2-(1-[(fluorescein-5-yl)thioureido]hexanamido)ethyl}-6-N-(4-nitrobenzyl)-5-thioadenosine (FTH-SAENTA, Fig. 3-6). Unlike NBMPR, FTH-SAENTA is membrane impermeable

and can only bind hENT1 on the extracellular surface of the plasma membrane, thereby allowing quantification of extracellular and intracellular NBMPR binding sites (Table 3-2). MCF-7 cells had the greatest percentage of NBMPR binding sites on extracellular surfaces, followed by A549, MIA PaCa-2, U251, A498, and Capan-2 cells. MIA PaCa-2 displayed the greatest number of extracellular NBMPR binding sites ($4.4 \times 10^5 \pm 7 \times 10^4$ sites/cell), which was 2.3-, 3.4-, 4.5-, 7.2-, and 220-fold greater than the extracellular NBMPR binding sites for MCF-7, A549, U251, A498, and Capan-2 cells, respectively.

3.2.7 Correlation between FLT uptake and extracellular NBMPR binding sites

There was a strong correlation between FLT uptake and extracellular NBMPR binding sites/cell in five of the six cell lines used in this study ($P = 0.0011$, $r^2 = 0.98$, Fig. 3-7). MIA PaCa-2, which was excluded from Fig. 3-7, had at least a 2-fold greater number of extracellular NBMPR binding sites per cell than any other cell line in this study but had similar FLT uptake to U251. For all cell lines except MIA PaCa-2, there was a clear relationship between the levels of extracellular plasma membrane hENT1 and FLT uptake.

3.3 Discussion

FLT-PET has been demonstrated useful for determining the proliferative status of various tumor types [24]. Although FLT metabolism is generally considered the rate-limiting step for cellular FLT accumulation [2, 4], a study by Perumal et al. [25] suggested that FLT transport is important for FLT accumulation. RIF-1 xenograft tumors in mice displayed a 1.8-fold increase in ^{18}F -FLT uptake when tumor-bearing mice were given 5-fluorouracil [25]. Although RIF-1 tumors displayed no change in TK1 protein or ATP levels, NBMPR binding to cultured RIF-1 cells increased 50% after a two-h incubation with 10 $\mu\text{g}/\text{ml}$ 5-fluorouracil, suggesting that FLT transport was the rate-limiting process for FLT accumulation in RIF-1 tumors. However, the increased tumor uptake of ^{18}F -FLT may have been caused by depletion of cellular thymidine monophosphate (TMP) pools due to inhibition of thymidylate synthase, which produces TMP from 2'-deoxyuridine monophosphate. Decreased TMP pools allow greater phosphorylation of FLT monophosphate to FLT diphosphate by thymidylate kinase, which is the rate-limiting enzyme involved in FLT metabolism [3].

The research described in this chapter examined interactions between hNTs and FLT and determined which hNTs were capable of mediating FLT transport. Substitution of the 3'-hydroxyl group of thymidine with a fluoro group increased K_i values for inhibition of uridine transport (a measure of affinity for hNTs) by 3- to 15-fold. This reduction in hNTs' apparent affinities for FLT was relatively small considering the importance of the 3'-hydroxyl group in uridine for

nucleoside-hNT interaction - *i.e.*, using the yeast inhibitor-sensitivity assay described herein, hCNT3, hENT1, hCNT2, and hCNT1 displayed, respectively, 39-, >54-, >107-, and 135-fold larger K_i values for 3'-deoxyuridine than for uridine [20, 26]. FLT interacted poorly with hCNT2, and this explains the low amount of FLT uptake observed in oocytes producing hCNT2. Oocytes producing recombinant hENT1, hENT2, hENT3, hCNT1, and hCNT3 displayed significant mediated [^3H]FLT uptake, suggesting that these hNTs are all capable of FLT transport. It was surprising to observe that rates of [^3H]FLT uptake were equal or greater than rates of [^3H]thymidine uptake in oocytes producing hCNT1, hENT1, hENT2, and hENT3 since in most cultured cell lines [^3H]thymidine accumulates to a greater extent than [^3H]FLT [1]. However, differences in nucleoside metabolism in mammalian cells and *Xenopus laevis* oocytes may explain the differences in rates of [^3H]FLT and [^3H]thymidine uptake in oocytes, since *Xenopus laevis* oocytes display little thymidine metabolism [21]. To the author's knowledge, there is no information regarding oocyte metabolism of FLT.

Analysis of hNT transcript levels by real-time PCR revealed relatively little hCNT mRNA expression in the six cell lines. These results are supported by the small changes in [^3H]FLT uptake displayed when most of the cell lines were incubated in NMDG buffer. A notable exception was MIA PaCa-2 cells, which displayed 59% [^3H]FLT uptake in NMDG buffer compared to Na^+ buffer, suggesting that 41% of [^3H]FLT uptake was mediated by hCNTs. However, MIA PaCa-2 cells incubated in Na^+ buffer with 100 μM dilazep displayed 17% [^3H]FLT uptake compared to Na^+ buffer alone, suggesting that 83% of [^3H]FLT

uptake was mediated by hENTs. The basis of this discrepancy in hNT activity in MIA PaCa-2 cells remains unclear and warrants further investigation. Although MIA PaCa-2 and Capan-2 are both pancreatic carcinoma cell lines, their hNT transcript expression patterns differed significantly. MIA PaCa-2 and Capan-2 displayed hENT1/hENT2 expression ratios of 11 and 0.35, respectively, demonstrating that hNT expression patterns may differ between cell lines of similar origin.

For all cell lines, incubation of NBMPR in Na⁺ buffer reduced hNT-mediated [³H]FLT uptake by at least 50%, suggesting that hENT1 was the predominant hNT involved in [³H]FLT uptake. Although hCNTs appeared to have greater affinities for FLT, the greater abundance of hENT1 in the cell lines studied resulted in its mediating the greatest amount of [³H]FLT uptake. For MCF-7, A549, and Capan-2 cells, inhibition of 50% hENT1 decreased hENT1-mediated [³H]FLT uptake by at least 50%, suggesting that changes in transport activities in these cell lines had an immediate effect on FLT uptake. For the other cell lines, FLT phosphorylation may be the rate-limiting process for FLT uptake and upon inhibition of a subset of hENT1 by NBMPR, FLT transport may become the rate-limiting process for FLT uptake.

For all cell lines except MIA PaCa-2, a strong correlation was observed between extracellular NBMPR binding sites and [³H]FLT uptake. MIA PaCa-2 displayed more than two-fold larger number of extracellular NBMPR binding sites per cell than the other cell lines but did not display proportionally greater FLT uptake, suggesting that FLT phosphorylation was the rate-limiting step for

FLT uptake in MIA PaCa-2. When analyzing TK1 mRNA levels using real-time PCR for MIA PaCa-2 and Capan-2, TK1 mRNA levels in MIA PaCa-2 were approximately 30% of those found in Capan-2 (Chapter 5, Fig. 5-2B), suggesting that MIA PaCa-2 had low levels of TK1.

Understanding membrane transport of FLT in cells may explain the relatively low sensitivity of FLT-PET compared to the commonly used 2-fluoro-2-deoxyglucose (FDG)-PET. Immunohistochemical staining of hENT1 in 33 frozen sections of primary breast cancers revealed significant variations in hENT1 staining between tumors. Using a 0-4+ intensity staining scale, 4, 5, 7, 14, and 3 sections scored 0, 1+, 2+, 3+, and 4+, respectively [27]. No detectable hENT1 staining was observed in 12% of tumors examined, suggesting that FLT-PET may provide false-negative images for these tumors. Data from FLT-PET pilot studies in breast cancer patients suggested that 7-20% of tumors are not detectable by FLT-PET [28, 29]. These tumors may have low levels of hENT1, explaining their unobservable nature in FLT-PET.

hNT levels are variable in almost all cancers studied. RNA analysis of four pancreatic cell lines (NP9, NP18, NP29, and NP31) revealed that hENT1, hENT2, hCNT1, hCNT2, and hCNT3 mRNA levels differed significantly between the four cell lines and only hENT1 mRNA was easily detected for all four cell lines [30]. When hENT1 levels were analyzed in 21 pancreatic adenocarcinomas using immunohistochemistry, 12 samples displayed no detectable hENT1 in 10-100% of adenocarcinoma cells, suggesting that hENT1 is not present in all pancreatic adenocarcinomas [31]. Variability in ¹⁸F-FLT uptake

between tumors may be partly explained by the considerable inter-individual variability in tumor hNT levels [32]. When comparing RNA levels for hENT1 using matched tumor/normal tissue individual arrays, there was no consistent difference in hENT1 expression levels for kidney, breast, uterus, ovary, colon, lung, stomach, and rectum [32]. Only prostate tumors consistently demonstrated decreased hENT1 expression compared to normal tissues (hENT1 tumor levels 47% of normal tissues). These same prostate arrays also exhibited consistently higher levels of hENT2 tumor expression (hENT2 tumor levels were 323% of those of normal tissues), suggesting prostate tumors still retain the capacity for FLT transport despite the decrease in hENT1 levels. hCNT1 was not detected in the majority of the matched tissue arrays (breast, prostate, cervix, colon, stomach, and rectum) and consistently displayed low levels in tumors for almost all other tested tissues (kidney, uterus, lung, and small intestine), suggesting that neoplastic transformation of these tissues may decrease capacity for FLT transport.

Cellular hENT1 levels correlated with FLT uptake (present study) and the therapeutic activity of gemcitabine in pancreatic adenocarcinomas [31]. Patients with pancreatic adenocarcinoma tumors in which over 90% of tumor cells displayed hENT1 staining had significantly longer median survival times after gemcitabine monotherapy than patients with tumors in which 0-90% of tumor cells displayed hENT1 staining. If hENT1 levels influence both FLT uptake and gemcitabine cytotoxicity in pancreatic cancers, it is proposed that FLT-PET would be useful to determine gemcitabine resistance in pancreatic cancers prior to gemcitabine treatment. Further studies are required to validate this hypothesis.

Prior to this study, only hENT1 was known to transport FLT across plasma membranes and it was unknown whether the other hNTs could transport FLT [5]. The work described in this chapter established that FLT can interact with and is transported by hENT1, hENT2, hCNT1 and hCNT3. Because of the greater relative abundance of hENT1 in the tested cell lines, [³H]FLT uptake was primarily mediated by hENT1. Small alterations of hENT1 transport activity by treatment with NBMPR reduced [³H]FLT uptake in MCF-7, A549, and Capan-2 cells. A strong correlation was observed between [³H]FLT uptake and the number of extracellular NBMPR binding sites/cell for five of the six cell lines tested, demonstrating the importance of hENT1 for FLT uptake.

Table 3-1. Kinetic parameters of [³H]FLT influx mediated by hNTs in oocytes

Oocytes (n = 10-12) producing recombinant hENT1, hENT2, hCNT1, or hCNT3 were incubated with graded [³H]FLT concentrations for 1 min as described in section 2.4.2. hNT K_m and V_{max} values (mean \pm SEM) for FLT were determined from the data shown in Figure 3-2B using non-linear regression analysis with GraphPad Prism software (version 4.03).

	K_M	V_{max}	V_{max}/K_M
hNT	mM	pmol/oocyte/min	ratio
hENT1	3.4 \pm 0.2	169 \pm 4	50
hENT2	2.6 \pm 0.4	180 \pm 13	69
hCNT1	0.13 \pm 0.01	52 \pm 1	400
hCNT3	0.11 \pm 0.01	37 \pm 1	340

Table 3-2. NBMPR binding parameters and IC₅₀ values for inhibition of [³H]FLT uptake in various cell lines

MCF-7, A549, U251, A498, MIA PaCa-2, and Capan-2 cells in 12-well plates were incubated with Na⁺ buffer containing 74 nM [³H]FLT and graded concentrations of NBMPR for 1 h to determine IC₅₀ values (NBMPR concentration that inhibited 50% of [³H]FLT uptake) as described in section 2.4.3. Equilibrium NBMPR binding assays were also performed by incubating cells in 12-well plates for 90 min with Na⁺ buffer containing graded concentrations of [³H]NBMPR as described in section 2.6. Experiments were performed at least three times (each experiment in triplicate) and data are expressed as mean ± SEM.

Cell Line	NBMPR			Extracellular NBMPR		
	IC ₅₀ (nM)	K _d (nM)	B _{max} (fmol/10 ⁶ cells)	Total Binding (10 ⁵ sites/cell)	%	Binding (10 ⁵ sites/cell)
MCF-7	0.21 ± 0.01	0.23 ± 0.04	450 ± 76	2.7 ± 0.5	71 ± 9	1.9 ± 0.3
A549	0.22 ± 0.13	0.26 ± 0.07	360 ± 18	2.2 ± 0.1	60 ± 7	1.3 ± 0.06
U251	0.93 ± 0.28	0.20 ± 0.03	340 ± 33	2.0 ± 0.2	47 ± 5	1.0 ± 0.09
A498	0.31 ± 0.07	0.18 ± 0.02	270 ± 25	1.6 ± 0.2	38 ± 4	0.6 ± 0.06
MIA PaCa-2	1.15 ± 0.11	0.38 ± 0.05	1300 ± 210	7.9 ± 1.3	56 ± 3	4.4 ± 0.7
Capan-2	0.21 ± 0.04	0.43 ± 0.05	180 ± 25	1.1 ± 0.2	1.6 ± 1.6	0.02 ± 0.002

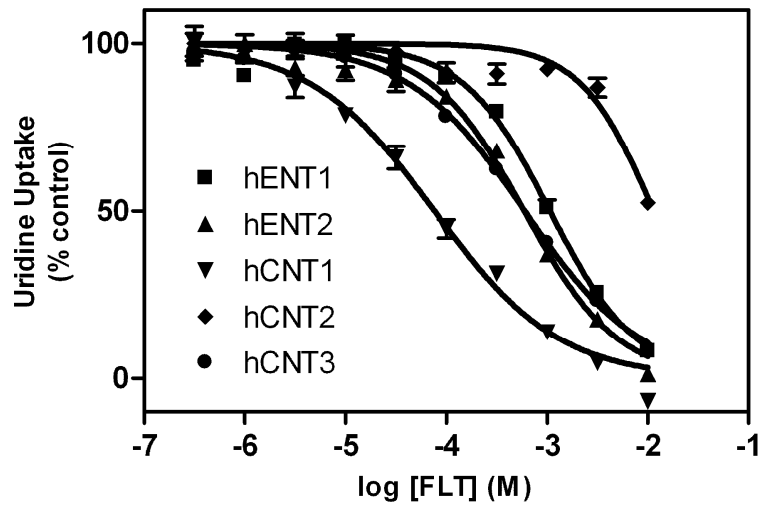


Figure 3-1. FLT inhibition of [³H]uridine uptake in yeast cells producing recombinant hNTs. Yeast cells producing the recombinant hNT indicated were incubated with 1 μ M [³H]uridine for up to 30 min as described in section 2.4.1. Shown are representative experiments performed in quadruplicate and data are expressed as mean \pm SEM. Error bars represent variability between replicates within each individual experiment. Uptake values represent the percentage of [³H]uridine uptake in the presence of FLT relative to that in its absence. Error bars are not shown where the SEM values were smaller than the size of the symbol.

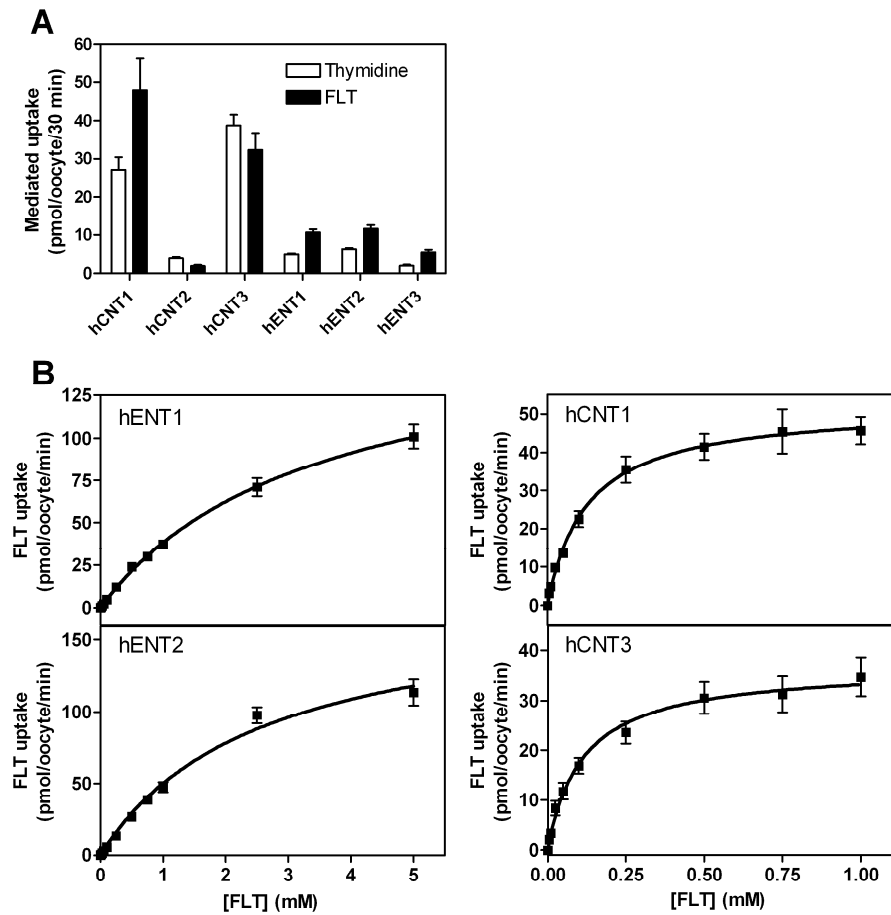


Figure 3-2. $[^3\text{H}]$ FLT uptake and kinetic analysis in oocytes producing recombinant hNTs. (A) Oocytes ($n = 10-12$) producing recombinant hCNT1, hCNT2, hCNT3, hENT1, hENT2, or hENT3 were incubated with $20 \mu\text{M}$ $[^3\text{H}]$ FLT or $[^3\text{H}]$ thymidine for 30 min and $[^3\text{H}]$ permeant uptake was measured as described in section 2.4.2. (B) Concentration dependent influx of $[^3\text{H}]$ FLT in oocytes producing hNT proteins. Oocytes ($n = 10-12$) producing recombinant hCNT1, hCNT3, hENT1, or hENT2 were incubated with graded $[^3\text{H}]$ FLT concentrations for 1 min and $[^3\text{H}]$ FLT uptake was measured as described in section 2.4.2. (A + B) Data from each figure are expressed as mean \pm SEM from a single experiment and error bars are not shown where the SEM values were smaller than the size of the symbol. Error bars represent variability between replicates within each individual experiment. Values are for mediated uptake (uptake in RNA transcript-injected oocytes minus uptake in control oocytes injected with water alone).

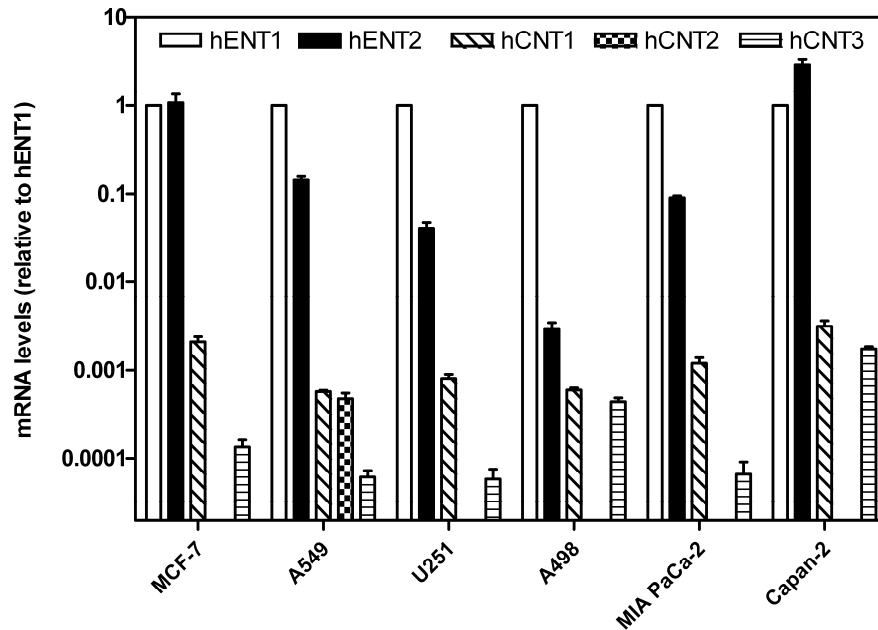


Figure 3-3. Relative quantitation of hNT transcript levels in various cell lines by real-time PCR. mRNA was isolated from MCF-7, A549, U251, A498, MIA PaCa-2, and Capan-2 cells and hNT transcript levels were quantified relative to those of hENT1 using TaqMan real-time RT-PCR as described in section 2.5. hCNT2 transcripts were only detectable in A549 cells. Three to five experiments were performed in triplicate and data are expressed as mean \pm SEM.

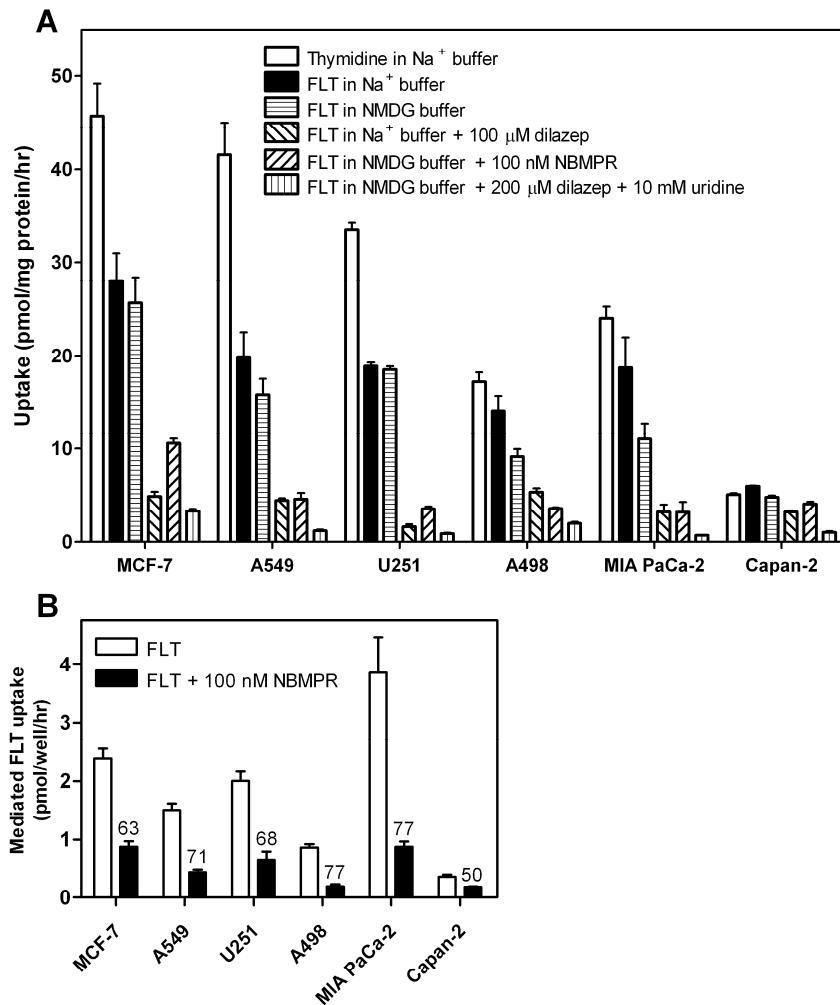


Figure 3-4. Characterization of hNTs responsible for FLT uptake in various cultured cancer cell lines. (A) MCF-7, A549, U251, A498, MIA PaCa-2, and Capan-2 cells in 12-well plates were incubated in Na⁺ or NMDG buffer containing 74 nM [³H]thymidine or [³H]FLT with or without hNT inhibitors for 1 h and [³H]permeant uptake was measured as described in section 2.4.3. (B) MCF-7, A549, U251, A498, MIA PaCa-2, and Capan-2 cells in 12-well plates were incubated in Na⁺ buffer containing 74 nM [³H]FLT with or without 100 nM NBMPR for 1 h and [³H]FLT uptake was measured as described in section 2.4.3. Numbers above black columns represent percent uptake inhibited by NBMPR. (A + B) At least three experiments were performed (each in triplicate) and data are expressed as mean ± SEM.

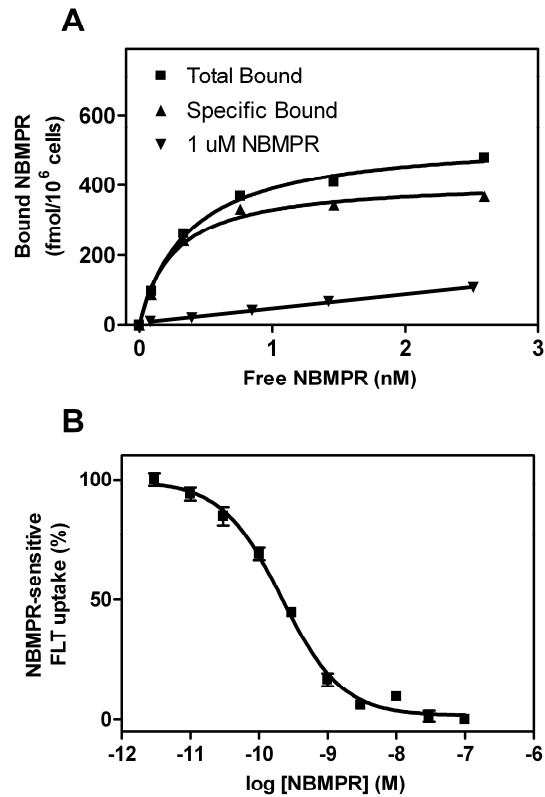


Figure 3-5. $[^3\text{H}]\text{NBMPR}$ binding sites and the effect of NBMPR on $[^3\text{H}]\text{FLT}$ uptake in MCF-7 cells. (A) Equilibrium NBMPR binding assays were performed by incubating MCF-7 cells in 12-well plate for 90 min with Na^+ buffer containing graded concentrations of $[^3\text{H}]\text{NBMPR}$ as described in section 2.6. Specifically bound $[^3\text{H}]\text{NBMPR}$ was calculated from differences between total bound and non-specifically bound (*i.e.*, in the presence of 1 μM non-radioactive NBMPR). **(B)** MCF-7 cells in 12-well plates were incubated in Na^+ buffer containing 74 nM $[^3\text{H}]\text{FLT}$ with graded concentrations of NBMPR for 1 h and $[^3\text{H}]\text{FLT}$ uptake was measured as described in section 2.4.3. The largest and smallest amounts of $[^3\text{H}]\text{FLT}$ uptake observed over the graded concentrations of NBMPR represented 100% and 0% uptake, respectively. **(A + B)** Shown are representative experiments performed in triplicate and data are expressed as mean \pm SEM. Error bars represent variability between replicates within each individual experiment. Error bars are not shown where the SEM values were smaller than the size of the symbol.

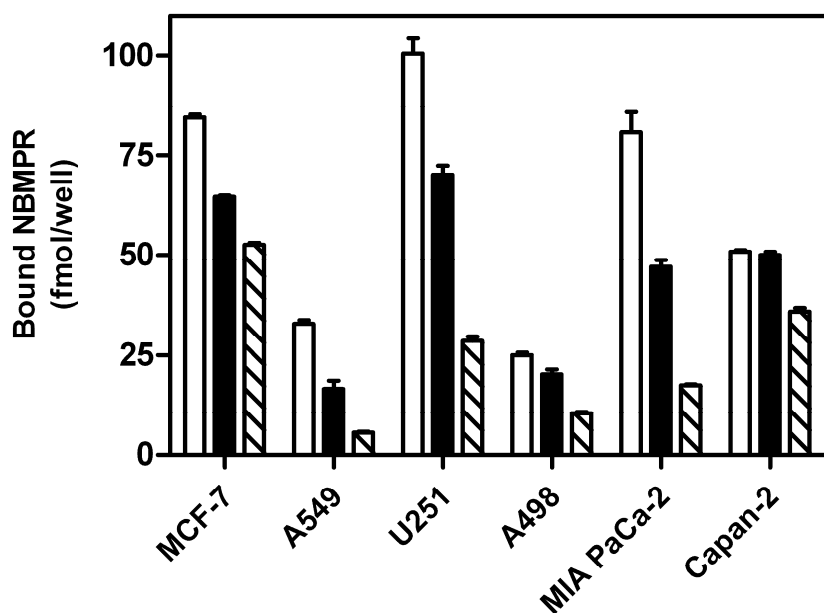


Figure 3-6. Extracellular and intracellular NBMPr binding in various cell lines. Equilibrium [³H]NBMPr binding assays were performed with MCF-7, A549, U251, A498, MIA PaCa-2, and Capan-2 cells in 12-well plates by incubating cells for 1 h with either 10 nM [³H]NBMPr (white columns), 10 nM [³H]NBMPr with 100 nM FTH-SAENTA (black columns), or 10 nM [³H]NBMPr with 10 μM NBMPr (striped column) as described in section 2.6. The differences between NBMPr binding with and without FTH-SAENTA represent extracellular specific NBMPr binding sites. Shown are representative experiments performed in triplicate and data are expressed as mean ± SEM. Error bars represent variability between replicates within each individual experiment.

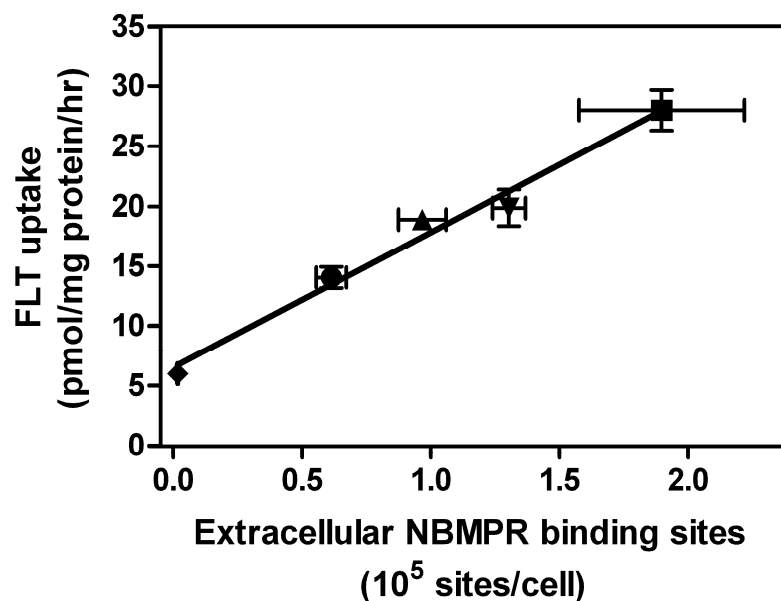


Figure 3-7. Linear regression analysis of [³H]FLT uptake and extracellular NBMPR binding sites per cell for all cell lines excluding MIA PaCa-2. Data in the figure were taken from Fig. 3-4 (FLT uptake in Na⁺ buffer) and Table 3-2 (extracellular NBMPR binding sites/cell). When analyzing Capan-2 (◆), A498 (●), U251 (▲), A549 (▼), and MCF-7 (■) cells, there was a significant correlation between [³H]FLT uptake and extracellular NBMPR binding sites ($P = 0.0011$, $r^2 = 0.98$).

3.4 Bibliography

- [1] Toyohara J, Waki A, Takamatsu S, Yonekura Y, Magata Y, Fujibayashi Y. Basis of FLT as a cell proliferation marker: comparative uptake studies with [3H]thymidine and [3H]arabinothymidine, and cell-analysis in 22 asynchronously growing tumor cell lines. *Nucl Med Biol* 2002;29:281-7.
- [2] Barthel H, Perumal M, Latigo J, He Q, Brady F, Luthra SK, et al. The uptake of 3'-deoxy-3'-[18F]fluorothymidine into L5178Y tumours in vivo is dependent on thymidine kinase 1 protein levels. *Eur J Nucl Med Mol Imaging* 2005;32:257-63.
- [3] Grierson JR, Schwartz JL, Muzi M, Jordan R, Krohn KA. Metabolism of 3'-deoxy-3'-[F-18]fluorothymidine in proliferating A549 cells: validations for positron emission tomography. *Nucl Med Biol* 2004;31:829-37.
- [4] Rasey JS, Grierson JR, Wiens LW, Kolb PD, Schwartz JL. Validation of FLT uptake as a measure of thymidine kinase-1 activity in A549 carcinoma cells. *J Nucl Med* 2002;43:1210-7.
- [5] Kong XB, Zhu QY, Vidal PM, Watanabe KA, Polsky B, Armstrong D, et al. Comparisons of anti-human immunodeficiency virus activities, cellular transport, and plasma and intracellular pharmacokinetics of 3'-fluoro-3'-deoxythymidine and 3'-azido-3'-deoxythymidine. *Antimicrob Agents Chemother* 1992;36:808-18.
- [6] Kong W, Engel K, Wang J. Mammalian nucleoside transporters. *Curr Drug Metab* 2004;5:63-84.
- [7] Latini S, Pedata F. Adenosine in the central nervous system: release mechanisms and extracellular concentrations. *J Neurochem* 2001;79:463-84.
- [8] Shryock JC, Belardinelli L. Adenosine and adenosine receptors in the cardiovascular system: biochemistry, physiology, and pharmacology. *Am J Cardiol* 1997;79:2-10.
- [9] Mackey JR, Baldwin SA, Young JD, Cass CE. Nucleoside transport and its significance for anticancer drug resistance. *Drug Resistance Updates* 1998;1:310-24.
- [10] Pastor-Anglada M, Felipe A, Casado FJ. Transport and mode of action of nucleoside derivatives used in chemical and antiviral therapies. *Trends Pharmacol Sci* 1998;19:424-30.
- [11] Baldwin SA, Yao SY, Hyde RJ, Ng AM, Foppolo S, Barnes K, et al. Functional characterization of novel human and mouse equilibrative

- nucleoside transporters (hENT3 and mENT3) located in intracellular membranes. *J Biol Chem* 2005;280:15880-7.
- [12] Barnes K, Dobrzynski H, Foppolo S, Beal PR, Ismat F, Scullion ER, et al. Distribution and functional characterization of equilibrative nucleoside transporter-4, a novel cardiac adenosine transporter activated at acidic pH. *Circ Res* 2006;99:510-9.
- [13] Griffiths M, Beaumont N, Yao SY, Sundaram M, Boumah CE, Davies A, et al. Cloning of a human nucleoside transporter implicated in the cellular uptake of adenosine and chemotherapeutic drugs. *Nat Med* 1997;3:89-93.
- [14] Griffiths M, Yao SY, Abidi F, Phillips SE, Cass CE, Young JD, et al. Molecular cloning and characterization of a nitrobenzylthioinosine-insensitive (ei) equilibrative nucleoside transporter from human placenta. *Biochem J* 1997;328 (Pt 3):739-43.
- [15] Ritzel MW, Ng AM, Yao SY, Graham K, Loewen SK, Smith KM, et al. Molecular identification and characterization of novel human and mouse concentrative Na⁺-nucleoside cotransporter proteins (hCNT3 and mCNT3) broadly selective for purine and pyrimidine nucleosides (system cib). *J Biol Chem* 2001;276:2914-27.
- [16] Ritzel MW, Yao SY, Huang MY, Elliott JF, Cass CE, Young JD. Molecular cloning and functional expression of cDNAs encoding a human Na⁺-nucleoside cotransporter (hCNT1). *Am J Physiol* 1997;272:C707-14.
- [17] Wang J, Su SF, Dresser MJ, Schaner ME, Washington CB, Giacomini KM. Na(+)-dependent purine nucleoside transporter from human kidney: cloning and functional characterization. *Am J Physiol* 1997;273:F1058-65.
- [18] Smith KM, Slugoski MD, Loewen SK, Ng AM, Yao SY, Chen XZ, et al. The broadly selective human Na⁺/nucleoside cotransporter (hCNT3) exhibits novel cation-coupled nucleoside transport characteristics. *J Biol Chem* 2005;280:25436-49.
- [19] Zhang J, Smith KM, Tackaberry T, Visser F, Robins MJ, Nielsen LP, et al. Uridine binding and transportability determinants of human concentrative nucleoside transporters. *Mol Pharmacol* 2005;68:830-9.
- [20] Zhang J, Visser F, Vickers MF, Lang T, Robins MJ, Nielsen LP, et al. Uridine binding motifs of human concentrative nucleoside transporters 1 and 3 produced in *Saccharomyces cerevisiae*. *Mol Pharmacol* 2003;64:1512-20.
- [21] Jarvis SM, Griffith DA. Expression of the rabbit intestinal N2 Na⁺/nucleoside transporter in *Xenopus laevis* oocytes. *Biochem J* 1991;278 (Pt 2):605-7.

- [22] Lai Y, Tse CM, Unadkat JD. Mitochondrial expression of the human equilibrative nucleoside transporter 1 (hENT1) results in enhanced mitochondrial toxicity of antiviral drugs. *J Biol Chem* 2004;279:4490-7.
- [23] Mani RS, Hammond JR, Marjan JM, Graham KA, Young JD, Baldwin SA, et al. Demonstration of equilibrative nucleoside transporters (hENT1 and hENT2) in nuclear envelopes of cultured human choriocarcinoma (BeWo) cells by functional reconstitution in proteoliposomes. *J Biol Chem* 1998;273:30818-25.
- [24] Been LB, Suurmeijer AJ, Cobben DC, Jager PL, Hoekstra HJ, Elsinga PH. [18F]FLT-PET in oncology: current status and opportunities. *Eur J Nucl Med Mol Imaging* 2004;31:1659-72.
- [25] Perumal M, Pillai RG, Barthel H, Leyton J, Latigo JR, Forster M, et al. Redistribution of nucleoside transporters to the cell membrane provides a novel approach for imaging thymidylate synthase inhibition by positron emission tomography. *Cancer Res* 2006;66:8558-64.
- [26] Vickers MF, Zhang J, Visser F, Tackaberry T, Robins MJ, Nielsen LP, et al. Uridine recognition motifs of human equilibrative nucleoside transporters 1 and 2 produced in *Saccharomyces cerevisiae*. *Nucleosides Nucleotides Nucleic Acids* 2004;23:361-73.
- [27] Mackey JR, Jennings LL, Clarke ML, Santos CL, Dabbagh L, Vsianska M, et al. Immunohistochemical variation of human equilibrative nucleoside transporter 1 protein in primary breast cancers. *Clin Cancer Res* 2002;8:110-6.
- [28] Been LB, Elsinga PH, de Vries J, Cobben DC, Jager PL, Hoekstra HJ, et al. Positron emission tomography in patients with breast cancer using (18)F-3'-deoxy-3'-fluoro-l-thymidine ((18)F-FLT)-a pilot study. *Eur J Surg Oncol* 2006;32:39-43.
- [29] Smyczek-Gargya B, Fersis N, Dittmann H, Vogel U, Reischl G, Machulla HJ, et al. PET with [18F]fluorothymidine for imaging of primary breast cancer: a pilot study. *Eur J Nucl Med Mol Imaging* 2004;31:720-4.
- [30] Garcia-Manteiga J, Molina-Arcas M, Casado FJ, Mazo A, Pastor-Anglada M. Nucleoside transporter profiles in human pancreatic cancer cells: role of hCNT1 in 2',2'-difluorodeoxycytidine- induced cytotoxicity. *Clin Cancer Res* 2003;9:5000-8.
- [31] Spratlin J, Sangha R, Glubrecht D, Dabbagh L, Young JD, Dumontet C, et al. The absence of human equilibrative nucleoside transporter 1 is associated with reduced survival in patients with gemcitabine-treated pancreas adenocarcinoma. *Clin Cancer Res* 2004;10:6956-61.

- [32] Pennycooke M, Chaudary N, Shuralyova I, Zhang Y, Coe IR. Differential expression of human nucleoside transporters in normal and tumor tissue. *Biochem Biophys Res Commun* 2001;280:951-9.

**Chapter 4: Biodistribution and uptake of 3'-deoxy-3'-
fluorothymidine in equilibrative nucleoside transporter 1 (ENT1)
knockout mice and in an ENT1 knockdown tumor model¹**

¹ A version of this chapter will be submitted to *The Journal of Nuclear Medicine*.

4.1 Introduction

Radiolabeled 3'-deoxy-3'-fluorothymidine (FLT) is a tracer used to indirectly monitor tissue proliferation using positron emission tomography (PET) [1]. Although several studies have demonstrated a significant correlation between FLT uptake and proliferation markers such as Ki-67 and Proliferating Cell Nuclear Antigen (PCNA) score in tumors [2-7], FLT is not a direct marker of proliferation since FLT is not significantly incorporated into DNA due to the lack of the 3'-hydroxyl group.

FLT is a permeant for four different human nucleoside transporters (hNTs) including human equilibrative nucleoside transporter 1 (hENT1), hENT2, human concentrative nucleoside transport 1 (hCNT1) and hCNT3 (Chapter 3, Fig. 3-2) [8]. Upon cellular entry, FLT is selectively phosphorylated by the cell-cycle regulated thymidine kinase 1 (TK1) [9]. TK1 expression is greatest during late G1/S-phase which allows proliferating cells to generate greater levels of FLT monophosphate [10]. Phosphorylated FLT is trapped inside cells since hNTs cannot transport nucleotides and most cells do not possess nucleotide-specific, outwardly directed transporters.

hNTs are membrane proteins involved in the transport of physiological nucleosides and various anti-cancer and anti-viral nucleoside analogs (see [11, 12] for reviews on hNTs). The two families of hNTs include hENTs and hCNTs. hENTs facilitate the bidirectional transport of nucleosides across membranes while hCNTs are symporters that mediate the influx of nucleosides and cations using the cation's electrochemical gradient as the energy source for transport. The

four hENT members are hENT1, hENT2, hENT3, and hENT4, although only hENT1 and hENT2 are considered important for cellular uptake of FLT since hENT3 is mainly found on intracellular membranes and hENT4 is selective for adenosine and monoamine/organic cations [13, 14]. hCNTs consist of three members, hCNT1, hCNT2, and hCNT3, although only hCNT1 and hCNT3 are capable of efficient FLT transport (Chapter 3, Fig. 3-2) since hCNT2 is purine nucleoside selective and has low affinity for FLT [8, 15].

Inhibition of hENT1 by nitrobenzylmercaptapurine ribonucleoside (NBMPR) caused at least 50% inhibition of mediated FLT uptake in six different cultured cell lines (Chapter 3, Fig. 3-4) [8]. To determine if ENT1 significantly affects FLT biodistribution, ENT1 knockout mice as well as wildtype mice injected with NBMPR phosphate (NBMPR-P) were analyzed using [¹⁸F]FLT small animal PET. To determine if hENT1 significantly affects FLT uptake in a tumor model, [¹⁸F]FLT PET was performed on mice bearing xenograft tumors comprised of the lung carcinoma A549 cell line that has been stably transfected with shRNA against either hENT1 or a scrambled sequence with no homology to any known mammalian gene. The results suggested that ENT1 significantly influenced [¹⁸F]FLT biodistribution in various tissues including the spleen and bone marrow. Decreased hENT1 expression in A549 xenograft tumors significantly decreased [¹⁸F]FLT uptake, suggesting that ENT1 is an important mediator of FLT uptake in *in vivo* models.

4.2 Results

4.2.1 Characterization of *ENT1* transcript levels in spleens of individual *ENT1*^{+/+} and *ENT1*^{-/-} mice

Spleens from individual *ENT1*^{+/+} and *ENT1*^{-/-} mice were analyzed for *ENT1* transcript levels using TaqMan real-time quantitative RT-PCR and Fig. 4-1 displays the results of the Taqman real-time reverse-transcriptase polymerase chain reaction (RT-PCR) experiment. *ENT1* transcripts were detectable in *ENT1*^{+/+} mouse spleen whereas no *ENT1* was detectable in *ENT1*^{-/-} mouse spleen (Fig. 4-1).

4.2.2 [¹⁸F]FLT PET with *ENT1* altered mice

To determine how *ENT1* affects FLT biodistribution, *ENT1*^{+/+}, *ENT1*^{-/-}, and *ENT1*^{+/-} mice underwent [¹⁸F]FLT PET for 1 h (Fig. 4-2). Four *ENT1*^{+/+} mice were also injected with 15 mg/kg NBMPR-P 1 h before imaging to determine if pharmacological blockage of *ENT1* affected [¹⁸F]FLT biodistribution in wildtype mice (Fig. 4-2). A previous study by Gati *et al.* [16] demonstrated that, when mice were injected with 15 mg/kg NBMPR-P, NBMPR-P was metabolized to NBMPR and plasma NBMPR concentrations were approximately 5 μM one hour after NBMPR-P injection. Low micromolar concentrations of NBMPR effectively inhibited m*ENT1* activity and produced no significant toxicities to mice [16, 17], suggesting that injection of mice with 15 mg/kg NBMPR-P should safely and effectively inhibit *ENT1* activity one hour after NBMPR-P injection.

One hour after [¹⁸F]FLT injection, *ENT1*^{+/+} mice displayed the typical FLT biodistribution observed in rodents [18] while injection of NBMPR-P

increased FLT uptake in the bone marrow and spleen of treated mice (Fig 4-2). ENT1^{-/-} mice displayed the greatest increase in FLT uptake in the bone marrow and spleen (Fig 4-2). When comparing [¹⁸F]FLT uptake in ENT1^{-/-} and ENT1^{+/+} mice 1 h after [¹⁸F]FLT injection, ENT1^{-/-} mice displayed significant ($P < 0.05$) 19-36% decreases in values of percent injected dose per gram (%ID/g) in blood, heart, kidney, liver, lungs, and brain (Table 4-1). Conversely, ENT1^{-/-} mice displayed significant ($P < 0.05$) 2.8-4.6 fold increases in [¹⁸F]FLT uptake (%ID/g) in bone, bone marrow, and spleen. When [¹⁸F]FLT uptake was normalized to blood levels [%ID/g (tissue)/%ID/g (blood)], only the bone, bone marrow, and spleen in ENT1^{-/-} mice displayed significant ($P < 0.05$) differences (3.1-5.9 fold increases) in [¹⁸F]FLT uptake.

Similar to ENT1^{-/-} mice, ENT1^{+/+} mice injected with NBMPR-P 1 h before imaging displayed significant ($P < 0.05$) 16-30% decreases in [¹⁸F]FLT uptake (%ID/g) compared to that of untreated ENT1^{+/+} mice in blood, brain, and liver (Table 4-1) and significant ($P < 0.05$) 1.5-2.7 fold increases in [¹⁸F]FLT uptake [%ID/g (tissue)/%ID/g (blood)] for bone, bone marrow, and spleen when compared to untreated ENT1^{+/+} mice (Table 4-1), suggesting that inhibition of ENT1 in ENT1^{+/+} mice by NBMPR-P altered FLT biodistribution similar to that found in ENT1^{-/-} mice. However, compared to ENT1^{-/-} mice, ENT1^{+/+} mice injected with NBMPR-P did not display reduced FLT uptake within the kidney and lungs, suggesting that decreased FLT uptake within these tissues in the ENT1^{-/-} mice may have been due to altered expression of genes encoding other NTs or proteins involved in FLT uptake.

ENT1^{+/-} mice were several months older and were slightly larger than the other mice, causing the ENT1^{+/-} mice to have reduced %ID/g [¹⁸F]FLT uptake values compared to the other mice. To compensate for the larger size of the ENT1^{+/-} mice, [¹⁸F]FLT uptake values for all mice were normalized using [%ID/g(tissue)]/[%ID/g(blood)] values. Compared to ENT1^{+/+} mice, ENT1^{+/-} mice displayed significant ($P < 0.05$) 1.1-1.3 fold increases in normalized [¹⁸F]FLT uptake for colon and bone (Table 4-1). In general, reducing ENT1 activity significantly affected [¹⁸F]FLT biodistribution in various tissues and the ENT1 knockout mice displayed the largest changes in [¹⁸F]FLT biodistribution compared to ENT1^{+/+} mice.

4.2.3 TK1 immunoblots of mouse spleens

Spleen tissues from ENT1^{+/+}, ENT1^{-/-}, and ENT1^{+/-} mice were excised and analyzed for TK1 (and β -actin as a control) using immunoblots to determine if there were differences in spleen TK1 protein levels between groups of mice since [¹⁸F]FLT uptake was significantly higher in spleens of ENT1^{-/-} mice compared to ENT1^{+/+} mice. Although spleen TK1 levels varied for each mouse, there were no significant differences when comparing standardized TK1 levels (TK1/ β -actin band intensities) from ENT1^{+/+}, ENT1^{-/-}, and ENT1^{+/-} mice ($P > 0.05$, Fig. 4-3A). The data indicates that spleen TK1 protein levels between mouse strains were not significantly different and could not account for the large differences observed in spleen FLT uptake.

4.2.4 NT immunohistochemistry of mouse spleens

Spleen tissues from ENT1^{+/+} and ENT1^{-/-} mice were excised and analyzed using immunohistochemistry to determine which mNTs were present. From the representative immunohistochemistry slides, mENT2 staining appeared stronger in ENT1^{-/-} mice and mCNT1 and mCNT3 staining appeared slightly stronger in ENT1^{+/+} mice (Fig. 4-3B). The data demonstrated that mCNT1 and mCNT3 were abundant in the spleens of both groups and that the absence of ENT1 may have caused a small increase in mENT2 protein levels and small decreases in mCNT1 and mCNT3 protein levels in spleens of ENT1^{-/-} mice.

4.2.5 Thymidine levels in mouse plasma

To determine if there were differences in plasma thymidine levels between ENT1^{+/+} and ENT1^{-/-} mice that may have influenced FLT biodistribution, mice were euthanized and plasma samples were collected and analyzed for thymidine using liquid chromatography-mass spectrometry (LC-MS). Representative chromatograms for individual ENT1^{+/+} and ENT1^{-/-} mice are shown in Figure 4-4A and mean values for results obtained for groups of three mice are shown in Figure 4-4B. ENT1^{-/-} mice displayed significantly greater plasma thymidine levels (1.65-fold, $P < 0.005$) than ENT1^{+/+} mice. The increased plasma thymidine levels in ENT1^{-/-} mice may have decreased the amount of unoccupied NTs and TK1 available for interacting with FLT, potentially explaining the reduced levels of [¹⁸F]FLT uptake in various tissues.

4.2.6 In vitro characterization of transfected A549 cells

To determine how altered ENT1 levels affect FLT uptake in a tumor model, A549 cells were stably transfected with pSUPER encoding a 1) shRNA

with a scrambled sequence with no homology to any known mammalian protein (A549-pSUPER-SC), or 2) shRNA targeted against hENT1 (A549-pSUPER-hENT1). The resulting A549-derived cell lines were analyzed for TK1 and hENT1 transcript levels using quantitative real-time RT-PCR (Fig. 4-5A). TK1 transcript expression was not significantly different between A549-pSUPER-SC and A549-pSUPER-hENT1 cells whereas hENT1 transcript expression in A549-pSUPER-hENT1 cells was significantly lower (55% decrease, $P < 0.0005$) than that of A549-pSUPER-SC cells.

Equilibrium NBMPR binding experiments were performed on the A549 cell lines since NBMPR binds to hENT1 molecules thereby allowing quantification of hENT1 protein levels. Extracellular NBMPR binding sites were determined by incubating A549 cell lines with or without 100 nM 5-*S*-{2-(1-[(fluorescein-5-yl)thioureido]hexanamido)ethyl}-6-*N*-(4-nitrobenzyl)-5-thioadenosine (FTH-SAENTA), which is membrane impermeant and blocks binding of NBMPR on extracellular specific NBMPR binding sites (*i.e.*, cell surface hENT1). The number of extracellular NBMPR binding sites/cell were not significantly different in untransfected A549 and A549-pSUPER-SC cells ($84,000 \pm 13,000$ vs $106,000 \pm 15,000$, respectively, $P > 0.05$) whereas A549-pSUPER-hENT1 cells displayed significantly lower (0.45-fold, $P < 0.01$) extracellular NBMPR binding sites/cell compared to that of A549-pSUPER-SC cells (Fig. 4-5B).

Cultured A549, A549-pSUPER-SC, and A549-pSUPER-hENT1 cells were incubated for 1 h with 100 nM [3 H]FLT to determine each cell line's

capacity for [³H]FLT uptake. Untransfected A549 and A549-pSUPER-SC cells displayed similar levels of [³H]FLT uptake (17.6 ± 1.1 vs 18.9 ± 1.7 pmol/mg protein/h, respectively, $P > 0.05$) whereas A549-pSUPER-hENT1 cells displayed significantly lower [³H]FLT uptake compared to that of A549-pSUPER-SC cells (0.68-fold, $P < 0.05$, Fig. 4-5C). These data suggested that A549-pSUPER-hENT1 cells had 1) lower levels of hENT1 transcripts and NBMPR binding sites (hENT1 molecules), and 2) lower FLT uptake than A549-pSUPER-SC cells.

4.2.7 *In vivo* characterization of transfected A549 cells

To determine if reduced hENT1 levels in tumors led to reduced FLT uptake, A549-pSUPER-SC and A549-pSUPER-hENT1 cells were, respectively, injected over the left and right thighs of NIH-III mice and, when tumors were at least 250 mm³ in volume, mice underwent dynamic [¹⁸F]FLT PET imaging for 1 h. Figure 4-6A provides a representative summarized maximum intensity projection [¹⁸F]FLT PET image of a single mouse 60-min post injection which displayed significantly greater [¹⁸F]FLT uptake in the A549-pSUPER-SC tumor compared to that of the A549-pSUPER-hENT1 tumor. Average tumor [¹⁸F]FLT standardized uptake values (SUVs) from five different mice were plotted over time to generate time-activity curves (TACs). The average [¹⁸F]FLT maximum SUV (SUV_{max}) was significantly larger for A549-pSUPER-SC tumors than that of A549-pSUPER-hENT1 tumors (0.82 ± 0.15 and 0.53 ± 0.12 , respectively, $P < 0.01$, Fig. 4-6B). Tumor [¹⁸F]FLT %ID/g values were determined by *ex vivo* gamma counting and produced results that were similar to that of PET image

analysis (4.9 ± 0.43 and 3.7 ± 0.26 for A549-pSUPER-SC and A549-pSUPER-hENT1 tumors, respectively, $P < 0.05$).

Kinetic analysis of A549-pSUPER-SC and A549-pSUPER-hENT1 xenograft tumors from data obtained from dynamic small animal [^{18}F]FLT PET experiments was performed using a previously described three-compartment model (Fig. 4-7) [19]. Apparent K_1 , k_2 , k_3 , and k_4 values, representing [^{18}F]FLT transport from blood to tissue, [^{18}F]FLT efflux from tissue to blood, [^{18}F]FLT phosphorylation, and [^{18}F]FLT dephosphorylation, respectively, are shown in Table 4-2. Compared to A549-pSUPER-SC tumors, A549-pSUPER-hENT1 tumors displayed 0.64-fold K_1 values ($P < 0.05$), suggesting that decreased hENT1 protein levels decreased [^{18}F]FLT K_1 values. Surprisingly, A549-pSUPER-hENT1 tumors displayed significantly greater k_3 values (1.5-fold, $P < 0.05$) compared to those of A549-pSUPER-SC tumors. Although k_3 values represent [^{18}F]FLT phosphorylation in tissue, which is considered the rate limiting step in [^{18}F]FLT retention [4, 20], the increased k_3 values displayed by A549-pSUPER-hENT1 tumors had minimal effects on [^{18}F]FLT uptake, which was lower in these tumors compared to those of A549-pSUPER-SC tumors. There were no significant differences in TK1 level between A549-pSUPER-SC and A549-pSUPER-hENT1 tumors (Fig. 4-6C), suggesting that the k_3 parameter in the described three compartment model (Fig. 4-7) may not have been completely dependent on TK1 activity.

A549-pSUPER-SC and A549-pSUPER-hENT1 tumors were excised and analyzed for TK1/ β -actin levels using immunoblots to determine if TK1 levels

varied between the two different tumors (Fig. 4-6C). Although TK1 levels differed substantially between tumors from different mice, average TK1/ β -actin band intensities did not significantly differ between A549-pSUPER-SC and A549-pSUPER-hENT1 tumors ($P > 0.05$), suggesting that differences in [^{18}F]FLT uptake between A549-pSUPER-SC and A549-pSUPER-hENT1 tumors were not caused by differences in TK1 activity.

4.3 Discussion

[¹⁸F]FLT is considered a PET proliferation tracer since phosphorylation of FLT by cell cycle-regulated TK1 ‘traps’ FLT within cells and allows cellular FLT accumulation [1]. However, FLT must cross plasma membranes before it may be phosphorylated by TK1, suggesting that permeation of FLT across plasma membranes is also an important step for cellular FLT accumulation. *In vitro* experiments with cultured cell lines demonstrated that hNTs play an important role in FLT uptake (Chapters 3 and 5; Fig. 3-4 and Table 5-3) [8, 21]. The work described in this chapter demonstrated the importance of NTs, in particular ENT1, in [¹⁸F]FLT biodistribution and tumor uptake using *in vivo* models.

ENT1^{-/-} mice had slightly altered levels of ENT2, CNT1, and CNT3 compared to those of ENT1^{+/+} mice (Fig. 4-3B), suggesting that differences in FLT biodistribution in the two strains of mice may have been caused by both the functional deletion of ENT1 and altered expression of other NTs. When comparing ENT1^{+/+} and ENT1^{-/-} mice, there may also have been differences in the levels of other proteins that may have altered FLT biodistribution, including uridine diphosphate glucuronosyltransferases, which are likely involved in the formation of FLT-glucuronide [22]. To determine the role of ENT1 in the biodistribution of [¹⁸F]FLT, ENT1^{+/+} mice were injected with 15 mg/kg NBMPR-P, which is rapidly metabolized to NBMPR and inhibits ENT1 [16, 23], followed by [¹⁸F]FLT small animal PET. Compared to ENT1^{+/+} mice, both ENT1^{-/-} mice and ENT1^{+/+} mice injected with NBMPR-P displayed decreased circulating

[¹⁸F]FLT levels and increased [¹⁸F]FLT uptake in the spleen and bone marrow 1 h after tracer injection (Table 4-1, Fig. 4-2).

[¹⁸F]FLT biodistribution in ENT1^{-/-} mice was similar to that of rats injected with thymidine phosphorylase, which displayed increased [¹⁸F]FLT accumulation in the bone marrow and spleen [18], suggesting that ENT1^{-/-} mice may have had decreased circulating thymidine levels compared to ENT1^{+/+} mice. However, LC-MS analysis of plasma thymidine levels showed that ENT1^{-/-} mice displayed a 1.65-fold increase in plasma thymidine levels compared to ENT1^{+/+} mice (Fig. 4-4) - i.e., the increase in [¹⁸F]FLT uptake in the spleen and bone marrow of ENT1^{-/-} mice was not caused by decreased levels of circulating thymidine.

Experiments in Chapters 3 and 5 demonstrated that inhibition of ENT1 decreased [³H]FLT uptake in cultured cells (Fig. 3-4 and Table 5-3) [8, 21], which was the opposite of what was observed in spleen and bone marrow tissues of ENT1^{-/-} mice when compared to ENT1^{+/+} mice. Since there was no difference in spleen TK1 protein levels between the two strains of mice (Fig. 4-3A), and since circulating thymidine levels were higher in ENT1^{-/-} compared to ENT1^{+/+} mice (Fig. 4-4), the data suggests that the increased [¹⁸F]FLT accumulation in these tissues was caused by increased CNT/ENT transport ratios. CNTs can only transport FLT into cells while ENTs can transport FLT both into and out of cells. If FLT influx mediated by CNTs was greater than FLT efflux mediated by ENTs, FLT could accumulate within cells without FLT phosphorylation by TK1. Although many cultured cell lines have significantly greater levels of ENTs

compared to CNTs [8, 21], cultured human renal cells hRPTC1 displayed 1) significant amounts of CNT-dependent uridine uptake, and 2) approximately 1.4-fold increased uridine uptake when incubated with dilazep (hENT1 and hENT2 inhibitor), suggesting that inhibition of ENTs may increase nucleoside uptake if significant levels of CNTs are present [24]. The mouse spleen displays significant levels of CNTs (Fig. 4-3B), which supports this hypothesis. Furthermore, human bone marrow has very high hCNT3 transcript expression [25], suggesting that focal uptake of [¹⁸F]FLT in human bone marrow may be primarily caused by relatively high hCNT transport activity.

Figure 4-8 summarizes these concepts and illustrates how FLT uptake may be affected by hNTs in the absence of TK1. Cells with large hENT/hCNT transport activity ratios allow equilibration of FLT across plasma membranes with relatively little intracellular FLT accumulation (Fig. 4-8A) whereas cells with large hCNT/hENT transport activity ratios allow concentration of FLT into cells even in the absence of TK1 (Fig. 4-8B). Inhibition of hENT1 in cells with large hENT/hCNT transport activity ratios decreases initial rates of FLT influx and may not concentrate FLT into cells if hENT2 efflux activity is greater than hCNT1/3 influx activities. Inhibition of hENT1 in cells with large hCNT/hENT transport activity ratios may allow greater FLT concentration into cells since hENT1 (and hENT2) predominantly mediate FLT efflux when intracellular FLT concentrations are greater than extracellular FLT concentrations.

Cultured A549-pSUPER-hENT1 cells displayed 0.45-fold extracellular NBMPR binding sites (i.e., cell-surface hENT1) and 0.68-fold [³H]FLT uptake

compared to A549-pSUPER-SC cells (Figs. 4-5B and 4-5C). [³H]FLT uptake in cultured A549 cells was also dependent on hENT2, which may explain why changes in cell surface hENT1 levels did not have an equivalent effect on [³H]FLT uptake [8]. Cultured A549 cells express very low levels of hCNT1 and hCNT3 transcripts compared to those of hENT1 and hENT2, potentially explaining why reducing ENT1 activity caused a decrease in [³H]FLT uptake [8]. A549-pSUPER-hENT1 xenograft tumors displayed 0.76-fold reduced [¹⁸F]FLT %ID/g values when compared to A549-pSUPER-SC tumors. The reduction in FLT uptake caused by shRNA against hENT1 was smaller in tumors compared to cultured cells which may be explained by the presence in tumors of some host-derived cells (*e.g.*, cells in blood vessels) that do not contain shRNA against hENT1.

A549-pSUPER-hENT1 tumors displayed reduced apparent K_1 values for [¹⁸F]FLT compared to A549-pSUPER-SC tumors. Although tumor blood flow was not determined, differences in blood flow between A549-pSUPER-SC and A549-pSUPER-hENT1 tumors may partly explain the observed differences in apparent K_1 values. However, the reduction in apparent K_1 values between tumors was likely caused by differences in hENT1 levels since cultured A549-pSUPER-hENT1 cells displayed reduced FLT uptake compared to that of A549-pSUPER-SC cells. Both *in vitro* and *in vivo* data suggest that decreased hENT1 activity in high hENT/hCNT ratio expressing cells decreases FLT uptake.

Although many clinical trials have shown correlations between [¹⁸F]FLT uptake and proliferation markers in tumors [26-31], other studies have not been

able to reproduce such correlations [32-34]. Differences in tumor hNT levels may explain such discrepancies since hNT transcript and protein levels differ significantly among tumors for many cancer types, with some tumors displaying no detectable hENT1 protein [35-37]. Additionally, some therapeutic agents inhibit hENT1 and/or hENT2 activities, including dipyridamole [38, 39] and various protein kinase inhibitors [40]. The use of such agents prior to [¹⁸F]FLT PET scans may alter [¹⁸F]FLT biodistribution and/or affect tumor uptake of [¹⁸F]FLT, suggesting that patients' therapy regimens should be known prior to analysis of [¹⁸F]FLT PET scans.

Table 4-1. [¹⁸F]FLT biodistribution in mice with various ENT1 activities.

ENT1^{+/+} mice with (n = 4) or without (n = 6) injection of 15 mg/kg NBMPR-P one h before imaging and ENT1^{+/-} (n = 5) and ENT1^{-/-} (n = 6) mice were injected with 2-10 MBq [¹⁸F]FLT and then subjected to small animal PET imaging for one hour as described in section 2.8.2. After [¹⁸F]FLT PET, mice were euthanized and tissues were excised, weighed, and analyzed for radioactivity with a gamma counter as described in section 2.8.2. Values represent mean ± standard error of the mean (SEM) and blood normalized [¹⁸F]FLT uptake values [(%ID/g tissue)/(%ID/g blood)] were obtained by dividing tissue %ID/g values with blood %ID/g value for the same mouse strain.

Organ	ENT1 ^{+/+} +				ENT1 ^{+/+} +			
	ENT1 ^{+/+}	NBMPR-P	ENT1 ^{+/-}	ENT1 ^{-/-}	ENT1 ^{+/+}	NBMPR-P	ENT1 ^{+/-}	ENT1 ^{-/-}
	%ID/g				(%ID/g tissue)/(%ID/g blood)			
Blood	5.7 ± 0.3	4.8 ± 0.3*	4.1 ± 0.2	4.6 ± 0.4	1.0 ± 0.05	1.0 ± 0.07	1.0 ± 0.1	1.0 ± 0.08
Heart	5.3 ± 0.2	4.7 ± 0.2	4.0 ± 0.2	3.9 ± 0.2	0.9 ± 0.04	1.0 ± 0.05	1.0 ± 0.1	0.8 ± 0.04
Brain	1.0 ± 0.1	0.7 ± 0.02	0.7 ± 0.1	0.7 ± 0.1	0.2 ± 0.02	0.1 ± 0.01	0.2 ± 0.01	0.1 ± 0.01
Small Intestine	7.4 ± 1.0	7.0 ± 1.1	7.3 ± 1.4	6.6 ± 1.0	1.3 ± 0.2	1.5 ± 0.2	1.8 ± 0.4	1.4 ± 0.2
Colon	5.4 ± 0.4	4.8 ± 0.2	4.7 ± 0.3	5.3 ± 0.6	0.9 ± 0.07	1.0 ± 0.04	1.2 ± 0.07	1.2 ± 0.1
Kidney	8.7 ± 0.6	8.7 ± 1.8	5.8 ± 0.8	6.2 ± 0.6	1.5 ± 0.1	1.8 ± 0.4	1.4 ± 0.2	1.3 ± 0.1
Liver	6.5 ± 0.4	5.3 ± 0.3	4.4 ± 0.2	5.1 ± 0.2	1.2 ± 0.07	1.1 ± 0.07	1.1 ± 0.04	1.1 ± 0.05
Muscle	4.6 ± 0.5	4.3 ± 0.3	2.8 ± 0.1	3.4 ± 0.4	0.8 ± 0.09	0.9 ± 0.07	0.7 ± 0.02	0.7 ± 0.09
Adipose tissue	0.6 ± 0.1	0.5 ± 0.01	0.4 ± 0.1	0.8 ± 0.2	0.1 ± 0.02	0.1 ± 0.01	0.1 ± 0.02	0.2 ± 0.03
Lungs	5.7 ± 0.4	5.0 ± 0.3	4.0 ± 0.2	4.3 ± 0.3	1.0 ± 0.07	1.1 ± 0.05	1.0 ± 0.06	0.9 ± 0.06
Bone	3.7 ± 0.2	5.5 ± 0.5	3.3 ± 0.2	10.3 ± 1.1	0.7 ± 0.04	1.1 ± 0.1	0.8 ± 0.05	2.2 ± 0.2
Bone Marrow	6.4 ± 2.5	17 ± 2	5.9 ± 0.9	29 ± 8	1.1 ± 0.4	3.6 ± 0.4	1.5 ± 0.2	6.4 ± 1.8
Spleen	6.4 ± 1.3	12 ± 2	12.2 ± 4.8	30 ± 9	1.1 ± 0.2	2.5 ± 0.4	3.0 ± 1.2	6.5 ± 2.0

* Values of %ID/g and (%ID/g tissue)/(%ID/g blood) in bold type are significantly different from those of ENT1^{+/+} mice (*P* < 0.05).

Table 4-2. [¹⁸F]FLT apparent kinetic values for A549-pSUPER-SC and A549-pSUPER-hENT1 tumors in NIH-III mice using a 3-compartment model.

Five NIH-III mice bearing A549-pSUPER-SC and A549-pSUPER-hENT1 tumors over the right and left thighs, respectively, underwent [¹⁸F]FLT PET for one hour as described in section 2.8.2. Apparent [¹⁸F]FLT kinetic parameters (K_1 , k_2 , k_3 , and k_4) in xenograft tumors were determined from PET images using a previously established 3-compartment model [19] as described in section 2.8.3. Values represent mean \pm SEM from the five mice imaged.

Kinetic parameter	A549-pSUPER-SC	A549-pSUPER-hENT1
K_1 (ml/min/g)	0.069 \pm 0.010	0.044 \pm 0.009*
k_2 (min ⁻¹)	0.124 \pm 0.008	0.161 \pm 0.019
k_3 (min ⁻¹)	0.040 \pm 0.008	0.061 \pm 0.011
k_4 (min ⁻¹)	0.024 \pm 0.002	0.035 \pm 0.006
$k_3/(k_2+k_3)$	0.235 \pm 0.038	0.269 \pm 0.014
$K_1*[k_3/(k_2+k_3)]$ (ml/min/g)	0.015 \pm 0.002	0.012 \pm 0.002

* Values in bold type are significantly different from the values obtained for A549-pSUPER-SC tumors ($P < 0.05$)

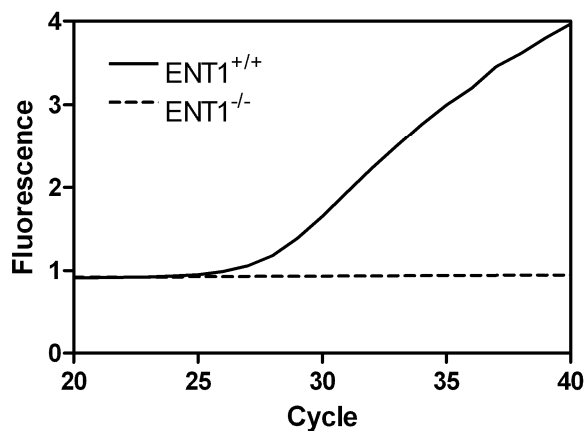


Figure 4-1. Analysis of mENT1 transcript levels in spleens of ENT1^{+/+} and ENT1^{-/-} mice. mRNA was isolated from spleens of ENT1^{+/+} and ENT1^{-/-} mice and ENT1 transcript levels were analyzed with TaqMan real-time RT-PCR as described in section 2.5. Shown are fluorescence levels, which represent the presence of ENT1 mRNA transcripts, from individual wells from a representative experiment.

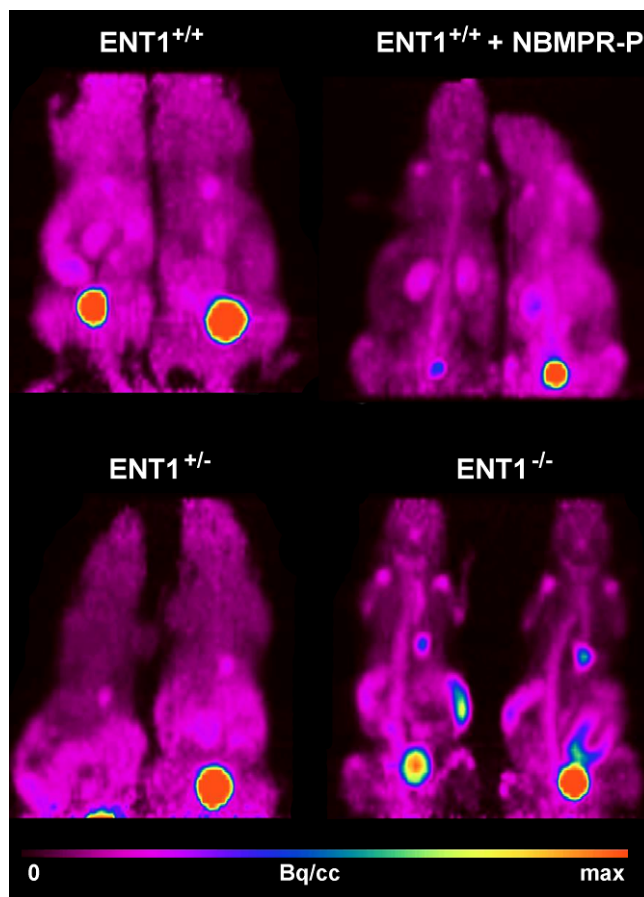


Figure 4-2. [^{18}F]FLT PET maximum intensity projection images of $ENT1^{+/+}$ mice, $ENT1^{+/+}$ mice injected with 15 mg/kg NBMPR-P 1 h before imaging, $ENT1^{+/-}$ mice, and $ENT1^{-/-}$ mice. Mice were injected with 2-10 MBq [^{18}F]FLT and underwent [^{18}F]FLT PET for one hour as described in section 2.8.2. Images were summations of radioactivity over 10 min from approximately 50-60 min after tracer injection.

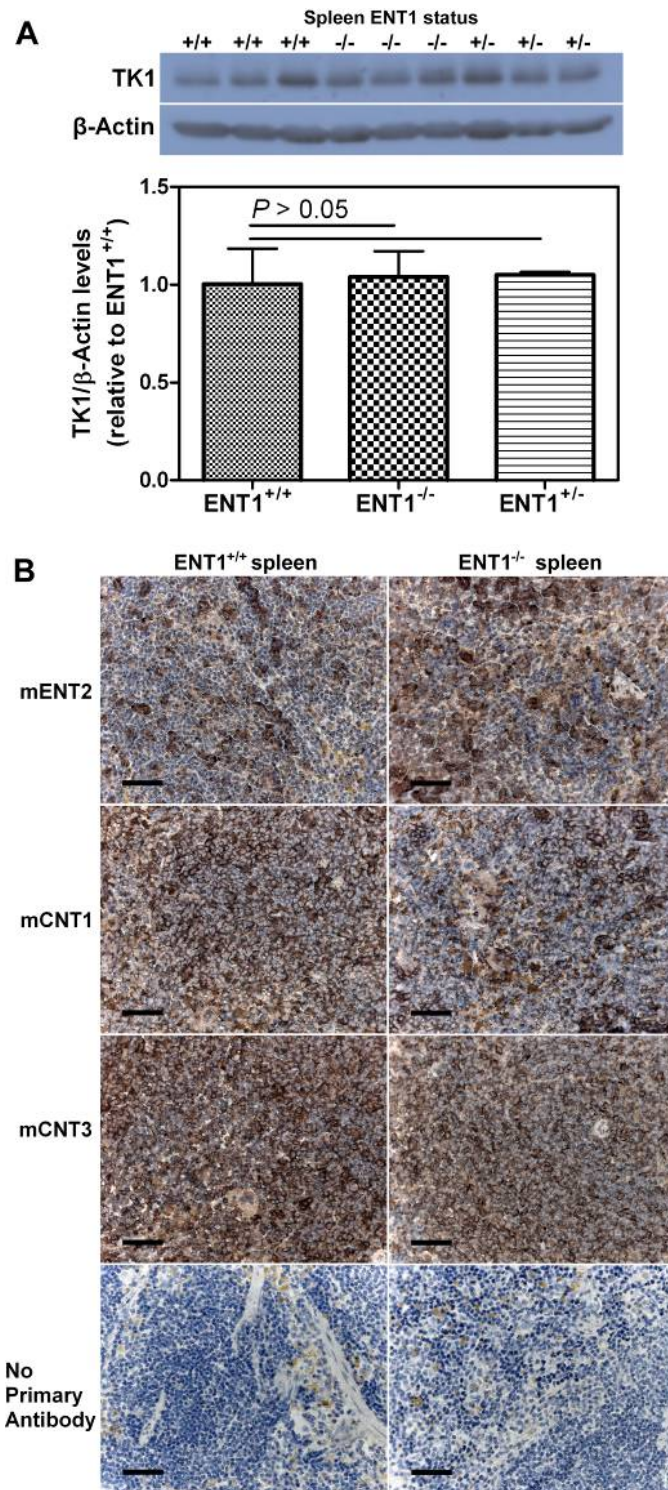


Figure 4-3. Characterization of TK1 and mNT levels in ENT1 altered mice.

(A) Three ENT1^{+/+}, ENT1^{-/-}, and ENT1^{+/-} mice were euthanized and spleens were excised and analyzed for TK1 and β-actin levels using immunoblotting as

described in section 2.9. Average TK1/ β -actin band intensity ratios were quantified with MetaMorph Offline software and bars represent mean \pm SEM values. **(B)** ENT1^{+/+} and ENT1^{-/-} mice were euthanized and spleens were excised and characterized for NT levels using immunohistochemistry as described in section 2.10. Scale bars represent 50 μ m lengths.

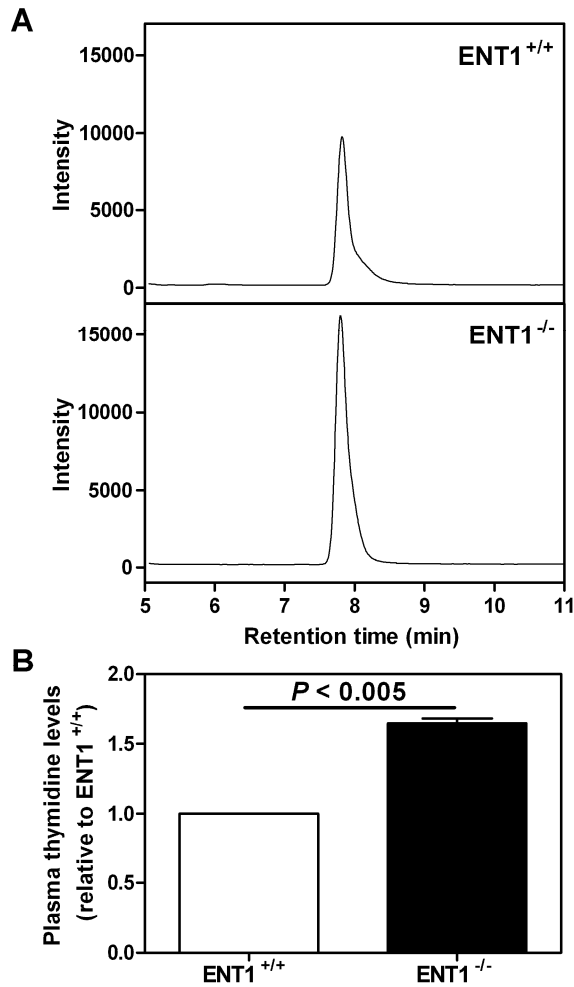


Figure 4-4. LC-MS analysis of plasma thymidine levels in ENT1^{+/+} and ENT1^{-/-} mice. Three ENT1^{+/+} and three ENT1^{-/-} mice were euthanized and blood was collected and centrifuged to isolate plasma. Thymidine levels were analyzed in plasma samples using LC-MS as described in section 2.11. **(A)** Representative single ion monitoring chromatograms for individual ENT1^{+/+} and ENT1^{-/-} mice are shown. **(B)** Values (mean \pm SEM) for plasma thymidine levels from three mice from each strain are shown.

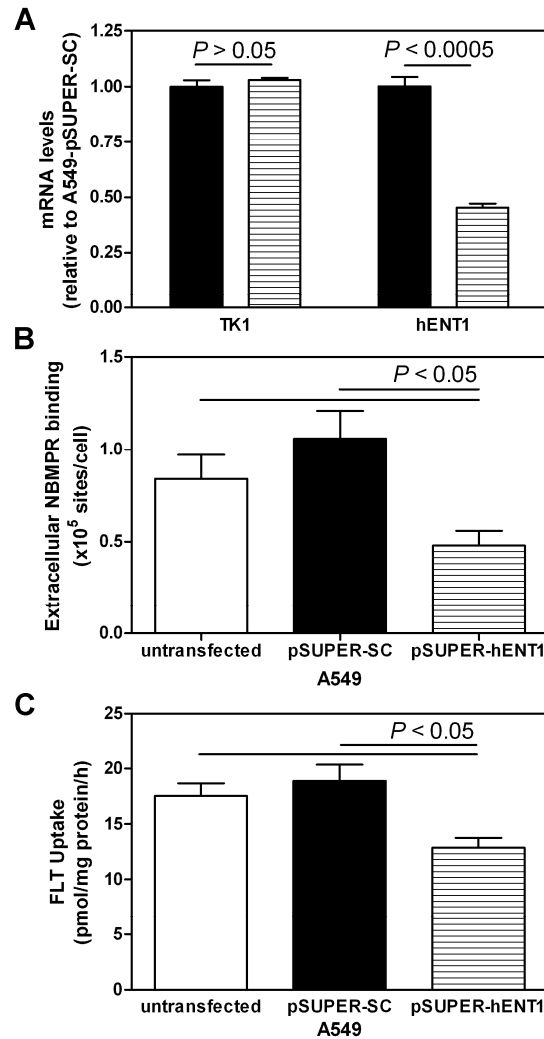


Figure 4-5. Characterization of hENT1 and TK1 transcript levels, NBMPR binding sites, and [³H]FLT uptake in A549-derived cells. (A) mRNA was isolated from cultured A549-pSUPER-SC (black bars) and A549-pSUPER-hENT1 (hatched bars) cells and hENT1 and TK1 mRNA transcripts were quantified relative to those of A549-pSUPER-SC by TaqMan real-time RT-PCR as described in section 2.5. **(B)** Equilibrium [³H]NBMPR binding assays were performed with untransfected A549 (white bars), A549-pSUPER-SC (black bars), and A549-pSUPER-hENT1 (hatched bars) cells in 24-well plates by incubating

cells for 1 h with either 10 nM [³H]NBMPR, 10 nM [³H]NBMPR with 100 nM FTH-SAENTA, or 10 nM [³H]NBMPR with 10 μM NBMPR as described in section 2.6. **(C)** A549 (white bars), A549-pSUPER-SC (black bars), and A549-pSUPER-hENT1 (hatched bars) cells in 24-well plates were incubated for 1 h in DMEM + 10% CS containing 100 nM [³H]FLT as described in section 2.4.3. **(A + B + C)** Bars represent mean ± SEM from at least three different experiments (each performed in triplicate).

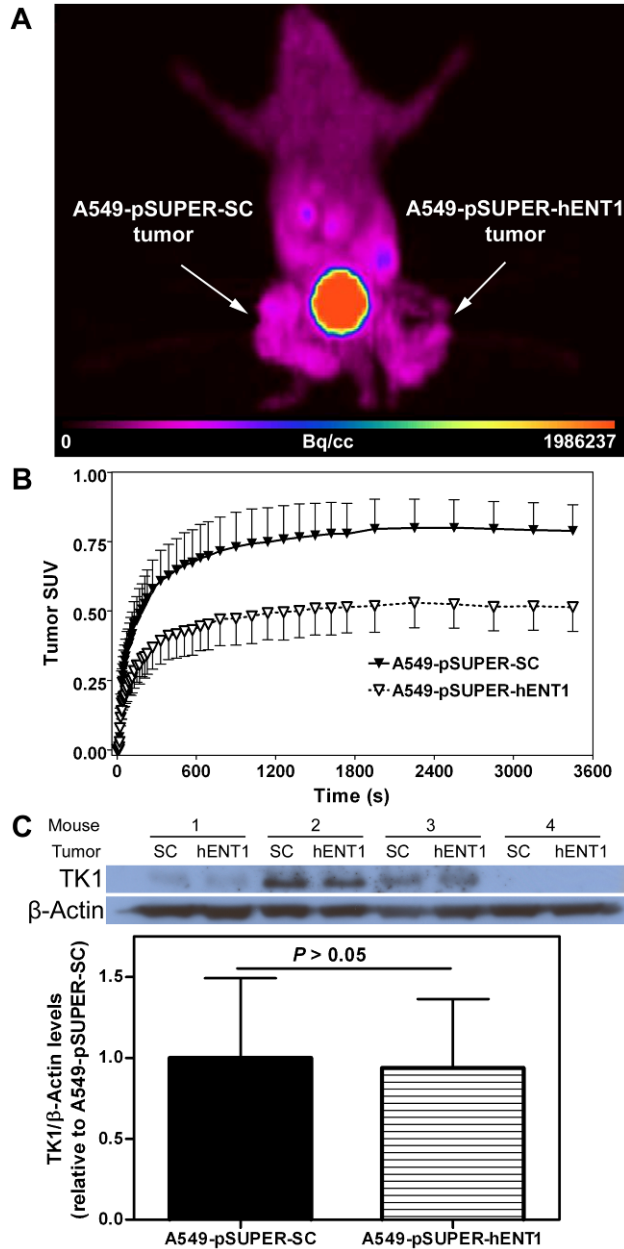


Figure 4-6. [¹⁸F]FLT uptake in A549-pSUPER-hENT1 and A549-pSUPER-SC xenograft tumors. (A) An individual NIH-III mouse bearing A549-pSUPER-SC and A549-pSUPER-hENT1 tumors near the left and right thighs, respectively, was injected with 6.6 MBq [¹⁸F]FLT and underwent [¹⁸F]FLT PET for one hour as described in section 2.8.2. The [¹⁸F]FLT PET maximum intensity projection

image is a summation of radioactivity from 0-60 min after tracer injection. **(B)** [^{18}F]FLT TACs of tumor SUVs from five different mice were generated from the dynamic [^{18}F]FLT PET images. Each symbol represents mean \pm SEM. [^{18}F]FLT accumulation in tumors increased for approximately 10 min post injection but remained relatively constant for the subsequent 50 min. A549-pSUPER-hENT1 tumors displayed significantly reduced [^{18}F]FLT SUV_{max} values compared to those of A549-pSUPER-SC tumors ($P < 0.01$). **(C)** A549-pSUPER-SC and A549-pSUPER-hENT1 tumors were excised from four different euthanized NIH-III mice and analyzed for TK1 and β -actin levels by immunoblotting as described in section 2.9. Average TK1/ β -actin band intensity ratios were quantified with MetaMorph Offline software and bars represent mean \pm SEM values.

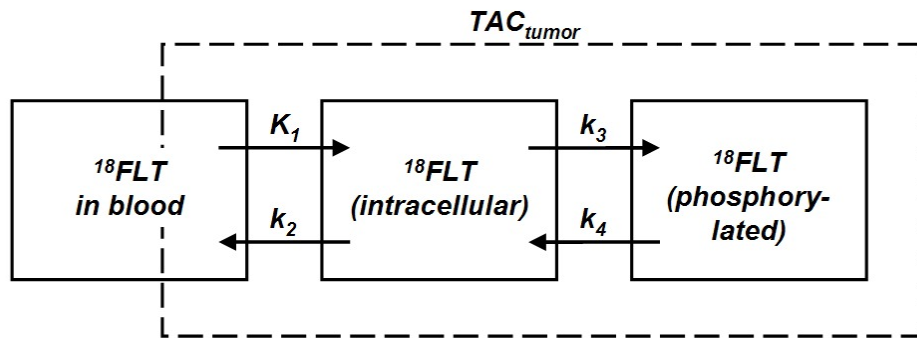


Figure 4-7. Three compartment model describing FLT kinetics. Based on the model described by Muzi et al. [19], radiolabeled FLT can be found in three compartments: FLT in the blood, FLT within cells, and phosphorylated FLT within cells. K_1 represents the amount of blood (ml) completely cleared of FLT per min per gram of tissue, while k_2 , k_3 , and k_4 represent the proportion of FLT transferred from one compartment to another per min as described in the figure. The time-activity curve for tumors (TAC_{tumor} ; shown in Fig. 4-6 B) includes FLT from all three compartments.

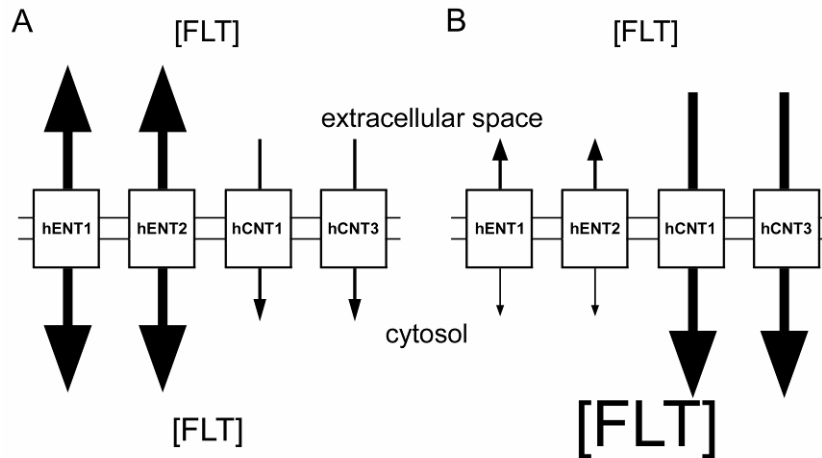


Figure 4-8. Models of FLT uptake mediated by hNTs in the absence of TK1.

(A) Cells with large hENT/hCNT transport activity ratios allow equilibration of FLT across plasma membranes with relatively little intracellular FLT accumulation. Inhibition of hENT1 transport activity in these cells will decrease initial rates of FLT influx and FLT may not concentrate in cells if hENT2 efflux transport activity is still larger than hCNT1/3 influx transport activities. **(B)** Cells with large hCNT/hENT transport activity ratios allow concentration of FLT inside cells. Inhibition of hENT1 transport activity in these cells also decreases initial rates of FLT influx but may allow increased intracellular FLT accumulation since, at later time points, hENTs will predominantly mediate FLT efflux due to larger intracellular FLT levels caused by high hCNT1/3 transport activities.

4.4 Bibliography

- [1] Been LB, Suurmeijer AJ, Cobben DC, Jager PL, Hoekstra HJ, Elsinga PH. [18F]FLT-PET in oncology: current status and opportunities. *Eur J Nucl Med Mol Imaging* 2004;31:1659-72.
- [2] Apisarnthanarax S, Alauddin MM, Mourtada F, Ariga H, Raju U, Mawlawi O, et al. Early detection of chemoradioresponse in esophageal carcinoma by 3'-deoxy-3'-3H-fluorothymidine using preclinical tumor models. *Clin Cancer Res* 2006;12:4590-7.
- [3] Barthel H, Cleij MC, Collingridge DR, Hutchinson OC, Osman S, He Q, et al. 3'-deoxy-3'-[18F]fluorothymidine as a new marker for monitoring tumor response to antiproliferative therapy in vivo with positron emission tomography. *Cancer Res* 2003;63:3791-8.
- [4] Barthel H, Perumal M, Latigo J, He Q, Brady F, Luthra SK, et al. The uptake of 3'-deoxy-3'-[18F]fluorothymidine into L5178Y tumours in vivo is dependent on thymidine kinase 1 protein levels. *Eur J Nucl Med Mol Imaging* 2005;32:257-63.
- [5] Kim SJ, Lee JS, Im KC, Kim SY, Park SA, Lee SJ, et al. Kinetic modeling of 3'-deoxy-3'-18F-fluorothymidine for quantitative cell proliferation imaging in subcutaneous tumor models in mice. *J Nucl Med* 2008;49:2057-66.
- [6] Leyton J, Latigo JR, Perumal M, Dhaliwal H, He Q, Aboagye EO. Early detection of tumor response to chemotherapy by 3'-deoxy-3'-[18F]fluorothymidine positron emission tomography: the effect of cisplatin on a fibrosarcoma tumor model in vivo. *Cancer Res* 2005;65:4202-10.
- [7] Ullrich RT, Zander T, Neumaier B, Koker M, Shimamura T, Waerzeggers Y, et al. Early detection of erlotinib treatment response in NSCLC by 3'-deoxy-3'-[F]-fluoro-L-thymidine ([F]FLT) positron emission tomography (PET). *PLoS ONE* 2008;3:e3908.
- [8] Paproski RJ, Ng AM, Yao SY, Graham K, Young JD, Cass CE. The role of human nucleoside transporters in uptake of 3'-deoxy-3'-fluorothymidine. *Mol Pharmacol* 2008;74:1372-80.
- [9] Munch-Petersen B, Cloos L, Tyrsted G, Eriksson S. Diverging substrate specificity of pure human thymidine kinases 1 and 2 against antiviral dideoxynucleosides. *J Biol Chem* 1991;266:9032-8.
- [10] Sherley JL, Kelly TJ. Regulation of human thymidine kinase during the cell cycle. *J Biol Chem* 1988;263:8350-8.

- [11] Pastor-Anglada M, Cano-Soldado P, Errasti-Murugarren E, Casado FJ. SLC28 genes and concentrative nucleoside transporter (CNT) proteins. *Xenobiotica* 2008;38:972-94.
- [12] Young JD, Yao SY, Sun L, Cass CE, Baldwin SA. Human equilibrative nucleoside transporter (ENT) family of nucleoside and nucleobase transporter proteins. *Xenobiotica* 2008;38:995-1021.
- [13] Baldwin SA, Yao SY, Hyde RJ, Ng AM, Foppolo S, Barnes K, et al. Functional characterization of novel human and mouse equilibrative nucleoside transporters (hENT3 and mENT3) located in intracellular membranes. *J Biol Chem* 2005;280:15880-7.
- [14] Barnes K, Dobrzynski H, Foppolo S, Beal PR, Ismat F, Scullion ER, et al. Distribution and functional characterization of equilibrative nucleoside transporter-4, a novel cardiac adenosine transporter activated at acidic pH. *Circ Res* 2006;99:510-9.
- [15] Wang J, Su SF, Dresser MJ, Schaner ME, Washington CB, Giacomini KM. Na(+)-dependent purine nucleoside transporter from human kidney: cloning and functional characterization. *Am J Physiol* 1997;273:F1058-65.
- [16] Gati WP, Paterson AR. Measurement of nitrobenzylthioinosine in plasma and erythrocytes: a pharmacokinetic study in mice. *Cancer Chemother Pharmacol* 1997;40:342-6.
- [17] Kiss A, Farah K, Kim J, Garriock RJ, Drysdale TA, Hammond JR. Molecular cloning and functional characterization of inhibitor-sensitive (mENT1) and inhibitor-resistant (mENT2) equilibrative nucleoside transporters from mouse brain. *Biochem J* 2000;352 Pt 2:363-72.
- [18] van Waarde A, Cobben DC, Suurmeijer AJ, Maas B, Vaalburg W, de Vries EF, et al. Selectivity of 18F-FLT and 18F-FDG for differentiating tumor from inflammation in a rodent model. *J Nucl Med* 2004;45:695-700.
- [19] Muzi M, Mankoff DA, Grierson JR, Wells JM, Vesselle H, Krohn KA. Kinetic modeling of 3'-deoxy-3'-fluorothymidine in somatic tumors: mathematical studies. *J Nucl Med* 2005;46:371-80.
- [20] Rasey JS, Grierson JR, Wiens LW, Kolb PD, Schwartz JL. Validation of FLT uptake as a measure of thymidine kinase-1 activity in A549 carcinoma cells. *J Nucl Med* 2002;43:1210-7.
- [21] Paproski RJ, Young JD, Cass CE. Predicting gemcitabine transport and toxicity in human pancreatic cancer cell lines with the positron emission tomography tracer 3'-deoxy-3'-fluorothymidine. *Biochem Pharmacol* 2010;79:587-95.

- [22] Schinazi RF, Boudinot FD, Doshi KJ, McClure HM. Pharmacokinetics of 3'-fluoro-3'-deoxythymidine and 3'-deoxy-2',3'-didehydrothymidine in rhesus monkeys. *Antimicrob Agents Chemother* 1990;34:1214-9.
- [23] Kolassa N, Paterson AR, Chou TC. Modification by nitrobenzylthioinosine-5'-monophosphate of pseudoisocytidine pharmacokinetics in mice and rats through inhibition of membrane transport. *Cancer Treat Rep* 1983;67:51-8.
- [24] Elwi AN, Damaraju VL, Kuzma ML, Baldwin SA, Young JD, Sawyer MB, et al. Human concentrative nucleoside transporter 3 is a determinant of fludarabine transportability and cytotoxicity in human renal proximal tubule cell cultures. *Cancer Chemother Pharmacol* 2009;63:289-301.
- [25] Ritzel MW, Ng AM, Yao SY, Graham K, Loewen SK, Smith KM, et al. Molecular identification and characterization of novel human and mouse concentrative Na⁺-nucleoside cotransporter proteins (hCNT3 and mCNT3) broadly selective for purine and pyrimidine nucleosides (system cib). *J Biol Chem* 2001;276:2914-27.
- [26] Buck AK, Halter G, Schirrmeister H, Kotzerke J, Wurziger I, Glatting G, et al. Imaging proliferation in lung tumors with PET: 18F-FLT versus 18F-FDG. *J Nucl Med* 2003;44:1426-31.
- [27] Chen W, Cloughesy T, Kamdar N, Satyamurthy N, Bergsneider M, Liau L, et al. Imaging proliferation in brain tumors with 18F-FLT PET: comparison with 18F-FDG. *J Nucl Med* 2005;46:945-52.
- [28] Cobben DC, Elsinga PH, Suurmeijer AJ, Vaalburg W, Maas B, Jager PL, et al. Detection and grading of soft tissue sarcomas of the extremities with (18)F-3'-fluoro-3'-deoxy-L-thymidine. *Clin Cancer Res* 2004;10:1685-90.
- [29] Kenny LM, Vigushin DM, Al-Nahhas A, Osman S, Luthra SK, Shousha S, et al. Quantification of cellular proliferation in tumor and normal tissues of patients with breast cancer by [18F]fluorothymidine-positron emission tomography imaging: evaluation of analytical methods. *Cancer Res* 2005;65:10104-12.
- [30] Vesselle H, Grierson J, Muzi M, Pugsley JM, Schmidt RA, Rabinowitz P, et al. In vivo validation of 3'-deoxy-3'-[(18)F]fluorothymidine ([18F]FLT) as a proliferation imaging tracer in humans: correlation of [18F]FLT uptake by positron emission tomography with Ki-67 immunohistochemistry and flow cytometry in human lung tumors. *Clin Cancer Res* 2002;8:3315-23.
- [31] Wagner M, Seitz U, Buck A, Neumaier B, Schultheiss S, Bangerter M, et al. 3'-[18F]fluoro-3'-deoxythymidine ([18F]-FLT) as positron emission

tomography tracer for imaging proliferation in a murine B-Cell lymphoma model and in the human disease. *Cancer Res* 2003;63:2681-7.

- [32] Kameyama R, Yamamoto Y, Izuishi K, Takebayashi R, Hagiike M, Murota M, et al. Detection of gastric cancer using 18F-FLT PET: comparison with 18F-FDG PET. *Eur J Nucl Med Mol Imaging* 2009;36:382-8.
- [33] Linecker A, Kermer C, Sulzbacher I, Angelberger P, Kletter K, Dudczak R, et al. Uptake of (18)F-FLT and (18)F-FDG in primary head and neck cancer correlates with survival. *Nuklearmedizin* 2008;47:80-5; quiz N12.
- [34] van Westreenen HL, Cobben DC, Jager PL, van Dullemen HM, Wesseling J, Elsinga PH, et al. Comparison of 18F-FLT PET and 18F-FDG PET in esophageal cancer. *J Nucl Med* 2005;46:400-4.
- [35] Farrell JJ, Elsaleh H, Garcia M, Lai R, Ammar A, Regine WF, et al. Human equilibrative nucleoside transporter 1 levels predict response to gemcitabine in patients with pancreatic cancer. *Gastroenterology* 2009;136:187-95.
- [36] Mackey JR, Jennings LL, Clarke ML, Santos CL, Dabbagh L, Vsianska M, et al. Immunohistochemical variation of human equilibrative nucleoside transporter 1 protein in primary breast cancers. *Clin Cancer Res* 2002;8:110-6.
- [37] Pennycooke M, Chaudary N, Shuralyova I, Zhang Y, Coe IR. Differential expression of human nucleoside transporters in normal and tumor tissue. *Biochem Biophys Res Commun* 2001;280:951-9.
- [38] Griffiths M, Beaumont N, Yao SY, Sundaram M, Boumah CE, Davies A, et al. Cloning of a human nucleoside transporter implicated in the cellular uptake of adenosine and chemotherapeutic drugs. *Nat Med* 1997;3:89-93.
- [39] Griffiths M, Yao SY, Abidi F, Phillips SE, Cass CE, Young JD, et al. Molecular cloning and characterization of a nitrobenzylthioinosine-insensitive (ei) equilibrative nucleoside transporter from human placenta. *Biochem J* 1997;328 (Pt 3):739-43.
- [40] Huang M, Wang Y, Cogut SB, Mitchell BS, Graves LM. Inhibition of nucleoside transport by protein kinase inhibitors. *J Pharmacol Exp Ther* 2003;304:753-60.

**Chapter 5: Predicting gemcitabine transport and toxicity in
human pancreatic cancer cell lines with the positron emission
tomography tracer 3'-deoxy-3'-fluorothymidine¹**

¹ A version of this chapter has been published:

Paproski et al. (2010) *Predicting gemcitabine transport and toxicity in human pancreatic cancer cell lines with the positron emission tomography tracer 3'-deoxy-3'-fluorothymidine*. *Biochem. Pharmacol.* **79**:587-595.

5.1 Introduction

Advanced pancreatic cancer is currently considered an incurable disease with median survival times of less than one year [1]. The standard treatment is single-agent gemcitabine, and, with the exception of erlotinib [2], other anticancer therapies have not shown any additional survival advantage when coupled with gemcitabine. As a cytidine nucleoside analog, gemcitabine requires human nucleoside transporters (hNTs) to cross plasma membranes of tumor cells before it is phosphorylated by deoxycytidine kinase (dCK) [3]. Recent studies suggest that pancreatic tumor levels of human equilibrative nucleoside transporter 1 (hENT1), as measured by immunohistochemistry, can be used to predict tumor response to gemcitabine. Patients with pancreatic tumors with abundant hENT1 display longer survival times than those with tumors with undetectable or low levels of hENT1 after treatment with gemcitabine [4, 5].

hNTs are capable of transporting physiological nucleosides and many different therapeutic nucleoside analogs across cellular membranes (see [6-8] for hNT reviews). Gemcitabine can be transported by members of both hENTs (SLC29 family) and human concentrative nucleoside transporters (hCNTs, SLC28 family).

hENTs mediate bidirectional transport of nucleosides across biological membranes and are considered to be ubiquitous throughout the body. The four hENT family members are hENT1/2/3/4 and all, except hENT3, have been shown to be plasma membrane transporters [9-12]. Both hENT1 and hENT2 have similar permeant selectivities, transporting purine and pyrimidine nucleosides as well as

many synthetic nucleosides, although hENT2 (unlike hENT1) also transports some nucleobases. Among hNTs, hENT1 can be functionally identified by its sensitivity to inhibition by nitrobenzylmercaptapurine ribonucleoside (NBMPR) at nanomolar concentrations and hENT1/2 by their sensitivities to inhibition by dilazep at micromolar concentrations [11, 12]. Both hENT1 and hENT2 transport gemcitabine although hENT1 displays a lower K_m value (*i.e.*, higher affinity) for gemcitabine than hENT2 [13]. hENT3 is an intracellular pH-dependent, broadly nucleoside-selective transporter [9, 14]. N-terminal deleted hENT3 produced in *Xenopus laevis* oocytes exhibits pH-dependent interaction with gemcitabine, suggesting that hENT3 may transport gemcitabine across intracellular membranes [14]. hENT4 displays pH-dependent adenosine-selective transport and is unlikely to be involved in gemcitabine transport [10].

hCNTs are nucleoside/cation symporters that concentrate nucleosides within cells by coupling the transport of nucleosides and cations down their cationic electrochemical gradients. The three hCNT family members (hCNT1/2/3) are all considered to be plasma membrane transporters [15-17]. hCNT1 is pyrimidine nucleoside-selective and hCNT2 is purine nucleoside-selective, although they are each capable of transporting both adenosine and uridine [16, 17]. hCNT3 has broad nucleoside selectivity, efficiently transporting a variety of purine and pyrimidine nucleosides [15]. Gemcitabine, a pyrimidine nucleoside, is transported by hCNT1 and hCNT3 but not by hCNT2 [13, 18].

Since hENT1 abundance has been shown by immunohistochemical staining of tumor samples to be a predictive marker for gemcitabine response in

patients with pancreatic cancer, a non-invasive method for *in vivo* identification of pancreatic cancers with low gemcitabine transport capacity would be useful in predicting clinical resistance to gemcitabine. The positron emission tomography (PET) tracer 3'-deoxy-3'-fluorothymidine (FLT), a pyrimidine nucleoside analog, may be a probe for tumor gemcitabine transport capacity since FLT is transported by the same hNTs (hENT1, hENT2, hCNT1, and hCNT3) as gemcitabine [19].

Upon entering cells, FLT is phosphorylated by thymidine kinase 1 (TK1), a cell-cycle specific kinase that exhibits its maximum activity during S-phase [20]. Phosphorylated forms of FLT are not transported by hNTs and are therefore trapped within cells. FLT, which preferentially accumulates in proliferating cells with high TK1 activities, is used clinically as a PET proliferation tracer [21].

The research described in this chapter was undertaken to determine if FLT transport and uptake predict gemcitabine transport and toxicity in six human pancreatic cancer cell lines. The results demonstrated that hENT transport inhibitors significantly reduced 1) gemcitabine and FLT transport and uptake, and 2) gemcitabine toxicity in all six cell lines. In five cell lines, there were significant positive correlations between FLT and gemcitabine initial rates of uptake and between FLT uptake and gemcitabine toxicity. Measurements of FLT and gemcitabine uptake were comparable for predicting gemcitabine toxicity, suggesting that [¹⁸F]FLT PET of pancreatic cancers may be useful clinically to predict gemcitabine sensitivity in patients.

5.2 Results

5.2.1. Quantification of extracellular hENT1 levels with [³H]NBMPR binding

Plasma membrane levels of hENT1 in the six pancreatic cancer cell lines were determined using equilibrium [³H]NBMPR binding assays with or without membrane impermeant 5-*S*-{2-(1-[(fluorescein-5-yl)thioureido]hexanamido)ethyl}-6-*N*-(4-nitrobenzyl)-5-thioadenosine (FTH-SAENTA) or excess non-radioactive NBMPR. Since nucleoside transporters must be on plasma membranes to import nucleosides/nucleoside analogs into cells, quantification of extracellular NBMPR binding sites is more meaningful than quantification of total NBMPR binding sites in assessing hENT1-mediated uptake capacity. Binding of 10 nM [³H]NBMPR with or without 100 nM FTH-SAENTA or 10 μM NBMPR is shown in Fig. 5-1 for representative experiments conducted with Capan-2 and PANC-1 cells. The difference in [³H]NBMPR binding with and without 10 μM NBMPR represented total specific [³H]NBMPR binding while the difference in [³H]NBMPR binding with and without 100 nM FTH-SAENTA represented cell-surface (*i.e.*, extracellular) specific [³H]NBMPR binding.

Total and extracellular NBMPR binding sites as well as the percentage of extracellular sites are presented in Table 5-1 for the six cell lines. Capan-2 cells displayed the lowest number of extracellular NBMPR binding sites with 2.1×10^4 sites/cell while AsPC-1, BxPC-3, PL45, MIA PaCa-2, and PANC-1 cells displayed, respectively, 1.4-, 1.6-, 2.6-, 18-, and 35-fold greater extracellular NBMPR binding sites per cell than Capan-2 cells. Less than 30% of the NBMPR binding sites were extracellular for Capan-2, BxPC-3, PL45, and AsPC-1 cells,

suggesting that hENT1 was not efficiently transferred to plasma membranes in these cell lines. In contrast, greater than 50% of the NBMPR binding sites were extracellular for MIA PaCa-2 and PANC-1 cells.

5.2.2 Quantification of relative levels of hNTs, dCK, TK1, and RRM1 mRNA with real-time PCR

A relationship has been shown between gemcitabine resistance and relative levels of transcripts encoding hENT1, dCK, ribonucleotide reductase subunit 1 (RRM1), and ribonucleotide reductase subunit 2 (RRM2) in a panel of human pancreatic cancer cell lines [22]. Studies were therefore undertaken using Taqman quantitative real-time reverse transcriptase polymerase chain reaction (RT-PCR) to determine and compare the relative transcript levels of hNTs, dCK, TK1, and RRM1 to those of hENT1 for the pancreatic cell lines used in this study (Fig. 5-2A). hENT2 transcript levels were greater than those of hENT1 in BxPC-3 (1.2-fold), Capan-2 (2.9-fold), and AsPC-1 (3.5-fold) cells, while hENT1 transcript levels were greater than those of hENT2 in MIA PaCa-2 (4.6-fold), PANC-1 (7.1-fold), and PL45 (20-fold) cells. For all cell lines, hENT1 transcripts were greater than those of hCNT1 (190 to 6200-fold), hCNT3 (78 to 34000-fold) and dCK (17 to 370-fold), indicating that hENT1 mRNA expression was greater than that of hCNTs or dCK. For five of the six cell lines, TK1 mRNA expression was greater than that of hENT1 (1.3 to 9.5-fold) whereas PANC-1 cells displayed 1.4-fold greater hENT1 mRNA expression than that of TK1. RRM1 transcript levels were greater than those of hENT1 in MIA PaCa-2 (1.3-fold), AsPC-1 (3.4-fold), BxPC-3 (4.5-fold), and Capan-2 (6.7-fold) cells while hENT1 transcript

levels were greater than those of RRM1 in PL45 (1.3-fold) and PANC-1 (2.6-fold) cells.

Gene expression levels were also compared between cell lines using Capan-2 as the reference (Fig. 5-2B). hENT1 mRNA expression was greatest in PL45 cells (12-fold) followed by PANC-1 (10-fold), MIA PaCa-2 (1.2-fold), Capan-2 (1.0-fold), BxPC-3 (0.65-fold), and AsPC-1 (0.6-fold) cells. The three cell lines with the greatest amount of NBMPR binding sites per cell (PANC-1, MIA PaCa-2, and PL45) in the experiments of Table 5-1 also displayed the greatest amount of hENT1 mRNA expression, although the ranking differed. hENT2 mRNA expression was greatest in Capan-2 cells (1.0-fold) followed by AsPC-1 (0.72-fold), PANC-1 (0.53-fold), BxPC-3 (0.27-fold), PL45 (0.22-fold), and MIA PaCa-2 (0.09-fold). hCNT1 and hCNT3 mRNA expression levels differed between the cell lines although, based on the relative levels of hCNT transcripts as compared to those of hENT (see above), the hCNTs probably did not contribute much to FLT or gemcitabine transport in any of the cell lines. Differences in dCK, TK1, and RRM1 mRNA expression between cell lines may have contributed to differences in gemcitabine uptake, FLT uptake, and gemcitabine toxicity, respectively. dCK mRNA expression was greatest in Capan-2 cells (1.0-fold) followed by that in PL45 (0.84-fold), PANC-1 (0.48-fold), AsPC-1 (0.41-fold), BxPC-3 (0.23-fold), and MIA PaCa-2 (0.1-fold) cells. TK1 mRNA expression was greatest in PL45 cells (2.6-fold) followed by that in PANC-1 (1.04-fold), Capan-2 (1.0-fold), BxPC-3 (0.87-fold), AsPC-1 (0.43-fold), and MIA PaCa-2 (0.26-fold) cells. RRM1 mRNA expression was greatest in

PL45 cells (1.3-fold) followed by that in Capan-2 (1.0-fold), PANC-1 (0.57-fold), BxPC-3 (0.43-fold), AsPC-1 (0.31-fold), and MIA PaCa-2 (0.22-fold) cells.

5.2.3. Correlation between FLT and gemcitabine transport in five cell lines

To compare transport of FLT and gemcitabine in the pancreatic cancer cell lines, initial rates of uptake were measured to obtain rates of inward permeation processes under conditions during which there was little or no influence of nucleoside phosphorylation. In an attempt to reproduce physiological conditions, transport buffer consisted of Dulbecco's Modified Eagle's Medium with 10% calf serum and assays were conducted at 37°C rather than the conditions that are commonly used in other cell culture transport assays – *i.e.*, a simplified Na⁺ buffer at room temperature. Cultured cells were incubated with 1 μM [³H]FLT or [³H]gemcitabine for short time periods (up to 45 s) in the absence or presence of 100 μM dilazep, and radioactivity in cells was analyzed; representative time courses of uptake of [³H]FLT or [³H]gemcitabine are shown for MIA PaCa-2 cells in Fig. 5-3A and Fig. 5-3B. FLT and gemcitabine initial uptake rates were relatively similar, ranging from 24-67 and 24-42 fmol/mg protein/s, respectively (see Table 5-2 for summary of data obtained for the six cell lines), with Capan-2 cells displaying the lowest rates of uptake of FLT and gemcitabine. In the presence of 100 μM dilazep, initial rates of uptake of FLT and gemcitabine were 41-55% and 0.3-5% of uninhibited rates, respectively, suggesting that hENT activity was important for uptake of both compounds, although substantial uptake of FLT, but not of gemcitabine, also occurred by dilazep-insensitive (*i.e.*, hENT1/2-independent) processes.

Passive uptake of FLT in BxPC-3 cells was determined by incubating cells for 45 s with transport buffer containing 1 μM [^3H]FLT with or without 1 mM non-radioactive FLT and 100 μM dilazep (Fig. 5-3C). The presence of 1 mM non-radioactive FLT and 100 μM dilazep decreased initial rates of FLT uptake to 32% of that without 1 mM FLT and 100 μM dilazep, suggesting that passive diffusion contributed significantly to FLT uptake in BxPC-3 cells. Initial rates of FLT uptake in BxPC-3 cells were reduced further when cells were incubated with both 100 μM dilazep and 1 mM FLT compared to that with 100 μM dilazep alone, suggesting that FLT uptake was mediated by at least one other dilazep-insensitive process that was not passive diffusion. When BxPC-3 cells were incubated for 45 s with [^3H]FLT and 100 μM dilazep with or without 1 mM thymidine, inosine or uridine, initial rates of FLT uptake were not significantly affected by the presence of 1 mM non-radioactive nucleosides ($P > 0.05$, Fig. 5-3D), suggesting that hCNTs were not responsible for the observed hENT1/2-independent FLT uptake.

For all cell lines except one, a significant positive correlation existed between FLT and gemcitabine initial rates of uptake ($P < 0.005$, $r^2 = 0.95$, Fig. 5-4). BxPC-3 cells displayed a 2.5-fold greater rate of FLT uptake than gemcitabine and therefore did not follow the trend of the other five cell lines. The explanation for this deviation is uncertain.

5.2.4. Dependence of FLT and gemcitabine uptake on hNT activity

During prolonged exposures to nucleoside analogs such as FLT and gemcitabine, uptake represents the combined effects of permeation through plasma membranes and intracellular nucleoside phosphorylation. In the

experiments of Fig. 5-5, uptake of 100 nM [³H]FLT and [³H]gemcitabine was measured after 1-h incubations to assess the impact of nucleoside phosphorylation. For the six pancreatic cell lines, FLT and gemcitabine uptake values ranged from 7-21 and 13-29 pmol/mg protein/h, respectively, with Capan-2 cells displaying the lowest values (Table 5-3), which was surprising given their high levels of dCK and TK1 mRNA (Fig. 5-2). When comparing all cell lines, there were no positive correlations between 1) TK1 mRNA expression and FLT uptake, or 2) dCK mRNA expression and gemcitabine uptake. In the presence of 100 nM NBMPR, FLT and gemcitabine uptake values were 27-74% and 7-24% of uninhibited values, respectively, suggesting that hENT1 activity affected both FLT and gemcitabine uptake but was more important for uptake of gemcitabine than for that of FLT. In the presence of 100 μM dilazep, which inhibits hENT1 and hENT2 activities, FLT and gemcitabine uptake values were reduced even further, to 12-58% and 1-2% of uninhibited values, respectively. As was the case with inhibition of hENT1 activity, the effect of inhibition of hENT1/2 activities was greater for gemcitabine than for FLT.

5.2.5. Dependence of gemcitabine toxicity on hNT activity

The sensitivities of the pancreatic cancer cell lines to gemcitabine cytotoxicity were determined using the Promega CellTiter 96[®] AQueous One Solution Cell Proliferation Assay. Cells were incubated with graded concentrations of gemcitabine with or without 100 nM NBMPR or 10 μM dilazep for 72 h to determine if hENT activity affected gemcitabine toxicity. Results for all cell lines are summarized in Table 5-4. Capan-2 cells displayed the greatest

EC₅₀ value (gemcitabine concentration that produced 50% of maximal effect) at 3500 nM, with lower values exhibited by PANC-1 (820 nM), PL45 (53 nM), AsPC-1 (39 nM), BxPC-3 (27 nM), and MIA PaCa-2 (8.3 nM) cells. Addition of 100 nM NBMPR increased gemcitabine EC₅₀ values 1.3 to 7.7-fold for all cell lines except PANC-1, which displayed gemcitabine EC₅₀ values that were not significantly different with or without NBMPR ($P > 0.05$). Addition of 10 μM dilazep increased gemcitabine EC₅₀ values 2.1 to 41-fold for all cell lines including PANC-1, suggesting that both hENT1 and hENT2 activities were important for gemcitabine toxicity since inhibition of both hENT1 and hENT2 caused greater gemcitabine resistance than inhibition of only hENT1.

5.2.6. Correlations between gemcitabine uptake, FLT uptake, or RRM1 mRNA expression and gemcitabine toxicity in five cell lines

To determine if FLT uptake could be used to predict gemcitabine toxicity in the pancreatic cancer cell lines, FLT uptake during 1-h incubations and gemcitabine toxicity data were analyzed; an incubation time of 1 h was selected since FLT PET scans in human patients are typically up to 1 hour after tracer injection. Gemcitabine uptake correlated negatively with gemcitabine resistance for all cell lines except PANC-1 ($P < 0.005$, $r^2 = 0.96$, Fig. 5-6A), which did not fit the trend since it displayed the greatest amount of gemcitabine uptake but was the second most resistant to gemcitabine. FLT uptake also displayed a significant negative correlation with gemcitabine resistance for five of the six cell lines ($P < 0.005$, $r^2 = 0.96$, Fig. 5-6B), although the cell line that did not fit the trend was PL45. The gemcitabine EC₅₀ value was similar to that of AsPC-1 cells, whereas

FLT uptake after 1 h was approximately only half of that of AsPC-1 cells. Interestingly, RRM1 mRNA expression also correlated positively with gemcitabine resistance ($P < 0.01$) when PL45 cells were excluded from analysis (Fig. 5-6C). Compared to the other cell lines, PL45 displayed the greatest expression of RRM1 mRNA (Fig. 5-2B) but was still relatively sensitive to gemcitabine (Table 5-4).

5.3 Discussion

Clinical resistance to gemcitabine has been well studied. hNTs are necessary for gemcitabine transport into tumor cells and a lack of hNT activity, especially that of hENT1, leads to gemcitabine resistance in cultured cell lines and pancreatic cancer patients [3-5]. dCK is the rate limiting enzyme in the phosphorylation of gemcitabine, which is necessary for the pharmacologic activation of gemcitabine, and decreased dCK protein levels correlates with gemcitabine resistance [23, 24]. RRM1 is also considered to be important in gemcitabine resistance since increased expression of RRM1 mRNA is associated with gemcitabine resistance [25, 26]. In the work described in this chapter, if PL45 cells were excluded from analysis, RRM1 mRNA expression positively correlated with gemcitabine resistance ($P < 0.01$), suggesting that RRM1 mRNA (and possibly also protein) levels may be useful to predict gemcitabine sensitivity. Predicting response of pancreatic cancer patients to gemcitabine has been achieved by assessing hENT1 abundance by immunohistochemistry on pancreatic tumors obtained at surgery [4]. Unfortunately, only 10-15% of pancreatic cancer patients are eligible for tumor resection [1], and a non-invasive assay is, therefore, necessary to predict response to gemcitabine for the majority of pancreatic cancer patients. Uptake of the recently developed PET tracer 1-(2'-deoxy-2'-fluoroarabinofuranosyl) cytosine (FAC), which is a dCK substrate, was used to determine tumor dCK activity (since FAC uptake is dependent on dCK activity) and predict gemcitabine toxicity in L1210 tumor-bearing mice [27]. The current study assessed if uptake of the clinically available PET tracer FLT predicts

gemcitabine toxicity in pancreatic cancer cell lines since FLT and gemcitabine are transported by the same hNTs.

Using an inhibitor-sensitivity assay in hNT-producing *Saccharomyces cerevisiae*, K_i values were previously calculated from concentrations that caused 50% inhibition of uridine transport for FLT and gemcitabine, respectively, for hENT1 (74 and 354 μM), hENT2 (160 and 780 μM), hCNT1 (20 and 13 μM), hCNT2 (1200 and 1320 μM), and hCNT3 (31 and 22 μM) [19, 28]. The data indicated that hENTs have higher affinities for FLT than for gemcitabine whereas hCNTs have very similar affinities for both FLT and gemcitabine. Thus, although FLT and gemcitabine are permeants for the same hNTs (hENT1/2 and hCNT1/3), differences between them in individual hNT transport efficiencies will likely be reflected in differences in hNT transport rates among various cell types.

In the current study, hENT1 and hENT2 were shown to be important for gemcitabine and FLT uptake and gemcitabine toxicity since co-incubation with NBMPR or dilazep significantly reduced gemcitabine and FLT uptake and increased gemcitabine resistance in the six pancreatic cancer cell lines tested. Capan-2 cells displayed the lowest amount of 1) extracellular NBMPR binding sites, 2) FLT and gemcitabine uptake, and 3) gemcitabine sensitivity. It should be noted that the amount and percent of extracellular NBMPR binding sites for Capan-2 were larger in this study than those previously reported in Chapter 3 (Table 3-2) although total NBMPR binding sites per cell were relatively similar. Capan-2 cells were cultured differently in the two studies (in Chapter 3, Capan-2 cells were inoculated in 12-well plates at 5×10^4 cells/well and cultured for 72 h

whereas in this Chapter, Capan-2 cells were inoculated in 24-well plates at 1×10^5 cells/well for 24 h). The different culture conditions may have caused cell cycle changes in Capan-2 cells during experiments, and, since plasma membrane levels of hENT1 are cell cycle-dependent [29], thereby leading to different quantities of extracellular NBMPR binding.

In five of six pancreatic cancer cell lines, a positive correlation existed between FLT and gemcitabine transport activities, as measured by initial rates of uptake. BxPC-3 cells did not fit the trend of the other cell lines since FLT transport was significantly greater than that of gemcitabine. BxPC-3 cells displayed significant levels of FLT passive diffusion. The octanol-water partition coefficients for FLT and gemcitabine are 0.68 [30] and 0.053 (Gemcitabine Hydrochloride for Injection Material Safety Data Sheet), respectively, indicating that FLT is significantly more hydrophobic than gemcitabine, thereby explaining the greater level of passive diffusion observed with FLT than with gemcitabine. Although passive diffusion of FLT in BxPC-3 cells was relatively large compared to that of gemcitabine, diffusional FLT uptake was relatively small compared to mediated FLT uptake, indicating the importance of hNTs in cellular uptake of FLT.

FLT and gemcitabine are phosphorylated by TK1 and dCK, respectively, and these differences in nucleoside phosphorylation may also cause differences in cellular uptake between FLT and gemcitabine. Tumor cells with low TK1 and high dCK activities would be expected to display relatively low and high levels of FLT and gemcitabine uptake, respectively. However, PL45 cells, which had low

and high levels of FLT and gemcitabine uptake, respectively, displayed greater TK1 than dCK mRNA expression (Fig. 5-2A). Compared to the other cell lines, PL45 cells displayed relatively high expression of several genes, including the greatest expression of hENT1 mRNA even though they had only moderate levels of NBMPR binding sites (representing hENT1 molecules, Table 5-1), suggesting that PL45 cells may not have efficiently translated hENT1 proteins (and perhaps other proteins) from RNA -- i.e., transcript levels in PL45 cells may not have reflected protein levels.

A significant negative correlation was observed between gemcitabine uptake and resistance in only five of six cell lines, suggesting that uptake analysis of any nucleoside analog, including gemcitabine, FAC or FLT, will never be 100% accurate for predicting gemcitabine toxicity since gemcitabine toxicity is dependent on more than just gemcitabine transport and phosphorylation. Although a perfect correlation was not observed between FLT uptake and gemcitabine resistance for the six pancreatic cancer cell lines included in this study, the results suggested that FLT PET could be used to identify pancreatic tumors with low gemcitabine transport capacity that would thus be resistant to gemcitabine therapy. hENT1 immunohistochemistry has proven to be a clinical predictive assay for gemcitabine response in pancreatic cancer even though the assay only monitors the abundance of a single hNT [4]. FLT PET may provide *functional* data on the combined transport capacities of hENT1, hENT2, hCNT1, and hCNT3 (*i.e.*, all of the hNTs known to transport gemcitabine). Pancreatic tumors with high FLT uptake are expected to have hNTs capable of FLT transport and are

likely to be similar to pancreatic tumors that were positive by immunohistochemistry for hENT1 in the Farrell *et al.* report [4]. In the current study, the three cell lines with the highest amounts of FLT uptake were also the three most sensitive to gemcitabine (Tables 5-3 and 5-4). When using hENT1 immunohistochemistry, 44 of 198 (22%) of pancreatic tumors had no detectable hENT1 and patients with these tumors displayed the lowest overall survival rates when taking gemcitabine [4]. Clinical [¹⁸F]FLT PET of pancreatic cancers have shown that a similar percentage of pancreatic cancers (6 of 21; 29%) do not display focally increased [¹⁸F]FLT uptake [31], suggesting that tumors with no focally increased [¹⁸F]FLT uptake may have low/no hENT1 and would not respond well to gemcitabine.

FLT uptake is dependent on the proportion of cells in S-phase [32, 33] and gemcitabine toxicity is also partly dependent on cells cycling through S-phase since gemcitabine-induced DNA fragmentation and toxicity are both enhanced when cells are in S-phase [34, 35]. Furthermore, levels of gemcitabine-triphosphate incorporation into DNA are positively correlated with gemcitabine toxicity [36], indicating that incorporation of gemcitabine into DNA is an important process for gemcitabine toxicity. Since both FLT uptake and gemcitabine toxicity are directly related to the proportion of cells in S-phase, monitoring tumor proliferative status with FLT PET may help predict which tumors are sensitive to gemcitabine. Theoretically, this is another reason why FLT uptake may predict gemcitabine toxicity although further studies are necessary to validate this hypothesis.

FLT PET is capable of distinguishing between benign and malignant pancreatic tumors since focal uptake of [¹⁸F]FLT was observed exclusively in malignant pancreatic tumors [31]. The current study provides an additional reason for performing FLT PET on untreated pancreatic cancer patients since FLT uptake may also predict gemcitabine sensitivity in pancreatic tumors. Performing FLT PET after gemcitabine therapy may also indicate response to therapy since gemcitabine causes an accumulation of cells in early S-phase, causing an increase in FLT uptake [37]. Therefore, future clinical studies should examine FLT PET images of pancreatic tumors before and after gemcitabine treatment since both may be useful for predicting gemcitabine response.

In summary, the work described in this chapter demonstrated that gemcitabine and FLT uptake in human pancreatic cancer cell lines was dependent on hNT activities and that FLT and gemcitabine uptake were comparable in predicting gemcitabine toxicity. Future FLT PET clinical trials of pancreatic cancer patients are warranted to determine the potential of FLT PET in predicting tumor gemcitabine sensitivity.

Table 5-1. Total and extracellular NBMPR binding sites per cell in pancreatic cancer cell lines

Equilibrium [³H]NBMPR binding assays were performed with Capan-2, AsPC-1, BxPC-3, PL45, MIA PaCa-2, and PANC-1 cells in 24-well plates by incubating cells for 1 h in either 10 nM [³H]NBMPR, 10 nM [³H]NBMPR with 100 nM FTH-SAENTA, or 10 nM [³H]NBMPR with 10 μM NBMPR as described in section 2.6. At least three [³H]NBMPR binding experiments were performed under equilibrium conditions (each experiment in triplicate) and data are expressed as mean ± standard error of the mean (SEM).

Cell line	Total NBMPR	Extracellular NBMPR	
	Binding sites/cell (x10 ⁵)		%
Capan-2	1.6 ± 0.3	0.21 ± 0.04	15 ± 4
AsPC-1	1.1 ± 0.1	0.29 ± 0.05	27 ± 4
BxPC-3	2.1 ± 0.1	0.33 ± 0.10	15 ± 5
PL45	2.4 ± 0.4	0.55 ± 0.09	23 ± 2
MIA PaCa-2	6.7 ± 1.0	3.8 ± 0.6	57 ± 6
PANC-1	11 ± 1	7.4 ± 0.5	65 ± 4

Table 5-2. Rates of uptake of FLT and gemcitabine with or without hNT inhibitors between 1-45 s in pancreatic cancer cell lines

Capan-2, AsPC-1, BxPC-3, PL45, MIA PaCa-2, and PANC-1 cells in 24-well plates were incubated for 1-45 s in Dulbecco's Modified Eagle's Medium (DMEM) + 10% calf serum (CS) containing 1 μ M [3 H]FLT or [3 H]gemcitabine with or without 100 μ M dilazep as described in section 2.4.3. At least three experiments were performed (each experiment in triplicate) and data are expressed as mean \pm SEM.

Cell line	1 μ M [3 H]FLT		1 μ M [3 H]Gemcitabine	
	no inh.*	100 μ M Dilazep	no inh.	100 μ M Dilazep
	fmol/mg protein/s			
Capan-2	24 \pm 1	12 \pm 2	24 \pm 2	1.2 \pm 0.4
AsPC-1	40 \pm 4	22 \pm 2	32 \pm 6	1.2 \pm 0.7
BxPC-3	67 \pm 7	31 \pm 6	27 \pm 2	0.2 \pm 0.1
PL45	39 \pm 7	16 \pm 3	35 \pm 7	0.1 \pm 0.1
MIA PaCa-2	59 \pm 5	31 \pm 3	41 \pm 5	0.8 \pm 0.4
PANC-1	57 \pm 5	28 \pm 3	42 \pm 4	0.7 \pm 0.3

* no inh. means no hNT inhibitor used in transport assays.

Table 5-3. FLT and gemcitabine uptake with or without hNT inhibitors after 1 h in pancreatic cancer cell lines

Capan-2, AsPC-1, BxPC-3, PL45, MIA PaCa-2, and PANC-1 cells in 24-well plates were incubated for 1 h in DMEM + 10% CS containing 100 nM [³H]FLT or [³H]gemcitabine with or without 100 nM NBMPR or 100 μM dilazep as described in section 2.4.3. At least three experiments were performed (each experiment in triplicate) and data are expressed as mean ± SEM.

Cell line	100 nM [³ H]FLT			100 nM [³ H]Gemcitabine		
	no inh.*	100 nM NBMPR	100 μM Dilazep	no inh.	100 nM NBMPR	100 μM Dilazep
	pmol/mg protein/h					
Capan-2	7.0 ± 0.2	4.9 ± 0.2	2.9 ± 0.2	13 ± 0.7	3.1 ± 0.2	0.16 ± 0.01
AsPC-1	18 ± 2	11 ± 0.4	7.9 ± 0.4	20 ± 1	3.6 ± 0.2	0.23 ± 0.02
BxPC-3	19 ± 1	14 ± 1	11 ± 1	21 ± 0.7	4.0 ± 0.4	0.17 ± 0.01
PL45	10 ± 2	2.7 ± 0.6	1.2 ± 0.3	22 ± 2	1.6 ± 0.2	0.30 ± 0.06
MIA PaCa-2	21 ± 2	10 ± 1	4.8 ± 0.6	22 ± 4	2.8 ± 0.3	0.23 ± 0.05
PANC-1	16 ± 1	6.5 ± 0.8	5.7 ± 0.7	29 ± 3	2.2 ± 0.3	0.15 ± 0.01

* no inh. means no hNT inhibitor used in uptake assays.

Table 5-4. Gemcitabine toxicity with or without hNT inhibitors in pancreatic cancer cell lines

Capan-2, AsPC-1, BxPC-3, PL45, MIA PaCa-2, and PANC-1 cells in 96-well plates were incubated for 72 h in medium containing graded concentrations of gemcitabine with or without 100 nM NBMPR or 10 μ M dilazep. Cell proliferation was analyzed using the CellTiter 96[®] AQueous One Solution Cell Proliferation Assay (Promega, Madison, WI) as described in section 2.7. At least three experiments were performed (each experiment in triplicate) and data are expressed as mean \pm SEM.

Cell line	Gemcitabine EC ₅₀ values (nM)		
	no inh.*	100 nM NBMPR	10 μ M Dilazep
Capan-2	3500 \pm 400	4600 \pm 1700	7500 \pm 1600
AsPC-1	39 \pm 5	300 \pm 80	510 \pm 30
BxPC-3	27 \pm 7	75 \pm 10	180 \pm 20
PL45	53 \pm 10	290 \pm 60	930 \pm 70
MIA PaCa-2	8.3 \pm 2.4	19 \pm 0.9	340 \pm 50
PANC-1	820 \pm 150	560 \pm 90	5000 \pm 400

* no inh. means no hNT inhibitor used in toxicity assays.

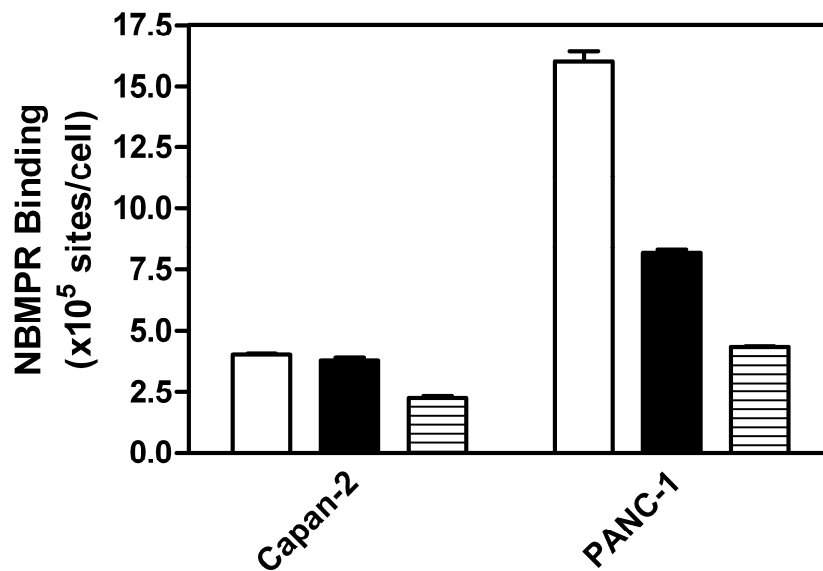


Figure 5-1. Quantification hENT1 sites with NBMPR binding in pancreatic cancer cells. Equilibrium [³H]NBMPR binding assays were performed with Capan-2 and PANC-1 cells in 24-well plates by incubating cells for 1 h in either 10 nM [³H]NBMPR (white columns), 10 nM [³H]NBMPR with 100 nM FTH-SAENTA (black columns), or 10 nM [³H]NBMPR with 10 μM NBMPR (striped column) as described in section 2.6. Shown is a representative experiment performed in triplicate. Bars represent mean ± SEM and error bars represent variability between replicates within each individual experiment.

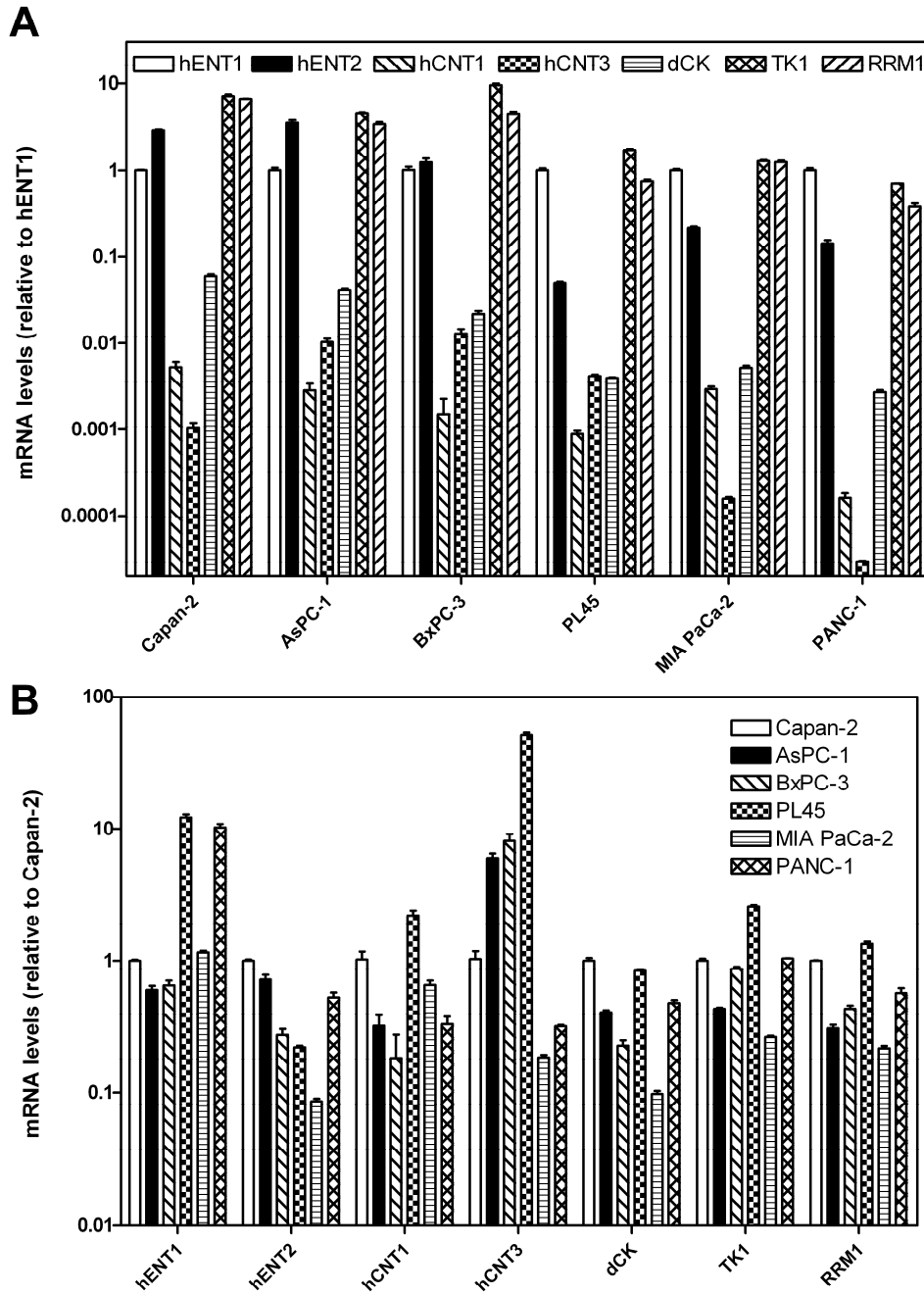


Figure 5-2. Quantification of hNT, dCK, TK1, and RRM1 mRNA levels in pancreatic cancer cell lines by real-time RT-PCR. Taqman quantitative real-time RT-PCR was performed on mRNA isolated from Capan-2, AsPC-1, BxPC-3, PL45, MIA PaCa-2, and PANC-1 cells as described in section 2.5. (A) Comparison of mRNA levels within each cell line with data normalized to the values for hENT1. The transcripts analyzed include those encoding hENT1 (white

bars), hENT2 (black bars), hCNT1 (down-right diagonal striped bars), hCNT3 (square checkered bars), dCK (horizontal striped bars), TK1 (diamond checkered bars) and RRM1 (down-left diagonal striped bars). **(B)** Comparison of mRNA levels between cell lines with data normalized to the values for Capan-2 cells. The cell lines from which mRNA was prepared and analyzed include Capan-2 (white bars), AsPC-1 (black bars), BxPC-3 (down-right diagonal striped bars), PL45 (square checkered bars), MIA PaCa-2 (horizontal striped bars), and PANC-1 (diamond checkered bars). **(A + B)** Relative mRNA levels were determined with the delta-delta-CT method using GAPDH as the loading control. At least three experiments were performed (each in triplicate) and bars represent mean values \pm SEM. Error bars are not shown where they are too small to be distinguished from data bars.

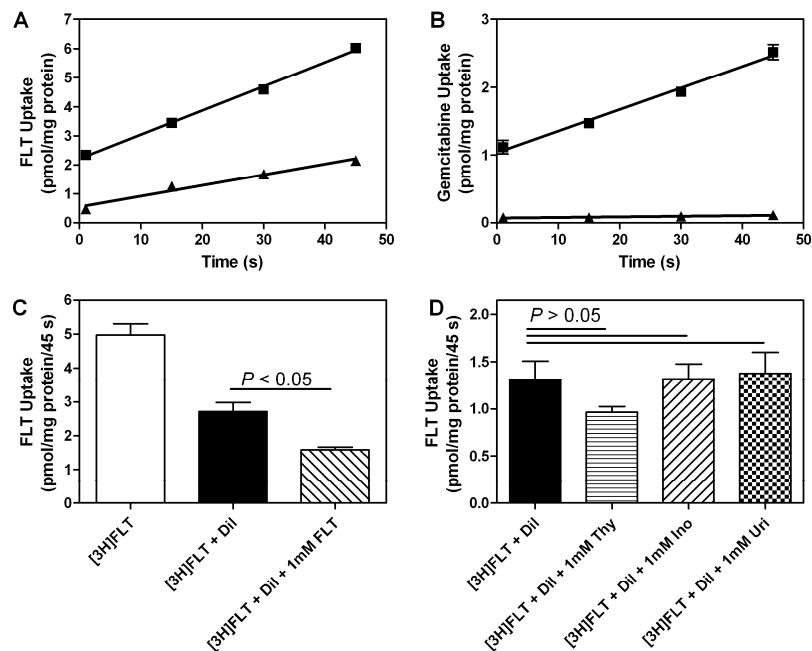


Figure 5-3. FLT and gemcitabine uptake in pancreatic cancer cell lines over short periods of time. MIA PaCa-2 cells in 24-well plates were incubated for 1-45 s in DMEM + 10% CS containing 1 μ M [³H]FLT (A) or [³H]gemcitabine (B) with (triangles) or without (squares) 100 μ M dilazep as described in section 2.4.3. (A + B) Shown are representative experiments performed in triplicate and symbols represent mean uptake values \pm SEM. Error bars represent variability between replicates within each individual experiment. Error bars are not shown when the bars are smaller than the symbols. (C) BxPC-3 cells in 24-well plates were incubated for 45 s in DMEM + 10% CS containing either 1 μ M [³H]FLT (white bar), 1 μ M [³H]FLT with 100 μ M dilazep (black bar), or 1 μ M [³H]FLT with 100 μ M dilazep and 1 mM non-radioactive FLT (hatched bar) as described in section 2.4.3. (D) BxPC-3 cells in 24-well plates were incubated for 45 s in DMEM + 10% CS containing 1 μ M [³H]FLT and 100 μ M dilazep without (black bar) or with 1 mM thymidine (horizontal-striped bar), 1 mM inosine (diagonal-striped bar), or 1 mM uridine (checkered bar) as described in section 2.4.3. (C + D) Experiments were performed three times except those with inosine (n = 2); each experiment was performed in triplicate and bars represent mean values \pm SEM.

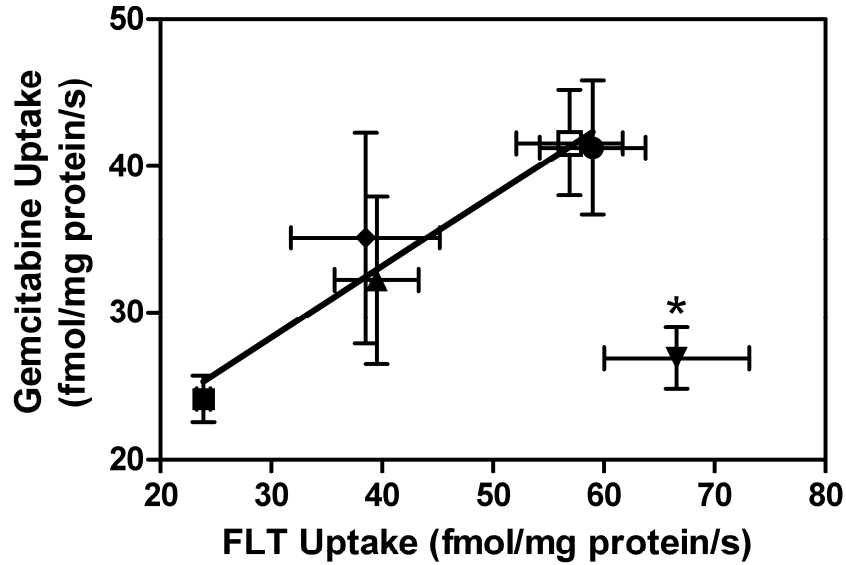


Figure 5-4. Linear regression analysis of FLT and gemcitabine initial rates of uptake in pancreatic cancer cell lines. FLT and gemcitabine initial rates of uptake are shown for Capan-2 (■), AsPC-1 (▲), PL45 (◆), MIA PaCa-2 (●), and PANC-1 (□) cells. Data were taken from Table 5-2 for FLT and gemcitabine transport in the absence of hNT inhibitors and symbols represent mean values \pm SEM. For the five cell lines included in the analysis, a significant positive correlation existed between FLT and gemcitabine transport ($P < 0.005$, $r^2 = 0.95$). BxPC-3 cells, indicated with the asterisk, were not included in the linear regression analysis.

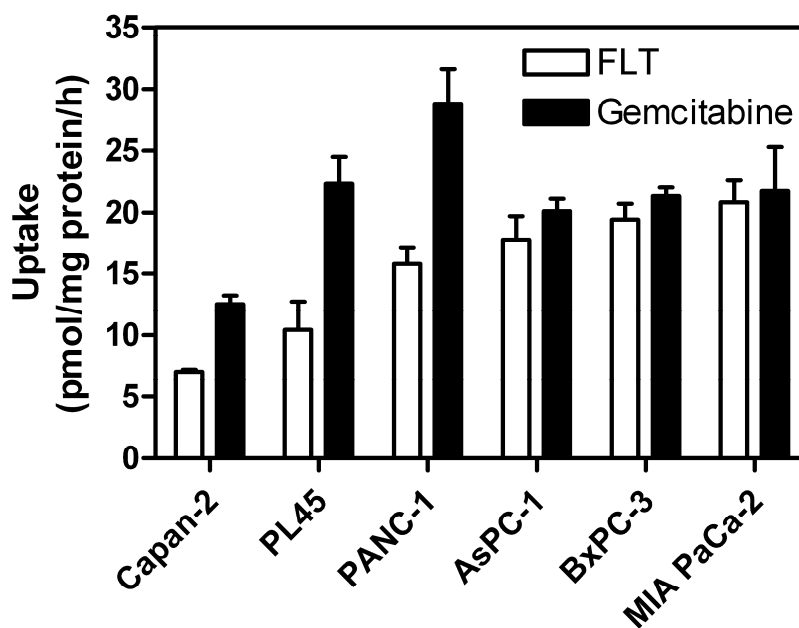


Figure 5-5. Uptake of 100 nM [³H]FLT and [³H]gemcitabine in pancreatic cancer cell lines. Capan-2, PL45, PANC-1, AsPC-1, BxPC-3, and MIA PaCa-2 cells in 24-well plates were incubated for 1 h in DMEM + 10% CS containing 100 nM [³H]FLT (white bars) or [³H]gemcitabine (black bars) as described in section 2.4.3. At least three experiments were performed (each in triplicate) and bars represent mean uptake values ± SEM. Error bars are not shown where they are too small to be distinguished from data bars.

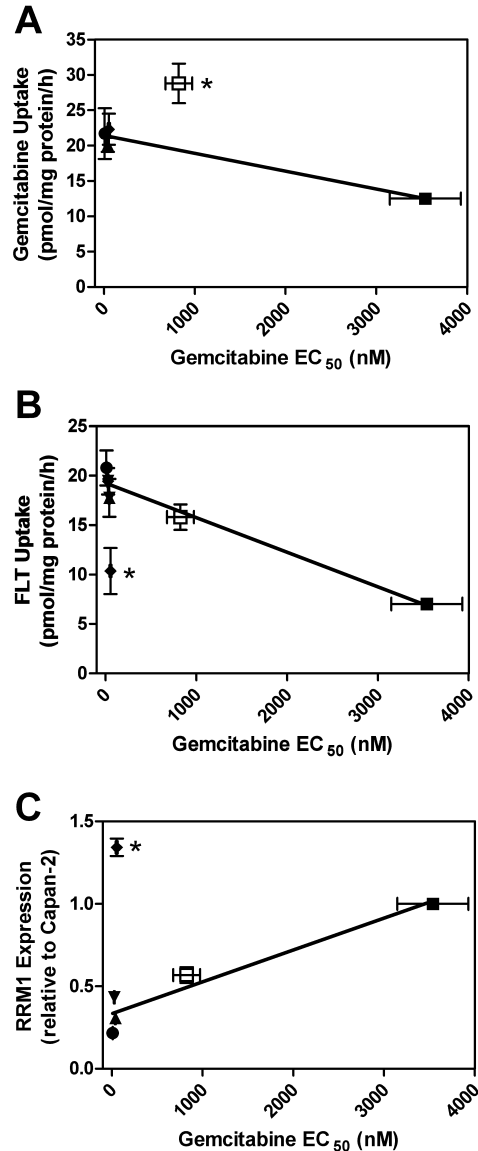


Figure 5-6. Linear regression analysis of gemcitabine toxicity in pancreatic cell lines with gemcitabine uptake, FLT uptake, or RRM1 expression. Data were taken from Table 5-3 (FLT and gemcitabine uptake), Fig. 5-2B (RRM1 expression) and Table 5-4 (gemcitabine toxicity) and symbols represent mean values \pm SEM. **(A)** For the five cell lines included in the analysis [Capan-2 (■), AsPC-1 (▲), BxPC-3 (▼), PL45 (◆), and MIA PaCa-2 (●)], significant correlations existed between gemcitabine resistance and gemcitabine uptake ($P < 0.005$, $r^2 = 0.96$). PANC-1 cells, indicated with the asterisk, were not included in the linear regression analysis. **(B + C)** For the five cell lines included in the

analysis [Capan-2 (■), AsPC-1 (▲), BxPC-3 (▼), MIA PaCa-2 (●), and PANC-1 (□)], significant correlations existed between gemcitabine resistance and 1) FLT uptake ($P < 0.005$, $r^2 = 0.96$) and 2) RRM1 expression ($P < 0.01$, $r^2 = 0.92$). PL45 cells, indicated with the asterisk, were not included in the linear regression analyses.

5.4 Bibliography

- [1] Cartwright T, Richards DA, Boehm KA. Cancer of the pancreas: are we making progress? A review of studies in the US Oncology Research Network. *Cancer Control* 2008;15:308-13.
- [2] Moore MJ, Goldstein D, Hamm J, Figer A, Hecht JR, Gallinger S, et al. Erlotinib plus gemcitabine compared with gemcitabine alone in patients with advanced pancreatic cancer: a phase III trial of the National Cancer Institute of Canada Clinical Trials Group. *J Clin Oncol* 2007;25:1960-6.
- [3] Mackey JR, Mani RS, Selner M, Mowles D, Young JD, Belt JA, et al. Functional nucleoside transporters are required for gemcitabine influx and manifestation of toxicity in cancer cell lines. *Cancer Res* 1998;58:4349-57.
- [4] Farrell JJ, Elsaleh H, Garcia M, Lai R, Ammar A, Regine WF, et al. Human equilibrative nucleoside transporter 1 levels predict response to gemcitabine in patients with pancreatic cancer. *Gastroenterology* 2009;136:187-95.
- [5] Spratlin J, Sangha R, Glubrecht D, Dabbagh L, Young JD, Dumontet C, et al. The absence of human equilibrative nucleoside transporter 1 is associated with reduced survival in patients with gemcitabine-treated pancreas adenocarcinoma. *Clin Cancer Res* 2004;10:6956-61.
- [6] Kong W, Engel K, Wang J. Mammalian nucleoside transporters. *Curr Drug Metab* 2004;5:63-84.
- [7] Molina-Arcas M, Trigueros-Motos L, Casado FJ, Pastor-Anglada M. Physiological and pharmacological roles of nucleoside transporter proteins. *Nucleosides Nucleotides Nucleic Acids* 2008;27:769-78.
- [8] Young JD, Yao SY, Sun L, Cass CE, Baldwin SA. Human equilibrative nucleoside transporter (ENT) family of nucleoside and nucleobase transporter proteins. *Xenobiotica* 2008;38:995-1021.
- [9] Baldwin SA, Yao SY, Hyde RJ, Ng AM, Foppolo S, Barnes K, et al. Functional characterization of novel human and mouse equilibrative nucleoside transporters (hENT3 and mENT3) located in intracellular membranes. *J Biol Chem* 2005;280:15880-7.
- [10] Barnes K, Dobrzynski H, Foppolo S, Beal PR, Ismat F, Scullion ER, et al. Distribution and functional characterization of equilibrative nucleoside transporter-4, a novel cardiac adenosine transporter activated at acidic pH. *Circ Res* 2006;99:510-9.

- [11] Griffiths M, Beaumont N, Yao SY, Sundaram M, Boumah CE, Davies A, et al. Cloning of a human nucleoside transporter implicated in the cellular uptake of adenosine and chemotherapeutic drugs. *Nat Med* 1997;3:89-93.
- [12] Griffiths M, Yao SY, Abidi F, Phillips SE, Cass CE, Young JD, et al. Molecular cloning and characterization of a nitrobenzylthioinosine-insensitive (ei) equilibrative nucleoside transporter from human placenta. *Biochem J* 1997;328 (Pt 3):739-43.
- [13] Mackey JR, Yao SY, Smith KM, Karpinski E, Baldwin SA, Cass CE, et al. Gemcitabine transport in xenopus oocytes expressing recombinant plasma membrane mammalian nucleoside transporters. *J Natl Cancer Inst* 1999;91:1876-81.
- [14] Govindarajan R, Leung GP, Zhou M, Tse CM, Wang J, Unadkat JD. Facilitated Mitochondrial Import of Anti-viral and Anti-cancer Nucleoside Drugs by Human Equilibrative Nucleoside Transporter-3 (hENT3). *Am J Physiol Gastrointest Liver Physiol* 2009.
- [15] Ritzel MW, Ng AM, Yao SY, Graham K, Loewen SK, Smith KM, et al. Molecular identification and characterization of novel human and mouse concentrative Na⁺-nucleoside cotransporter proteins (hCNT3 and mCNT3) broadly selective for purine and pyrimidine nucleosides (system cib). *J Biol Chem* 2001;276:2914-27.
- [16] Ritzel MW, Yao SY, Huang MY, Elliott JF, Cass CE, Young JD. Molecular cloning and functional expression of cDNAs encoding a human Na⁺-nucleoside cotransporter (hCNT1). *Am J Physiol* 1997;272:C707-14.
- [17] Wang J, Su SF, Dresser MJ, Schaner ME, Washington CB, Giacomini KM. Na(+)-dependent purine nucleoside transporter from human kidney: cloning and functional characterization. *Am J Physiol* 1997;273:F1058-65.
- [18] Hu H, Endres CJ, Chang C, Umaphathy NS, Lee EW, Fei YJ, et al. Electrophysiological characterization and modeling of the structure activity relationship of the human concentrative nucleoside transporter 3 (hCNT3). *Mol Pharmacol* 2006;69:1542-53.
- [19] Paproski RJ, Ng AM, Yao SY, Graham K, Young JD, Cass CE. The role of human nucleoside transporters in uptake of 3'-deoxy-3'-fluorothymidine. *Mol Pharmacol* 2008;74:1372-80.
- [20] Arner ES, Eriksson S. Mammalian deoxyribonucleoside kinases. *Pharmacol Ther* 1995;67:155-86.
- [21] Been LB, Suurmeijer AJ, Cobben DC, Jager PL, Hoekstra HJ, Elsinga PH. [18F]FLT-PET in oncology: current status and opportunities. *Eur J Nucl Med Mol Imaging* 2004;31:1659-72.

- [22] Nakano Y, Tanno S, Koizumi K, Nishikawa T, Nakamura K, Minoguchi M, et al. Gemcitabine chemoresistance and molecular markers associated with gemcitabine transport and metabolism in human pancreatic cancer cells. *Br J Cancer* 2007;96:457-63.
- [23] Ruiz van Haperen VW, Veerman G, Eriksson S, Boven E, Stegmann AP, Hermsen M, et al. Development and molecular characterization of a 2',2'-difluorodeoxycytidine-resistant variant of the human ovarian carcinoma cell line A2780. *Cancer Res* 1994;54:4138-43.
- [24] Sebastiani V, Ricci F, Rubio-Viqueira B, Kulesza P, Yeo CJ, Hidalgo M, et al. Immunohistochemical and genetic evaluation of deoxycytidine kinase in pancreatic cancer: relationship to molecular mechanisms of gemcitabine resistance and survival. *Clin Cancer Res* 2006;12:2492-7.
- [25] Bepler G, Kusmartseva I, Sharma S, Gautam A, Cantor A, Sharma A, et al. RRM1 modulated in vitro and in vivo efficacy of gemcitabine and platinum in non-small-cell lung cancer. *J Clin Oncol* 2006;24:4731-7.
- [26] Rosell R, Danenberg KD, Alberola V, Bepler G, Sanchez JJ, Camps C, et al. Ribonucleotide reductase messenger RNA expression and survival in gemcitabine/cisplatin-treated advanced non-small cell lung cancer patients. *Clin Cancer Res* 2004;10:1318-25.
- [27] Laing RE, Walter MA, Campbell DO, Herschman HR, Satyamurthy N, Phelps ME, et al. Noninvasive prediction of tumor responses to gemcitabine using positron emission tomography. *Proc Natl Acad Sci U S A* 2009;106:2847-52.
- [28] Clarke ML, Damaraju VL, Zhang J, Mowles D, Tackaberry T, Lang T, et al. The role of human nucleoside transporters in cellular uptake of 4'-thio-beta-D-arabinofuranosylcytosine and beta-D-arabinosylcytosine. *Mol Pharmacol* 2006;70:303-10.
- [29] Pressacco J, Wiley JS, Jamieson GP, Erlichman C, Hedley DW. Modulation of the equilibrative nucleoside transporter by inhibitors of DNA synthesis. *Br J Cancer* 1995;72:939-42.
- [30] Schinazi RF, Boudinot FD, Doshi KJ, McClure HM. Pharmacokinetics of 3'-fluoro-3'-deoxythymidine and 3'-deoxy-2',3'-didehydrothymidine in rhesus monkeys. *Antimicrob Agents Chemother* 1990;34:1214-9.
- [31] Herrmann K, Eckel F, Schmidt S, Scheidhauer K, Krause BJ, Kleeff J, et al. In vivo characterization of proliferation for discriminating cancer from pancreatic pseudotumors. *J Nucl Med* 2008;49:1437-44.

- [32] Rasey JS, Grierson JR, Wiens LW, Kolb PD, Schwartz JL. Validation of FLT uptake as a measure of thymidine kinase-1 activity in A549 carcinoma cells. *J Nucl Med* 2002;43:1210-7.
- [33] Schwartz JL, Tamura Y, Jordan R, Grierson JR, Krohn KA. Monitoring tumor cell proliferation by targeting DNA synthetic processes with thymidine and thymidine analogs. *J Nucl Med* 2003;44:2027-32.
- [34] Huang P, Plunkett W. Induction of apoptosis by gemcitabine. *Semin Oncol* 1995;22:19-25.
- [35] Huang P, Plunkett W. Fludarabine- and gemcitabine-induced apoptosis: incorporation of analogs into DNA is a critical event. *Cancer Chemother Pharmacol* 1995;36:181-8.
- [36] Veltkamp SA, Pluim D, van Eijndhoven MA, Bolijn MJ, Ong FH, Govindarajan R, et al. New insights into the pharmacology and cytotoxicity of gemcitabine and 2',2'-difluorodeoxyuridine. *Mol Cancer Ther* 2008;7:2415-25.
- [37] Dittmann H, Dohmen BM, Kehlbach R, Bartusek G, Pritzkow M, Sarbia M, et al. Early changes in [18F]FLT uptake after chemotherapy: an experimental study. *Eur J Nucl Med Mol Imaging* 2002;29:1462-9.

Chapter 6: General discussion and conclusions

6.1 Human nucleoside transporters (hNTs) capable of 3'-deoxy-3'-fluorothymidine (FLT) transport

Prior to the initiation of the research described in this thesis, human equilibrative nucleoside transporter 1 (hENT1) was known to transport FLT since the majority of FLT uptake in cultured HL-60 (human promyelocytic leukemia) cells was inhibited by nitrobenzylmercaptapurine ribonucleoside (NBMPR) phosphate (NBMPR-P) [1]. Since it was not known if the other plasma membrane human nucleoside transporters (hNTs) were capable of FLT transport, the first goal of this project was to determine the potential transportability of FLT by hENT2, human concentrative nucleoside transporter 1 (hCNT1), hCNT2, and hCNT3. K_i values for inhibition of hENT1/2 and hCNT1/3 in yeast cells producing a single recombinant hNT were significantly greater than those of thymidine (12-, 3.4-, 5.0-, >8.3-, and 15-fold, respectively), suggesting that substitution of a 3'-floro group for the 3'-hydroxyl group in thymidine significantly decreased the affinities of the various hNTs for FLT. These results were expected since previous studies had demonstrated that the 3'-hydroxyl group of uridine is important for interaction with hENT1, hENT2, hCNT1, hCNT2, and hCNT3 [2-4]. The transport experiments with yeast cells producing recombinant hNTs demonstrated that FLT binds to various hNTs, thereby indicating that FLT is potentially a permeant of hNTs. Transport experiments involving [³H]FLT were subsequently performed with *Xenopus laevis* oocytes to directly determine which hNTs were capable of FLT transport.

Xenopus laevis oocytes producing recombinant hNTs were used to study FLT transport since oocytes do not exhibit any significant amounts of endogenous thymidine transport or phosphorylation [5], allowing relatively sensitive and accurate measurements of FLT transport in oocytes producing recombinant hNTs. Oocytes producing recombinant hENT1, hENT2, hCNT1, or hCNT3, but not those producing recombinant hCNT2, were capable of efficient FLT transport. Each hENT1- or hENT2-producing oocyte that was incubated with 20 μM [^3H]FLT for 30 min displayed approximately 11 pmol FLT uptake (Fig. 3-2). Assuming that oocytes have an average diameter of 1 mm with a spherical shape and an intracellular environment that contains primarily water, the volume of individual oocytes (volume = $4/3 \cdot \pi \cdot \text{radius}^3$) was estimated to be approximately 500 nl. Thus, the [^3H]FLT concentration within oocytes producing hENT1 or hENT2 was approximately 20 μM , suggesting that oocytes producing hENT1 or hENT2 could only equilibrate FLT across membranes. Oocytes producing recombinant hCNT3 or hCNT1 displayed intra-oocyte FLT concentrations of approximately 60 and 90 μM , respectively, suggesting that FLT was concentrated within oocytes producing hCNT1 or hCNT3 despite the lack of FLT metabolism inside oocytes. Considering that the intracellular environment within oocytes contains significant amounts of lipids and proteins, intracellular FLT concentrations within hCNT-producing oocytes were likely greater than the estimated values suggested above. The data suggested that FLT could accumulate within human cells in the absence of thymidine kinase 1 (TK1) if FLT influx by

hCNT1 and/or hCNT3 activity is greater than FLT efflux by hENT1 and/or hENT2 activity.

6.2 Importance of hNTs for FLT uptake

To determine the importance of hNTs for FLT uptake, cultured human cancer cell lines of various origin, including MCF-7 (breast adenocarcinoma), A549 (lung carcinoma), U251 (glioblastoma), A498 (renal carcinoma), and five pancreatic carcinoma cell lines (Capan-2, AsPC-1, BxPC-3, PL45, MIA PaCa-2, and PANC-1), were incubated with [³H]FLT with or without various hNT inhibitors and/or hNT permeants. Incubation of cells with the hENT1 inhibitor NBMPR caused a relatively large decrease in FLT uptake in all of the cell lines, indicating that hENT1 was an important mediator of FLT uptake (Fig. 3-4 and Table 5-3). For many cell lines, incubation of cells with dilazep reduced FLT uptake to a greater extent than NBMPR, indicating that hENT2 was also an important mediator of FLT uptake (Fig. 3-4 and Table 5-3). The cell lines incubated in Na⁺-free buffer displayed relatively similar FLT uptake compared to that observed in Na⁺-containing buffer, suggesting that hCNT1 and hCNT3 had relatively minor effects on FLT uptake in the cells lines tested (Fig. 3-4). When BxPC-3 cells were incubated with 100 nM [³H]FLT, 100 μM dilazep, and 1 mM non-radioactive FLT, [³H]FLT uptake was 32% of that in the absence of dilazep and non-radioactive FLT (Fig. 5-3), suggesting that this residual [³H]FLT uptake was due to passive diffusion. Passive diffusion of FLT in PL45 cells was likely lower than that in BxPC-3 cells since FLT uptake in PL45 cells incubated with 100 μM dilazep was 12% of that in its absence (Fig 5-3). The results suggested

that passive diffusion of FLT across plasma membranes 1) significantly contributed to FLT uptake (although to a lesser extent than that of mediated transport in all cell lines), and 2) differed between cell lines.

Although transcript levels of hENT1 and hENT2 differed significantly between cell lines, all the cell lines tested displayed hENT1/2 transcript levels that were approximately 2-4 orders of magnitude greater than those of hCNT1/3 (Fig. 3-3 and Fig. 5-2). These data were consistent with the observations that hENT1/2 transport activities were responsible for the majority of hNT-mediated FLT uptake in all cell lines tested (Fig. 3-4 and Table 5-3).

Previous studies have shown that FLT uptake in cultured A549 cells correlated with TK1 activity, suggesting that TK1 is important for FLT uptake in A549 cells [6]. Results from Chapter 3 showed that inhibition of 50% of hENT1 by NBMPR in cultured A549 cells inhibited at least 50% of mediated FLT uptake (Table 3-2), suggesting that hENT1 was also important for FLT uptake in A549 cells. Both FLT transport and phosphorylation by hNTs and TK1, respectively, were apparently important for FLT uptake since TK1 can only phosphorylate intracellular FLT and hNTs are required for rapid permeation of FLT across plasma membranes.

To determine if altering hENT1 activity in tumors affected FLT uptake, A549 cells were stably transfected with pSUPER encoding shRNA targeting 1) hENT1 (A549-pSUPER-hENT1 cells) or, 2) a scrambled sequence with no homology against any known mammalian gene (A549-pSUPER-SC cells). Compared to cultured A549-pSUPER-SC cells, A549-pSUPER-hENT1 cells

displayed 1) 0.45-fold hENT1 mRNA levels and extracellular NBMPR binding sites (Fig. 4-5A and Fig. 4-5B), and 2) 0.68-fold FLT uptake (Fig. 4-5C), suggesting that reducing expression of hENT1 mRNA in cultured A549 cells significantly reduced FLT uptake.

In vivo experiments were performed with immunocompromised NIH-III mice bearing A549-pSUPER-SC and A549-pSUPER-hENT1 xenograft tumors over the left and right thighs, respectively, that underwent [^{18}F]FLT microPET. Compared to A549-pSUPER-SC tumors, A549-pSUPER-hENT1 tumors displayed significantly reduced FLT uptake 1 h after [^{18}F]FLT injection using *ex vivo* gamma counting (0.76-fold %ID/g values) and microPET image analysis (0.65-fold SUV_{max}). These results demonstrated that altering expression of hENT1 mRNA, and presumably altering hENT1 protein levels, in A549 cells affected FLT uptake in both *in vitro* and *in vivo* models.

Kinetic analysis of FLT uptake by tumors using a three compartment model suggested that, compared to A549-pSUPER-SC tumors, A549-pSUPER-hENT1 tumors displayed significantly reduced apparent K_1 values, which represented transport of FLT from plasma to tissues. Although direct measures of tumor blood flow were not made, it is possible that differences in blood flow between A549-pSUPER-SC and A549-pSUPER-hENT1 xenograft tumors may partly explain the observed differences in apparent K_1 values. However, the difference in apparent K_1 values between the tumor types were likely caused by differences in hENT1 since the reduction in hENT1 mRNA expression 1) caused a reduction in FLT uptake in cultured A549-pSUPER-hENT1 cells compared to

that of A549-pSUPER-SC cells, and 2) was the only known molecular difference between the two cell lines.

To assess the role of ENT1 in the biodistribution of FLT, [^{18}F]FLT microPET was performed in ENT1^{+/+}, ENT1^{+/-}, ENT1^{-/-} mice, as well as ENT1^{+/+} mice injected with 15 mg/kg NBMPR-P 1 hour before imaging. Mice injected with 15 mg/kg NBMPR-P display micromolar levels of NBMPR in the plasma one hour after NBMPR-P injection, suggesting that this dosage of NBMPR-P can be used to pharmacologically inhibit ENT1 in mice [7, 8]. FLT biodistribution in ENT1^{+/+} mice was typical for rodents in that there was relatively little FLT accumulation in the bone marrow (Fig. 4-2) [9]. Compared to ENT1^{+/+} mice, ENT1^{+/+} mice injected with 15 mg/kg NBMPR-P and ENT1^{-/-} mice displayed significantly reduced levels of circulating FLT with increased FLT uptake in the bone marrow and spleen with ENT1^{-/-} mice displaying the greatest change in FLT biodistribution (Fig 4-2 and Table 4-1). These results showed that the absence of functional ENT1 significantly affected FLT biodistribution in mice.

For all of the cultured cell lines tested in the work described in this thesis, inhibition of hENT1 activity with NBMPR reduced FLT uptake. However, in mice without ENT1 activity, FLT uptake increased in mouse bone marrow and spleen tissue. Since TK1 protein levels in spleens of different mouse strains were similar, the differences in FLT uptake were not due to differences in FLT phosphorylation. Plasma thymidine levels in ENT1^{-/-} mice were higher than those of ENT1^{+/+} mice, suggesting that increased FLT accumulation in the bone marrow and spleen tissues of ENT1^{-/-} mice was not caused by decreased plasma thymidine

levels which would provide less competition for interaction with hNTs and TK1. Mouse spleen tissues displayed significant immunohistochemical staining for both CNT1 and CNT3, suggesting that the greater FLT accumulation in spleen and bone marrow cells of ENT1^{-/-} than ENT1^{+/+} mice may have resulted from the combined effects of 1) negligible FLT efflux via ENT1 in cells and 2) high levels of FLT influx via CNT1 and/or CNT3. Cells with large CNT/ENT transport activity ratios will concentrate FLT into cells if FLT influx via CNT1 and/or CNT3 is greater than FLT efflux via ENT1 and/or ENT2. Inhibition of ENT1 in these cells will increase FLT concentration into cells since ENT1 will predominantly mediate FLT efflux when intracellular FLT levels are greater than extracellular FLT levels (Fig. 4-7B).

6.3 Clinical implications of FLT transport by hNTs

FLT was originally used in PET imaging to determine tumor proliferation [10]. The assumption was that FLT uptake is primarily dependent on TK1 activity since several studies have shown that TK1 transcript and protein expression and activity is regulated during the cell-cycle, with highest levels during late G1- and S-phase [11]. The results of this thesis suggest that FLT uptake in human cancer cells is strongly dependent on hNT activity, especially that of hENT1, and the influence of hNTs on FLT uptake may interfere with the ability of FLT PET to determine tumor proliferation. For example, rapidly dividing tumor cells with low hENT1/2 and hCNT1/3 activities may display relatively little FLT uptake. Similarly, slowly dividing tumor cells with low and high hENT1/2 and hCNT1/3 activities, respectively, may display relatively high FLT uptake when compared to

surrounding tissues. Inter-tumor levels of hNT mRNA and protein differ significantly for many cancers and some tumors have no detectable levels of hENT1 protein [12-14]. Immunohistochemical staining of hENT1 in human primary breast and pancreatic cancers showed that 12% and 22%, respectively, of specimens had no detectable hENT1 [12, 13]. Interestingly, two different FLT PET studies of human breast cancer and one study of human pancreatic cancer showed that 7-20% and 29% of breast and pancreatic cancers, respectively, were not detectable by FLT PET [15-17], suggesting that breast and pancreatic cancers with no detectable hENT1 may be “invisible” with FLT PET.

In many FLT PET clinical trials, tumor uptake of FLT correlated with other markers of proliferation. However, in those clinical trials that exhibited a significant correlation between FLT uptake and tumor proliferation, there was a large range in squared correlation coefficient (r^2) values (0.30 to 0.85, [18-22]), suggesting that FLT PET does not consistently predict tumor proliferation. Moreover, several FLT PET clinical trials lack significant correlations between FLT uptake and tumor proliferation [23-25]. The results presented in this thesis suggest that differences in tumor hNT levels may explain this phenomenon.

FLT biodistribution and tumor uptake may also be affected by various clinically used therapeutics that inhibit hENT activity. Dipyridamole, which is an antiplatelet agent used to reduce thrombus formation, is a potent hENT1 and hENT2 inhibitor at micromolar concentrations [26, 27]. Various protein kinase inhibitors including 1) tyrosine kinase inhibitors (AG825, AG1517, AG1478, STI-571), 2) protein kinase C inhibitors (staurosporine, GF 109203X, R0 31-

8220, arcyriarubin A), and 3) cyclin-dependent kinase inhibitors (roscovitine, olomoucine, indirubin-3'-monoxime), inhibited [³H]uridine uptake in cultured myelogenous leukemia K562 cells [28], suggesting that the kinase inhibitors affect NT activity. Further research is necessary to determine if clinically used multi-target protein kinase inhibitors, including sorafenib and sunitinib, affect FLT uptake in normal and diseased tissues.

Although the necessity of hNTs for efficient FLT uptake may complicate the use of FLT as a proliferation PET tracer, the necessity of hNTs for efficient FLT uptake may also provide clinically useful information of tumor capacity for nucleoside transport. Several anticancer drugs, including fludarabine, cladribine, clofarabine, cytarabine, gemcitabine and capecitabine, are nucleoside analogs and most clinically used nucleoside analogs require hNTs for efficient permeation inside tumor cells to exert their effects [29]. The positive correlation between the presence of hNTs, especially hENT1, and tumor response to chemotherapy has been most extensively studied and validated with pancreatic cancer response to gemcitabine [12, 30-32]. Interestingly, FLT and gemcitabine are pyrimidine nucleoside analogs and are both transported by the same hNTs, including hENT1/2 and hCNT1/3 [33-35]. The objective of Chapter 5 was to determine if FLT uptake could predict gemcitabine response in cultured pancreatic cancer cells since 1) pancreatic tumor response to gemcitabine, and 2) FLT uptake in cultured cancer cells is dependent on hNTs, especially hENT1.

To determine if FLT uptake predicts gemcitabine response, five different human pancreatic cancer cell lines (Capan-2, AsPC-1, BxPC-3, PL45, MIA PaCa-

2, and PANC-1) were analyzed for FLT and gemcitabine uptake over short (45 s) and long (60 min) periods and for gemcitabine sensitivity. Experiments were performed with or without NBMPR or dilazep to determine how hENT1/2 affected FLT uptake and gemcitabine uptake and toxicity. FLT and gemcitabine uptake over both short and long periods and gemcitabine sensitivity were reduced by simultaneous exposure to NBMPR and further reduced by simultaneous exposure to dilazep, suggesting that hENT1 and hENT2 were involved in these processes (Tables 5-2, 5-3, 5-4). In 5 of 6 cell lines, linear regression analysis of data demonstrated correlations between FLT and gemcitabine uptake over short periods (Fig. 5-4), gemcitabine uptake over long periods and gemcitabine sensitivity (Fig. 5-6A), and FLT uptake over long periods and gemcitabine sensitivity (Fig. 5-6B), suggesting that FLT uptake may predict gemcitabine response in the majority of pancreatic cancer cell lines.

When all of the pancreatic cell lines used in this research were compared, there was no correlation between FLT and gemcitabine uptake over long periods. However, FLT and gemcitabine are phosphorylated by different kinases (deoxycytidine kinase and TK1, respectively) and differences in TK1 and deoxycytidine kinase activities within tumor cells may have caused differences in the uptake of FLT and gemcitabine over prolonged periods of time. Despite differences between FLT and gemcitabine metabolism, the tested pancreatic cancer cell lines displayed similar correlations between 1) gemcitabine response, and 2) gemcitabine or FLT uptake over long periods.

Correlations between gemcitabine uptake over long periods and gemcitabine sensitivity were observed in five of six cell lines, suggesting that it will be impossible for uptake analysis of any nucleoside analog to predict gemcitabine response in *all* tumors since gemcitabine toxicity is determined by multiple processes in addition to gemcitabine transport and retention within tumor cells. Increased expression of mRNA encoding ribonucleotide reductase subunit 1, a downstream target of gemcitabine, correlated with increased gemcitabine resistance [36, 37], suggesting that gemcitabine toxicity is also dependent on levels of ribonucleotide reductase activity. Incorporation of gemcitabine within DNA inhibits DNA synthesis, and tumor proliferation rates (which affect FLT uptake) and DNA repair capacity will therefore also likely affect gemcitabine toxicity [38, 39]. Gemcitabine initiates apoptosis in cells and proteins involved in apoptosis are believed to affect gemcitabine toxicity since siRNA knockdown of Bcl-2 enhances gemcitabine toxicity in xenograft pancreatic tumors [40, 41]. Although many different factors may affect tumor response to gemcitabine, the data presented in Chapter 5 showed that FLT uptake correlated with gemcitabine response in the majority of cultured pancreatic cancer cell lines, presumably because gemcitabine permeation across plasma membranes was an important step in gemcitabine toxicity. Its absence is a major potential mechanism of gemcitabine resistance in pancreatic cancer cells.

6.4 Future work

Clinical trials are needed to determine if FLT PET is beneficial for patients with unidentified pancreatic lesions. A group of untreated patients with

pancreatic lesions should undergo FLT PET before treatment to determine FLT uptake in pretreated lesions. Lesions would also need to be characterized by magnetic resonance imaging, computed tomography, and/or biopsies if possible. Patients being treated with gemcitabine should undergo several more FLT PET scans days to weeks after initial treatment to determine how gemcitabine treatment affects tumor uptake of FLT. Gemcitabine causes cells to arrest in S-phase, leading to a transient increase in FLT uptake, suggesting that FLT PET after gemcitabine treatment may also be able to predict gemcitabine response [42]. Initial FLT uptake and changes in FLT uptake for pancreatic tumors should be compared with gemcitabine response to determine if FLT PET may be clinically useful for predicting gemcitabine response. A previous study by Hermann et al. [16] demonstrated that focal FLT uptake was exclusively observed in malignant pancreatic lesions, suggesting that initial FLT uptake and malignant status of pancreatic lesions should also be compared to verify if FLT PET is useful for identifying malignant pancreatic tumors.

If FLT PET is capable of predicting gemcitabine response in the majority of pancreatic cancers, cost-benefit analysis would need to be performed to determine if such imaging is warranted. Compared to other clinically used imaging modalities, PET is very expensive and uses relatively large amounts of radiation. Currently, very few treatments other than gemcitabine are available for pancreatic cancer patients since only gemcitabine and gemcitabine with erlotinib have been proven to increase survival [43, 44], therefore, determining if pancreatic cancers respond to gemcitabine would provide minimal benefit without

a proven second line treatment. However, performing FLT PET with patients with unidentified pancreatic lesions may distinguish benign from malignant pancreatic lesions which would provide useful information to guide subsequent clinical treatment [16]. Determining which pancreatic cancers are gemcitabine resistant may also minimize the unnecessary prescription of gemcitabine in patients that would not receive benefit, reducing chemotherapy side-effects and improving patient quality of life. Finally, determining which pancreatic cancer are resistant to gemcitabine would be beneficial as additional proven treatments for pancreatic cancers are eventually discovered.

6.5 Bibliography

- [1] Kong XB, Zhu QY, Vidal PM, Watanabe KA, Polsky B, Armstrong D, et al. Comparisons of anti-human immunodeficiency virus activities, cellular transport, and plasma and intracellular pharmacokinetics of 3'-fluoro-3'-deoxythymidine and 3'-azido-3'-deoxythymidine. *Antimicrob Agents Chemother* 1992;36:808-18.
- [2] Vickers MF, Zhang J, Visser F, Tackaberry T, Robins MJ, Nielsen LP, et al. Uridine recognition motifs of human equilibrative nucleoside transporters 1 and 2 produced in *Saccharomyces cerevisiae*. *Nucleosides Nucleotides Nucleic Acids* 2004;23:361-73.
- [3] Zhang J, Smith KM, Tackaberry T, Visser F, Robins MJ, Nielsen LP, et al. Uridine binding and transportability determinants of human concentrative nucleoside transporters. *Mol Pharmacol* 2005;68:830-9.
- [4] Zhang J, Visser F, Vickers MF, Lang T, Robins MJ, Nielsen LP, et al. Uridine binding motifs of human concentrative nucleoside transporters 1 and 3 produced in *Saccharomyces cerevisiae*. *Mol Pharmacol* 2003;64:1512-20.
- [5] Jarvis SM, Griffith DA. Expression of the rabbit intestinal N2 Na⁺/nucleoside transporter in *Xenopus laevis* oocytes. *Biochem J* 1991;278 (Pt 2):605-7.
- [6] Rasey JS, Grierson JR, Wiens LW, Kolb PD, Schwartz JL. Validation of FLT uptake as a measure of thymidine kinase-1 activity in A549 carcinoma cells. *J Nucl Med* 2002;43:1210-7.
- [7] Gati WP, Paterson AR. Measurement of nitrobenzylthioinosine in plasma and erythrocytes: a pharmacokinetic study in mice. *Cancer Chemother Pharmacol* 1997;40:342-6.
- [8] Kiss A, Farah K, Kim J, Garriock RJ, Drysdale TA, Hammond JR. Molecular cloning and functional characterization of inhibitor-sensitive (mENT1) and inhibitor-resistant (mENT2) equilibrative nucleoside transporters from mouse brain. *Biochem J* 2000;352 Pt 2:363-72.
- [9] van Waarde A, Cobben DC, Suurmeijer AJ, Maas B, Vaalburg W, de Vries EF, et al. Selectivity of 18F-FLT and 18F-FDG for differentiating tumor from inflammation in a rodent model. *J Nucl Med* 2004;45:695-700.
- [10] Shields AF, Grierson JR, Dohmen BM, Machulla HJ, Stayanoff JC, Lawhorn-Crews JM, et al. Imaging proliferation in vivo with [F-18]FLT and positron emission tomography. *Nat Med* 1998;4:1334-6.

- [11] Munch-Petersen B, Cloos L, Jensen HK, Tyrsted G. Human thymidine kinase 1. Regulation in normal and malignant cells. *Adv Enzyme Regul* 1995;35:69-89.
- [12] Farrell JJ, Elsaleh H, Garcia M, Lai R, Ammar A, Regine WF, et al. Human equilibrative nucleoside transporter 1 levels predict response to gemcitabine in patients with pancreatic cancer. *Gastroenterology* 2009;136:187-95.
- [13] Mackey JR, Jennings LL, Clarke ML, Santos CL, Dabbagh L, Vsianska M, et al. Immunohistochemical variation of human equilibrative nucleoside transporter 1 protein in primary breast cancers. *Clin Cancer Res* 2002;8:110-6.
- [14] Pennycooke M, Chaudary N, Shuralyova I, Zhang Y, Coe IR. Differential expression of human nucleoside transporters in normal and tumor tissue. *Biochem Biophys Res Commun* 2001;280:951-9.
- [15] Been LB, Elsinga PH, de Vries J, Cobben DC, Jager PL, Hoekstra HJ, et al. Positron emission tomography in patients with breast cancer using (18)F-3'-deoxy-3'-fluoro-L-thymidine ((18)F-FLT)-a pilot study. *Eur J Surg Oncol* 2006;32:39-43.
- [16] Herrmann K, Eckel F, Schmidt S, Scheidhauer K, Krause BJ, Kleeff J, et al. In vivo characterization of proliferation for discriminating cancer from pancreatic pseudotumors. *J Nucl Med* 2008;49:1437-44.
- [17] Smyczek-Gargya B, Fersis N, Dittmann H, Vogel U, Reischl G, Machulla HJ, et al. PET with [18F]fluorothymidine for imaging of primary breast cancer: a pilot study. *Eur J Nucl Med Mol Imaging* 2004;31:720-4.
- [18] Buck AK, Halter G, Schirrmeister H, Kotzerke J, Wurziger I, Glatting G, et al. Imaging proliferation in lung tumors with PET: 18F-FLT versus 18F-FDG. *J Nucl Med* 2003;44:1426-31.
- [19] Buck AK, Schirrmeister H, Hetzel M, Von Der Heide M, Halter G, Glatting G, et al. 3-deoxy-3-[(18)F]fluorothymidine-positron emission tomography for noninvasive assessment of proliferation in pulmonary nodules. *Cancer Res* 2002;62:3331-4.
- [20] Cobben DC, Elsinga PH, Suurmeijer AJ, Vaalburg W, Maas B, Jager PL, et al. Detection and grading of soft tissue sarcomas of the extremities with (18)F-3'-fluoro-3'-deoxy-L-thymidine. *Clin Cancer Res* 2004;10:1685-90.
- [21] Francis DL, Freeman A, Visvikis D, Costa DC, Luthra SK, Novelli M, et al. In vivo imaging of cellular proliferation in colorectal cancer using positron emission tomography. *Gut* 2003;52:1602-6.

- [22] Vesselle H, Grierson J, Muzi M, Pugsley JM, Schmidt RA, Rabinowitz P, et al. In vivo validation of 3'deoxy-3'-[(18)F]fluorothymidine ([18)F]FLT) as a proliferation imaging tracer in humans: correlation of [18)F]FLT uptake by positron emission tomography with Ki-67 immunohistochemistry and flow cytometry in human lung tumors. *Clin Cancer Res* 2002;8:3315-23.
- [23] Kameyama R, Yamamoto Y, Izuishi K, Takebayashi R, Hagiike M, Murota M, et al. Detection of gastric cancer using 18F-FLT PET: comparison with 18F-FDG PET. *Eur J Nucl Med Mol Imaging* 2009;36:382-8.
- [24] Linecker A, Kermer C, Sulzbacher I, Angelberger P, Kletter K, Dudczak R, et al. Uptake of (18)F-FLT and (18)F-FDG in primary head and neck cancer correlates with survival. *Nuklearmedizin* 2008;47:80-5; quiz N12.
- [25] van Westreenen HL, Cobben DC, Jager PL, van Dullemen HM, Wesseling J, Elsinga PH, et al. Comparison of 18F-FLT PET and 18F-FDG PET in esophageal cancer. *J Nucl Med* 2005;46:400-4.
- [26] Griffiths M, Beaumont N, Yao SY, Sundaram M, Boumah CE, Davies A, et al. Cloning of a human nucleoside transporter implicated in the cellular uptake of adenosine and chemotherapeutic drugs. *Nat Med* 1997;3:89-93.
- [27] Griffiths M, Yao SY, Abidi F, Phillips SE, Cass CE, Young JD, et al. Molecular cloning and characterization of a nitrobenzylthioinosine-insensitive (ei) equilibrative nucleoside transporter from human placenta. *Biochem J* 1997;328 (Pt 3):739-43.
- [28] Huang M, Wang Y, Cogut SB, Mitchell BS, Graves LM. Inhibition of nucleoside transport by protein kinase inhibitors. *J Pharmacol Exp Ther* 2003;304:753-60.
- [29] Zhang J, Visser F, King KM, Baldwin SA, Young JD, Cass CE. The role of nucleoside transporters in cancer chemotherapy with nucleoside drugs. *Cancer Metastasis Rev* 2007;26:85-110.
- [30] Giovannetti E, Del Tacca M, Mey V, Funel N, Nannizzi S, Ricci S, et al. Transcription analysis of human equilibrative nucleoside transporter-1 predicts survival in pancreas cancer patients treated with gemcitabine. *Cancer Res* 2006;66:3928-35.
- [31] Marechal R, Mackey JR, Lai R, Demetter P, Peeters M, Polus M, et al. Human equilibrative nucleoside transporter 1 and human concentrative nucleoside transporter 3 predict survival after adjuvant gemcitabine therapy in resected pancreatic adenocarcinoma. *Clin Cancer Res* 2009;15:2913-9.

- [32] Spratlin J, Sangha R, Glubrecht D, Dabbagh L, Young JD, Dumontet C, et al. The absence of human equilibrative nucleoside transporter 1 is associated with reduced survival in patients with gemcitabine-treated pancreas adenocarcinoma. *Clin Cancer Res* 2004;10:6956-61.
- [33] Hu H, Endres CJ, Chang C, Umaphathy NS, Lee EW, Fei YJ, et al. Electrophysiological characterization and modeling of the structure activity relationship of the human concentrative nucleoside transporter 3 (hCNT3). *Mol Pharmacol* 2006;69:1542-53.
- [34] Mackey JR, Yao SY, Smith KM, Karpinski E, Baldwin SA, Cass CE, et al. Gemcitabine transport in xenopus oocytes expressing recombinant plasma membrane mammalian nucleoside transporters. *J Natl Cancer Inst* 1999;91:1876-81.
- [35] Paproski RJ, Ng AM, Yao SY, Graham K, Young JD, Cass CE. The role of human nucleoside transporters in uptake of 3'-deoxy-3'-fluorothymidine. *Mol Pharmacol* 2008;74:1372-80.
- [36] Bepler G, Kusmartseva I, Sharma S, Gautam A, Cantor A, Sharma A, et al. RRM1 modulated in vitro and in vivo efficacy of gemcitabine and platinum in non-small-cell lung cancer. *J Clin Oncol* 2006;24:4731-7.
- [37] Rosell R, Danenberg KD, Alberola V, Bepler G, Sanchez JJ, Camps C, et al. Ribonucleotide reductase messenger RNA expression and survival in gemcitabine/cisplatin-treated advanced non-small cell lung cancer patients. *Clin Cancer Res* 2004;10:1318-25.
- [38] Ewald B, Sampath D, Plunkett W. ATM and the Mre11-Rad50-Nbs1 complex respond to nucleoside analogue-induced stalled replication forks and contribute to drug resistance. *Cancer Res* 2008;68:7947-55.
- [39] Huang P, Plunkett W. Fludarabine- and gemcitabine-induced apoptosis: incorporation of analogs into DNA is a critical event. *Cancer Chemother Pharmacol* 1995;36:181-8.
- [40] Huang P, Plunkett W. Induction of apoptosis by gemcitabine. *Semin Oncol* 1995;22:19-25.
- [41] Okamoto K, Ocker M, Neureiter D, Dietze O, Zopf S, Hahn EG, et al. bcl-2-specific siRNAs restore gemcitabine sensitivity in human pancreatic cancer cells. *J Cell Mol Med* 2007;11:349-61.
- [42] Dittmann H, Dohmen BM, Kehlbach R, Bartusek G, Pritzkow M, Sarbia M, et al. Early changes in [18F]FLT uptake after chemotherapy: an experimental study. *Eur J Nucl Med Mol Imaging* 2002;29:1462-9.

- [43] Cartwright T, Richards DA, Boehm KA. Cancer of the pancreas: are we making progress? A review of studies in the US Oncology Research Network. *Cancer Control* 2008;15:308-13.
- [44] Moore MJ, Goldstein D, Hamm J, Figer A, Hecht JR, Gallinger S, et al. Erlotinib plus gemcitabine compared with gemcitabine alone in patients with advanced pancreatic cancer: a phase III trial of the National Cancer Institute of Canada Clinical Trials Group. *J Clin Oncol* 2007;25:1960-6.